NOTE TO USERS

Robust Control Techniques for Aerospace Vehicles

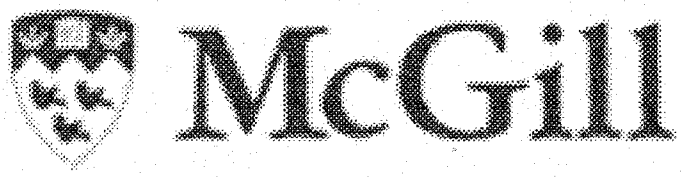

By

Nabil Aouf

A thesis submitted in conformity with the requirements
For the degree of Doctor of Philosophy
Graduate Department of Electrical and Computer Engineering
McGill University

Abstract

The research work presented in this thesis deals with flight control problems. Based on robust control techniques such as H_∞ control and $\mu-$synthesis, we develop control laws that are efficient in reducing gust loads on flexible aircraft. Uncertainty models for flexible aircraft are proposed and shown to be well adapted for robust control design, while tightly covering unknown but bounded variations of flexible mode parameters. One of the models presented introduces a new complex-rational controller design methodology that takes advantage of the uncertain plant structure and achieves good performance criteria. Other uncertainty models are presented for the first time for the purpose of closed-loop reduction of flexible models. We propose a new model/controller order reduction method for flexible aircraft preserving robust performance in closed loop. Two case studies of complex aircraft are presented with the objective of full flight envelope control. Solutions for scheduled control laws are given to maintain performance objectives along the entire flight envelope. We adapt to our complex aircraft case study known gain scheduling techniques such as observer-form controller scheduling, and we propose new gain scheduling techniques, including a robust performance blending/interpolation design, an optimal multi-switching methodology and a scheduled-partitioned controller.

Résumé

Dans cette thèse, on développe des lois de commande robustes, comme la commande H_∞ et la synthèse μ, qui sont appliquées à plusieurs problèmes en aéronautique. Cette thèse contribue à plusieurs aspects de la commande de vol evoluée. On résout plusieurs problèmes théoriques dont les solutions élaborées sont susceptibles de donner satisfaction sur des modèles complexes d'avions réels. Nous traitons le problème des rafales et leurs effets sur un avion flexible. Nous montrons l'efficacité d'intégrer des lois de commande robustes afin d'alléger les effets de rafales sur l'avion. L'étude de la commande robuste nous amène à parler de modélisation d'incertitudes. Nous proposons dans cette thèse de nouveaux modèles d'incertitudes qui représentent finement les variations des paramètres caractérisant les modes flexibles ainsi que pour la réduction de modèles d'avions. Ce dernier objectif est pris en compte dans notre recherche et une méthode de réduction d'ordre du modèle et du compensateur pour les structures flexibles, en boucle fermée et préservant la performance robuste est proposée. S'ajoute à ceci une étude du *gain scheduling* avec de nouvelles méthodes proposées pour un avion STOVL Harrier et pour un avion flexible B1. Une loi de commande a performance robuste est réalisée et on prouve la stabilité pour des approches basées sur l'interpolation et jugées *ad hoc* dans la littérature.

I Dedicate this Thesis in Memory of My Parents: Taya, Med Lakhdar, and My Brother Elyasse,
To All Who Love Me.

Acknowledgements

First and foremost, I would like to thank Professor Benoit Boulet, my thesis advisor, for his guidance, support and friendship throughout my Ph.D. studies. The quality of this thesis owes much to his rigorous reading and many constructive criticisms.

I owe a debt of gratitude to Professor Ruxandra Botez for her advices at every stage of this work.

I thank Professor Postlethwaite and Dr. Bates of University of Leicester, UK, for the research collaboration they provided during my visits to Leicester.

I must also thank the Centre for Intelligent Machines (CIM) for providing an excellent atmosphere for conducting research. Many fellow graduate students deserve my appreciation for constant exchange of ideas and lively debates. Some of them are: Shahid Shaikh, Ammar Haurani, Miguel Torres-Toretti, Khaled El widyan, among many others.

I would like to thank the Natural Sciences and Engineering Research Council (NSERC) of Canada for providing financial support.

I wish to thank my brother Lotfi, my sisters Naima, Salima, Mounira, Rahima and their husbands and children for their love, support and advice. My uncle El-Hadi and his family must also be thanked for their love and encouragement.

Finally, I would like to thank my wife, Samira, for constant love, support and encouragement.

Claims of originality

Flexible aircraft and gust load alleviation problem

One of the main objectives of this thesis is to study aircraft flexible models. These models are of high order and tend to be difficult for robust control design. However, these flexible models are more realistic than rigid-body models typically used in the flight control literature. Neglecting the flexibility aspect of an aircraft, especially large aircraft, can have dangerous consequences when control laws are implemented. Since the flexible models are sensitive to gust effects, we focus on designing robust control laws, using H_∞ control and $\mu-$synthesis, shown through this thesis to be able to reduce undesirable acceleration caused by gust loads. A motivating justification for the use of H_∞ control for optimal gust load alleviation is given. This problem has not been treated in the literature using robust control techniques in application to flexible aircraft. We include in the robust control setup for gust loads alleviation problem, representative models for severe gust generation. The use of such models in this thesis gives a realistic study of the effects of gusts on the flexible aircraft. Comparisons of results we obtain using robust control techniques (weighted H_2 and H_∞ control) with modern control techniques such as LQG or classical H_2, are given in Chapter 2 for a B52 flexible bomber. These results show significant difference in reducing the acceleration of the aircraft due to the gust effects in favor of robust control techniques

Uncertainty modeling

Robust control design needs tight bounds of uncertainties when variations in the aircraft dynamics are taken into account. For flexible aircraft, we investigate modeling the variations of flexible mode parameters. In the literature, e.g., [Bal99], [Mad], no tight models, without unrealistic heuristics, have been proposed. We present in Chapter 4 two uncertainty models based on coprime factorization approach and modal coordinates approach, respectively. These models are well adapted for a less conservative robust control design. The uncertainty model, based on the modal coordinates approach, leads to an efficient complex-rational controller design newly introduced in this thesis. This complex-rational control methodology achieves good robust performance indices and is shown to be the first step of the controller design. The second step will be that of recovering a robust real-rational controller for implementation purposes. The efficiency of the uncertainty models and the complex-rational control methodology is shown on three-mass flexible models.

In addition, we present in Chapter 3 a new uncertainty model for flexible modes called "inverse uncertainty", with lower upper bounds than the usual additive uncertainty model, that is efficient for robust control design under a closed-loop order reduction framework.

Order reduction techniques

Many order reduction techniques [Glo84], [Enn84b] were proposed in the literature. However, these techniques are usually for open-loop order reduction. Although, some techniques, [Wortel94], are developed for closed-loop order reduction, the physical meaning of the state is lost after reduction. For this reason and because each flexible mode has its specific state representation, we introduce a model/controller closed-loop order reduction preserving performance indices. The method we propose in Chapter 3 has the virtue of treating the reduction of the flexible model and the controller in the same framework. Using new parametric uncertainty models, which include reduction effects of a given number of flexible modes and with a robust performance $\mu-$analysis, we are able in the first step of our methodology to give the statement of the best flexible mode combination to truncate, without losing performance specifications. We propose then Theorem 3.1 that gives a sufficient condition under which, starting from the full-order controller of the best flexible mode combination, and under certain conditions, a reduced-order controller preserving the robust performance specifications obtained by the full-order controller can be obtained. Applicability of the proposed technique is validated by many examples from flexible aircraft to flexible structures models.
In addition to this technique, we propose uncertain closed-loop order reduction methodology for which we use the inverse uncertainty model developed in this thesis. Results in favor of this uncertainty model compared with additive uncertainty model are highlighted through examples in Chapter 3.

Gain scheduling

Huge progress in gain scheduling research has been achieved this last decade because of its importance for flight control research. In general, we classify gain-scheduling techniques into simple, practical methods, however ad hoc, and sophisticated parameter-varying techniques that offer some stability guarantees. In this thesis and through Chapter 5 and Chapter 6, we propose gain-scheduling techniques based on the simplicity of the *ad hoc* methods, while providing robust stability and performance guarantees (see Chapter 6). In fact, complexity of STOVL Harrier aircraft studied in Chapter 5 is a hard constraint that imposes the use of simple gain-scheduling schemes such as the new blending/interpolating technique that we propose in this thesis. In addition to this technique, we provide an observer-form controller solution and a multi-switching

algorithm based on the linear quadratic bumpless transfer technique. All these developments are made under an Integrated Flight Propulsion Control methodology used in this thesis. This methodology leads to a sub-optimal decentralized controller easy to implement and for which we propose a new scheduling-partitioning technique.

In Chapter 6, for the model of a flexible B1 bomber, and based on the availability of linear parameter varying model, we propose techniques based on interpolation of Riccati equation solutions and a redesign technique. In addition to this, we propose, based on the blending/interpolating technique developed in Chapter 5, a robust performance controller design and analysis tools for the entire envelope of the aircraft considered. We propose a methodology to represent the nonlinear system of the flexible B1 bomber by a linear uncertain model, which covers the aircraft flight envelope by the variation of its parametric uncertainty. Then we propose Theorem 6.1, which uses $\mu-$robust performance setup properties to give a necessary and sufficient condition to obtain a gain-scheduled controller guaranteeing robust performance specifications. This result allows us to use simpler techniques than linear parameter varying control, while still guaranteeing stability and performance specifications. In addition to Theorem 6.1, we present in Lemma 6.1 general necessary tools for the stability and performance analysis of the gain-scheduled controller, based on the blending/interpolating technique presented in Chapter 5. In particular these tools can be used for the analysis of the robust performance gain-scheduled controller obtained by Theorem 6.1.

Content

Chapter 1: Introduction 1

1.1 Robust flight control 1

1.2 Aircraft and gust modeling 2

1.2.1 Rigid body aircraft model 3

1.2.2 Longitudinal motion 6

1.2.3 Background on flexible structures 7

1.2.4 Flexible aircraft model 10

1.3 Gust load alleviation problem 11

1.3.1 Turbulence modeling 11

1.3.2 Load gusts on aircraft 13

Chapter 2: Robust control techniques with application to gust load alleviation of flexible aircraft 16

2.1 Introduction 16

2.2 Problem setup 16

2.3 Weighted H_2 Optimal control 18

2.3.1 Motivations on weighted H_2 design 18

2.3.2 Briefs on Algebraic Riccatti equations 20

2.3.3 H_2 synthesis 21

2.3.4 H_2 State Feedback via LMI 23

2.4 H_∞ Optimal control 25

2.5 LMI approach to H_∞ control 26

2.6 Uncertainty modeling 29

2.6.1 Unstructured uncertainties 29

2.6.1.1 Additive uncertainty model 29

2.6.1.2 Output multiplicative uncertainty 31

2.6.1.3 Input multiplicative uncertainty 31

2.6.1.4 LFT uncertainty representation 32

2.6.2 Robust stability theorem 34

2.6.3 Structured uncertainty 36

2.6.3.1 Parametric uncertainties 37

2.6.3.2 Structured singular value 39
2.6.3.3 Robust stability with structured uncertainty 43
2.6.3.4 Robust performance 44
2.7 H_∞ loopshaping design 45
2.7.1 Robust stabilization 46
2.7.2 Loopshaping procedure 47
2.8 μ – Synthesis using H_2 controllers 48
2.9 B52 flexible bomber application 50
2.9.1 Introduction 50
2.9.2 Vertical gust model 52
2.9.3 Flexible model description 52
2.9.4 Problem setup 53
2.9.5 H_∞ control 55
2.9.6 Weighted H_2 and H_∞ optimal control 56
2.9.6.1 Weighted H_2 controller 56
2..9.6.2 H_∞ optimal design 56
2.9.6.2.1 weighting functions for nominal performance 57
2.9.6.2.2 H_∞ optimal controller 58
2.9.6.3 μ – controller 58
2.9.6.4 Simulation results 60

Chapter 3: Order reduction techniques for flexible structures 64
3.1 Introduction 64
3.2 Open-loop order reduction methods 64
3.2.1 Algebraic dominance 64
3.2.2 Devillemagne-Skelton approach 65
3.2.3 Cost decomposition order reduction 66
3.2.4 Modern, optimal order reduction techniques 67
3.2.4.1 Balanced reduction 69
3.2.4.2 Mode balanced modal reduction 69
3.2.4.3 Optimal H_2 norm reduction 70
3.2.4.4 Optimal Hankel-norm reduction 71
3.2.4.5 H_∞ optimal reduction 71

3.2.5 Weighted order reduction 72
3.3 Closed-loop order reduction 73
3.3.1 LQG and H_∞ balanced reduction 74
3.3.2 Closed-loop balanced reduction 75
3.3.3 Closed loop preserving performance controller reduction methods 76
3.4 Order reduction of flexible systems in a closed loop framework 78
3.4.1 Uncertain flexible modes truncation 79
3.4.1.1 Additive uncertainty reduction 79
3.4.1.2 Inverse uncertainty reduction 81
3.4.2 Model and controller Reduction for flexible aircraft preserving robust performance 84
3.4.2.1 Introduction 84
3.4.2.2 Problem setup 86
3.4.2.3 Uncertainty model 87
3.4.2.4 Model and controller reduction 90
3.4.2.5 Modal reduction over the full flight envelope of a flexible aircraft 95
3.4.2.6 Flexible system example 96
3.4.2.7 Flexible aircraft example 99
3.4.3 Discussion of μ – sensitivity order reduction for flexible aircraft 101
3.4.3.1 μ – sensitivity 102
3.4.3.2 μ – sensitivity for order reduction 102

Chapter 4: Uncertainty models and robust complex-rational controller design 104
4.1 Introduction 104
4.2 Problem setup 105
4.3 Coprime factorization approach 106
4.4 Modal coordinates approach 107
4.5 Control design 109
4.6 Simulation and new control design strategy 110
Chapter 5: Gain scheduling techniques for STOVL harrier aircraft 115
5.1 Introduction 115
5.2 Integrated methodology for propulsion and airframe control 116
5.3 STVOL Harrier aircraft 117
5.4 Centralized IFPC system design 121

5.5 Observer-form implementation and scheduling 123
5.6 Antiwindup methodology 133
5.6.1 Problem statement 133
5.6.2 Antiwindup technique 136
5.6.3 Application of the observer from antiwindup technique 137
5.7 A control signal blending/Interpolating approach 140
5.8 Optimal multi-switching technique 147
5.8.1 Introduction 147
5.8.2 Linear quadratic bumpless transfer 148
5.8.2.1 Finite horizon compensator formulae 148
5.8.2.2 Infinite horizon compensator formulae 152
5.8.2.3 Stability 154
5.8.3 A multi-switching technique for controller implementation 154
5.8.3.1 Supervisory control 154
5.8.3.2 A multi-switch methodology for the VSTOL aircraft 156
5.8.4 Nonlinear simulation Results 158
5.8.4.1 Without the bumpless transfer scheme 158
5.8.4.2 With the bumpless transfer scheme 161
5.9 Partitioning-scheduling of IFPC design 163
5.9.1 Introduction 163
5.9.2 Centralized controller and partitioning procedure 164
5.9.3 Scheduling the partitioned controllers 167
5.9.4 Non-linear simulation 168

Chapter 6: Advanced scheduling techniques for a flexible aircraft 173
6.1 Introduction 173
6.2 LPV gain-scheduled control theory 173
6.3 Gain-scheduled LFT control theory 177
6.4 Riccati solutions interpolation technique 179
6.4.1 Introduction 179
6.4.2 Problem setup 180
6.4.2.1 Aircraft model 180
6.4.2.1 Controller design 181
6.4.3 Scheduling technique 184

6.4.4 Results and nonlinear simulation 185
6.5 Concept of online redesign of controller 187
6.6 Robust Gain scheduling controller design 190
6.6.1 Introduction 190
6.6.2 Uncertain model representation 191
6.6.3 Parameterization of stabilizing controllers 193
6.6.4 Robust performance gain scheduling approach 195
6.6.5 Optimization based control 197
6.6.6 Robust performance analysis technique 199
6.6.7 Application example 200
Chapter 7 Summary and Conclusion 204
7.1 Future research 206
7.1.1 Order reduction 206
7.1.2 Uncertainty and gain scheduling 207
Bibliography 208

Appendix 218

List of Figures

Figure1.1: Body and Earth axes system

Figure 1.2 Aircraft subject forces

Figure 1.3: Turbulence effect on aircraft velocity

Figure 2.1: Typical feedback control system

Figure 2.2: plant augmentation

Figure 2.3: equivalent setup

Figure 2.4: Additive uncertainty

Figure 2.5: Output multiplicative uncertainty

Figure 2.6: Input multiplicative uncertainty

Figure 2.7: LFT uncertainty representation

Figure 2.8: Equivalent LFT and $M-\Delta$ interconnections

Figure 2.9: structured uncertainty setup

Figure 2.10: Parametric uncertainty setup

Figure 2.11: robust performance setup

Figure2.11: H_{∞} robust stabilization problem

Figure2.12: B52 bomber

Figure 2.13: Problem setup

Figure 2.14: Norms of closed-loop transfer matrices

Figure 2.15. Setup for robust control design

Figure 2.16: Gust signals and open-loop response

Figure2.17: Simulation results

Figure 2.18: Norm bounds for uncertainties

Figure 2.19: Upper and lower bounds on μ for μ design

Figure 2.20 Upper and lower bounds on μ, $\mathcal{H}_{\infty}$ design

Figure 3.1: Additive uncertainty reduction

Figure 3.2: Inverse uncertainty reduction

Figure3.3: open loop frequency response

Figure3.4: Additive uncertainty bounds

Figure3.5: Inverse uncertainty bounds

Figure3.6: μ – upper bounds for flexible mode3 truncation

Figure3.7: μ – upper bounds for flexible mode1 truncation

Figure3.8 :Parametric uncertainty injection

Figure3.9 :SVD decomposition of the uncertainty

Figure3.10 : augmented plant representation

Figure3.11 : Robust analysis setup

Figure3.12 : Robust performance setup

Figure3.13 : Controller reduction setup

Figure3.14 Augmented plant with the reduced order controller

Figure3.15 : Uncertainty block augmentation

Figure3.16: Introduction of the closeness of the full and reduced controllers

Figure3.17 : Augmentation of the plant by adding $\tilde{\Delta}_K$ uncertainty

Figure3.18 : Magnitude of Δ_K and W_k^{-1}

Figure3.19 : μ bounds for both full and reduced controllers

Figure3.20: Magnitudes of the norm of $(K_r - \hat{K}_f)$ and of W_k^{-1}

Figure3.21: μ bounds for both full and reduced controllers

Figure3.22 : Magnitudes of the two entries of $(K_r - K_{f1})$ and of W_k^{-1}

Figure3.23 : μ bounds for both full and reduced controllers

Figure4.1: Coprime factorization Control setup

Figure4.2: Upper bound on magnitudes of perturbations for Example 1

Figure4.3: Upper bound on μ for Example 1

Figure4.4: Upper bound on magnitudes of perturbations for Example 2

Figure4.5: Upper bound on μ with complex-rational controller for Example 2

Figure4.6: Upper bound on μ with real-rational controller for Example 2

Figure 5.1 : A version of STVOL Harrier aircraft

Figure5.2: Spey engine scheme

Figure 5.3: H_∞ loopshaping controller implementation for piloted trials

Figure 5.4 : Scheduled Observer implementation of the H_∞ loopshaping

Figure 5.5 : observer form(dashed)/1DOF H_∞ loopshaping structure for $\dot{\gamma}$ demand. airframe and engine variables

Figure 5.6 : observer form(dashed)/1DOF H_∞ loopshaping structure for $\dot{\gamma}$ demand. Actuator efforts

Figure 5.7 : observer form(dashed)/1DOF H_∞ loopshaping structure for $\dot{\gamma}$ demand. Actuator efforts

Figure 5.8 : Observer form(dashed)/1DOF H_∞ loopshaping structure for velocity demands: airframe and engine variables
Figure 5.9 : Respnse of scheduled IFPC system for pilot demands VT in the acceleration from hover
Figure 5.10 : Airframe actuator responses of pilot demands on VT in the acceleration from hover
Figure 5.11 : Engine variables of pilot demands on VT in the acceleration from hover
Figure 5.12 Engine actuators of pilot demands on VT in the acceleration from hover
Figure 5.13 : comparison of VT responses to pilot, scheduled IFPC system (-), single controller designed at hover (--)
Figure 5.14 :comparison of $\dot{\gamma}$ coupling for pilot demands on VT, scheduled IFPC system (-), single controller designed at hover (--)
Figure5.15: Results of 150kn controller: Velocity tracking
Figure5.16: Results of scheduled controller from hover to150kn without antiwindup technique. (a)
Figure5.17: Results of scheduled controller from hover to150kn without antiwindup technique. (b)
Figure5.18: Results of scheduled controller from hover to150kn without antiwindup technique. (c)
Figure5.19: Results of scheduled controller from hover to150kn without antiwindup technique. (d)
Figure5.20: Observer form antiwindup technique
Figure5.21: Results of 150kn safe controller: Velocity tracking
Figure5.22: Results of scheduled controller from hover to150kn with antiwindup technique. (a)
Figure5.23: Results of scheduled controller from hover to150kn with antiwindup technique. (b)
Figure5.24: Results of scheduled controller from hover to150kn with antiwindup technique. (c)
Figure5.25: Results of scheduled controller from hover to150kn with antiwindup technique. (d)
Figure 5.26 : Blended/Interpolated implementation
Figure 5.27 : Blending/interpolating scheduling for velocity demands (20kn to 120kn)

Figure 5.28 Blending/Interpolating scheduling for velocity demands (20kn to 120kn). Engine variables
Figure 5.29 : Blending/Interpolating scheduling for velocity demands(20kn to 120kn). Airframe actuators
Figure 5.30 : Blending/Interpolating scheduling for velocity demands(20kn to 120kn). engine actuators
Figure 5.31 : Blending/Interpolating scheduling for velocity demands(0kn to 120kn)
Figure 5.32 : Blending/Interpolating scheduling for velocity demands(0kn to 120kn). Engine variables
Figure 5.33 : Blending/Interpolating scheduling for velocity demands(0kn to 120kn). Airframe actuators
Figure 5.34 : Blending/Interpolating scheduling for velocity demands(0kn to 120kn). engine actuators
Figure 5.35 : Bumpless transfer scheme
Figure 5.36 : An example of switching boundaries which are manifolds
Figure 5.37 : Switching points on an interval
Figure 5.38 : Airframe responses without bumpless transfer scheme
Figure 5.39 : Engine variables without bupless transfer scheme
Figure 5.40 : Actuator responses without bumpless transfer scheme
Figure 5.41 : Actuator responses without bumpless transfer sheme
Figure 5.42 : Airframe variables with the bumpless transfer scheme
Figure 5.43 : Engine variables with the bumpless transfer scheme
Figure 5.44 : Actuaor responses with bumless transfer scheme
Figure 5.45 : Actuator responses with bumpless transfer scheme
Figure5.46: Partitioning IFPC controller scheme
Figure5.47: Blending/interpolating portioned controller
Figure 5.48: Airframe variables with 50kn partioned controller
Figure 5.49: Engine variables with 50kn-partitioned controller
Figure 5.50: Actuator responses with 50kn-partitioned controller
Figure 5.51: Actuator responses for 50kn-partitioned controller
Figure 5.52: Airframe variables with a partitioned scheduled controller
Figure 5.53: Engine variables for scheduled partitioned controller
Figure 5.54: Engine variables for scheduled partitioned controller
Figure 5.55: Actuator responses for scheduled partitioned controller

Figure6.1: Parameter-dependent plant
Figure6.2: Parameter-dependent controller
Figure6.3: Gain scheduled LFT control setup
Figure6.4: Optimal control setup
Figure6.5: Frozen controller results (pitch tracking and actuator responses)
Figure6.6: gain scheduled controller results (pitch tracking and actuator responses)
Figure6.7: Constrained gain scheduled controller results (pitch tracking and actuator responses)
Figure6.8: Controller redesign setup
Figure6.9: Robustness measures
Figure6.10: pitch angle tracking for redesigned controller
Figure6.11: actuator responses for redesigned controller
Figure6.12: Standard robust controller setup
Figure6.13: Parameterization of stabilizing controller
Figure6.14: Blending/interpolating parameterized controllers
Figure6.15: Augmented system into robust controller setup
Figure6.16: $S-\Delta$ structure
Figure6.17: $\mu-bounds$ for robust performance
Figure6.18: $\mu-bounds$ for robust stability
Figure6.19: $\mu-bounds$ with relaxed performance specification
Figure6.20: pitch tracking for weighted H_2 control
Figure6.21: actuator responses for weighted H_2 control
Figure6.22: $\mu-bounds$ for robust performance
Figure6.23: pitch tracking for robust gain scheduling control
Figure6.24: pitch tracking for robust gain scheduling control

List of Tables

Table 1.1: Gust models.

Table 2.1: Flexible modes.

Table 3.1: Results for truncation of a single flexible mode.

Table 3.2: Flexible modes.

Table 6.1: Operating points and performance indices.

Chapter 1

Introduction

1.1 Robust flight control

In this thesis, we develop robust techniques for various flight control problems including gust load alleviation for flexible aircraft. Open research questions are treated using advanced control techniques such as H_∞ control, μ - synthesis and gain scheduling.

The gust load alleviation problem for flexible aircraft is defined with the necessity of integrating robust control techniques in Chapter 2. Flexible aircraft models are chosen as case studies for this problem because taking into account the flexibility in the aircraft and its interaction with gust effects is more realistic than simply using rigid-body models. Motivation to use H_∞ and weighted-H_2 control for the gust load alleviation problem is given and efficiency of these proposed control technologies demonstrated and compared to other classical types of control strategies.

Flexible aircraft, which are represented in general by high-order models, naturally led us to consider the order reduction problem for the model and/or the controller. This problem is treated in Chapter 3 by our new model/controller order reduction technique achieving closed-loop robust performance criteria. The proposed method is suitable for flexible models, which up to now have been usually reduced in open loop using classical order reduction techniques that do not take into account the physical interpretation of the flexible modes. In addition to this method, we discuss uncertain models for closed-loop reduction methods for which we introduced a new type of uncertainty, suitable for reduction of the flexible systems, and called "inverse uncertainty". This type of uncertainty facilitates the controller design based on the reduced-order model chosen.

In modeling flexible aircraft, or in general flexible structures, one needs to have information about the accuracy of the values for the damping ratios and natural frequencies of the flexible modes. This is not generally the case, which spurred research to develop parametric uncertainty models for these uncertain coefficients. Existing uncertainty models in the literature [Mad98], [Bald99] often suffer from being too conservative and sometimes use questionable heuristics. Thus, we propose in Chapter 4

two tight uncertainty models based on coprime factorization and that are suitable for robust control design. In addition, we present a way of calculating μ, the structured singular value, that can be very useful when the uncertainty models contain many uncertainty blocks, real and complex. The problem of calculating μ is still open for research, and existing solutions are not always satisfactory for high-order uncertain models. For real flight control applications, aircraft control should obviously function over the entire flight envelope considered. This leads to the study in Chapter 5, of the gain scheduling problem, which is still open for discussion and improvements. Noting the complexity and numerical problems associated with gain scheduling techniques such as linear parameter-varying control, we prefer to adapt ad-hoc methods in the literature that have proved to achieve acceptable performance on a complex Short take-off and vertical landing (STOVL) Harrier aircraft. In this chapter, an integrated flight propulsion control (IFPC) framework is introduced and described in some details. Under this framework, and in addition to adapting an observer-form interpolating scheduling technique [Aouf2000d], we propose a new blending/interpolating [Aouf2000c] technique and extend a bumpless switching technique [Turn2002] for a multi-switching control structure. We close Chapter 5 with the introduction of a partitioning technique for IFPC systems and propose a scheduling approach for a partitioned controller. Starting from a linear parameter-varying model of the nonlinear B1 flexible aircraft, we present in the first part of Chapter 6 two gain scheduling techniques: one based on interpolation of the solution of Riccati equations used in robust control techniques, and the second technique is based on controller redesign along the flight envelope as the dynamics change. In the second part of this chapter, we present a new gain scheduling robust performance controller design and analysis based on blending/interpolation technique, which is introduced in Chapter 5. A proof of stability is given for the gain scheduling controller based on interpolation methods. This represents a step forward as such controllers have been designated as *ad-hoc* methods for their lack of guarantee on the stability of the gain-scheduled closed-loop system.

1.2 Aircraft and gust modeling

In this section we give some background and generalities on aircraft modeling and specifically for flexible aircraft, which is one of our applications of interest. Aircraft models that include structural flexibility are more realistic than rigid-body models. For small aircraft, it is often admissible to ignore the flexibility that exists in the aircraft, e.g., in the aircraft wings. However for commercial aircraft that

are usually of large dimension, ignoring the flexible modes of the aircraft may systematically cause a problem of accuracy of the model representing the real aircraft.

We introduce the problem of gust load alleviation as a flight performance objective of interest. We will study the effect of turbulence on the acceleration of the aircraft, and by means of advanced control techniques, we will propose control laws to reduce passenger discomfort caused by vibration induced by the turbulence.

1.2.1 Rigid-body aircraft model

In this aircraft motion modeling analysis, we use the earth frame axes $X_E Y_E Z_E$ and the aircraft frame axes $X_B Y_B Z_B$. The rigid aircraft is assumed to have the same distance between any two points on its structure over the entire flight envelope. When an aircraft is assumed to be rigid, its motion has six degrees of freedom. The following study is derived from the textbook [Mcl90] where detailed information can be obtained. The motion equations of a rigid-body aircraft are deduced by applying Newton's second law. The forces acting on the aircraft along the aircraft axes are:

$$F = \frac{d}{dt}\{m_0 V_T\} \tag{1.1}$$

$$F = \mathrm{i}F_X + \mathrm{j}F_Y + \mathrm{k}F_Z \ , \quad \begin{aligned} F_X &= m_0(\dot{U} + QW - VR) \\ F_Y &= m_0(\dot{V} + UR - PW) \\ F_Z &= m_0(\dot{W} + VP - UQ) \end{aligned} \tag{1.2}$$

and $V_T = \mathrm{i}U + \mathrm{j}V + \mathrm{k}W$,

where m is the mass of the aircraft, V_T is the velocity of the aircraft, expressed in the aircraft's frame, with derivatives: $\left.\frac{d}{dt}V_T\right|_B = \mathrm{i}\dot{U} + \mathrm{j}\dot{V} + \mathrm{k}\dot{W}$, (i, j, k) are the orthonormal vectors associated with the body axes $X_B Y_B Z_B$ and parameters P, Q, R represent the angular roll, pitch and yaw velocities respectively.

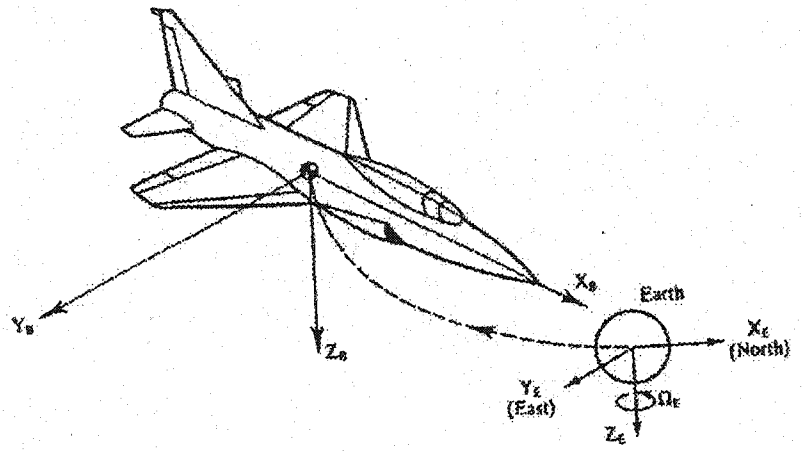

Figure1.1: Body and Earth axes system

Other types of forces such as the gravitational forces acting on the aircraft should be taken into account in the modeling of motion equations. For the following we define ϕ,θ,ψ as the roll, pitch and yaw angles, respectively. The coordinates of the gravitational forces along the aircraft axes are:

$$\begin{aligned} F_X &= -m_0 g \sin\theta \\ F_Y &= m_0 g \cos\theta \sin\phi \\ F_z &= m_0 g \cos\theta \cos\phi \end{aligned} \quad . \tag{1.3}$$

Using Newton's second law for the moments applied on the aircraft, we obtain:

$$M = \frac{d}{dt} H + \omega \times H \tag{1.4}$$

where $H = I\omega$ is the angular moment, ω is the angular velocity, and $I = \begin{bmatrix} I_{xx} & -I_{xy} & -I_{xz} \\ -I_{xy} & I_{yy} & -I_{yz} \\ -I_{xz} & -I_{yz} & I_{zz} \end{bmatrix}$ is the inertia matrix.

The simplified coordinates of the moments along the aircraft axes $X_B Y_B Z_B$ are given respectively as follows [Mcl90]:

$$M = \begin{bmatrix} \Delta L \\ \Delta M \\ \Delta N \end{bmatrix}, \quad \begin{aligned} \Delta L &= I_{xx}\dot{P} - I_{xz}\left(\dot{R} + PQ\right) \\ \Delta M &= I_{yy}\dot{Q} + I_{xz}\left(P^2 - R^2\right) \\ \Delta N &= I_{zz}\dot{R} - I_{xz}\left(\dot{P} - QR\right) \end{aligned} \tag{1.5}$$

Using perturbation theory, which considers the movement of an aircraft as small deviations from equilibrium around a stationary operating point, the equations of motion of a rigid-body aircraft are given for the equilibrium operating point represented by subscript 0, as:

$$
\begin{aligned}
F_{X_0} &= m_0\left[Q_0W_0 - R_0V_0 + g\sin\Theta_0\right] \\
F_{Y_0} &= m_0\left[U_0R_0 - P_0W_0 - g\cos\Theta_0\sin\Phi_0\right] \\
F_{Z_0} &= m_0\left[P_0V_0 - Q_0U_0 - g\cos\Theta_0\cos\Phi_0\right] \\
L_0 &= Q_0R_0(I_{zz} - I_{yy}) - P_0Q_0I_{xz} \\
M_0 &= (P_0^2 - R_0^2)I_{xz} + (I_{xx} - I_{zz})P_0R_0 \\
N_0 &= I_{xz}Q_0R_0 + (I_{yy} - I_{xx})P_0Q_0
\end{aligned}
\tag{1.6}
$$

For the perturbed part:

$$
\begin{aligned}
\Delta F_X &= m_0\left[\dot{u} + W_0q + Q_0w - V_0r - R_0v + g\cos\Theta_0\theta\right] \\
\Delta F_Y &= m_0\left[\dot{v} + U_0r + R_0u - W_0p - P_0w - \left(g\cos\Theta_0\cos\Phi_0\right)\phi + \left(g\sin\Theta_0\sin\Phi_0\right)\theta\right] \\
\Delta F_Z &= m_0\left[\dot{w} + V_0P + P_0v - U_0q - Q_0u + \left(g\cos\Theta_0\sin\Phi_0\right)\phi + \left(g\sin\Theta_0\cos\Phi_0\right)\theta\right] \\
\Delta \boldsymbol{L} &= I_{xx}\dot{p} - I_{xz}\dot{r} + \left(I_{zz} - I_{yy}\right)\left(Q_0r + R_0q\right) - I_{xz}\left(P_0q + Q_0p\right) \\
\Delta \boldsymbol{M} &= I_{yy}\dot{q} + \left(I_{xx} - I_{zz}\right)\left(P_0r + R_0p\right) - \left(2R_0r - 2P_0p\right)I_{xz} \\
\Delta \boldsymbol{N} &= I_{zz}\dot{r} - I_{xz}\dot{p} + \left(I_{yy} - I_{xx}\right)\left(P_0q + Q_0p\right) + I_{xz}(Q_0r + R_0q)
\end{aligned}
\tag{1.7}
$$

where each variable X is written $X_0 + x$; X_0 is the value of the variable X at the equilibrium.

Using certain assumptions, [Mcl90], on the motion of the aircraft, a simplified representation of the perturbed coordinates can be given as:

$$
\begin{aligned}
\Delta F_X &= m_0\left[\dot{u} + W_0q + g\cos\Theta_0\theta\right] \\
\Delta F_Y &= m_0\left[\dot{v} + U_0r - W_0p + g\cos\Theta_0\phi\right] \\
\Delta F_Z &= m_0\left[\dot{w} - U_0q + q\sin\Theta_0\theta\right]
\end{aligned}
\tag{1.8}
$$

$$
\begin{aligned}
\Delta \boldsymbol{L} &= I_{xx}\dot{p} - I_{xz}\dot{r} \\
\Delta \boldsymbol{M} &= I_{yy}\dot{q} \\
\Delta \boldsymbol{N} &= I_{zz}\dot{r} - I_{xz}\dot{p}
\end{aligned}
\tag{1.9}
$$

and the coordinates of angular velocity ω of the aircraft, which represent the rotation of the aircraft axes to the earth axes, are given as:

$$\begin{aligned} p &= \dot{\phi} - \dot{\psi}\sin\Theta_0 \\ q &= \dot{\theta} \\ r &= \dot{\psi}\cos\Theta_0 \end{aligned} \tag{1.10}$$

1.2.2 Longitudinal motion

Throughout this thesis, we consider the longitudinal motion of different types of aircraft. Thus we give more details on the longitudinal motion, rather than the lateral motion of the aircraft. Under equilibrium operating conditions, the longitudinal and lateral equations of motion could be separated as given in the following:

$$\begin{cases} \Delta F_x = x = m_0\left[\dot{u} + W_0 q - g\cos\Theta_0\theta\right] \\ \Delta F_z = z = m_0\left[\dot{w} - U_0 q + g\sin\Theta_0\theta\right] \\ \Delta M = m = I_{yy}\dot{q} \end{cases} \tag{1.11}$$

where: x, z, m are the variations of displacement on X_B axe, of displacement on Z_B axe and of pitching moment, respectively.

$$\begin{cases} y = m_0\left[\dot{v} + U_0 r - W_0 P - g\cos\Theta_0\phi\right] \\ l = I_{xx}p - I_{xz}\dot{r} \\ n = I_{zz}\dot{r} - I_{xz}\dot{p} \end{cases} \tag{1.12}$$

where: y, l, n are the variations of displacement on Y_B axe, of rolling moment and of yawing moment, respectively.

In the following, the only actuator considered for the longitudinal motion is the elevator. Developing in Taylor series the coordinates of the forces acting on the aircraft in (1.7), we obtain the following equations:

$$
\begin{aligned}
&\frac{\partial F_X}{\partial u}u+\frac{\partial F_X}{\partial \dot{u}}\dot{u}+\frac{\partial F_X}{\partial w}w+\frac{\partial F_X}{\partial \dot{w}}\dot{w}+\frac{\partial F_X}{\partial q}q+\frac{\partial F_X}{\partial \dot{q}}\dot{q}+\frac{\partial F_X}{\partial \delta_E}\delta_E\\
&+\frac{\partial F_X}{\partial \dot{\delta}_E}\dot{\delta}_E=m_0[\dot{u}+W_0q+g\cos\Theta_0\theta]\\
&\frac{\partial F_Z}{\partial u}u+\frac{\partial F_Z}{\partial \dot{u}}\dot{u}+\frac{\partial F_Z}{\partial w}w+\frac{\partial F_Z}{\partial \dot{w}}\dot{w}+\frac{\partial F_Z}{\partial q}q+\frac{\partial F_Z}{\partial \dot{q}}\dot{q}+\frac{\partial F_Z}{\partial \delta_E}\delta_E\\
&+\frac{\partial F_Z}{\partial \dot{\delta}_E}\dot{\delta}_E=m_0\left[\dot{w}-U_0q+g\sin\Theta_0\theta\right]\\
&\frac{\partial M}{\partial u}u+\frac{\partial M}{\partial \dot{u}}\dot{u}+\frac{\partial M}{\partial w}w+\frac{\partial M}{\partial \dot{w}}\dot{w}+\frac{\partial M}{\partial q}q+\frac{\partial M}{\partial \dot{q}}\dot{q}+\frac{\partial M}{\partial \delta_E}\delta_E\\
&+\frac{\partial M}{\partial \dot{\delta}_E}\dot{\delta}_E=I_{yy}\dot{q}
\end{aligned}
\tag{1.13}
$$

Note that if we considered other command surfaces such as the horizontal canard δ_{hc}, then terms such as $\frac{\partial \vartheta}{\partial \delta_E}\delta_E+\frac{\partial \vartheta}{\partial \dot{\delta}_E}\dot{\delta}_E$ could be added for each Taylor series developed for variables: $\vartheta=F_x,F_z$ or M.

Using the standard notations in aeronautics:

$$
\begin{aligned}
X_x&=\frac{1}{m_0}\frac{\partial F_X}{\partial x}\\
Z_x&=\frac{1}{m_0}\frac{\partial F_Z}{\partial x}\\
M_x&=\frac{1}{I_{yy}}\frac{\partial M_X}{\partial x}
\end{aligned}
\tag{1.14}
$$

where X_x,Z_x,M_x are called stability derivatives, the longitudinal equations of motion are given as:

$$
\begin{aligned}
\dot{u}&=X_uu+X_{\dot{u}}\dot{u}+X_ww+X_{\dot{w}}\dot{w}+X_qq+X_{\dot{q}}\dot{q}+W_0q\\
&\quad -g\cos\Theta_0\theta+X_{\delta_E}\delta_E+X_{\dot{\delta}_E}\dot{\delta}_E\\
\dot{w}&=Z_uu+Z_{\dot{u}}\dot{u}+Z_ww+Z_{\dot{w}}\dot{w}+Z_qq+Z_{\dot{q}}\dot{q}+U_0q\\
&\quad -g\sin\Theta_0\theta+Z_{\delta_E}\delta_E+Z_{\dot{\delta}_E}\dot{\delta}_E\\
\dot{q}&=M_uu+M_{\dot{u}}\dot{u}+M_ww+M_{\dot{w}}\dot{w}+M_qq+M_{\dot{q}}\dot{q}\\
&\quad +M_{\delta_E}\delta_E+M_{\dot{\delta}_E}\dot{\delta}_E\\
\dot{\theta}&=q
\end{aligned}
\tag{1.15}
$$

The stability derivatives mentioned above depend on the type of aircraft and the operating point in the flight envelope. They are generally estimated offline by wind tunnel tests.

If certain stability derivatives are neglected [Mcl90], the longitudinal equations of motion can be simplified to:

$$\begin{aligned}
\dot{u} &= X_u u + X_w w + W_0 q - g\cos\Theta_0\theta \\
\dot{w} &= Z_u u + Z_w w + U_0 q - g\sin\Theta_0\theta + Z_{\delta_E}\delta_E \\
\dot{q} &= M_u u + M_w w + M_{\dot{w}}\dot{w} + M_q q + M_{\delta_E}\delta_E \\
\dot{\theta} &= q
\end{aligned} \tag{1.16}$$

These equations are more suitably written, for control system objectives, in a state-space representation $G(s) = \left[\begin{array}{c|c} A & B \\ \hline C & D \end{array}\right] := C(sI - A)^{-1}B + D$. By choosing the state variables vector as: $x = [u \quad w \quad q \quad \theta]^T$ and the actuator vector as δ_E, we get the matrices

$$A = \begin{bmatrix} X_u & X_w & W_0 & -g\cos\Theta_0 \\ Z_u & Z_w & U_0 & -g\sin\Theta_0 \\ \bar{M}_u & \bar{M}_w & \bar{M}_q & \bar{M}_\theta \\ 0 & 0 & 1 & 0 \end{bmatrix} \tag{1.17}$$

and

$$B = \begin{bmatrix} X_{\delta_E} \\ Z_{\delta_E} \\ \bar{M}_{\delta_E} \\ 0 \end{bmatrix} \tag{1.18}$$

where:

$\bar{M}_u = (M_u + M_{\dot{w}} Z_u)$
$\bar{M}_w = (M_w + M_{\dot{w}} Z_w)$
$\bar{M}_q = (M_q + U_0 M_{\dot{w}})$
$\bar{M}_0 = (-g M_w \sin\gamma_0)$
$\bar{M}_{\delta_E} = (M_{\delta_E} + M_{\dot{w}} Z_{\delta_E})$

If a short-period approximation is desired, which means neglecting the variations of speed due to deflections of control surfaces, then $u = 0$; thus the state variables for the longitudinal motion are reduced to $x = \begin{bmatrix} w \\ q \end{bmatrix}$ and

$$A=\begin{bmatrix} Z_w & U_0 \\ (M_w+M_{\dot{w}}Z_w) & (M_q+U_0M_{\dot{w}}) \end{bmatrix} \tag{1.19}$$

$$B=\begin{bmatrix} Z_{\delta_E} \\ (M_{\delta_E}+Z_{\delta_E}M_{\dot{w}}) \end{bmatrix} \tag{1.20}.$$

1.2.3 Background on flexible structures

Using the Hamilton principle for undamped systems

$$\int_{t_1}^{t_2}\delta(\mathcal{T}-\mathcal{U})dt=\int_{t_1}^{t_2}\delta\tau dt \tag{1.21}$$

where τ is the effort of the non-conservative forces, $\mathcal{T}$ is the kinetic energy and $\mathcal{U}$ is the deformation energy. If we discretize the structure studied into a finite number of elements represented by n nodes located on the contour of the structure, then an approximation of the displacements of the structure is given as:

$$u_j(x,y,z,t)=\sum_{i=1}^{n}\eta_i(x,y,z)q_i(t) \tag{1.22}$$

where:

$q_i(t)$ are generalized coordinates,

$\eta_i(x,y,z,t)$ are the basis functions of the approximation.

Reformulating the Hamilton principle by taking into account Equation (1.22) leads to the Lagrange equations as:

$$\frac{\partial}{\partial t}\left(\frac{\partial \mathcal{T}}{\partial \dot{q}_i}\right)-\frac{\partial \mathcal{T}}{\partial q_i}+\frac{\partial \mathcal{U}}{\partial q_i}=F_i \tag{1.23}$$

where F_i is generalized force corresponding to the generalized coordinates q_i and given as: $\delta\tau=F_i\delta q_i$.

For small displacements of the elastic systems, an approximation of the kinetic energy and the deformation energy is given as:

$$\mathcal{T}=1/2\sum_{i=1}^{n}\sum_{j=1}^{n}\dot{q}_i^TM_{ij}\dot{q}_i=1/2\,\dot{q}^TM\dot{q} \tag{1.24}$$

$$\mathcal{U}=1/2\sum_{i=1}^{n}\sum_{j=1}^{n}q_i^TK_{ij}q_i=1/2\,q^TKq \tag{1.25}$$

then the Lagrange equation in (1.23) is rewritten as:

$$M\ddot{q}(t) + Kq(t) = F(t) \tag{1.26}$$

For damped systems, we need to add a term to model the force of viscosity dissipation. Thus the global flexible structure model is given as:

$$M\ddot{q}(t) + C\dot{q}(t) + Kq(t) = F(t) \tag{1.27}$$

where: M: is the semi-definite mass matrix.

C : viscosity-damping matrix.

K: positive stiffness matrix.

F: generalized forces.

1.2.4 Flexible aircraft model

In this thesis, we are interested in models of aircraft that include structural flexibility. These models are more realistic and have the potential to yield more reliable controller designs than rigid-body models neglecting the flexibility aspect of the aircraft. In the following, we show how, starting from rigid-body dynamics, aeroelastic effect can be included in the state-space representation of the flexible aircraft model. As explained above for general flexible structures, and assuming small aircraft structure displacements, each flexible damped mode i can be represented by generalized coordinates

$$q_i: \; A_i\ddot{q}_i + B_i\dot{q}_i + C_i q_i = Q_i . \tag{1.28}$$

where A_i, B_i, C_i are the coefficients of the generalized coordinate q_i and Q_i represents a generalized aerodynamic force. Each differential equation in (1.28) representing the *ith* flexible mode can be included in the global state space representation of the flexible aircraft. This can be done by adding, for each flexible mode taken into account, two states

$$\begin{bmatrix} \dot{x}_{i1} \\ \dot{x}_{i2} \end{bmatrix} = \begin{bmatrix} 0 & 1 \\ -C_i/A_i & -B_i/A_i \end{bmatrix} \begin{bmatrix} \dot{x}_{i1} \\ \dot{x}_{i2} \end{bmatrix} + \begin{bmatrix} 0 \\ 1/A_i \end{bmatrix} Q_i \tag{1.29}$$

In general the state-space matrix A of flexible aircraft model can be partitioned as:

$A = \begin{bmatrix} A_{rr} & A_{re} \\ A_{er} & A_{ee} \end{bmatrix}$ where A_{rr}, A_{ee} are the state matrices of the rigid-body part and the elastic part of the aircraft. A_{re}, A_{er} are the coupling matrices of the rigid part to the flexible part and of the flexible part to the rigid part. The coupling terms can be estimated from wind tunnel tests.

To be more generic in our modeling of the aircraft, we do not specify the output equations of the models. This depends on the type of aircraft and the performance objectives. The vector of outputs can include acceleration measurements with different position accelerometer on the aircraft. Also roll, pitch and yaw angles can be measured using gyros. For instance, some of the outputs variables do not necessarily have to be sensed. They may be aircraft or engine variables that need to be simulated or controlled indirectly.

1.3 Gust load alleviation problem

Problems caused by gusts acting on aircraft started to be studied in the early fifties and research programs were elaborated to overcome those problems. In 1949 a program, concerning the aircraft Bristol Barbazon, was proposed to develop a system that would alleviate loads due to turbulence and flight maneuvers. The objective of this program was to reduce wing deflection due to turbulence, and execute the required flight maneuvers. This program resulted in a prototype but was never flight-tested, as opposed to other programs developed between 1955 and 1960 in England for the Avro Lancaster aircraft. All of these early systems had difficulty reacting fast enough to counteract the turbulence effects on the aircraft. These deficiencies have been noted by Attwood, Canon, Johnson and Andrew [Att61], who applied for a patent, which was awarded in 1961. This work proposed to measure the normal and angular acceleration of the aircraft and use its auxiliary control surfaces to produce the necessary forces and moments to minimize the undesirable accelerations caused by wind gusts.

In 1964, damages to a military B52 aircraft caused by severe turbulence, of 35m/s maximal velocity, accelerated the development of a research program including extensive flight testing called Load Alleviation and Mode Suppression (LAMS) in 1965. Results of this program were presented in [Bur68] and continued until 1973. Other programs focused on gust alleviation objectives have been described in [Sto73].

Starting from the early seventies, the use of control surfaces became widespread for the gust alleviation problem. The incorporation of classical control design techniques for this problem was obvious. Research works as in [Mcl78], [Krag79], [Abel82], [Van86], [Mats88], treated some aspects of gust alleviation problem using classical control techniques. In [Osb94] [Muk92], [Ban92] modern robust control methods started to be applied to aerospace problems, especially for rigid aircraft, where unmodelled perturbation effects have been studied. One objective of this thesis is to adapt modern robust control techniques to flexible aircraft subjected to wind gusts.

1.3.1 Turbulence modeling

Atmospheric perturbations may have a considerable effect on the performance of an aircraft. They may cause premature airframe fatigue and reduce passenger comfort. As mentioned above, one of the objectives of active control surfaces is the suppression of undesirable effects of turbulence on the movement of the aircraft.

Turbulence can be defined as a series of discrete gusts acting on the aircraft at different times. Two functions modeling gusts are generally used in the literature: the first one consists in $w_g(t) = \frac{k}{T}\left[1 - \cos(2\pi/T)t\right]$ where: $T = L/U_0$ is the period of the gust, U_0 is the velocity of the aircraft at the equilibrium point and L is the wavelength. The second function modeling the gust is the delta gust and mathematically is given as:

$$w_g(t) = \begin{cases} A\frac{t}{t_1} \text{ for } 0 \le t \le t_1 \\ -A\frac{t}{t_1} + 2A \text{ for } t_1 < t \le t_2 \\ 0 \text{ elsewhere} \end{cases}$$ where A is the maximum of gust magnitude.

A turbulence acting on the aircraft is a random phenomenon, which can be defined by its root mean square value (rms) and its gaussian amplitude distribution. As shown in the literature [Hob88], this phenomenon can be generated by a superposition of infinite sinusoidal components as:

$$y(t) = \sum_{i=1}^{\infty} \sqrt{\phi(\omega_i)\Delta\omega}.\cos(\omega_i t + \psi_i) \tag{1.30}$$

where: $\sqrt{\phi(\omega_i)\Delta\omega}$, ψ_i represent the magnitude and the phase, respectively; $\omega_i, \phi(\omega_i)$ are the frequency and the total average power of sinusoid of frequency ω_i, respectively.

Defining $y_T(t) = \begin{cases} y(t) \text{ for } -T \le t \le T \\ 0 \text{ elsewhere} \end{cases}$ and assuming the existence of the Fourier transform of $y_T(t)$ as:

$F(\omega) = \int_{-\infty}^{\infty} y_T(t) e^{-j\omega t} dt$, the power spectral density (PSD) of the function $y(t)$ is given as:

$$\phi(\omega) = \lim_{T\to\infty} \frac{1}{2\pi T} |F(\omega)|^2 = \lim_{T\to\infty} \frac{1}{2\pi T} F(\omega)F(-\omega) = \lim_{T\to\infty} \frac{1}{2\pi T} \int_{-\infty}^{+\infty} \int_{-\infty}^{\infty} y_T(t) y_T(\varepsilon) e^{j\omega t} e^{-j\omega\varepsilon} d\varepsilon dt \quad (1.31)$$

assuming $\varepsilon = t + \tau$ then

$$\phi(\omega) = \frac{1}{\pi} \int_{-\infty}^{\infty} [\lim_{T\to\infty} \frac{1}{2T} \int_{-\infty}^{\infty} y_T(t) y_T(t+\tau) dt] e^{-j\omega\tau} d\tau = \frac{1}{\pi} \int_{-\infty}^{\infty} R(\tau) e^{-j\omega\tau} d\tau \quad (1.32)$$

where: $\phi(\omega), R(\tau)$ are the real, even, positive PSD function and the autocorrelation function defined as: $R(\tau) := \lim_{T\to\infty} \frac{1}{2T} \int_{-T}^{T} y(t) y(t+\tau) dt = \overline{y(t).y(t+\tau)}$, respectively.

The autocorrelation function $R(\tau)$ is connected to the PSD function, through the Fourier transform, as follows:

$$R(\tau) = \int_{0}^{+\infty} \phi(\omega) \cos(\omega\tau) d\omega \quad (1.33)$$

This implies that σ (the rms), which represents the intensity of the turbulence, is calculated as: $R(0) = \overline{y^2(t)} = \sigma^2 = \int_0^{\infty} \phi(\omega) d\omega \Rightarrow \sigma = \sqrt{\int_0^{\infty} \phi(\omega) d\omega}$.

Analytic, continuous forms of the PSD of the turbulence acting on the aircraft are available in the literature [Mcl90]. The most known forms are the Von Karman model [Von37] and Dryden model. These are given in Table1.1:

Table 1.1: Gust models

Von Karman models	$\phi_i(\Omega) = \frac{\sigma_i L_i \left[1 + \frac{8}{3}(1{,}339 L_i \Omega)^2\right]}{\pi \left[1 + (1{,}339 L_i \Omega)^2\right]^{11/6}} \quad i = w, v$	$\phi_u(\Omega) = \frac{2\sigma_u{}^2 L_u}{\pi \left[1 + (1{,}339 L_u \Omega)^2\right]^{5/6}}$
Dryden models	$\phi_i(\Omega) = \frac{\sigma_i{}^2 L_i \left[1 + 3(L_i \Omega)^2\right]}{\pi \left[1 + (L_i \Omega)^2\right]^2} \quad i = w, v$	$\phi_u(\Omega) = \frac{2\sigma_u{}^2 L_u}{\pi \left[1 + (L_u \Omega)^2\right]^2}$

where $\Omega = \omega / U_0$, which implies that $\phi(\omega) = \phi(U_0\Omega)$. The indices $i = w, v$ is for the vertical and transversal gusts, respectively. Subscript u is for the longitudinal gusts.

1.3.2 Gust loads on aircraft

On Figure 1.2, we represent the most influent forces acting on an aircraft along its flight.

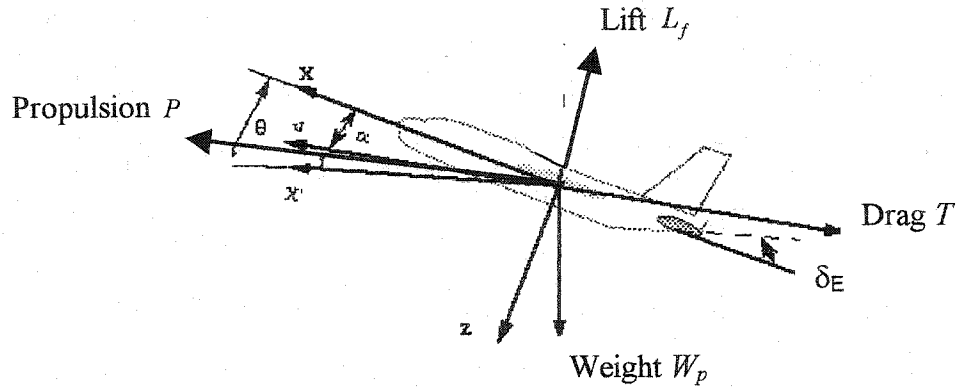

Figure 1.2 Aircraft subject to forces

where: θ is the pitch angle and α is the angle of attack.

Mainly, L_f, called the lift force, is the vertical component of the aerodynamic force that opposes the weight force W to allow the aircraft to fly. The "drag" force, T, has an opposite direction to the velocity of the aircraft and opposes the propulsion force P. Note that for horizontal flight $L_f = W$ and $P=T$.

Assuming that the trim velocity of a flying aircraft is U_0, then wind gusts acting on the aircraft results in a change in the angle of attack α by $\Delta\alpha$. In Figure 1.3 we show how a vertical gust affects the angle of attack of the aircraft.

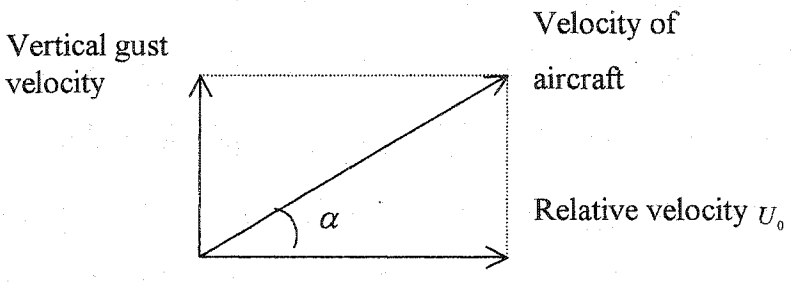

Figure 1.3: Turbulence effect on aircraft velocity

This change in the angle of attack and thus the velocity of the aircraft has a direct effect on the lift force L. This effect has been studied in [Hob88], where it is quantified as:

$$\Delta L_{gust} = \frac{\rho}{2} U_0^2 S C_{L_\alpha} \Delta\alpha \tag{1.34}$$

where:

ρ: air density,

S: wing surface,

$C_{l\alpha}$: tangent of L_{gust} on α axis,

w_g: velocity of the vertical gust,

$\Delta\alpha = w_g/U_0$.

In practice, the effect of the gust on the aircraft is measured by a factor of gut load given as:

$$\Delta n = \frac{\Delta L_g}{W} = \frac{\left[\frac{\rho}{2} w_g U_0 S C_{L_\alpha}\right]}{W} \tag{1.35}$$

At this stage, we have a specific description of the turbulence, its statistical characteristics and how it affects the aircraft. In the next chapter, we will present a real application of turbulence modeling, starting from a white noise perturbation, in a system ready for use in a feedback control design.

Chapter2

Robust control techniques with application to gust load alleviation of flexible aircraft

2.1 Introduction

The aim of this chapter is to introduce the reader to some optimal and robust design techniques that will be used along this thesis. These days, a modern multivariable feedback control strategy is needed, especially for aerospace applications where the complexity of the models and performance objectives need efficient control algorithms meeting realistic constraints. General control objective concerns a minimization of the effect of exogenous input signals (w) on some error signals (e). These signals (w) can include reference signals to be tracked and/or disturbances signals. The formulation of optimal control problems, in state-space representation, initially developed in [Doy89] spurred the adaptation of this optimal control theory to complex industrial problems [Skog96], and applications to aerospace vehicles [Vid95], [Nie96]. In fact, theories such as H_2, H_∞ and μ control received a great deal of interest since the 90`s, compared to the classical optimal LQR and LQG/LTR [Kal60], [Gup80] actively used in the 80`s. The optimization framework of these theories, based in general on a common setup, provides solutions in state space using efficient solutions to Riccati equations as well as linear matrix inequalities.

2.2 Problem setup

Consider the general block diagram of a unity feedback control system shown below.

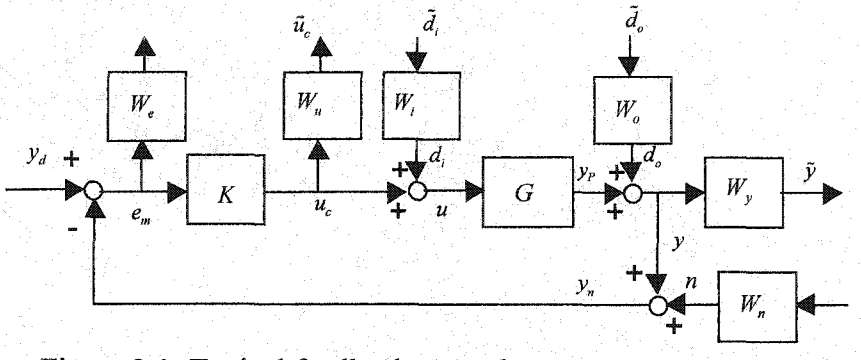

Figure 2.1: Typical feedback control system

The weighting functions W_x are added for different reasons (although they are rarely all present in a given design):

-To enforce closed-loop performance specifications (weighting functions on output signals and error signals).

- To represent the frequency contents of disturbances and noises

- To limit actuator responses to reasonable control effort.

The choice of the weighting functions W_d, W_e, W_y, W_u is not trivial. It varies from an application to the next, and from objective to objective. The weighting functions essentially have to take into account the closed-loop performance objectives with realistic constraints imposed on the system.

For simplicity, we assume that $\tilde{d}_i = 0, \tilde{n} = 0$, and we consider the regulator problem where the effect of the output disturbance $\tilde{d}_o$ on the weighted output $\tilde{y}$ must be minimized. This system can be recast as a linear fractional transformation (LFT) as shown below in figures 2.2 and 2.3.

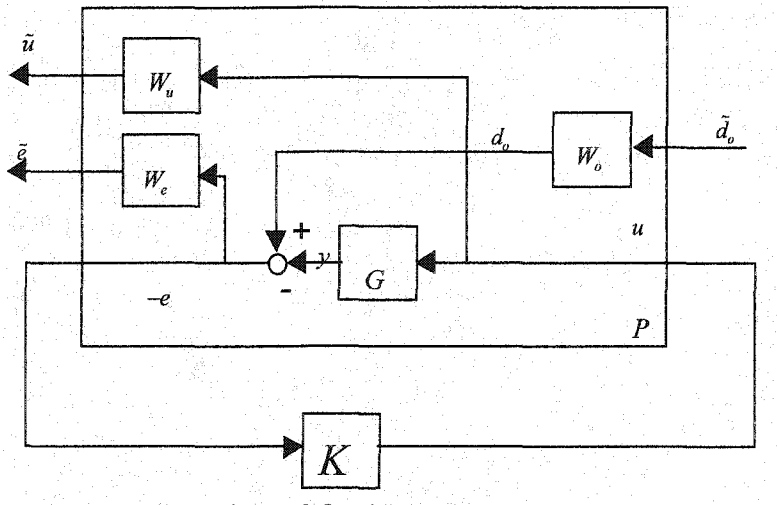

Figure 2.2: plant augmentation

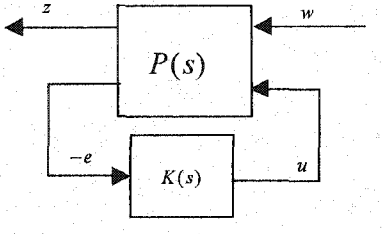

Figure 2.3: equivalent setup

where $P(s) := \begin{bmatrix} P_{11}(s) & P_{12}(s) \\ P_{21}(s) & P_{22}(s) \end{bmatrix}$, and the transfer matrix entries of this generalized plant are readily obtained from the paths relating each input signal to each output signal. Here we have:

$$\begin{aligned} P_{11}(s) &= \begin{bmatrix} 0 \\ W_e W_o \end{bmatrix} \\ P_{12}(s) &= \begin{bmatrix} W_u \\ -W_e G \end{bmatrix} \\ P_{21}(s) &= W_o \\ P_{22}(s) &= -G \end{aligned} \tag{2.1}$$

The closed-loop transfer function from w to z, T_{zw}, is represented as an LFT given below:

$$T_{zw}(s) = F_L\left[P(s), K(s)\right] = P_{11}(s) + P_{12}(s)K(s)\left[I - P_{22}(s)K(s)\right]^{-1} P_{21}(s) \tag{2.2}$$

Depending on the application, the exogenous input w, in Figure2.3, can include references for tracking, and then the generalized plant P of the problem setup can be constructed in an analog manner.

2.3 Weighted H_2 optimal control

2.3.1 Motivations on weighted H_2 design

The performance criterion used in this control design theory is defined over the space RH_2, which consists in the real-rational, strictly proper transfer matrix functions that have all their poles in $\mathbb{C}^-$, the open left-half of the complex plane. The inner product in this space is:

$$\langle F, G \rangle_2 = \frac{1}{2\pi} \int_{-\infty}^{+\infty} Tr\left\{F^*(j\omega)G(j\omega)\right\} d\omega \tag{2.3}$$

for two elements F and $G \in RH_2$, and where $Tr\{.\}$ denotes the trace of the matrix .

The objective of the H_2 control design, given an augmented plant P as in Figure 2.3, is to find a state-space controller K, which internally stabilizes P and minimizes $\left\|F_L\left[P(s), K(s)\right]\right\|_2$ defined in (2.4).

Let us , before going into the synthesis procedure, give basic information on the H_2 norm. If $P \in RH_2$ with a state space realization:

$P = \left[\begin{array}{c|c} A & B \\ \hline C & 0 \end{array}\right]$ where A is Hurwitz. Then the H_2 norm of P is defined as:

$$\|P\|_2^2 := \langle P, P \rangle_2 = \frac{1}{2\pi} \int_{-\infty}^{+\infty} Tr\left\{P^*(j\omega)P(j\omega)\right\} d\omega = \int_{-\infty}^{+\infty} |P(t)|^2 \, dt = \int_{-\infty}^{+\infty} Tr\left\{B^* e^{A^* t} C^* C e^{At} B\right\} dt = Tr(B^* Y_0 B) \tag{2.4}$$

where Y_0 denotes the observability grammian. Similary, we show that $\|P\|_2^2 = Tr(CX_0C^*)$ where X_0 is the controllability grammian of the state-space realization.

The requirement to minimize the H_2 norm of the map from w to z in the synthesis of the stabilizing controller K has a significant meaning on performance objectives. In fact, If we consider w as a stationary random process, the signal variance is given by:

$$Var|w(t)|^2 = Tr\left\{R_w(0)\right\} = \frac{1}{2\pi} \int_{-\infty}^{+\infty} Tr\left\{S_w(\omega)\right\} d\omega \tag{2.5}$$

where R_w and S_w represent respectively, the autocorrelation matrix an its Fourier transform, for the signal w. If $z = Pw$ then $S_z(\omega) = P(j\omega)S_w(j\omega)P(j\omega)^*$ and then

$$Var|z(t)|^2 = \frac{1}{2\pi} \int_{-\infty}^{+\infty} Tr\left\{P(j\omega)S_w(j\omega)P^*(j\omega)\right\} d\omega = \int_{-\infty}^{+\infty} Tr\left\{P^*(j\omega)P(j\omega)S_w(j\omega)\right\} d\omega \tag{2.6}$$

If the signal w is just a unit intensity white noise, then $S_w(j\omega) = I$, which results in $Var|z(t)|^2 = \|P\|_2^2$. Thus the H_2 norm can be interpreted as the output variance for a white noise input.

In the case where the spectrum of the input signal is known, another interpretation of the H_2 norm can be given. Let us consider the case where $w(t)$ is scalar-valued, given as a delta Dirac function $w(t) = \delta(t)$, then:

$$\|z\|_2^2 = \int_{-\infty}^{+\infty} z^*(t)z(t)dt = \frac{1}{2\pi}\int_{-\infty}^{+\infty} z^*(j\omega)z(j\omega)d\omega = \frac{1}{2\pi}\int_{-\infty}^{+\infty} P^*(j\omega)P(j\omega)d\omega = \|P\|_2^2 \qquad (2.7)$$

This means that when the system input is scalar-valued, the H_2 norm of P gives us a direct measure of the system output energy.

Now that we have shown the importance of performance measure delivered by the H_2 norm of a mapping of input, output signals of a closed loop system, we give, in the following, the steps needed for an H_2 control synthesis:

2.3.2 Background on algebraic Riccati equations

Let A, Q, R be real $n \times n$ matrices with Q, R symmetric. Then an algebraic Riccati equation (ARE) is the following matrix equation:

$$A^*X + XA + XRX + Q = 0 \qquad (2.8)$$

Associated with this ARE is the $2n \times 2n$ Hamiltonian matrix:

$$H := \begin{bmatrix} A & R \\ -Q & -A^* \end{bmatrix} \qquad (2.9)$$

This matrix will be used to solve the ARE for the matrix X. A direct relation between this Hamiltonian matrix and the ARE is the following reformulation of the ARE as:

$$\begin{bmatrix} X & -I \end{bmatrix} H \begin{bmatrix} I \\ X \end{bmatrix} = \begin{bmatrix} X & -I \end{bmatrix} \begin{bmatrix} A & R \\ -Q & -A^* \end{bmatrix} \begin{bmatrix} I \\ X \end{bmatrix} = 0. \qquad (2.10)$$

The Ric function is now defined. Assume that Hamiltonian matrix H has no eigenvalue on the imaginary axis. Then, H has n eigenvalues in the open right half-plane and n eigenvalues in the open left half-plane. Consider the n-dimensional invariant spectral subspace $\mathcal{X}_-(H)$ corresponding to the n eigenvalues of H in the open left half-plane. By finding a basis for $\mathcal{X}_-(H)$, we get:

$$\mathcal{X}_{-}(H) = Ra\left\{\begin{bmatrix} X_1 \\ X_2 \end{bmatrix}\right\}, \quad X_1, X_2 \in \mathbb{C}^{n\times n} \tag{2.11}$$

If X_1 is nonsingular, then we can define $X := X_2 X_1^{-1}$ and the Hamiltonian matrix H uniquely defines X. Thus the function $H \mapsto X$ is called Ric and defined explicitly on:

$$\text{Ric: dom}\{\text{Ric}\} \subset \mathbb{R}^{2n\times 2n} \to \mathbb{R}^{n\times n} \tag{2.12}$$

where $\text{dom}\{\text{Ric}\}$ is taken to be Hamiltonian matrices that have no eigenvalues on the imaginary axis, and have a nonsingular X_1.

The following result states that $X := X_2 X_1^{-1}$ is a solution to the algebraic Riccati equation:

Theorem 2.1 [Kuc72]

Suppose that $H \in \text{dom}\{\text{Ric}\}$, and X=Ric(H). Then:

(i) X is real symmetric,

(ii) X satisfies the ARE,

(iii) $A + RX$ is stable (all of its eigenvalues are in the open LHP).

2.3.3 H_2 synthesis

Suppose that a state-space realization of $P(s)$ is given by

$$P(s) = \left[\begin{array}{c|cc} A & B_1 & B_2 \\ \hline C_1 & 0 & D_{12} \\ C_2 & D_{21} & 0 \end{array}\right] \tag{2.13}$$

Notice the special off-diagonal structure of D: D_{22} is assumed to be 0 so that $P_{22}(s)$ is strictly proper, and D_{11} is assumed to be 0 so that $P_{11}(s)$ is also strictly proper (which is a necessary condition for $P_{11}(s)$ to be in H_2.). This off-diagonal structure allows us to give details on the synthesis procedure with the maximum of simplifications. Details on how to construct a H_2 controller with the general structure (D_{11} and $D_{22} \neq 0$) are given in [Gre95]. Further assume that D_{12} has full column rank and D_{21} has full row rank.

First define $R_1 = D_{12}^* D_{12}$ and $R_2 = D_{21} D_{21}^*$, and the two Hamiltonian matrices:

$$H_2 := \begin{bmatrix} A - B_2 R_1^{-1} D_{12}^* C_1 & -B_2 R_1^{-1} B_2^* \\ -C_1^* \left(I - D_{12} R_1^{-1} D_{12}^* \right) C_1 & -\left(A - B_2 R_1^{-1} D_{12}^* C_1 \right)^* \end{bmatrix} \tag{2.14}$$

$$J_2 := \begin{bmatrix} \left(A - B_1 D_{21}^* R_2^{-1} C_2 \right)^* & -C_2^* R_2^{-1} C_2 \\ -B_1 \left(I - D_{21}^* R_2^{-1} D_{21} \right) B_1^* & -\left(A - B_1 D_{21}^* R_2^{-1} C_2 \right) \end{bmatrix} \tag{2.15}$$

Note that $H_2, J_2 \in \text{dom(Ric)}$ and $X_2 := \text{Ric}(H_2) \geq 0$, $Y_2 := \text{Ric}(J_2) \geq 0$.

Theorem 2.2 [Doy89]:

If the following assumptions hold:

1.The pair (A, B_2) is stabilizable and the pair (A, C_2) is detectable (This assumption is necessary and sufficient for P to be internally stabilizable).

2. $R_1 = D_{12}^* D_{12} > 0$ and $R_2 = D_{21} D_{21}^* > 0$

3. $\begin{bmatrix} A - j\omega I & B_2 \\ C_1 & D_{12} \end{bmatrix}$ has full column rank for all ω

4. $\begin{bmatrix} A - j\omega I & B_1 \\ C_2 & D_{21} \end{bmatrix}$ has full row rank for all ω

Then, the unique H_2-optimal output controller minimizing $\left\| F_L \left[P(s), K(s) \right] \right\|_2$ is given by

$$K_{opt}(s) = \left[\begin{array}{c|c} \hat{A}_2 & -L_2 \\ \hline F_2 & 0 \end{array} \right] \tag{2.16}$$

where :

$$L_2 := -\left(Y_2 C_2^* + B_1 D_{21}^* \right) R_2^{-1}, \tag{2.17}$$

$$F_2 := -R_1^{-1}\left(B_2^* X_2 + D_{12}^* C_1\right), \tag{2.18}$$

$$\hat{A}_2 := A + B_2 F_2 + L_2 C_2 . \tag{2.19}$$

Remark: Assumptions 3 and 4 ensure that $H_2, J_2 \in \text{dom(Ric)}$

2.3.4 H_2 State feedback via LMIs

In the following, we treat the special case of state feedback controller design with an efficient solution method, which consists in the solution of a system of linear matrix inequalities. The availability of the states as outputs of the aircraft model will certainly simplify the design and permit the use of efficient tools of controller synthesis. This is not in general the case in reality, but it may be possible for certain models, as the ones we have in our applications.

The following proposition introduces a relation between the H_2 norm and the feasibility of special linear matrix inequalities.

Proposition 2.1

Suppose P is a system with state-space realization $(A,B,C,0)$. Then

$\|P\|_2 < 1$ and A is Hurwitz, iff

$\exists$ symmetric matrix $X > 0$ such that $Tr\{CXC^*\} < 1$ and $AX + XA^* + BB^* < 0$.

The augmented plant P in the case of state feedback synthesis has the following state space representation:

$$P(s) = \left[\begin{array}{c|cc} A & B_1 & B_2 \\ \hline C_1 & 0 & D_{12} \\ I & 0 & 0 \end{array}\right] \tag{2.20}$$

and the controller in this case is just a static feedback gain $K(s) = K$.

Theorem 2.3

$\exists K(s) = K$ that internally stabilizes P and satisfies $\left\| F_L\left[P(s), K(s)\right]\right\|_2 < 1$ if and only if

there exist a matrix Y such that : $K = YX^{-1}$ where $X > 0$ is symmetric and satisfies :

$$\begin{bmatrix} A & B_2 \end{bmatrix}\begin{bmatrix} X \\ Y \end{bmatrix} + \begin{bmatrix} X & Y^* \end{bmatrix}\begin{bmatrix} A^* \\ B_2^* \end{bmatrix} + B_1 B_1^* < 0 \text{ and } Tr\left\{C_1 X C_1^*\right\} + 2Tr\left\{D_{12} Y C_1^*\right\} + Tr\left\{D_{12} Y X^{-1} Y^* D_{12}^*\right\} < 1$$

The above trace condition cannot be directly analyzed by means of LMI tools because of the nonlinear term existing in the third trace. Therefore, we have to introduce a new variable, which permit us to write this trace condition in the form of an LMI.

Using the following Schur complement operation result we can transform the above constraint into an LMI.

Proposition 2.3 (Schur-Complement result) [Horn85]

Suppose R is a complex matrix, and M and Q are symmetric complex matrices then:

$Q < 0$ and $M - RQ^{-1}R^* < 0$ are true is equivalent that $\begin{bmatrix} M & R \\ R^* & Q \end{bmatrix} < 0$ is satisfied.

Assuming the monotonicity of the trace under matrix inequalities:

$$Tr\left\{D_{12} Y X^{-1} Y^* D_{12}^*\right\} = \inf_Z Tr\left\{Z\right\} \tag{2.21}$$

where $D_{12} Y X^{-1} Y^* D_{12}^* < Z$.

Using the result of proposition 2.3, the above inequality can be written into the following LMI:

$\begin{bmatrix} Z & D_{12}Y \\ Y^* D_{12}^* & X \end{bmatrix} > 0$ which simplify the trace condition in the given theorem into the following LMI condition, easy to analyze:

$$TrC_1 X C_1^* + 2TrD_{12} Y C_1^* + TrZ < 1 \tag{2.22}$$

2.4 H_∞ Optimal control

Refering to Figure 2.3, the standard H_∞ optimal control problem is to find all stabilizing controllers K which minimize:

$$\left\| F_L\left[P(s), K(s)\right]\right\|_\infty = \sup_\omega \bar{\sigma}\left[F_L\left(P, K\right)(j\omega)\right] \tag{2.23}$$

where $\bar{\sigma}(.)$ denotes the maximum singular value of the matrix.

We note that using the H_∞ norm as a performance criterion introduces a more severe constraint compared to the H_2 norm. In fact, the H_2 norm specification expresses an average behavior of the linear closed-loop system. The optimization based on H_2 criterion corresponds to an optimization of the average behavior of a system's response to a white noise, i.e., it minimizes the total average energy of the frequency response. In contrast, the H_∞ criterion corresponds to the maximum gain of energy, and also to the worst case of an input signal producing an output signal of maximum amplitude. Minimization of the H_∞ norm ensures that for all possible sinusoidal input signals, the amplitude of the output signals will be less than or equal to the H_∞ norm times the amplitude of the input signal.

The H_∞ optimization consists then in minimizing the peak of the maximum singular value of the closed loop system $F_L\left[P(s), K(s)\right]\Big|_{s=j\omega}$. It can be also interpreted in the time domain as the induced 2-norm: If $z = F_L\left[P(s), K(s)\right]w$ then $\left\| F_L\left[P(s), K(s)\right]\right\|_\infty = \max_{w(t)\neq 0} \frac{\|z\|_2}{\|w\|_2}$ where $\|z\|_2 = \sqrt{\int_{-\infty}^{+\infty} \sum_i |z_i(t)|^2 \, dt}$ is the 2-norm of the vector signal.

The H_∞ minimization problem can be written as:

$$\min_{K \in S} \left\| F_L\left[P(s), K(s)\right]\right\|_\infty \tag{2.24}$$

where : S represents the set of all stabilizing controller K and $F_L\left[P(s), K(s)\right]$ is the closed-loop transfer matrix from the exogenous input w to the output z. The optimization of (2.24) is very difficult theoretically and numerically. Thus, for practical design, a solution to the suboptimal H_∞ problem stated as:

Let $\gamma_{\min}$ be the minimum value of $\|F_L[P(s),K(s)]\|_\infty$ over all stabilizing controllers. Then, given $\gamma > \gamma_{\min} > 0$, find all stabilizing controllers such that $\|F_L[P(s),K(s)]\|_\infty < \gamma$.

2.5 LMI approach to H_∞ control

The LMI solution for the H_∞ control problem avoids the restrictive assumptions that are usually needed in the classical solution initially presented in [Doy89]. The LMI approach is actually an efficient way to solve the sub-optimal H_∞ controller synthesis. In addition to the numerical efficiency of the LMI solvers, this approach of solving the H_∞ control problem gets rid of constraining assumptions that must be satisfied in the state space solution of [Doy89]. In the following we introduce a useful lemma for the solution of the H_∞ sub-optimal problem presented below:

Lemma 2.1 (Bounded real lemma revisited) [Gah93,Gah94a,Wan98]

If we consider the transfer function $P(s) = D + C(sI - A)^{-1}B$ then the following statements are equivalent:

- $P(s) \in RH_\infty$ and $\|P(s)\|_\infty < 1$.

- There exists $X = X^T > 0$ such that $\begin{bmatrix} A^TX + XA & XB & C^T \\ B^TX & -I & D^T \\ C & D & -I \end{bmatrix} < 0$.

Now if we consider a minimal realization of the plant $P(s) = \begin{bmatrix} D_{11} & D_{12} \\ D_{21} & 0 \end{bmatrix} + \begin{bmatrix} C_1 \\ C_2 \end{bmatrix} (sI - A)^{-1} \begin{bmatrix} B_1 & B_2 \end{bmatrix}$

where $A \in \Re^{n \times n}$, $D_{11} \in \Re^{p_1 \times m_1}$, $D_{22} \in \Re^{p_2 \times m_2}$

and we assume that:

- The pair (A, B_2) is stabilizable and the pair (A, C_2) is detectable

Given a proper controller K, the closed loop realization with this controller has the following state space representation: $F_L(P,K) := \left[\begin{array}{c|c} A_{cl} & B_{cl} \\ \hline C_{cl} & D_{cl} \end{array}\right]$ where :

$$A_{cl}=\begin{bmatrix} A+B_2D_KC_2 & B_2C_K \\ B_KC_2 & A_K \end{bmatrix};B_{cl}=\begin{bmatrix} B_1+B_2D_KD_{21} \\ B_KD_{21} \end{bmatrix};C_{cl}=\begin{bmatrix} C_1+D_{12}D_KC_2 & D_{12}C_K \end{bmatrix};$$
$$D_{cl}=D_{11}+D_{12}D_KD_{21}$$

By using the Bounded real lemma presented above, we can statute on the stability and the H_∞ norm constraint of the closed-loop system $\|F_L(P,K)\|_\infty < \gamma$. For this H_∞ norm constraint, the matrix inequality

$$\begin{bmatrix} A_{cl}{}^T X_{cl}+X_{cl}A_{cl} & X_{cl}B_{cl} & C_{cl}{}^T \\ B_{cl}{}^T X_{cl} & -\gamma I & D_{cl}{}^T \\ C_{cl} & D_{cl} & -\gamma I \end{bmatrix} < 0 \tag{2.25}$$

for some symmetric matrix $X_{cl} > 0$ of dimension $(n+k)\times(n+k)$ will be used. However, this inequality is not an LMI since the unknown variables are X_{cl}, A_{cl}, B_{cl}, C_{cl} and D_{cl}.

The following theorem provides a system of LMI's, whose solvability represents a sufficient and necessary condition for the existence of a stabilizing controller that verifies the H_∞ norm constraint.

Theorem 2.5 [Gah93a]

Assuming that

$$X_{cl}:=\begin{bmatrix} S & N \\ N^T & * \end{bmatrix};X_{cl}^{-1}:=\begin{bmatrix} R & M \\ M^T & * \end{bmatrix} \tag{2.26}$$

with $R,S\in\Re^{n\times n}$ and $M,N\in\Re^{n\times k}$. Consider the minimal realization of $P(s)$ given in (2.12), assume that the pair (A,B_2) is stabilizable and the pair (A,C_2) is detectable, and let $\mathbf{N}_{12}$ and $\mathbf{N}_{21}$ denote orthonormal bases of the null spaces of $\left(B_2^T, D_{12}^T\right)$ and $\left(C_2, D_{21}\right)$ respectively.

Then the suboptimal H_∞ problem of performance γ is solvable if and only if there exists two symmetric matrices $R,S\in\Re^{n\times n}$ satisfying the following system of LMIs:

$$\begin{bmatrix} \mathrm{N}_{12} & 0 \\ 0 & I \end{bmatrix}^T \begin{bmatrix} AR+RA^T & RC_1^T & B_1 \\ C_1R & -\gamma I & D_{11} \\ B_1^T & D_{11}^T & -\gamma I \end{bmatrix} \begin{bmatrix} \mathrm{N}_{12} & 0 \\ 0 & I \end{bmatrix} < 0 \tag{2.27}$$

$$\begin{bmatrix} \mathrm{N}_{21} & 0 \\ 0 & I \end{bmatrix}^T \begin{bmatrix} A^TS+SA & SB_1 & C_1^T \\ B_1^TS & -\gamma I & D_{11}^T \\ C_1 & D_{11} & -\gamma I \end{bmatrix} \begin{bmatrix} \mathrm{N}_{12} & 0 \\ 0 & I \end{bmatrix} < 0 \tag{2.28}$$

$$\begin{bmatrix} \mathrm{R} & I \\ I & S \end{bmatrix} \geq 0 \tag{2.29}$$

Moreover, there exist γ-suboptimal controllers of order $k < n$ iff the constraints (2.27-2.29) hold for some R, S that verify:

$$Rank(I - RS) \leq k \tag{2.30}$$

The optimization problem given by the LMI system (2.27-2.29) is convex and its feasibility results in pairs (R,S) that solve the γ-suboptimal $\mathcal{H}_\infty$ problem. Many efficient algorithms were developed, in [Gah94b], to solve the LMI feasibility problem . For a reduced order controller the matrix inequality (2.27) imposes a constraint that verifies the possibility of $\mathcal{H}_\infty$ stabilisable reduced controller [Gah93].

Let us define the convex set of feasible pairs (R,S) as $\mathfrak{M}_\gamma$. Any feasible pair (R,S) determines a set of γ-suboptimal controllers. Consider $k := Rank(I - RS)$ and compute the two full-column-rank matrices $M, N \in \Re^{n \times k}$ using the singular value decomposition (SVD) such that: $MN^T = I - RS$. These matrices uniquely define the matrix X_{cl} using (2.26). X_{cl} is the unique solution of the linear equation:

$$X_{cl} \begin{bmatrix} R & I \\ M^T & 0 \end{bmatrix} = \begin{bmatrix} I & S \\ 0 & N^T \end{bmatrix} \tag{2.31}$$

Once an $X_{cl} > 0$ is calculated,[Gah93], the matrix inequality in (2.25) becomes an LMI with respect to controller parameters A_K, B_K, C_K and D_K. Thus , we can associate to X_{cl} a convex set of γ-suboptimal controllers $\mathsf{K}(R,S,\gamma)$. This set is, in fact, the set of controllers $K(s) = D_K + C_K(sI - A_K)^{-1}B_K$ such that (2.25) holds for some X_{cl} compatible with (2.26).

The controllers $\mathsf{K}(R,S,\gamma)$ can be calculated by solving efficiently the LMI (2.27-2.29). For that, algorithms are available in the literature [Gah94b]. When no additional constraints on A_K, B_K, C_K and D_K are made, analytical solution can be found and explicit formulas can be used to construct the γ-suboptimal H_∞ controller [Gah93].

2.6 Uncertainty modeling

Any mathematical representation of a physical system needs approximations, which lead to model uncertainties. Different forms exist to represent these uncertainties according to what information we want to include. These representations reflect at the same time the knowledge of the physical phenomena that cause these uncertainties and our capacity to represent them in an easy to manipulate form. For an aircraft, whose parameters vary with the flight conditions, a linear mathematical model can be obtained by linearizing the equations of the aircraft at different points of flight. This will lead to an interval of variation for each parameter of the model obtained. These intervals of variations can represent structurally and accurately the uncertainties in the model but are not easy to manipulate. On the other hand, we can use a global form representation of the uncertainties as dynamical perturbation of the nominal model of the aircraft.

2.6.1 Unstructured uncertainties

2.6.1.1 Additive uncertainty model

Suppose that the unknown perturbed transfer matrix $G_p(s)$ of a system (aircraft) differs from a nominal transfer matrix model $G(s)$ that we have of it. The difference between these two models comes from an unknown dynamical perturbation $\Delta(s)$ representing the unmodeled dynamics of the aircraft. Suppose that this perturbation is additive, call it $\Delta_a(s)$, and that we know a function $\delta_a(\omega) \geq 0$ that bounds its norm (maximum singular value) for each frequency:

$$G_p(s) = G(s) + \Delta_a(s) \tag{2.32}$$

with

$$\left\|\Delta_a(j\omega)\right\| < \delta_a(\omega), \forall \omega \tag{2.33}$$

Note that the upper bound $\delta_a(\omega)$ represents the "size" of the uncertainty of the model at each frequency. It is often taken to be the magnitude of a scalar transfer function. This form of representation is called additive uncertainty because the perturbation's transfer matrix is added to the nominal model. This type of uncertainty is also called unstructured because the only information we use is just the upper bound of the norm of the uncertainty, and not its structure.

The figure below shows a closed loop system with such an additive uncertainty model. Again, it is important to emphasize that we do not know what $\Delta_a(s)$ is, we only know that it is bounded by $\|\Delta_a(j\omega)\| < \delta_a(\omega), \forall \omega$.

We can define a family of perturbed plant models as the set

$$\mathcal{P} := \left\{ G_p(s) : \|\Delta_a(j\omega)\| < \delta_a(\omega) \right\} \tag{2.34}$$

Then, robust control theory assumes that the unknown, "true" plant model belongs to $\mathcal{P}$. Thus, robust control design consists of designing a controller that can maintain a desired performance level for all plants in $\mathcal{P}$ (robust performance) or just stabilize all plants in $\mathcal{P}$ (robust stability).

Returning to the aircraft example, we might choose the nominal model $G(s)$ as the transfer matrix corresponding to an average flight condition. We can obtain $\delta_a(\omega)$ by calculating a large, but finite number of perturbed transfer matrices $\left\{ G_{pi}(s) \right\}_{i=1}^{N}$ corresponding to various possible flight conditions (altitudes and Mach numbers). It is then reasonable to expect that the corresponding additive perturbation $\Delta_a(s)$ would be bounded by:

$$\max_{i=1,\ldots,N} \left\| G_{pi}(j\omega) - G(j\omega) \right\| \tag{2.35}$$

at each frequency. We would then try to find an uncertainty bound $\delta_a(\omega)$ such that

$$\max_{i=1,\ldots,N} \left\| G_{pi}(j\omega) - G(j\omega) \right\| < \delta_a(\omega) \tag{2.36}$$

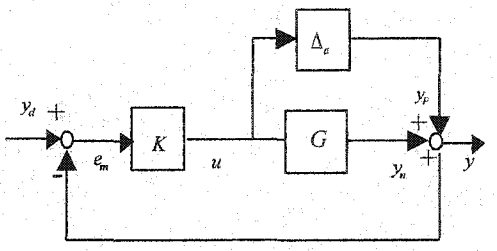

Figure 1.4: Additive uncertainty

Another way to represent the uncertainty in the system under study is the direct multiplicative uncertainty that can be related to additive uncertainty. This uncertainty has two forms of representation:

2.6.1.2 Output multiplicative uncertainty

The first representation is for direct multiplicative uncertainty taken at the output of the system:

$$G_p(j\omega) = (I_p + \Delta_m(j\omega))G(j\omega) \tag{2.37}$$

with $$\|\Delta_m(j\omega)\| < \delta_m(\omega) \quad \forall\omega \tag{2.38}$$

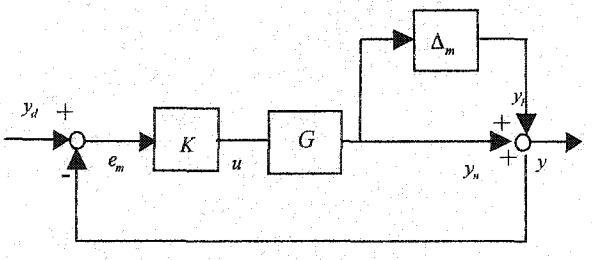

Figure 2.5: Output multiplicative uncertainty

2.6.1.3 Input multiplicative uncertainty

The second perturbed model is such that the direct multiplicative uncertainty appears at the input of the system:

$$G_p(j\omega) = G(j\omega)(I_m + \Delta_m(j\omega)) \tag{2.39}$$

with $$\|\Delta_m(j\omega)\| < \delta_m(\omega) \quad \forall \omega . \tag{2.40}$$

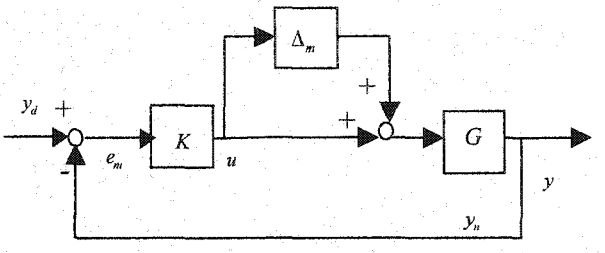

Figure 2.6: Input multiplicative uncertainty

Other models of representing dynamic uncertainties exist but are not widely used in industrial applications. We mention the input inverse multiplicative uncertainty and the output inverse multiplicative uncertainty, which can be useful to represent uncertainties that appear in the denominators (e.g., poles) of sensor and actuator transfer functions respectively.

Such unstructured models of uncertainty can be conservative and even lose information about the uncertainty in the physical system, but these kinds of models are general and can represent different uncertainties of various nature.

2.6.1.4 LFT uncertainty representation

Most of the uncertainty models described above can be cast into an LFT uncertainty representation. The perturbed model is a linear fractional transformation (LFT) of the nominal system model on the perturbation:

$$\begin{aligned} G_p(s) &= F_U\left[P(s), \Delta_l(s)\right] = P_{22}(s) + P_{21}(s)\left[I - \Delta_l(s)P_{11}(s)\right]^{-1} \Delta_l(s)P_{12}(s) \\ &= P_{22}(s) + P_{21}(s)\Delta_l(s)\left[I - P_{11}(s)\Delta_l(s)\right]^{-1} P_{12}(s) \end{aligned} \tag{2.41}$$

with $\|\Delta_l(j\omega)\| < \delta_l(\omega), \ \forall \omega .$

The figure below shows a feedback controlled upper LFT with the perturbation.

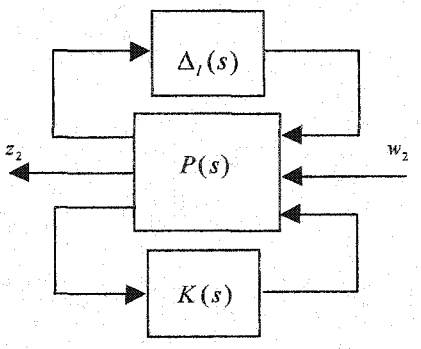

Figure 2.7: LFT uncertainty representation

Example 2.1

Output multiplicative uncertainty expressed in LFT form

Output multiplicative uncertainty can be written as

$$\begin{aligned} G_p(s) &= \left[I_p + \Delta_m(s) \right] G(s) \\ &= G(s) + \Delta_m(s) G(s) \\ &= P_{22}(s) + P_{21}(s) \left[I - \Delta_m(s) P_{11}(s) \right]^{-1} \Delta_m(s) P_{12}(s) \end{aligned}$$

and by identification with the entries of $P(s)$, we get

$$P_{22}(s) = G(s), \quad P_{21}(s) = I, \quad P_{11}(s) = 0, \quad P_{12}(s) = G(s)$$

In the following we consider different types on uncertainties and see what models can represent these uncertainties:

a- Parametric uncertainty: The variation in the parameters of the model can be represented by the additive, the direct multiplicative model and the also the reverse model if the system is square by comparing $G(j\omega)^{-1}$ and $G_p(j\omega)^{-1}$.

b- Actuators uncertainties: This comes essentially from the fact that the dynamics of actuators may not be well known or may even be neglected. These uncertainties can be take into account by using the two forms of the direct and reverse multiplicative uncertainty at the input.

c- Sensors uncertainties: The sensors are often fragile devices, so they can be partially damaged and deliver erroneous measures. These kinds of uncertainties can be represented by the direct and the reverse multiplicative uncertainties at the output.

d- Nonlinearity and reduction of the model: The nonlinearities can be taken into account if their effect can be bounded in the frequency domain. Reduction of the model is often used to simplify the control design. When we are using this technique we can take into account the neglected dynamics as uncertainty and can be represented by any type of model uncertainty.

2.6.2 Robust stability theorem

We now discuss the robust stability problem, using the small-gain theorem. Consider in the LFT in Figure 2.8. The matrix $\Delta(s)$ represents the uncertainty in the model and $M(s)$ the nominal matrix transfer function of the closed-loop system. All of the models with different types of uncertainties can be recast in the $M-\Delta$ format. The intermediate step to achieve this is to transform the block diagram into an LFT first as sown below: Then $M(s)=\mathcal{F}_L\left[P(s),K(s)\right]$.

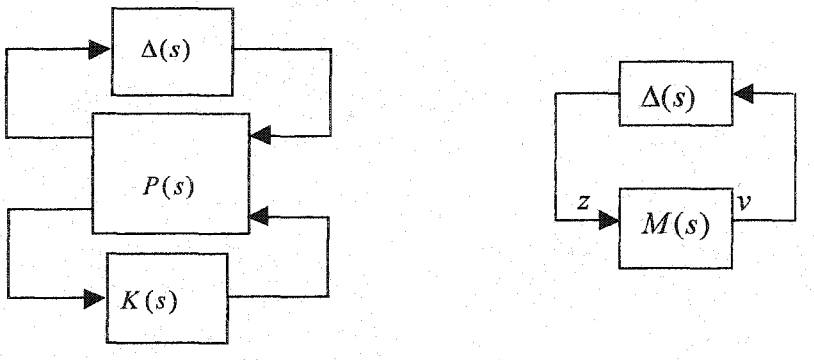

Figure 2.8: Equivalent LFT and $M-\Delta$ interconnection

Theorem 2.6 (Small-Gain Theorem) [Zam66]

Under the assumption that $M(s)$ and $\Delta(s)$ are stable and real-rational, i.e., $M(s)\in RH_\infty$, $\Delta(s)\in RH_\infty$, the $M-\Delta$ interconnection shown above is stable for every perturbation $\Delta(s)$ such that $\|\Delta\|_\infty<1$ iff $\|M\|_\infty\le 1$.

This theorem gives a necessary and sufficient condition for robust stability under the assumptions that the nominal closed-loop system $M(s)$ is stable, and that the uncertainty $\Delta(s)$ is also stable and normalized to have an H_∞-norm less than 1. The assumption that $\Delta(s)$ be stable is not too restrictive since such perturbations can generate *unstable* perturbed plant models with appropriate uncertainty models, such as inverse multiplicative or feedback uncertainty models.

Using this theorem to the different uncertain systems presented above will result in conditions of robust stability depending on the uncertainty model chosen. We will show explicitly the application of the above theorem for an LFT type uncertainty and we will give a robust stability condition specific to that uncertainty model.

Theorem 2.7 (Robust stability with linear fractional uncertainty)

Under assumptions that:

- Nominal open loop and perturbed open-loop have the same number of unstable poles.

- Any unstable pole of the perturbed open-loop system is also an unstable pole of the nominal open-loop system.

- The nominal closed-loop system is stable.

then closed-loop system of Figure 2.8 is stable if:

$$\forall \omega \in \mathbb{R}\ ,\ \left\|\Delta_s(j\omega)\right\|\left\|\mathcal{F}_L\left[P(j\omega),K(j\omega)\right]\right\| < 1, \tag{2.42}$$

or, equivalently, $$\left\|\mathcal{F}_L\left[P(j\omega),K(j\omega)\right]\right\| < \delta_l^{-1}(\omega) \tag{2.43}$$

Furthermore, under assumption that $M(s)$ and $\Delta(s)$ are stable, the closed-loop system of Figure2.8 is stable if and only if:

$$\forall \omega \in \mathbb{R}\ ,\ \left\|\mathcal{F}_L\left[P(j\omega),K(j\omega)\right]\right\| < \delta_l^{-1}(\omega) \tag{2.44}$$

The block diagram of a feedback controlled upper LFT with the perturbation (Figure 2.8) is the most general representation as all other robust stability conditions (for other types of uncertainty) can be obtained from the LFT one. Typically, the generalized plant $P(s)$ would embed all of the weighting functions used to specify performance and also weighting functions that shape the uncertainty.

The first condition given in the above theorem is just sufficient conditions for robust stability. But the second condition given based on the small-gain theorem is necessary and sufficient, and proves to be the most useful to control engineers.

The uncertainty bound $\delta(\omega)$ is usually specified by a *scalar* stable rational weigthing function $W(s)$ as follows. Let the perturbation be defined as $\Delta(s) := W(s)\tilde{\Delta}(s)$ where $\tilde{\Delta}(s)$ is a normalized perturbation in RH_∞ such that $\|\tilde{\Delta}(s)\|_\infty < 1$. Then

$$\begin{aligned} &\|\Delta(j\omega)\| < |W(j\omega)| = \delta(\omega), \quad \forall \omega \in \mathbb{R} \\ &\Leftrightarrow \\ &\|W^{-1}(j\omega)\Delta(j\omega)\| = \|\tilde{\Delta}(j\omega)\| < 1, \quad \forall \omega \in \mathbb{R} \\ &\Leftrightarrow \\ &\|\tilde{\Delta}(s)\|_\infty < 1 \end{aligned}$$

Thus, the upper bound $\|\tilde{\Delta}(s)\|_\infty < 1$ on the H_∞-norm of the normalized perturbation can be used in the theorems, along with the weighting functions.

2.6.3 Structured uncertainty

If the system studied is subjected to multiple sources of uncertainties or take into account the robust performance objective, a representation of a multiple uncertainty structure is needed. The uncertainties $\Delta_i(s) \in \mathbb{C}^{m_i \times p_i}$ and $\delta_i \in \mathbb{R}$ $i = 1, ..., n$ present in the first control setup, when this setup is transformed to an

LFT representation for a control design procedure, have to be pulled out into one structured uncertainty block as shown in Figure 2.9 below.

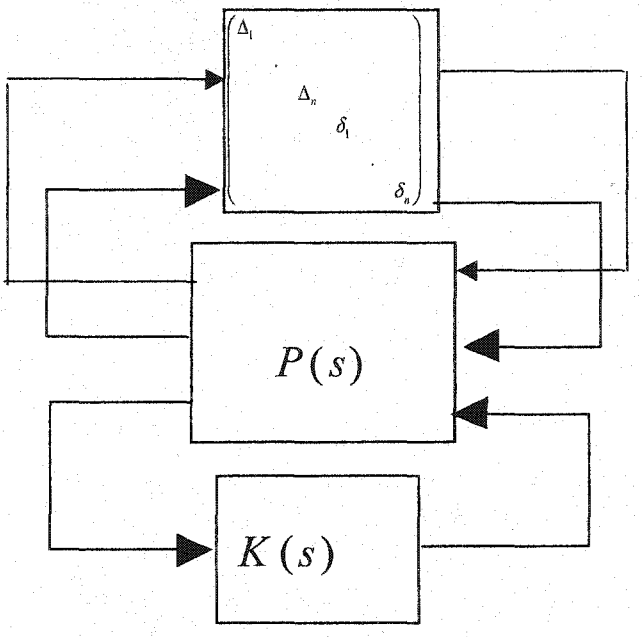

Figure 2.9: structured uncertainty setup

The best example to introduce the structured uncertainties is the use of parametric uncertainties to describe this aspect of multiple uncertainty blocks.

2.6.3.1 Parametric uncertainties

Let us define the transfer matrix $P(s,\rho) := \left[\begin{array}{c|c} A(\rho) & B(\rho) \\ \hline C(\rho) & D(\rho) \end{array}\right]$ where ρ is a vector of parameters. From this transfer matrix, we extract a constant matrix $\tilde{P}(s) := \left[\begin{array}{c|c} A & B \\ \hline C & D \end{array}\right]$ augmented by exogenous input $\tilde{w}$, outputs $\tilde{z}$ connected to the parameter dependent uncertainty block $\Delta(\rho)$, as shown below:

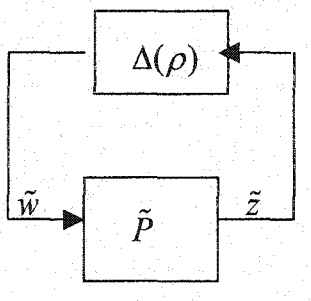

Figure 2.10: Parametric uncertainty setup

A general method is proposed, in [Bal95] to lead to the structure representation given in Figure 2.10.

Consider $\begin{bmatrix} A(\rho) & B(\rho) \\ C(\rho) & D(\rho) \end{bmatrix} = \begin{bmatrix} A_0 & B_0 \\ C_0 & D_0 \end{bmatrix} + \rho_i \begin{bmatrix} A_{ti} & B_{ti} \\ C_{ti} & D_{ti} \end{bmatrix}$ $i = 1,...,r$ where $\begin{bmatrix} A_0 & B_0 \\ C_0 & D_0 \end{bmatrix}$ is the nominal system and $\begin{bmatrix} A_{ti} & B_{ti} \\ C_{ti} & D_{ti} \end{bmatrix}$ represent the amount of uncertainty in the nominal system parameters. For simplicity, we suppose variations of system parameters at the same time (we mean if one parameter vary along an interval, it has one corresponding combination variation of the other uncertain parameters along their respective intervals of variation), thus $\begin{bmatrix} A_{ti} & B_{ti} \\ C_{ti} & D_{ti} \end{bmatrix} = \begin{bmatrix} A_t & B_t \\ C_t & D_t \end{bmatrix}$ and $i = 1$.

Two ways of constructing the uncertainty structure given in Figure 2.10 are discussed:

a-Classical method

Depending on the number, η, of non-zero elements of $\begin{bmatrix} A_t & B_t \\ C_t & D_t \end{bmatrix}$, we can extract, one by one, η augmented input/output link $\tilde{w}_i / \tilde{z}_i$.

Example2.2

Let us define a perturbed system in its state-space representation:

$$\begin{aligned} \dot{x} &= ax + u = (a_0 + \rho a_1)x + u = a_0 x + \rho a_1 x + u \\ y &= x \end{aligned} \tag{2.45}$$

If we propose a new variable to control $z = a_1 x$ and an exogenous input $\tilde{w} = \rho a_1 x$ then $\tilde{w} = \rho \tilde{z}$. This will allow us to write, as follows, an augmented system based on the nominal system of .

$$\begin{aligned} \dot{x} &= a_0 x + u + \tilde{w} \\ \tilde{z} &= a_1 x \\ y &= x \end{aligned} \tag{2.46}$$

This procedure can be applied to all non-zero elements of $\begin{bmatrix} A_t & B_t \\ C_t & D_t \end{bmatrix}$. However this approach is not automatic and can be conservative. In the following a systematic approach is presented.

b-SVD approach

In this approach we generate a number η_1 of repeated uncertainties such that $\eta_1 = rank\left(\begin{bmatrix} A_t & B_t \\ C_t & D_t \end{bmatrix}\right) \leq \eta$.

This can be achieved by means of an singular value decomposition of $\begin{bmatrix} A_t & B_t \\ C_t & D_t \end{bmatrix}$.

$$\begin{bmatrix} A_t & B_t \\ C_t & D_t \end{bmatrix} = U \begin{bmatrix} \Sigma_r & \\ & 0 \end{bmatrix} V^T = \begin{bmatrix} U_1 \\ U_2 \end{bmatrix} \begin{bmatrix} \Sigma_r & \\ & 0 \end{bmatrix} \begin{bmatrix} V_1 & V_2 \end{bmatrix} = U_1 W_1$$

where $r = rank(\begin{bmatrix} A_t & B_t \\ C_t & D_t \end{bmatrix})$ and $W_1 = \Sigma_r V_1$.

Thus the original system can be written as:

$\begin{bmatrix} A(\rho) & B(\rho) \\ C(\rho) & D(\rho) \end{bmatrix} = \begin{bmatrix} A_0 & B_0 \\ C_0 & D_0 \end{bmatrix} + \rho \begin{bmatrix} A_t & B_t \\ C_t & D_t \end{bmatrix}$ which is written as: $\begin{bmatrix} A(\rho) & B(\rho) \\ C(\rho) & D(\rho) \end{bmatrix} =$

$$\begin{bmatrix} A_0 & B_0 \\ C_0 & D_0 \end{bmatrix} + \begin{bmatrix} U_{11} \\ U_{12} \end{bmatrix} \tilde{w}$$

with $\tilde{w} = \rho I \tilde{z}$, $\tilde{z} = \begin{bmatrix} W_{11} & W_{12} \end{bmatrix}$, $U_1 = \begin{bmatrix} U_{11} \\ U_{12} \end{bmatrix}$ and $W_1 = \begin{bmatrix} W_{11} & W_{12} \end{bmatrix}$ then the augmented system is given as:

$$\tilde{P}(s) := \begin{bmatrix} A_0 & B_0 & U_1 \\ C_0 & D_0 & U_2 \\ V_1 & V_2 & 0 \end{bmatrix} \tag{2.47}$$

2.6.3.2 Structured singular value

The structured singular value is a generalization of the maximum singular value of constant complex matrices. Consider the feedback interconnection presented in Figure 2.8. The closed-loop poles are given by $\det[I - M(s)\Delta(s)] = 0$, and the feedback system becomes unstable if $\det[I - M(s)\Delta(s)] = 0$ for some $s \in \overline{\mathbb{C}}_+$ (closed RHP). Using the small gain theorem the robust stability margin $\beta_{\max}$ is defined as:

$$\frac{1}{\beta_{\max}} = \|M\|_\infty := \sup_{s\in\overline{\mathbb{C}}_+} \bar{\sigma}\left(M(s)\right) = \sup_{\omega} \bar{\sigma}\left(M(j\omega)\right) \tag{2.48}$$

such that $\|\Delta\|_\infty < \beta_{\max}$ and $\Delta(s)$ is unstructured.

For any fixed complex number $s_0 \in \overline{\mathbb{C}}_+$, the maximum singular value, [Doy82], $\bar{\sigma}\left(M(s)\right)$ can be written as:

$$\left\|M(s_0)\right\| = \bar{\sigma}\left(M(s_0)\right) = \frac{1}{\min\left\{\bar{\sigma}(\Delta) : \det\left(I - M(s_0)\Delta\right) = 0, \Delta \in \mathbb{C}^{p\times p}\right\}} \tag{2.49}$$

Therefore, the reciprocal of the *largest singular value* of $M(s_0)$ is a measure of the smallest unstructured $\Delta \in \mathbb{C}^{p\times p}$ that can cause instability of the feedback system.

For the smallest destabilizing *structured* complex Δ_s, the concept of maximum singular value needs to be generalized. We define,[Doy85],

$$\mu_\Delta\left(M(s_0)\right) := \begin{cases} \dfrac{1}{\min\left\{\bar{\sigma}(\Delta_s) : \det\left(I - M(s_0)\Delta_s\right) = 0, \Delta_s \text{ is structured}\right\}} \\ 0, \ \det\left(I - M(s_0)\Delta_s\right) \neq 0 \ \forall \Delta_s \end{cases} \tag{2.50}$$

as the largest structured singular value of $M(s_0)$ with respect to the structured complex perturbation Δ_s. Then, the robust stability margin $\beta_{\max}$ of the feedback system with structured complex uncertainty Δ_s is given by:

$$\frac{1}{\beta_{\max}} = \sup_{s\in\overline{\mathbb{C}}_+} \mu_\Delta\left(M(s)\right) = \sup_{\omega\in\mathbb{R}} \mu_\Delta\left(M(j\omega)\right) \tag{2.51}$$

In the following, we consider the general case of a S-scalar-block, F-full-block structured perturbation, where the scalar blocks may be repeated. Let $M \in \mathbb{C}^{n\times n}$, and $r_1,\ldots,r_q, m_1,\ldots,m_l$ be positive integers satisfying $\sum_{i=1}^{S} r_i + \sum_{j=1}^{F} m_j = n$ (this is just for bookkeeping of the dimensions of the uncertainty blocks).

We define the block structure $\Gamma \subset \mathbb{C}^{n\times n}$ as

$$\Gamma := \left\{ \Delta_s = \operatorname{diag}\left\{ \delta_1 I_{r_1}, \ldots, \delta_q I_{r_q}, \Delta_1, \ldots, \Delta_l \right\} : \delta_i \in \mathbb{C}, \Delta_j \in \mathbb{C}^{m_j \times m_j} \right\} \tag{2.52}$$

Definition2.1 structured singular value

For a complex matrix $M \in \mathbb{C}^{n\times n}$, the function $\mu_\Gamma : \mathbb{C}^{n\times n} \to \mathbb{R}_+$ is defined as

$$\mu_\Gamma(M) := \left[\min \left\{ \|\Delta_s\| : \Delta_s \in \Gamma, \det(I - M\Delta_s) = 0 \right\} \right]^{-1} \tag{2.53}$$

unless no $\Delta_s \in \Gamma$ makes $\det(I - M\Delta_s)$ singular, in which case $\mu_\Gamma(M) = 0$.

Define the " unit open ball" of complex structured perturbations:

$$\mathcal{B}\Gamma := \left\{ \Delta \in \Gamma : \|\Delta\| < 1 \right\} \tag{2.54}$$

Then, an alternative expression for $\mu_\Gamma(M)$ follows from the definition:

$$\mu_\Gamma(M) = \max_{\Delta_s \in \mathcal{B}\Gamma} \rho(M\Delta_s) \tag{2.55}$$

Where $\rho(.)$ is the spectral radius.

Since the spectral radius is a continuous function, the structured singular value $\mu_\Gamma : \mathbb{C}^{n\times n} \to \mathbb{R}_+$ is also a continuous function. However, $\mu_\Gamma(\cdot)$ is not a norm, since it does not satisfy the triangle inequality.

In the special cases of only a single scalar block, and only a single full block, $\mu_\Gamma(M)$ reduces to the following.

If $\Gamma = \{\delta I : \delta \in \mathbb{C}\}$ $(S = 1, F = 0, r_1 = n)$, then

$$\mu_\Gamma(M) = \rho(M), \tag{2.56}$$

which is the spectral radius of M.

If $\Gamma = \mathbb{C}^{n\times n}$ $\left(S = 0, F = 1, m_1 = n\right)$, then

$$\mu_{\Gamma}(M) = \bar{\sigma}(M) \tag{2.57}$$

Obviously, for a general uncertainty structure Γ as defined in the beginning, we must have

$$\{\delta I_n : \delta \in \mathbb{C}\} \subset \Gamma \subset \mathbb{C}^{n\times n}.$$

The bigger the uncertainty set, the more possible it is for a small perturbation to make $I - M\Delta_s$ singular. We conclude that:

$$\rho(M) \le \mu_{\Gamma}(M) \le \bar{\sigma}(M) \tag{2.58}$$

The gap between $\rho(M)$ and $\bar{\sigma}(M)$ can be large, which makes the evaluation of the structured singular value using these bounds difficult.

However, the bounds can be refined by considering transformations on M that *do not affect* $\mu_{\Delta}(M)$, but do affect $\rho(M)$ and $\bar{\sigma}(M)$. To do this, define the following two subsets of $\mathbb{C}^{n\times n}$:

$$\mathcal{U} := \left\{U \in \Gamma : UU^* = I_n\right\}, \tag{2.59}$$

which is the set of structured unitary matrices, and

$$\mathrm{D} := \left\{\mathrm{diag}\left\{D_1, \ldots, D_s, d_1 I_{m_1}, \ldots, d_{F-1} I_{m_{F-1}}, I_{m_F}\right\} : D_i \in \mathbb{C}^{r_i \times r_i}, D_i = D_i^* > 0, d_j \in \mathbb{R}, d_j > 0\right\} \tag{2.60}$$

which is the set of matrices that commute with any $\Delta_s \in \Gamma$. Mathematically, for any $\Delta_s \in \Gamma, U \in \mathcal{U}, D \in \mathcal{D}$, we have the following properties:

$$U^* \in \mathcal{U}, \quad U\Delta_s \in \Gamma, \quad \Delta_s U \in \Gamma, \quad \bar{\sigma}(U\Delta_s) = \bar{\sigma}(\Delta_s U) = \bar{\sigma}(\Delta_s),$$

$$D\Delta_s = \Delta_s D.$$

Consequently, we have:

For all $U \in \mathcal{U}, D \in \mathcal{D}$:

$$\mu_\Gamma(MU) = \mu_\Gamma(UM) = \mu_\Gamma(M) = \mu_\Gamma\left(DMD^{-1}\right) \tag{2.61}$$

Therefore, the lower and upper bounds on μ in (2.58) can be tightened to:

$$\max_{U\in\mathcal{U}} \rho(UM) \le \max_{\Delta_s\in\mathcal{B}\Gamma} \rho(\Delta_s M) = \mu_\Gamma(M) \le \inf_{D\in\mathcal{D}} \bar{\sigma}\left(DMD^{-1}\right) \tag{2.62}$$

The lower bound of the expression obtained above is always an equality:

$$\max_{U\in\mathcal{U}} \rho(UM) = \mu_\Gamma(M) \le \inf_{D\in\mathcal{D}} \bar{\sigma}\left(DMD^{-1}\right) \tag{2.63}$$

Unfortunately, the function $\rho(UM)$ can have multiple local maxima which are not global. Thus local search cannot be guaranteed to obtain $\mu_\Gamma(M)$, but can only yield a lower bound. The upper bound can be reformulated as a convex optimization problem, so the global minimum can, in principle, be found. Unfortunately, the upper bound is not always equal to $\mu_\Gamma(M)$. For block structures Γ with a number of scalar blocks and full blocks satisfying $2S+F \le 3$, the upper bound is always equal to $\mu_\Gamma(M)$, and for block structures with $2S+F > 3$, there exist matrices for which $\mu_\Gamma(M)$ is less than the infimum [Pack88].

2.6.3.3 Robust stability with structured uncertainty

In the following we give conditions of robust stability of a closed loop system subjected to a block of structured uncertainties. Let us define the set of real-rational, proper, stable structured perturbations:

$$\mathrm{S} := \left\{\Delta_s(s) \in RH_\infty : \Delta_s(s_0) \in \Gamma, \forall s_0 \in \overline{\mathbb{C}}_+\right\} \tag{2.64}$$

and consider the perturbed feedback loop in Figure2.8 where $\Delta(s) = \Delta_s(s) \in \mathbb{S}$. The LFT is simply reduced to an $M(s) - \Delta_s(s)$ interconnection, such that $F_L[P(s), K(s)]$, and we can use a generalization of the small gain theorem to assess robust stability.

Theorem2.8 Robust stability with structured perturbation (small-μ theorem)

Assume controller $K(s)$ is stabilizing for the nominal plant $P(s)$. Then given $\beta > 0$, the closed-loop system in Figure 2.8 is well-posed and internally stable for all $\Delta_s \in \mathcal{S}, \|\Delta_s\|_\infty < \beta$ if and only if: $\sup_{\omega \in \mathbb{R}} \mu_{\mathbb{T}} \{\mathcal{F}_L[P(j\omega), K(j\omega)]\} \leq \frac{1}{\beta}$.

In particular, if the structured perturbation is normalized, i.e., $\tilde{\Delta}_s \in \mathcal{S}, \|\tilde{\Delta}_s\|_\infty < 1$, the condition becomes: $\sup_{\omega \in \mathbb{R}} \mu_{\mathbb{T}} \{\mathcal{F}_L[P(j\omega), K(j\omega)]\} \leq 1$.

2.6.3.4 Robust performance

Consider the closed-loop system presented in Figure 2.11 where $z_2(t) \in \mathbb{R}^{n_{z_2}}$ and $w_2(t) \in \mathbb{R}^{n_{w_2}}$. Define the new uncertainty structure : $\Omega := \left\{ \begin{bmatrix} \Delta_s & 0 \\ 0 & \Delta_p \end{bmatrix} : \Delta_s \in \Gamma, \Delta_p \in \mathbb{C}^{n_{w_2} \times n_{z_2}} \right\}$. A fictitious uncertainty Δ_p was added to the structure. It accounts for the performance objectives under a classical robust stability framework described above.

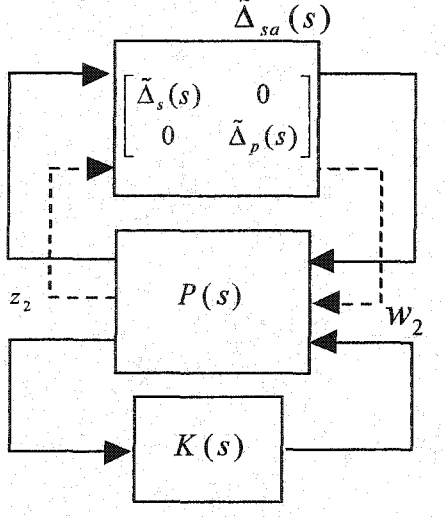

Figure 2.11: robust performance setup

The following theorem gives the conditions for robust performance criteria.

Theorem2.9: Robust performance with structured perturbation

Assume controller $K(s)$ is stabilizing for the nominal plant $P(s)$. Then for the closed-loop system in the figure, for all $\Delta_s \in \mathcal{S}, \|\Delta_s\|_\infty < \beta$ the closed-loop system is well-posed, internally stable and $\|T_{z_2 w_2}\|_\infty \le \frac{1}{\beta}$ if and only if

$$\sup_{\omega \in \mathbb{R}} \mu_\Omega \left\{ \mathcal{F}_L \left[P(j\omega), K(j\omega) \right] \right\} \le \frac{1}{\beta}, \tag{2.65}$$

where $T_{z_2 w_2}$ is the transfer matrix from the input w_2 to the output z_2.

The controller design technique called μ – synthesis is based on the use of the upper bound on μ in (2.58). We minimize the supremum of $\mu_\Omega \left\{ \mathrm{F}_L \left[P(j\omega), K(j\omega) \right] \right\}$ over all frequencies by solving the optimization problem:

$$\min_{K(s), D(s)} \left\| \begin{bmatrix} D & 0 \\ 0 & I \end{bmatrix} F_L(P, K) \begin{bmatrix} D^{-1} & 0 \\ 0 & I \end{bmatrix} \right\|_\infty \tag{2.66}$$

where K must stabilize the plant perturbed by any $\Delta_s \in S$ and $\|\Delta_s\|_\infty \le 1$. The $D(s)$ scales must be minimum phase and invertible in RH_∞. The optimization in (2.66) can be solved iteratively by fixing the D scales and solving $\min_{K(s)} \left\| D \mathcal{F}_L \left(G, K \right) D^{-1} \right\|_\infty$, then for a given controller $K(s)$, by solving $\inf_{D, D^{-1} \in \mathcal{H}_\infty} \left\| D \mathcal{F}_L \left(G, K \right) D^{-1} \right\|_\infty$. This optimization procedure is called *D-K iteration* and is detailed in [Bal95]. However, this procedure is not optimal in the sense that the controller $K(s)$ obtained only achieves a sub-optimal μ value in closed loop. This procedure depends on the nature of the uncertainties, complex, real or a mix of the two, and the D-scales used. Many papers, e.g., [You90], [You92], treated this open research topic and obtained results on what D-scales are best to use in the D-K iteration procedure to match the plant uncertainty. For the mixed uncertainty control problem, a similar algorithm called D-G-K iteration [You93] was developed to cope to the conservatism presented by the D-K iteration algorithm.

2.7 H_∞ loopshaping design

The loop-shaping design technique is based on the H_∞ robust stabilization procedure developed in [Mcf90],[Hyd91], where the plant is robustly stabilized with respect to coprime factor uncertainty using H_∞ optimization. The plant has to be shaped, following a well-developed procedure [Hyd91], by means of pre and post compensators to give a desired shape to the singular values of the open-loop system, specifying the performance objectives over the frequency range considered.

In the following, we briefly review the H_∞ robust stabilization procedure that has the virtue to be systematic in its solution and takes into account the uncertainty modeling or the choice of the performance weighting functions.

2.7.1 Robust stabilization

The dynamic, bounded norm uncertainty used in the classical $\mu-$synthesis must be stable to use robustness theorems presented earlier. H_∞ loopshaping approach avoids constraints that restrict the plant and the perturbed plant to have the same number of unstable poles. We consider the stabilization of a plant G which has a normalized left-coprime factorization:

$$G = M^{-1}N \tag{2.67}$$

then the perturbed plant model G_p can then be written as:

$$G = (M + \Delta_M)^{-1}(N + \Delta_N) \tag{2.68}$$

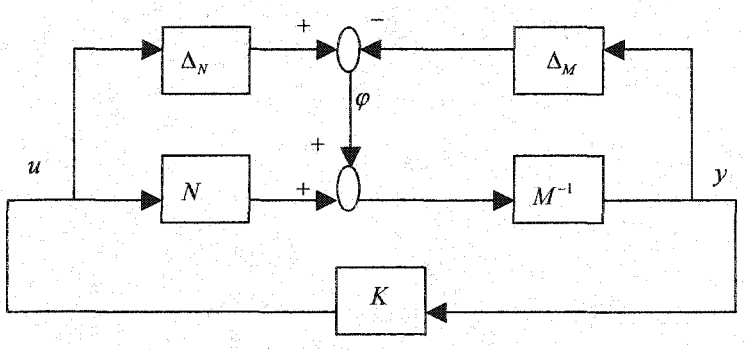

Figure 2.12: H_∞ robust stabilization problem

where Δ_M, Δ_N are stable unknown transfer functions representing the uncertainty in the nominal model G. The objective of H_∞ robust stabilization it to stabilize the family of perturbed plants defined by

$$G_p := \left\{ (M+\Delta_M)^{-1}(N+\Delta_N) : [\Delta_N \ \Delta_M] \in RH_\infty, \left\| [\Delta_N \ \Delta_M] \right\|_\infty < \varepsilon \right\} \tag{2.69}$$

where $\varepsilon > 0$ is the stability margin.

The stability of the interconnection in Figure 2.12 is robust if and only if the nominal feedback system is stable and

$$\gamma := \left\| \begin{bmatrix} K \\ I \end{bmatrix} (I-GK)^{-1} M^{-1} \right\|_\infty \leq \frac{1}{\varepsilon} \tag{2.70}$$

where γ is the H_∞ norm of the transfer matrix linking ϕ to $\begin{bmatrix} u \\ y \end{bmatrix}$. The objective of this robust stabilization is to obtain the lowest value of γ which represents the maximum stability margin. The lowest achievable γ obtained in [Mcf90] is given by:

$$\gamma_{\min} = \varepsilon_{\max}^{-1} = \left\{ 1 - \left\| [N \ M] \right\|_H^2 \right\}^{-\frac{1}{2}} = \left(1+\rho(XZ)\right)^{\frac{1}{2}} \tag{2.71}$$

where $\| \ . \ \|_H$ denotes the Hankel norm, ρ denotes the spectral radius and Z, X are the solutions of the following Riccati equations:

$$\left(A - BS^{-1}D^TC\right)Z + Z\left(A - BS^{-1}D^TC\right)^T - ZC^TR^{-1}CZ + BS^{-1}B^T = 0 \tag{2.72}$$

$$\left(A - BS^{-1}D^TC\right)^T X + X\left(A - BS^{-1}D^TC\right) - XBS^{-1}B^TX + C^TR^{-1}C = 0 \tag{2.73}$$

where: $R = I + DD^T, S = I + D^TD$.

A central controller, which guarantees that

$$\left\| \begin{bmatrix} K \\ I \end{bmatrix} (I-GK)^{-1} M^{-1} \right\|_\infty \leq \gamma \tag{2.74}$$

for a specified $\gamma > \gamma_{\min}$, is given in [Mcf90] by

$$K = \left[\begin{array}{c|c} A + BF + \gamma^2 \left(L^T\right)^{-1} ZC^T (C+DF) & \gamma^2 \left(L^T\right)^{-1} ZC^T \\ \hline B^TX & -D^T \end{array} \right] \tag{2.75}$$

where: $F = -S^{-1}\left(D^TC + B^TX\right), \ L = \left(1-\gamma^2\right)I + XZ.$

As mentioned above, the plant which has to be used in the previous H_∞ robust stabilization is indeed a shaped plant model of the real system. In the literature, [Mcf90], [Hyd91], [Pap98], the loop shaping

procedure was developed to become more and more systematic. In fact, we can summarize it in two steps [Hyd91]:

2.7.2 Loopshaping procedure

1- Scale all inputs and outputs of the plant to reflect the bandwidth of the actuator efforts and to unify the output units, respectively. Reorder the plant to present it as diagonal as possible.

2-Based on the frequency responses of the transfer functions linking each actuator to all outputs and all actuators to each output, propose weighting functions W_1 and W_2 in order to obtain a roll-off of 20db/decade at the desired frequency bandwidths. For that, include an integral action in the proposed W_1 weighting function.

At this point, a shaped plant including performance specifications is obtained. It has been shown [Mcf90], that the performance specifications included in the shaped plant reflect also the performance specifications of the closed-loop system after the controller procedure design. The shaped plant is now ready to be used in the H_∞ robust stabilization procedure presented earlier. The indicator $\gamma_{\min}$, related to the robustness of the system, can be used as a criterion of controller design satisfaction. Practically the best value of $\gamma_{\min}$ is between 4 and 5, which allows at minimum 25% of robust stability margin for the system.

2.8 μ – Synthesis using H_2 controllers

The synthesis procedure typically used for the μ – controller design is based on the D-K (eventually D-G-K for the mixed uncertainty type [You93]) iteration algorithm. This algorithm presents certain major deficiencies that cause problems in its adaptation for real flight control systems. Adding to the problem that the μ value can not be exactly calculated, especially for a robust performance criterion, the scalings needed to solve the optimization problem in the D-K (D-G-K) iteration can have certain dynamics that will dramatically increase the order of the system submitted to a large number of uncertainties. In fact, with these problems the complexity of the μ – controller design will increase and the upper bound of the μ value will be conservative, which does not guarantee the convergence to the μ – optimal controller and does not statute on the performance objective criteria used. All these inconveniences pushed us to explore other possible ways of implementing μ – controller design. A

method of designing a $\mu-$controller using weighted H_2 optimization [Yan97] is adapted in our work and proved useful when compared to the classical D-K iteration algorithm. In the following, we give a description of the method proposed:

Theorem2.10 [Yan97]

Suppose there exists a scalar frequency-dependent weight $W(s)$ such that the H_2 controller

$$K_0 = \arg\inf_K \left\| WF_L(P,K) \right\|_2 \tag{2.76}$$

satisfies

$$\mu_\Delta[F_L(P,K_0)(j\omega)] = \gamma_0 = const \ \forall\omega \tag{2.77}$$

$$\mu_\Delta[F_L(P,K_0)(j\omega)] = \left\| WF_L(P,K) \right\|_2 \ \forall\omega \tag{2.78}$$

then K_0 is the optimal $\mu-$controller

$$\inf_K \sup_\omega \mu_\Delta[F_L(P,K)(j\omega)] = \mu_\Delta[F_L(P,K_0)(j\omega)] = \gamma_0 \tag{2.79}$$

This theorem gives a sufficient condition of the existence of $\mu-$controller originally synthesized using H_2 optimization as in (2.76) and satisfying the conditions in (2.77), (2.78). Once the concept of designing such controllers is admitted, the main issue is to find the weighting function $W(s)$ that satisfies:

$$K_0 = \arg\inf_K \left\| WF_L(P,K) \right\|_2 = \inf_K \sup_\omega \mu_\Delta[F_L(P,K)(j\omega)] \tag{2.80}$$

The optimization in (2.76) is solved iteratively, where a weighting function $\hat{W}_i(s)$ is used for each iteration to lead to the optimal controller. Note that in practice there is no guarantee of the convergence to an optimal controller with the best $\mu-$bound.

An algorithm for designing the $\mu-$controller based on weighted H_2 optimization is presented in the following:

1-Set $\hat{W}_0(s) = I,\ i = 0.$

2-Compute $K_0 = \arg\inf_K \left\| \hat{W}_0 F_L(P,K) \right\|_2$ using the H_2 optimization technique

3-Compute $\mu_\Delta[\hat{W}_0 F_L(P,K_0)(j\omega)]$.

Do the following step unless $\sup_{\omega} \mu_{\Delta}[\hat{W}_i F_L(P,K_i)(j\omega)] - \sup_{\omega} \mu_{\Delta}[\hat{W}_{i-1} F_L(P,K_{i-1})(j\omega)] < \varepsilon$ where $\varepsilon > 0$ is the a tolerance value.

4-Set $\deg(\hat{W}_i) = n_w$, where $\hat{W}_i$ is a scalar, minimum phase function.

5-Fit $\mu_{\Delta}[\hat{W}_{i-1} F_L(P,K_{i-1})(j\omega)]$ by $\left|\hat{W}_i(j\omega)\right|$.

6-Compute $K_i = \arg\inf_K \left\|\hat{W}_i F_L(P,K)\right\|_2$

7-Compute $\mu_{\Delta}[\hat{W}_i F_L(P,K_i)(j\omega)]$.

The incorporation of the weighting function $\hat{W}_i(s)$ with the nominal plant P in the augmented P_a can be done as following: $P_{a_i} = \begin{bmatrix} W_i(s) I_l & 0 \\ 0 & I_m \end{bmatrix} P$ where l is the dimension of the variable to control z and m is the dimension of the output y. This method of $\mu-$controller design has the virtue of decreasing the order of the augmented system by half compared to the D-K iteration algorithm. It also decreases the complexity of the design by using H_2 optimization and can reach a less conservative upper bound of the $\mu-$value. This method allows one to design, at each iteration, a $\mu-$controller based on H_2 optimization. In our adaptation of this method to our work, we ran many design iterations design and we take the $\mu-$optimal controller leading to the smallest $\mu-$value. Because the weighting function proposed in the above algorithm is based on a fitting procedure of a $\mu-$frequency response, the convergence cannot be guaranteed as claimed theoretically [Yan97]. Even with this drawback, the method often leads to satisfactory upper bounds for μ for high-order uncertain systems compared to the classical D-K iteration. Another advantage of this method is the fact that it yields a $\mu-$controller based on an H_2 design with an observer-based structure facilitating implementation and lending itself to gain scheduling.

In the rest of this chapter, we treat the gust load alleviation problem by using robust control techniques. We give motivation of applicability of the H_∞ control design to an optimal control problem and compare results of other control techniques.

2.9 B52 flexible bomber application

2.9.1 Introduction

H_2 (LQG), weighted-H_2 and H_∞ techniques are used to establish a nominal performance baseline for the vertical acceleration control of a B-52 aircraft model with flexibilities.

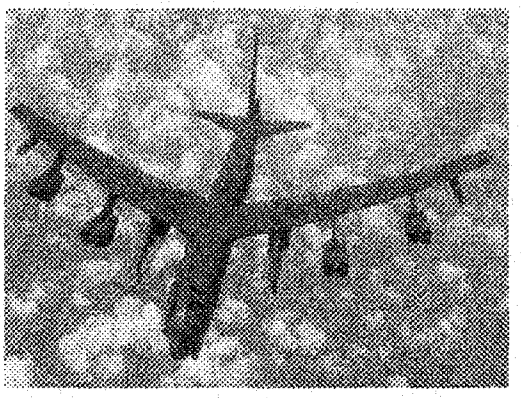

Figure 2.13: B52 bomber

The dynamic model of the aircraft used for control design includes five flexible modes. Such a model is more realistic than a rigid-body model, but it can also make the Gust Load Alleviation (GLA) feedback control design problem more challenging. The aircraft is assumed to be subjected to severe wind gusts causing undesirable vertical motion. The purpose of the controllers is to reduce the transient peak loads on the airplane caused by the gust. Our designs account for the flexible modes of the aircraft model. The gust signals are assumed to be generated by the Dryden power spectral density model. This model lends itself well to frequency-domain performance specifications in the form of weighting functions. Since the Dryden gust model is simply a white noise driving a stable real-rational linear time-invariant filter, it is natural to consider the design of an *LQG* controller, or its equivalent deterministic H_2 counterpart. However, as a bumpy flight experience would suggest, wind gusts are acting only over brief periods of time. Air turbulence in a localized area may last for a time long enough to warrant the Dryden colored noise approximation. But the point here is that an aircraft momentarily passing through the turbulence will only experience its effect for a brief period of time. Thus, rather than using signals of finite average power for LQG GLA control design, we suggest that such behavior may be best captured by bounded-energy signals with spectral contents given by the magnitude of the Dryden filter. In the deterministic, worst-case $\mathcal{L}_2$ setting, this remark gives some motivation to design a baseline GLA controller with an H_∞ performance

specification. The technique of μ-synthesis and analysis is used to study the robust performance of the aircraft taking into account specific input and output multiplicative uncertainty models. Robust performance is achieved with a μ-synthesis controller design using a *D-K* iteration procedure.

2.9.2 Vertical gust model

An expression for the Dryden filter $G_w(s)$ can be found with more details in chapter 1 as following:

$$G_w(s) = \sqrt{\frac{3U_0\sigma^2{}_w}{\pi L_w}} \frac{\frac{U_0}{\sqrt{3}L_w} + s}{\left[\frac{U_0}{L_w} + s\right]^2} \tag{2.81}$$

where: $L_w = 580$ m (1750 ft), $\sigma_w = 7m/s(21ft/s)$.

A proposed alternative use of the Dryden model is to consider the noise n to be any deterministic finite-energy signal in $\mathsf{N} := \{n \in \mathcal{L}_2[0,\infty) : \|n\|_2 \le 1\}$. The gust signal then lives in $\mathsf{W} := \{G_w n : n \in \mathsf{N}\} \subset \mathcal{L}_2[0,\infty)$,and its energy is bounded by $\|w_g\|_2 \le \|G_w\|_\infty = 0.9\sqrt{2}\sigma_w\sqrt{L_w/\pi U_0}$. Furthermore, such signals taper off at infinity in the time domain. Hence, they may be more representative of real wind gusts acting on an aircraft passing through turbulence. Although the stochastic nature of the signal is lost, the resulting set of bounded-energy gust signals can be used for a worst-case H_∞ design, which may be desirable in a safety critical application such as GLA.

2.9.3 Flexible model description

The short-period approximation for the rigid-body motion of the B-52 aircraft is considered. The rigid-body dynamics are augmented by a set of modal coordinates associated with the normal bending modes of the B-52. The i^{th} flexible mode is represented by the following equation in terms of its modal coordinate η_j:

$$\ddot{\eta}_i + 2\varsigma_i\omega_i\dot{\eta}_i + \omega_i^2\eta_i = \rho_i\phi_i \tag{2.82}$$

where $\varsigma_i, \omega_i, \rho_i$ are the damping ratio, frequency and gain of the i^{th} flexible mode, and ϕ_i is its corresponding generalized force. Thus, the rigid-body dynamics may be augmented with pairs of first-

order equations corresponding to each flexible mode considered. Five structural flexible modes were considered significant and were kept in the B-52 aircraft longitudinal dynamic model taken from [Mcl90]. The control inputs for the longitudinal motion are the deflection angles (in radians) of the elevator δ_{el} and the horizontal canard δ_{hc}. The longitudinal dynamics of the flexible aircraft are given by:

$$\begin{aligned} \dot{x} &= Ax + Bu + B_g w_g \\ y &= Cx + Du \end{aligned} \tag{2.83}$$

where $x(t) \in \mathbb{R}^{12}$ is the state vector given by:

$x^T = [\alpha \;\; q \;\; \eta_1 \;\; \dot{\eta}_1 \;\; \eta_2 \;\; \dot{\eta}_2 \;\; \eta_3 \;\; \dot{\eta}_3 \;\; \eta_4 \;\; \dot{\eta}_4 \;\; \eta_5 \;\; \dot{\eta}_5]$ $u(t) = \begin{bmatrix} \delta_{el} & \delta_{hc} \end{bmatrix}^T \in \mathbb{R}^2$ is the control vector (rad) $y(t) \in \mathbb{R}$ is the vertical acceleration (g), $w_g(t) = \begin{bmatrix} w_{g1} & w_{g2} & w_{g3} \end{bmatrix}^T \in \mathbb{R}^3$ is the vertical gust velocity at three stations along the airplane (m/s), $\alpha(t) \in \mathbb{R}$ is the angle of attack (rad), $q(t) \in \mathbb{R}$ is the pitch rate (rad/s). There are couplings between the flexible modes and the rigid-body mode. The eigenvalues of A corresponding to the rigid-body mode are $\lambda_{1,2} = -1.803 \pm j2.617$. The five flexible modes are listed in Table 2.1 below.

Table2.1: Flexible modes

	1	2	3	4	5
ω_i (rd/s)	7.60	15.2	19.73	20.24	38.29
ς_i	0.39	0.05	0.011	0.067	0.023

Note that the second and third gust signals w_{g2} and w_{g3} are actually delayed versions of w_{g1}. The second gust is delayed by $\tau_1 = U_0/x_1 = 0.06$ s, where x_1 is the distance from the first body station to the second. The third gust input is delayed by $\tau_2 = U_0/x_2 = 0.145$ s. First-order lag approximations of the time delays are used, e.g., $w_{g2} = \dfrac{1}{0.06s + 1} w_{g1}$.

2.9.4 Problem setup

A block diagram of the closed-loop GLA design problem with weighting functions is shown in Figure2.14 below:

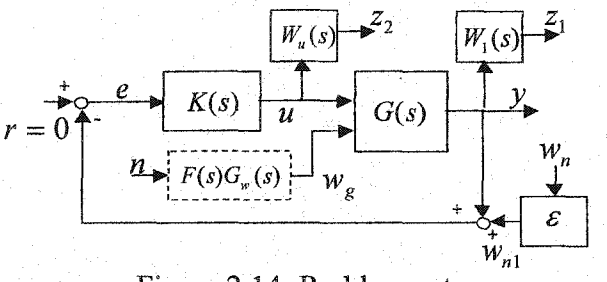

Figure 2.14: Problem setup

where $w_{n1}(t) \in \mathbb{R}$ is an acceleration measurement noise used to regularize the controller design problem, with amplitude specified by $\varepsilon = 10^{-4}$ as w_n is normalized, $r(t) \in \mathbb{R}$ is the vertical acceleration setpoint ($r(t) = 0$), $e(t) \in \mathbb{R}$ is the measured error, $z_1(t) \in \mathbb{R}$ is the weighted measured acceleration, $z_2(t) \in \mathbb{R}^2$ is the weighted controller output, and $F(s)$ contains the lags approximating the delays. The plant transfer matrix $G(s)$ mapping $[u\ w_g{}^T]^T$ to y is given by

$$G(s) = \left[\begin{array}{c|c} A & [B\ B_g] \\ \hline C & [D\ 0] \end{array}\right] \tag{2.84}$$

The GLA problem of Figure2.14 can be recast into the standard H_2 and H_∞ optimal control problem of Figure2.3.

The vector of exogenous inputs in Figure2.3 is $w := [n\ w_n]^T$ for the H_2 controller designs, or $w := [w_g{}^T\ w_n]^T$ for the H_∞ controller design. The signals to be minimized are collected in $z := \begin{bmatrix} W_1 y \\ W_u u \end{bmatrix}$.

The nominal generalized plant

$$P(s) = \begin{bmatrix} P_{11}(s) & P_{12}(s) \\ P_{21}(s) & P_{22}(s) \end{bmatrix} \tag{2.85}$$

has a minimal state-space realization

$$\begin{aligned} \dot{x} &= A_P x + B_{P1} w + B_{P2} u \\ z &= C_{P1} x + D_{P11} w + D_{P12} u \\ y &= C_{P2} x + D_{P21} w + D_{P22} u \end{aligned} \tag{2.86}$$

which combines the aircraft model, the Dryden filter (for the H_2 controller) and the weighting functions. For convenience, we will use the notation $T_{xy} := x \mapsto y$ for closed-loop transfer matrices.

2.9.5 H_2 control

Assuming that the origin of the gust is a zero-mean gaussian white noise of unit intensity, we first design an unweighted H_2 controller that is more related to classical LQG design technique. This control design is based on the generalized plant with exogenous inputs $w = [n \;\; w_n]^T$ and outputs $z = \begin{bmatrix} z_1 & z_2^T \end{bmatrix}^T$. Thus, the gust vector generator FG_w is embedded in the generalized plant P. For regular $\mathcal{H}_2$ control design, we used the weighting functions $W_1 = 1$ and $W_u = 1$. Closed-loop performance is indirectly specified by G_w. For instance, choosing $\sigma_w = 7m/s$ and $L_w = 580m$ in G_w for simulation purposes, we obtain a gust that has most of its power concentrated in the frequency band [0.1, 6] Hz. The objective of the $\mathcal{H}_2$ controller design is to minimize

$$\|T_{wz}\|_2 = \left[\frac{1}{2\pi} \int_{-\infty}^{\infty} \mathrm{Tr}\{T_{wz}^*(j\omega) T_{wz}(j\omega)\} d\omega \right]^{\frac{1}{2}} \tag{2.87}$$

the $\mathcal{H}_2$ norm of T_{wz}, over all finite-dimensional, linear time-invariant stabilizing controllers $K(s)$. Assuming that $z(t)$ is ergodic, its average power is then minimized as

$\lim_{T\to\infty} \frac{1}{2T} \int_{-T}^{T} \|z(t)\|^2 dt = E\left\{ \|z(t)\|^2 \right\} = \|T_{wz}\|_2^2$. This has the effect of decreasing the $\mathcal{H}_2$ norm of sub matrices of T_{wz} by virtue of the fact that $\left\| \begin{bmatrix} G_1 & G_2 \end{bmatrix} \right\|_2^2 = \|G_1\|_2^2 + \|G_2\|_2^2$. For example, the closed-loop vertical acceleration of the aircraft can be written in terms of the uncorrelated white noises n and w_n as follows:

$$y = T_{wy} w = T_{ny} n + T_{w_n y} w_n \tag{2.88}$$

The H_2 norms of the transfer matrices T_{ny} and $T_{w_n y}$ satisfy $\|T_{ny}\|_2^2 + \|T_{w_n y}\|_2^2 \le \|T_{wz}\|_2^2$. The H_2 controller obtained had 20 states and achieved $\|T_{wz}\|_2 = 0.2$. Figure 2.14(a) shows the spectral norms of $T_{ny}(j\omega)$ and $T_{w_{n1}y}(j\omega)$ with the H_2 controller for comparison with the other controllers.

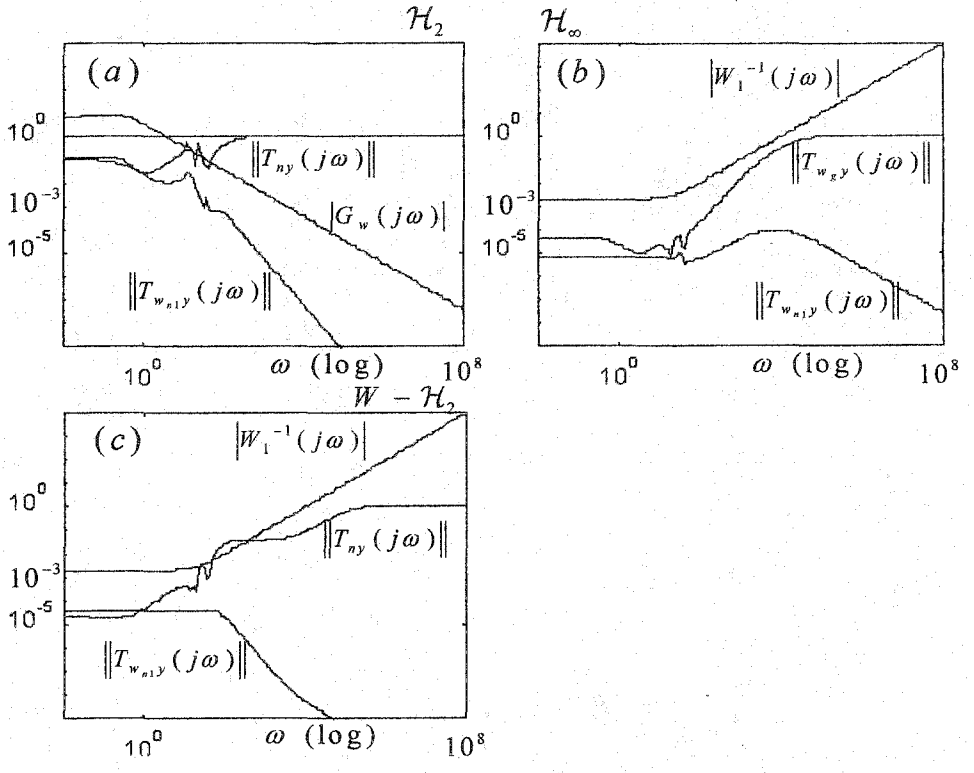

Figure 2.15: Norms of closed-loop transfer matrices

2.9.6 WEIGHTED H_2 AND H_∞-OPTIMAL CONTROL

2.9.6.1 Weighted H_2 Controller

In order to improve the performance obtained with the regular $\mathcal{H}_2$ controller, we introduce a performance weighting function

$$W_1(s) = \frac{k_1}{a_0 s + 1} \tag{2.89}$$

on the acceleration y, with $k_1 = 500$, $a_0 = 0.05$. This weighting function is the same as the one used for the $\mathcal{H}_\infty$ design in order to compare the results obtained for both controllers. We obtained $\|T_{wz}\|_2 = 1.5$ with the weighted- $\mathcal{H}_2$ controller, which means that $\|W_1 T_{ny}\|_2^2 + \|W_1 T_{w_n y}\|_2^2 \le 2.25$. Figure

2.15(c) shows that the weighting function led to much better GLA performance at low frequencies by trading off sensor noise rejection, which deteriorated slightly, but remained acceptable.

2.9.6.2 H_∞-Optimal Design

As gusts act over a relatively short period of time, they can be considered as signals with finite energy. Such signals can have spectral contents similar to the *PSD* of stochastic Dryden gust signals by using $G_w(s)$ as a filter. This remark provides motivation for $\mathcal{H}_\infty$ GLA control design as $\min_{K\in S}\max_{w\in W}\|T_{wz}w\|_2 = \min_{K\in S}\max_{n\in N}\|T_{wz}G_w n\|_2 = \min_{K\in S}\|T_{wz}G_w\|_\infty$ where S is the set of all stabilizing controllers.

2.9.6.2.1 Weighting functions for nominal performance

The specification is that our controller has to be able to regulate the vertical acceleration in the gust bandwidth with an amplitude attenuation of at least -54 dB (500). The closed-loop vertical acceleration of the aircraft can be written in terms of the gust vector w_g and the noise w_n:

$$y = T_{w_g y}w_g + T_{w_n y}w_n \tag{2.90}$$

The gust alleviation performance specification on $\|T_{w_g y}(j\omega)\|$ can be enforced through the use of a weighting function W_1 of magnitude at least 500 over [0.1, 6] Hz, as long as we get $\|W_1 T_{w_g y}\|_\infty < 1$ with the controller K, which implies

$$\|T_{w_g y}(j\omega)\| < |W_1(j\omega)|^{-1} \tag{2.91}$$

The weighting function is as given in (2.22). A plot of $|W_1(j\omega)|^{-1}$ is shown in Figure 2.15(b)(c). The controller outputs consist of deflection angles (in radians) of the aircraft's elevators and horizontal canards. In order to keep these angles within acceptable limits, we used a suitable weighting function W_u on u such that $\|W_u T_{wu}\|_\infty < 1$. The weighting function W_u is a constant diagonal matrix $W_u = \text{diag}\{k_{u_1}, k_{u_2}\}$ so that the above H_∞-norm condition implies

$$\|T_{wu1}(j\omega)\| < k_{u_1}^{-1} \tag{2.92}$$

and

$$\|T_{wu2}(j\omega)\| < k_{u_2}^{-1} \tag{2.93}$$

where $T_{wu} = \begin{bmatrix} T_{wu1} \\ T_{wu2} \end{bmatrix}$. Here $k_{u_1}^{-1} = 0.2$, $k_{u_2}^{-1} = 0.5$ are the maximum allowed control gains in closed loop. It is preferable to use a constant weighting matrix for this application, since it does not increase the order of $P(s)$. Hence, the resulting H_∞ controller has a lower order.

2.9.6.2.2 H_∞ optimal Controller

The overall objective in this H_∞ controller design was to minimize $\|T_{wz}\|_\infty$ over all finite-dimensional, linear time-invariant stabilizing controllers $K(s)$, in order to get $\|T_{wz}\|_\infty < 1$. This would guarantee that the performance specification is satisfied. A norm of $\|T_{wz}\|_\infty = 0.68$ was achieved. Figure 2.15 shows that our H_∞ controller meets the GLA performance specification given above. We can see that the maximum singular value of $T_{w_g y}$ is well below 10^{-5} over $2\pi[0.1, 6]$ rd / s. The spectral norms of the frequency responses of T_{wu1} and T_{wu2} satisfy the constraints of (2.91), (2.92) and (2.93) respectively.

2.9.6.3 μ – controller

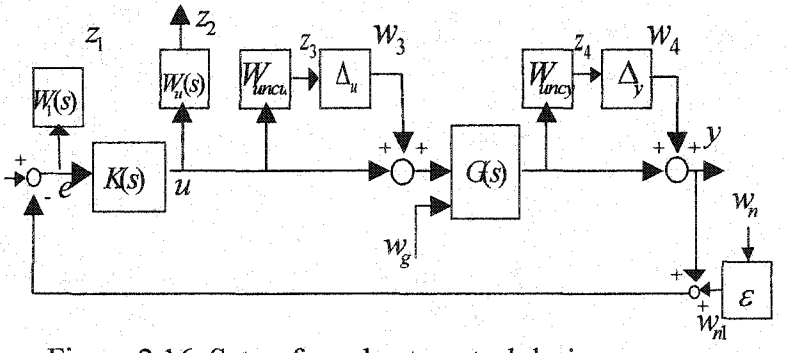

Figure 2.16. Setup for robust control design

The H_∞ controller design of the previous section provides nominal performance. That is, performance is guaranteed only if the model represents the aircraft's dynamics perfectly, which is clearly too optimistic. In this section, uncertainty in the frequency responses of the actuators and sensors is taken into account in the model and the controller design. Note that this uncertainty may also include

variations in the aerodynamics of the control surfaces, which may be caused by changes in altitude and velocity of the aircraft. As shown in Figure 2.16, we include two complex multiplicative uncertainty blocks in the model: $\Delta_u := \text{diag}\{\Delta_{u1}, \Delta_{u2}\}$, $\Delta_{u1}, \Delta_{u2} \in \mathbb{C}$ and $\Delta_y \in \mathbb{C}$. These perturbations represent the uncertainty in the frequency responses of the actuators and the sensor, respectively. We chose the corresponding weighting functions to be:

$$W_{unu} = \begin{bmatrix} \frac{0.75s+50}{s+400} & 0 \\ 0 & \frac{0.75s+22.5}{s+400} \end{bmatrix} \tag{2.94}$$

$$W_{uncy} = \frac{0.15s+30}{s+1000} \tag{2.95}$$

These weighting functions are selected such that the magnitudes of their frequency responses represent the maximum error in the actuators and sensor models at each frequency. Typically, multiplicative perturbations are small at low frequencies and rise towards or above one at high frequencies. The weighting functions can be obtained by finding an upper bound on several Bode plots of possible perturbations. For example, suppose that an uncertain, parameterized model $G_s(p,s)$ of the sensor is available, where p is the vector of parameters with known bounds. Then, one can fit a weighting function $W_{uncy}(j\omega)$ such that its magnitude is a tight upper bound of all the plots of $|G_s(p_i, j\omega) - 1|$ for $i = 1,\ldots,M$, where p_i is a set of parameters within their bounds. The weighting functions can also be obtained from experimental frequency-response input-output data.

One must keep in mind that these weights represent the size of the uncertainty and should thus be seen as hard constraints, not design parameters. It is the performance weighting functions that may be changed until a good robustness/performance tradeoff is obtained in the design.

The block diagram of Figure 2.16 can be recast into the general $\mu-$synthesis setup as given by Figure 2.9. Define the complex structured uncertainty set

$$\Omega := \left\{\Delta = \text{blockdiag}\left\{\Delta_{u1}, \Delta_{u2}, \Delta_y\right\} : \Delta_{u1}, \Delta_{u2}, \Delta_y \in \mathbb{C}\right\} \subset \mathbb{C}^{3\times 3} \tag{2.96}$$

and the augmented structured uncertainty set

$$\Gamma := \left\{\Delta_s = \text{blockdiag}\left\{\Delta, \Delta_p\right\} : \Delta \in \Omega, \Delta_p \in \mathbb{C}^{4\times 3}\right\} \subset \mathbb{C}^{7\times 6} \tag{2.97}$$

where $\Delta_p \in \mathbb{C}^{4\times 3}$ is a fictitious uncertainty linking the exogenous inputs $\begin{bmatrix} w_g & w_n \end{bmatrix}^T$ to the output variables $\begin{bmatrix} z_1 & z_2 \end{bmatrix}^T$. This fictitious perturbation is included to transform a robust performance design problem into an equivalent robust stability problem, which is easier to solve [Bal95] as explained earlier. The inputs and outputs of the structured uncertainty $\Delta_s(s) \in H_\infty, \Delta_s(j\omega) \in \Gamma$ in Figure 2.9 are, respectively, the vectors $z_s = \begin{bmatrix} z_3^T & z_4 & z_1 & z_2^T \end{bmatrix}^T \in \mathbb{R}^6$ and $w_s = \begin{bmatrix} w_3^T & w_4 & w_g^T & w_n \end{bmatrix}^T \in \mathbb{R}^7$.

A robust controller design based on μ_Γ (which is the structured singular value with respect to the uncertainty structure Γ) is less conservative than a robust H_∞ design (not to be confused with our H_∞ controller of the previous section which is optimal for the nominal model, but was not designed to be robust to model uncertainty). This is because the structured uncertainty Δ_s is taken into account as a full block of uncertainty in a typical robust H_∞ design.

We used the D-K iteration [Bal95] algorithm to design the $\mu-$controller able to give the best robust performance level[Aou2000b].

2.9.6.4 Simulation results

We used the Dryden model with parameters σ_w=7 m/s, $L_w = 580m$ to generate severe wind gust signals for simulation purposes. Figure 2.17(a),(b),(c) shows the resulting gust signals. The open-loop vertical acceleration response of the B-52 to these gust signals is shown in Figure 2.17(d).

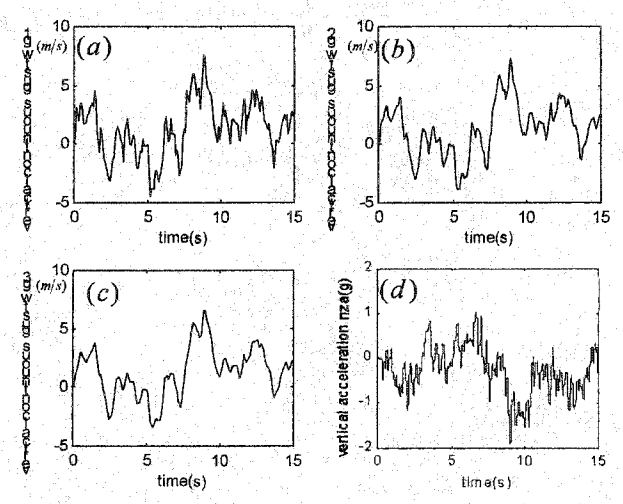

Figure 2.17: Gust signals and open-loop response

Figure 2.15(a) shows a magnitude plot of the frequency response of the Dryden filter for the simulation. We see that the performance specification enforced by the weighting function W_1 used for the weighted-H_2 and H_∞ controllers (Figure 2.15(b)(c)) should result in efficient gust alleviation. Time-domain simulations were conducted and results are presented below. The results shown in Figure 2.18(a)(b) confirm that the H_∞ controller can dramatically reduce the effect of wind gusts on the vertical acceleration of the aircraft for the nominal model. This controller also seems suitable from the point of view of control effort. From Figure 2.18(a), it can be seen that the elevator angle remained within ± 0.25 radians ($\pm 14^\circ$) in the simulation. The H_∞ controller gave the best GLA performance without exciting the flexible modes of the model or generating large control angles that could saturate the control surfaces. A comparison of peak vertical accelerations with the H_∞ controller (Figure 2.18(b)) and without any feedback control (Figure 2.17(d)) indicates that the H_∞ controller reduced the acceleration by a factor of 10^5. This could translate into dramatic improvements in flight comfort and reduced airframe loads.

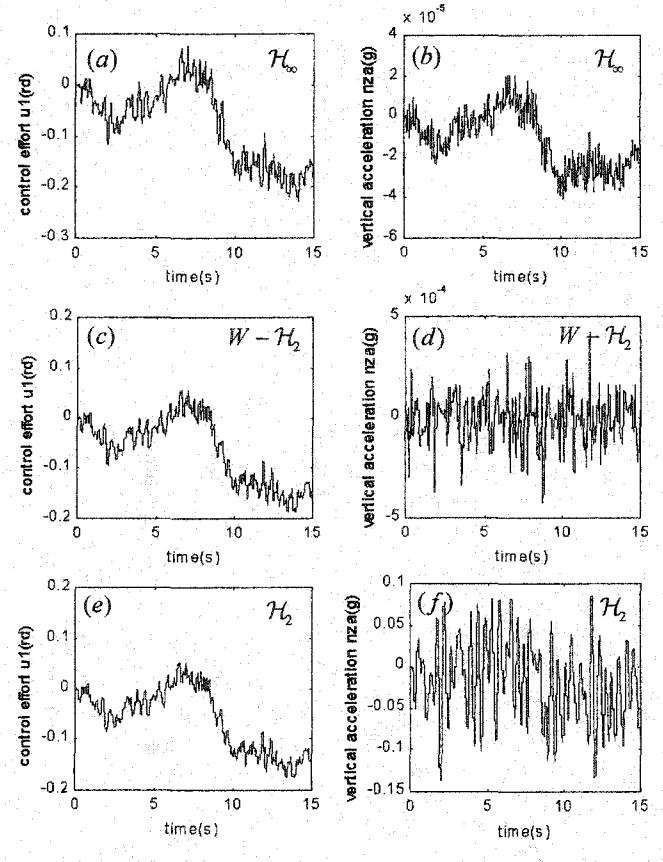

Figure2.18: Simulation results

In contrast to the H_∞ controller, the H_2 controller only reduced the peak acceleration by a factor of 14 as seen in Figure 2.18(f).

A significant performance improvement was obtained over regular H_2 by using a weighted-H_2 control approach, as evidenced by Figure 2.18 (d). The performance obtained with the weighted-H_2 controller is more comparable to the performance of the H_∞ controller, although still about 20 times worse in terms of peak acceleration. The $\mathcal{H}_\infty$ controller appeared to control the flexible modes better, which is not surprising in view of its low closed-loop $\left\|T_{w_g y}(j\omega)\right\|$ in the frequency range of the flexible modes (see Figure 2.15(b)).

Figure 2.19 below shows the magnitude of the weighting functions $W_{uncu}(s) = \begin{bmatrix} W_{uncu1}(s) & 0 \\ 0 & W_{uncu2}(s) \end{bmatrix}$, $W_{uncy}(s)$. These weighting functions specify the amount of uncertainty in the actuators and the sensor, respectively. We specified nearly 20% of uncertainty at low frequencies for the first actuator (elevator) and around 8% of uncertainty for the second actuator (horizontal canard). For the sensor we assumed an uncertainty of 3.5% at low frequencies. These uncertainties grow with frequency until they reach a constant level at high frequencies.

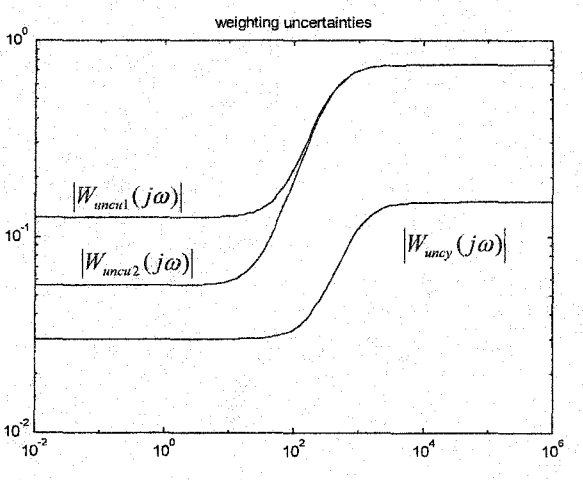

Figure 2.19: Norm bounds for uncertainties

Our μ controller obtained using D-K iteration reached the robust performance specified. Figure 2.20 shows the $\mu-$bounds for the controller obtained in the second D-K iteration. The maximum of the upper bound for μ across frequencies is equal to 0.792, and therefore robust performance was achieved.

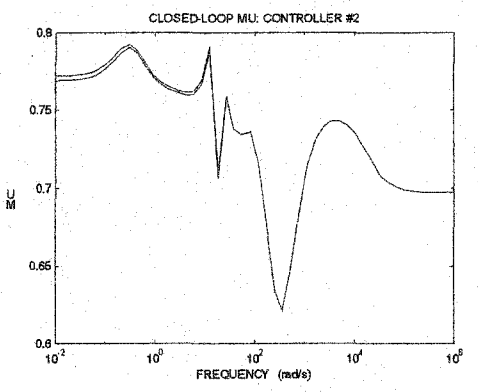

Figure 2.20: Upper and lower bounds on μ for μ design

An H_∞ controller designed for the model with uncertainties led to an maximum norm of the frequency response of the closed-loop system equal to 15.35. This is too high and hence unacceptable from a robust performance point of view. A $\mu-$analysis was done for the H_∞ controller and the results are shown in Figure 2.21. It is seen that the maximum of μ obtained with the H_∞ controller is equal to 3.1.This value being much larger than one confirms the loss of robust performance.

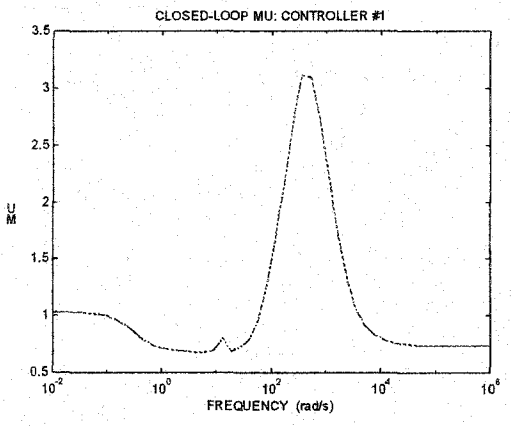

Figure 2.21 Upper and lower bounds on μ, $\mathcal{H}_\infty$ design

This was expected because the H_∞ design is unable to take into account the structure of the uncertainty as opposed to the $\mu-$design.

Chapter 3

Order reduction techniques for flexible aircraft

3.1 Introduction

High-order plant models make robust control design techniques difficult to use and often lead to conservative results. Although controllers satisfying the performance specifications could be obtained, the resulting high-order controllers would be difficult to implement. Thus, order reduction methods have to be considered, especially for flexible systems that generally are of high order. In the literature, starting from [Ske80], [Enn84a], [Enn84b], [Glo84] going to [Ske90], [Wor94], [Godd93], [Beck96], methods have been proposed for either model order reduction or controller reduction. These methods use open-loop or closed-loop performance criteria. In this chapter, we give an overview of a few well-developed order reduction methods, and we propose new approaches adapted to our main problem of interest, namely order reduction of flexible dynamics through modal truncation.

3.2 Open-loop order reduction methods

The objective in these methods is to obtain either a reduced order model or controller that has an input/output behavior close to that of the full-order system considered. Different approaches have been proposed in the past to guarantee a minimum error between the reduced-order system and the full-order system based on various measures of the closeness of these systems. We describe in the following, proven, efficient reduction methods that appeared in the literature.

3.2.1 Algebraic dominance [Woe85]

Consider the stable transfer matrix $G(s)$ of the system to be reduced as:

$$G(s) = \left[\begin{array}{c|c} A & B \\ \hline C & 0 \end{array}\right], \quad y = C(sI - A)^{-1}Bu \tag{3.1}$$

Any transfer function linking the kth output to the jth input can be written as follows:

$y_k = G_{kj}(s)u_j = \left[\sum_{i=1}^{n} G_{kj}(s)^{(i)}\right]u_j$ where $G_{kj}(s)^{(i)}$ is the contribution of mode i to the transfer function $G_{kj}(s)$.

Let us define: $\lim_{t\to 0} y_k(t) = \lim_{s\to\infty} \sum_{i=1}^{n} sG_{kj}(s)^{(i)} = \sum_{i=1}^{n} R_{kj}^{(i)}$ where the coefficient $R_{kj}^{(i)}$ represents the contribution of mode *I* to the inial value of the output due to an input $u_j(s) = 1$, i.e., $u_j(t) = \delta(t)$.

$\lim_{t\to\infty} y_k(t) = \lim_{s\to 0} \sum_{i=1}^{n} G_{kj}(s)^{(i)} = \sum_{i=1}^{n} S_{kj}^{(i)}$ where $S_{kj}^{(i)}$ is a static gain and represents the steady state contribution of mode i due to an input $u_j(s) = 1/s$.

For example, if we assume that $G_{kj}(s)^{(i)} = \dfrac{As+B}{s^2 + 2\zeta_i\omega_i s + \omega_i^2}$ then $R_{kj}^{(i)} = A$ and the static gain $S_{kj}^{(i)} = B/\omega_i^2$.

In this proposed method, we associate the modal dominance parameter $D_i = \max_{k,j} \left|F_{kj}^{(i)}\right|$, where $F_{kj}^{(i)} = R_{kj}^{(i)}$ or $S_{kj}^{(i)}$, to mode *i*. We use this parameter as a criterion for order reduction. In fact, mode *i* is kept in the model whenever D_i is larger than a threshold.

If we decompose, through each mode i, the effect from the input *u* to the output *y* as:

$$y = \left[\sum_{i=1}^{n} G(s)^{(i)}\right]u = \sum_{i=1}^{n} \left[\tilde{C}_i(sI - \tilde{A}_i)^{-1}\tilde{B}_i\right]u \tag{3.2}$$

where $\tilde{A}_i = \begin{bmatrix} -2\zeta_i\omega_i & \omega_i^2 \\ 1 & 0 \end{bmatrix}, \tilde{B}_i = \begin{bmatrix} \tilde{b}_i \\ 0 \end{bmatrix}, \tilde{C}_i = \begin{bmatrix} \tilde{c}_{i1} & \tilde{c}_{i2} \end{bmatrix}$ where $\tilde{c}_{i1}, \tilde{c}_{i2}$ are functions of the frequency mode ω_i.

In this case the modal dominance parameter is:

$$D_i = \left|F^{(i)}\right| = \begin{cases} \left|R^{(i)}\right| = \left\|\tilde{C}_i\tilde{B}_i\right\| = \left\|\tilde{c}_1\tilde{b}_i\right\| \text{ if } u(s) = 1 \\ \left|S^{(i)}\right| = \left\|-\tilde{C}_i\tilde{A}_i^{-1}\tilde{B}_i\right\| = \left\|\dfrac{\tilde{b}_i\tilde{c}_2}{\omega_i^2}\right\| \text{ if } u(s) = 1/s \end{cases} \tag{3.3}$$

3.2.2 Devillemagne-Skelton approach

Based on the approximation of the transfer matrix of the system by its series development in a frequency interval, this method was proposed in the seventies by Devillemagne-Skelton [Dev87].

This method, developed for an asymptotically stable system, does not preserve the physical meaning of the states of the full-order model. The original model $G(s)$ as given in (3.1) can be expanded around the zero frequency as :

$$G(s) = -\sum_{i=1}^{\infty} s^{i-1} C A^{-i} B \tag{3.4}$$

where at $M_i^{s0} = CA^{-i}B$ are the moments at the frequency 0.

$G(s)$ can be also expanded around the infinite frequency as:

$G(s) = -\sum_{i=1}^{\infty} \frac{1}{s^{i+1}} CA^{i}B$ where $M_i^{s\infty} = CA^{i}B$ are the moments at the frequency ∞.

The objective in this method is to be able to find a matrix transformation applied to full- order state-space system such that the reduced state-space system can recover the moment's expansion of the full order system. To make this more clear. Let suppose we have a state-space representation of a single input/single output full-order system with n modes as (A,B,C,D) then a reduced order model of order r that recovers $2r$ first low frequency moments of the full-order model expansion can be given as follows:

$$\begin{aligned} A_r &= LAR \\ B_r &= LB \\ C_r &= CR \end{aligned}$$

$$\text{where: } L = \begin{bmatrix} CA^{-r} \\ \vdots \\ CA^{-1} \end{bmatrix}, Z = \begin{bmatrix} A^{-r} & \cdots & A^{-1}B \end{bmatrix}, R = Z(LZ)^{-1}. \tag{3.5}$$

3.2.3 Cost decomposition order reduction

Assuming the asymptotic stability of the system with no direct transmission from the inputs to outputs, each component of the system, either input, output or state has an effect on the performance of the system. This effect can be measured using a quadratic criterion. In [Ske80], Skelton proposed the cost contribution of the component p_i as $V_{p_i} = 1/2 \frac{\partial V}{\partial p_i} p_i$ where V represents the total cost of the system and express an energy criterion:

$$V = \int_{t=0}^{\infty} y(t)^T Q_y y(t) dt \tag{3.6}$$

$y(t)$ is the output of the system to an impulse input.

The total cost can be easily calculated as $V = trace(X_v C' Q_y C) = trace(Y_v B Q_u B')$ where:

Q_u is a diagonal matrix related to the magnitude of the inputs, X_v and Y_v are the solutions of the following Lyapunov equations, respectively:

$$\begin{aligned} X_v A^T + A X_v + B Q_u B^T &= 0 \\ Y_v A + A^T Y_v + C^T Q_y C &= 0 \end{aligned} \tag{3.7}$$

Because our interest in the order reduction is the state of the system, we orient our cost evaluation for the components states $p_i = x_i$. The cost contribution for each state can be given as:

$$V_{x_i} = [X_v C' Q_y C]_{(i,i)} \tag{3.8}$$

For specific state-space representations, another way to calculate the global cost value can be given. If we could obtain a balanced representation of the system, then the global cost value could be obtained as:

$V = -2Tr\left\{\Sigma^2 A\right\}$ where: Σ is the diagonal matrix of singular values of A.

$$Q_y = I \text{ and } Q_u = I.$$

The objective of the reduction technique proposed in this method is to eliminate the states that have less influence on the performance of the system. Thus we discard the states that have the smallest cost value V_{x_i}. More specifically, we can propose to minimize the cost difference $\Delta V = V - V_r$ where V_r represents the global cost value of the system reduced to order r.

3.2.4 Modern, optimal order reduction techniques

The objective of model order reduction is to preserve the behavior of the outputs of the full-order model and the reduced order model subject to the same type of inputs. To do so, the reduced model is viewed as an approximation to the full-order model. This can be done as follows:

$$\min_{G_r(s) \in RH_\infty} \left\| G(s) - G_r(s) \right\|_p \tag{3.9}$$

Where p specifies the type of system norm used.

The objective then, is to find a reduced-order system $G_r(s)$ that is close enough, in terms of a specified norm, to the full-order system $G(s)$. The norms that are typically used for that approximation problem are the H_2 norm for an average approximation problem and the H_∞ norm for a minmax approximation problem.

This approximation criterion can be extended to include a desired frequency range of approximation. This can be done by minimizing a weighted approximation criterion:

$$\min_{G_r(s)\in RH_\infty} \left\| W(s)(G(s)-G_r(s)) \right\|_p \tag{3.10}$$

where $W(s)$ a weighting function that specifies the frequency interval where the minimization should be effective.

Before giving more details on modern, optimal order reduction techniques we will give a brief introduction to some concepts used later in the thesis:

a- Truncation of order *r*

Consider a nominal model of order n $G = \left[\begin{array}{c|c} A & B \\ \hline C & D \end{array}\right]$. This state-space representation can be partitioned as $G = \left[\begin{array}{cc|c} A_r & A_{rt} & B_r \\ A_{tr} & A_t & B_t \\ \hline C_r & C_t & D \end{array}\right]$ then a reduced rth order model could be defined in state space representation as: $G_r = \left[\begin{array}{c|c} A_r & B_r \\ \hline C_r & D_r \end{array}\right]$. This state-space representation can be deduced by simply applying the truncation transformation $T_r = \begin{bmatrix} I_r \\ 0_{tr} \end{bmatrix}$ to the original system, which results in:

$$G_r = \left[\begin{array}{c|c} T_r^* A T_r & T_r^* B \\ \hline C T_r & D \end{array}\right] \tag{3.11}$$

This method would give a good reduced order model if we could represent the full-order model in a modal form where the modes can effectively be decoupled ($A_{rt}, A_{tr} \approx 0$).

b- Residualization of order *r*

Let G be the full-order system as specified earlier in (3.1), then a residualization of rth order can be given in its state-space representation as:

$$G_r = \left[\begin{array}{c|c} A_r - A_{rt}A_t^{-1}A_{tr} & B_r - A_{rt}A_t^{-1}B_t \\ \hline C_r - C_t A_t^{-1} A_{tr} & D - C_t A_t^{-1} B_t \end{array}\right] \tag{3.12}$$

The residualization offers, compared to the classical truncation method, the possibility to keep the reduced system close to the full-order system in the low frequencies, generally of main interest.

3.2.4.1 Balanced reduction

Balanced reduction was first presented by Moore [Moo81] and was revisited by Glover in [Glo84], [Bal91b] and [Ske88]. Let us define a balanced realization of a system. Stability of the full-order model G is assumed. Then the controllability and observability gramians of G, denoted as P and Q respectively, are calculated. We define the balancing transformation pair (L,R), which transforms the gramians P and Q into

$$L^*PL = R^*QR = \Sigma \tag{3.13}$$

where Σ is the diagonal matrix of the ordered Hankel singular values of the system G.

The balanced realization of G is defined as follows:

$$G_{bal} = \left[\begin{array}{c|c} L^*AR & L^*B \\ \hline CR & D \end{array}\right] \tag{3.14}$$

The balanced reduction can be now defined as the truncation of the balanced realization of the full balanced model:

$$G_{r,bal} = \left[\begin{array}{c|c} L_r^*AR_r & L_r^*B \\ \hline CR_r & D \end{array}\right] \tag{3.15}$$

where

$$PL_r = R_r \begin{bmatrix} \sigma_1 & & \\ & \ddots & \\ & & \sigma_r \end{bmatrix}$$

$$QR_r = L_r \begin{bmatrix} \sigma_1 & & \\ & \ddots & \\ & & \sigma_r \end{bmatrix}.$$

It has been proven in [Glo84] that the distance of the reduced balanced realization from the nominal model can be measured in H_∞ as :

$$\left\| G - G_{r,bal} \right\|_\infty \leq 2(\sigma_{(r+1)} + \ldots\ldots + \sigma_{(n)}) \tag{3.16}$$

Using the residualization technique, a balanced residualization can be obtained starting from the balanced realization of the full-order model G_{bal}.

3.2.4.2 Mode balanced modal reduction

The modal reduction technique was discussed in many papers as [Bon82], [Dec76]. In the following, we present an overview of this technique on a balanced approach. In fact a mode-balanced reduction

begins with a balanced modal realization, followed by a truncation of the less significant modes in the dynamics.

If we assume that the nominal system G has a block diagonal A matrix, then a mode-balanced realization is given as:

$$G_{\mathrm{mode},bal} = \left[\begin{array}{cc|c} \Lambda_r & 0 & B_r \\ 0 & \Lambda_t & B_t \\ \hline C_r & C_t & D \end{array}\right] \tag{3.17}$$

where $\Lambda_r = diag\{\lambda_1,...,\lambda_r\}$ and $\Lambda_t = diag\{\lambda_{r+1},...,\lambda_t\}$.

For this balanced representation, the mode-balanced reduction is given as: $G_{r,\mathrm{mode}} = \left[\begin{array}{c|c} \Lambda_r & B_r \\ \hline C_r & D \end{array}\right]$ and the mode-balanced residualization is given as: $G_{resid,\mathrm{mode}} = \left[\begin{array}{c|c} \Lambda_r & B_r \\ \hline C_r & D - C_t\Lambda_t^{-1}B_t \end{array}\right]$.

3.2.4.3 Optimal H_2 norm reduction

As mentioned before different norms can be used to characterize the approximation in (3.10). Consider a full-order system given in its minimal state-space representation as in (3.1). The objective then is to find a reduced state-space representation of a system $G_r = \left[\begin{array}{c|c} A_r & B_r \\ \hline C_r & 0 \end{array}\right]$ solving the following minimization problem:

$$\min_{A_r,B_r,C_r} \left\| C(sI_n - A)^{-1}B - C_r(sI_r - A_r)^{-1}B_r \right\|_2 \tag{3.18}$$

The first results for the H_2 norm reduction was obtained by Wilson in [Wil70], [Wil74]. Then Hyland and Bernstein [Hyl85] proposed optimal projections that are used for the H_2 norm reduction as follows:

Compute P and Q by solving

$$\begin{aligned} \Pi_r(AP + PA^* + BB^*) &= 0 \\ (A^*Q + QA + C^*C)\Pi_r &= 0 \end{aligned} \tag{3.19}$$

where $rank(P) = rank(Q) = rank(PQ) = r$, then the optimal solution of projection (L_r, R_r) proposed is given as:

$$\begin{aligned} PQ &= R_r M L_r^* \\ L_r^* R_r &= I_r \\ \Pi_r &= R_r L_r^* \end{aligned} \tag{3.20}$$

where Π_r, M are chosen and diagonal matrices.

Finally, a reduced-order model could be obtained as $G_r = \left[\begin{array}{c|c} L_r^* A R_r & L_r^* B \\ \hline C R_r & 0 \end{array}\right]$.

3.2.4.4 Optimal Hankel-norm reduction

Optimal Hankel-norm reduction was originally developed by Glover in 1984 [Glo84] and was used also by Safonov in [Saf90]. The minimization objective of the optimal Hankel-norm reduction is:

$$\min_{G_r(s)\in RH_\infty} \|G(s)-G_r(s)\|_H \tag{3.21}$$

It was shown in [Glo84] that: $\|G(s)-G_r(s)\|_H \geq \breve{\sigma}_{r+1}(G)$ where $\breve{\sigma}$ is the Hankel singular value ($\breve{\sigma}_i = [\lambda_i(PQ)]^{1/2}$) and the norm $\|G(s)-G_r(s)\|_\infty$ using the reduced model G_r obtained from the hankel-norm reduction can be bounded by $2\sum_{i=r+1}^{n} \breve{\sigma}_i$ as the balanced reduction method presented above. The research done by Glover showed that by manipulating the D matrix of the full-order system, one can obtain $\|G(s)-G_r(s)\|_\infty \leq \sum_{i=r+1}^{n} \breve{\sigma}_i$.

3.2.4.5 H_∞ optimal reduction

Most of the research on order reduction has been based on the H_∞ norm approximation problem [Had89], [Kav93], [Kav94]. Kavranoglu in [Kav93] derived a solution to the H_∞ norm reduction problem: $\min_{G_r} \|G(s)-G_r(s)\|_\infty \leq \gamma$ for every $\gamma > \gamma_0$ (3.22)

where γ_0 is the minimum value.

In [Kav94], Kavranoglu proposed an algorithm, based on the solution of specific Riccati equations and a balancing procedure, that gives a sub-optimal solution to the problem in (3.22).

The use of LMI's in control has shown their efficiency to find solutions to complex control problems. Helmersson in [Helm95b] proposed an order reduction method that leads to the solution of a set of LMIs. He used the Hankel norm approximation, and he tried to improve the H_∞ norm of the error. Helmersson proposed that

$$\min \|G_e\|_\infty = \min \|G-G_r\|_\infty \tag{3.23}$$

is equivalent to finding the smallest γ and symmetric positive definite matrix X such that :

$$\begin{bmatrix} A_v^T X + X A_v & X B_v & C_v^T \\ B_v^T X & -\gamma I & D_v^T \\ C_v & D_v & -\gamma I \end{bmatrix} < 0 \tag{3.24}$$

where $\left[\begin{array}{c|c} A_v & B_v \\ \hline C_v & D_v \end{array}\right] = \left[\begin{array}{cc|c} A & 0 & B \\ 0 & A_r & B_r \\ \hline C & -C_r & D - D_r \end{array}\right]$

By partitioning X as $X = \begin{bmatrix} X_{11} & X_{12} \\ X_{12}^T & X_{22} \end{bmatrix} > 0$ then the inequality (3.24) can be written as:

$$\begin{bmatrix} A^T X_{11} + X_{11} A & A^T X_{12} + X_{12} A_r & X_{11} B - X_{12} B_r & C^T \\ A_r^T X_{12}^T + X_{12}^T A & A_r^T X_{22} + X_{22} A_r & X_{12}^T B - X_{22} B_r & C_r^T \\ B^T X_{11} - B_r^T X_{12}^T & B^T X_{12} - B_r^T X_{22} & -\gamma I & D^T - D_r^T \\ C & C_r & D - D_r & -\gamma I \end{bmatrix} < 0 \tag{3.25}$$

Helmersson proposed an iterative algorithm to solve the minimization problem in (3.23) through the solution of the LMI in (3.24).

Based on the reduced model, $G_r = \left[\begin{array}{c|c} A_r & B_r \\ \hline C_r & D_r \end{array}\right]$, obtained from Hankel-norm reduction, we keep the matrices A_r and B_r constant and solve the LMI in (3.25) by minimizing γ with variables X, C_r and D_r. Keeping X_{12} and X_{22} in (3.24) and minimizing γ we obtain a solution $X_{11}, A_r, B_r, C_r, D_r$. These last two steps can be repeated until one could obtain an acceptable approximation error: $\|G - G_r\|_\infty$.

3.2.5 Weighted order reduction

The general problem of a weighted order reduction can be posed as:

$$\min_{G_r(s) \in RH_\infty} \|W(s)(G(s) - G_r(s))V(s)\|_p \tag{3.26}$$

Where $V(s)$ and $W(s)$ are input and output weighting matrices. Minimization of the Hankel-norm, the H_2 norm and the H_∞ norm can be extended to the weighted order reduction problem. Worterboer [Wor94] gave necessary conditions for the extension of Hankel-norm approximation and extended his iterative algorithm of H_2 norm for the weighted approximation case. Perhaps the best-known method used for the weighted order reduction problem is the balanced truncation method. Enns in 1984 [Enn84a], [Enn84b] was the first to extend the balanced reduction problem to a weighted case.

Consider the state space representations: $G=\left[\begin{array}{c|c} A & B \\ \hline C & 0 \end{array}\right], V_i=\left[\begin{array}{c|c} A_i & B_i \\ \hline C_i & D_i \end{array}\right], W_o=\left[\begin{array}{c|c} A_o & B_o \\ \hline C_o & D_o \end{array}\right]$ where the order of the nominal system is n, then

$$W_oGV_i=\left[\begin{array}{ccc|c} A & 0 & BC_i & BD_i \\ B_oC & A_o & 0 & 0 \\ 0 & 0 & A_i & B_i \\ \hline D_oC & C_o & 0 & 0 \end{array}\right]:=\left[\begin{array}{c|c} \overline{A} & \overline{B} \\ \hline \overline{C} & 0 \end{array}\right] \tag{3.27}$$

Consider $\overline{P}$ and $\overline{Q}$ the solutions of the Lyapunov equations: $\begin{array}{l} \overline{A}\overline{P}+\overline{P}\overline{A}^*+\overline{B}\overline{B}^*=0 \\ \overline{Q}\overline{A}+\overline{A}^*\overline{Q}+\overline{C}^*\overline{C}=0 \end{array}$. The input and output weighted gramians P and Q can be calculated as:

$$P=[I_n \quad 0]\overline{P}\begin{bmatrix} I_n \\ 0 \end{bmatrix}, Q=[I_n \quad 0]\overline{Q}\begin{bmatrix} I_n \\ 0 \end{bmatrix}.$$

Consider a nonsingular matrix T such that: $TPT^*=(T^{-1})^*QT^{-1}=\begin{bmatrix} \Sigma_1 & 0 \\ 0 & \Sigma_2 \end{bmatrix}$ where $\Sigma_1=diag(\sigma_1,...,\sigma_r), \Sigma_2=diag(\sigma_{r+1},...,\sigma_n)$. This transformation T leads to a balanced sate-space representation of the nominal system as: $\left[\begin{array}{c|c} TAT^{-1} & TB \\ \hline CT^{-1} & 0 \end{array}\right]=\left[\begin{array}{cc|c} A_{11} & A_{12} & B_1 \\ A_{21} & A_{22} & B_2 \\ \hline C_1 & C_2 & 0 \end{array}\right]$ and then a reduced order model of order r, can be obtained as: $G_r=\left[\begin{array}{c|c} A_{11} & B_1 \\ \hline C_1 & 0 \end{array}\right]$.

3.3 Closed-loop order reduction

The techniques proposed earlier deal with open-loop order reduction but do not take into account the performance objectives of the closed-loop system. The order reduction of a closed-loop system means either a reduction of the plant or the controller designed while keeping an acceptable level of performance of the nominal closed-loop system. Much research effort has been directed towards obtaining a systematic methodology for closed-loop order reduction [Hay90], [Har94]. Standard ways to achieve this include: reducing the model order, and based on the achieved reduced order model, design a reduced-controller; reducing the full-order controller designed based on the full-order model; and starting from a full-order model, directly design a reduced-order controller. The first method of closed-loop order reduction presented above is probably the most frequently cited in the literature. However there is a danger to have the reduced-controller, designed based on the dominant modes of the system, destabilize the full-order system.

Consider the standard optimal setup of Figure2.2 where G represents the nominal model of the system without the performance weighting functions. The closed-loop system is written as a combination of the model and the controller: $\Im(G,K)$. The order of the closed-loop system is then given by the order of the plant n_G plus the order of the controller n_K. The transfer matrix $\Im$ can be written in terms of G and K as $\begin{bmatrix} SG & S-I \\ S-I & SK \end{bmatrix}$ where $S=(I+GK)^{-1}$ is the sensitivity matrix.

3.3.1 LQG and H_∞ balanced reduction

The LQG balanced reduction uses results obtained by Jonckheere in [Jonc83] and assumes that the controller designed for the nominal plant G is an unweighted H_2 controller, known as the normalized LQG controller. This controller, which minimizes the H_2 norm of the closed loop system $\Im$, has a state-space representation as:

$$K_{LQG}=\left[\begin{array}{c|c} A-BB^*\theta-\Phi C^*C & \Phi C^* \\ \hline -B^*\theta & 0 \end{array}\right] \tag{3.28}$$

where Φ and θ are the solutions of the Riccati equations:

$$\begin{aligned} A\Phi+\Phi A^*+BB^*-\Phi C^*C\Phi=0 \\ A^*\theta+\theta A+C^*C-\theta BB^*\theta=0 \end{aligned} \tag{3.29}$$

The matrices Φ and θ are related to the closed loop gramians $P_\Im$ and $Q_\Im$ by:

$$\begin{aligned} P_\Im&=\begin{bmatrix}\Phi & 0\\ 0 & 0\end{bmatrix}+\begin{bmatrix}I\\ I\end{bmatrix}\Omega\begin{bmatrix}I & I\end{bmatrix} \\ Q_\Im&=\begin{bmatrix}\theta & 0\\ 0 & 0\end{bmatrix}+\begin{bmatrix}I\\ -I\end{bmatrix}\Psi\begin{bmatrix}I & -I\end{bmatrix} \end{aligned} \tag{3.30}$$

where

Ω is the controllability gramian of $\left[\begin{array}{c|c} A-BB^*\theta & \Phi C^* \\ \hline . & . \end{array}\right]$

Ψ is the observability gramian of $\left[\begin{array}{c|c} A-\Phi C^*C & . \\ \hline B^*\theta & . \end{array}\right]$

An LQG balanced realization is obtained by finding a transformation matrix pair (L,R) that yields $\Phi=\theta=diag(\varphi)$ where $\varphi=diag(\sqrt{\lambda(\Phi\theta)})$. This transformation pair can be applied to either the

plant or the controller to get their respective balanced realization. Finally, a reduced rth order model or controller is deduced by truncating the states that are less important according to the balanced gramians $\Phi = \theta$.

The results obtained for the LQG type of controller can be extended to the case of H_∞ type of control as given in [Must89]. The controller design is based on the minimum entropy H_∞ solution, which is not optimal, but gives a bound $\gamma > \gamma_0$ on the H_∞-norm of the closed-loop system $\mathfrak{I}(G,K)$. However, this controller can be calculated in one step, as opposed to the classical H_∞ controller.

Following the same methodology of LQG balanced reduction; the matrices Φ and θ used for the balancing procedure are calculated for this case as:

$$\begin{aligned} A^*\theta + \theta A - (1-\gamma^{-2})\theta BB^*\theta + C^*C = 0 \\ A\Phi + \Phi A^* - (1-\gamma^{-2})\Phi C^*C\Phi + BB^* = 0 \end{aligned} \tag{3.31}$$

Once these matrices are obtained, an H_∞ balanced reduction of the plant or the controller is possible.

3.3.2 Closed-loop balanced reduction

Much research has been conducted to develop normalized balanced reduction for closed-loop system [Wor93], [Cet93]. Wortelboer in [Wor94] was inspired from the work of Enns [Enn84b] on frequency-weighted reduction presented earlier. He extended this approach to the closed-loop system case. Let us note the controllability and observability gramians of the closed loop system $\mathfrak{I}(G,K)$ are: $P_{\mathfrak{I}}$ and $Q_{\mathfrak{I}}$ then P_G and Q_G are the gramians of G that can be deduced from the gramians of the closed-loop system. Similarly, P_K and Q_K are the gramians of the controller.

Define the Hankel singular values of the sub-systems G and K in the closed loop system as:

$$\begin{aligned} \breve{\sigma}_G &= \sqrt{\lambda(P_G Q_G)} \\ \breve{\sigma}_K &= \sqrt{\lambda(P_K Q_K)} \end{aligned} \tag{3.32}$$

Remark that in general: $\breve{\sigma}_G, \breve{\sigma}_K \not\subset \breve{\sigma}_{\mathfrak{I}}$ where $\breve{\sigma}_{\mathfrak{I}}$ are the Hankel singular values of the closed-loop system $\mathfrak{I}(G,K)$.

Note that $\breve{\sigma}_G$ and $\breve{\sigma}_K$ are independent of the realizations $G(s)$ and $K(s)$. By partitioning the controllability and observability gramians of the closed-loop system according to the sub-systems G and K as follows:

$$P_{\Im} = \begin{bmatrix} P_G & P_{GK} \\ P_{GK}^* & P_K \end{bmatrix}, Q_{\Im} = \begin{bmatrix} Q_G & Q_{GK} \\ Q_{GK}^* & Q_K \end{bmatrix} \tag{3.33}$$

The balanced model realization can be obtained by finding the pair (L,R) that yields to $P_G = Q_G = diag(\sigma_G)$. Similarly for the controller, the objective is to find a pair (L,R) to have $P_K = Q_K = diag(\sigma_K)$. Note that the gramians of the closed-loop system using the balanced realizations G_{bal} and K_{bal}, have the following structure:

$$P_{\Im,bal} = \begin{bmatrix} \cdot & & & - & - & - \\ & \sigma_G & & - & - & - \\ & & \cdot & - & - & - \\ - & - & - & \cdot & & \\ - & - & - & & \sigma_K & \\ - & - & - & & & \cdot \end{bmatrix}, Q_{\Im,bal} = \begin{bmatrix} \cdot & & & - & - & - \\ & \sigma_G & & - & - & - \\ & & \cdot & - & - & - \\ - & - & - & \cdot & & \\ - & - & - & & \sigma_K & \\ - & - & - & & & \cdot \end{bmatrix} \tag{3.34}$$

Where (-) means ignored terms.

The balanced reduction can be carried out on either the plant G or the controller K as used in the open-loop balanced reduction technique.

In [Wor94] an explicit link between the closed-loop balanced reduction and the frequency-weighted balancing procedure has been established. In fact, it has been shown that taking the weighting transfer matrices as $W_0 = \begin{bmatrix} S \\ KS \end{bmatrix}, W_i = \begin{bmatrix} S & SK \end{bmatrix}$ in the frequency-weighted balanced reduction developed by Enns will lead to the closed-loop balanced reduction presented above.

3.3.3 Closed-loop performance preserving controller reduction methods

The closed-loop reduction methods presented above have no explicit link to the performance degradation of the closed-loop system, except some of the results obtained by wortelboer in [Wor94]. As explained earlier a closed-loop system reduction can be either carried out as a reduction of the controller, the plant or both. In the following, we describe a few additional methods for controller reduction, which preserve the level of performance of the closed-loop system. Anderson and Liu [And89] extended Enn's approach to find weighting functions for the controller reduction problem that can maintain closed-loop performance. The more recent reduction methods guarantee the preservation of closed-loop stability and performance, especially for controller reduction techniques. Goddard and Glover [Godd93], [Godd98] developed sufficient conditions to design a stabilizing

reduced-order controller achieving a preserved level of performance. This work was based on the following idea: Given a full-order controller K_f achieving the performance level $\gamma := \left\| \mathcal{F}_L(P, K_f) \right\|_\infty$, and selecting $\gamma_1 > \gamma$, weighting functions W_1, W_2 are derived such that

$$\left\| W_2^{-1}(K_r - K_f)W_1^{-1} \right\|_\infty < 1 \Rightarrow \left\| \mathcal{F}_L(P, K_r) \right\|_\infty < \gamma_1 \tag{3.35}$$

Where K_r is the reduced-order controller, P is the nominal full-order generalized plant model, and $\mathcal{F}_L(P, K_r) := P_{11} + P_{12}\left(I - K_r P_{22}\right)^{-1} K_r P_{21}$ is the lower linear fractional transformation whose $\mathcal{H}_\infty$-norm should be kept small. The work of Lenz in [Len88a], [Len88b] proposed a choice of weighting functions for controller reduction in an H_∞ framework. The sufficient condition proposed is as follows: $\left\| W_2^{-1}(K_r - K_f)W_1^{-1} \right\|_\infty < 1/\sqrt{2} \Rightarrow \left\| F_L(P, K_r) \right\|_\infty < \sqrt{2}\gamma_1$. This means that given a frequency weighted error less than $1/\sqrt{2}$ then H_∞ performance is degraded by at most a factor of $\sqrt{2}$. Goddard improved the bound on closed-loop performance obtained by Lenz. He proposed a perturbed form of the controller. For an additive perturbation, $K = K^0 + W_2 \Delta W_1$, $\Delta \in \Re H_\infty$, where K^0 is a nominal controller. For coprime factor perturbation case $\begin{bmatrix} \tilde{U} & \tilde{V} \end{bmatrix} = \begin{bmatrix} \tilde{U}_0 & \tilde{V}_0 \end{bmatrix} + W_2 \begin{bmatrix} \Delta_{\tilde{U}} & \Delta_{\tilde{V}} \end{bmatrix} W_1$ where $K = \tilde{V}^{-1}\tilde{U}$, $K^0 = \tilde{V}_0^{-1}\tilde{U}_0$ and $\Delta = \begin{bmatrix} \Delta_{\tilde{U}} & \Delta_{\tilde{V}} \end{bmatrix}, \Delta \in RH_\infty$. A set of weighting functions W_1 and W_2 proving the existence of a reduced stabilizing controller has been found in [Godd98]. For the closed-loop performance preservation, a theorem, which was the basis of the solution provided by Goddard, has been presented in [Godd98]. It says that for any well-dimensioned $F_l(N, Q)$, where $N = \begin{bmatrix} N_{11} & N_{12} \\ N_{21} & N_{22} \end{bmatrix}$, assuming the feedback is well posed; and if N_{21} has full row rank (N_{12} has full column rank) with $N^{\sim}N = I$ ($NN^{\sim} = I$), where $N^{\sim}(s) = N^T(-s)$, then $\left\| F_l(N, Q) \right\|_\infty < 1$ if and only if $\left\| Q \right\|_\infty < 1$. Structures have been proposed to transform the closed-loop system analysis of $F_l(G, K)$ into an analysis of $F_l(\tilde{R}, \Delta)$ where $\tilde{R} = \begin{bmatrix} \gamma^{-1/2} I & 0 \\ 0 & W_1 \end{bmatrix} \begin{bmatrix} R_{11} & R_{12} \\ R_{21} & R_{22} \end{bmatrix} \begin{bmatrix} \gamma^{-1/2} I & 0 \\ 0 & W_2 \end{bmatrix}$ and $R = \begin{bmatrix} R_{11} & R_{12} \\ R_{21} & R_{22} \end{bmatrix}$ is the redheffer star product $\mathbb{S}\left(G, \begin{bmatrix} K^0 & I \\ I & 0 \end{bmatrix} \right)$ ($\mathbb{S}\left(G, \begin{bmatrix} K^0 & \tilde{V}_0^{-1} \\ I & 0 \\ -K^0 & -\tilde{V}_0^{-1} \end{bmatrix} \right)$ for the coprime factor case). Note that $R = \mathbb{S}(G, K) = \begin{bmatrix} F_l(G, K_{11}) & G_{12}(I - K_{11}G_{22})^{-1}K_{12} \\ K_{21}(I - G_{22}K_{11})^{-1}G_{21} & F_u(K, G_{22}) \end{bmatrix}$ such that

$G=\begin{bmatrix} G_{11} & G_{12} \\ G_{21} & G_{22} \end{bmatrix}, K=\begin{bmatrix} K_{11} & K_{12} \\ K_{21} & K_{22} \end{bmatrix}$. Δ is the additive uncertainty or the coprime factor uncertainty on the controller, depending on the case considered. Using the results of the theorem presented above and the structures proposed, the following can be proven:

$$\begin{aligned} &\|\Delta\|_\infty < 1 \Leftrightarrow \left\| W_2^{-1}\left(K-K^0\right)W_1^{-1} \right\|_\infty < 1 \\ &\left(\left\| W_2^{-1}\left\{\begin{bmatrix}\tilde{U} & \tilde{V}\end{bmatrix}-\begin{bmatrix}\tilde{U}_0 & \tilde{V}_0\end{bmatrix}\right\}W_1^{-1}\right\|_\infty < 1 \text{ for coprime factor perturbation case}\right) \\ &\Rightarrow \left\|F_l(\tilde{R},\Delta)\right\|_\infty < 1 \Rightarrow \left\|F_l(G,K)\right\|_\infty < 1 \end{aligned} \quad (3.36)$$

To guarantee a preserved level of closed-loop performance with a reduced-order controller, it is sufficient to find weighting functions W_1 and W_2 such that the matrix $\tilde{R}$ is inner, which has been achieved in [Godd98]. The main criticism that could be addressed to Goddard's method is the numerical complexity to find the weighting functions W_1 and W_2 and their high order. Wang and Sreeram in [Wang2001], based on an additive perturbation description of the closed-loop system, proposed low-order weighting functions W_1 and W_2 that minimize the following criterion:

$\left\| W_2^{-1}V_2(K_r-K_f)V_1W_1^{-1} \right\|_\infty$ where $V_1=\left(I-P_{22}K\right)^{-1}P_{21}, V_1=P_{12}\left(I+K\left(I-P_{22}K\right)^{-1}P_{22}\right)$.

3.4 Order reduction of flexible systems in a closed loop framework

Our main interest in order reduction is the truncation of the less influent flexible modes on the closed-loop system behaviour of the flexible system studied. All of the above order reduction methods do not take into account the physical interpretation of the truncated states. An optimal reduced-order model (or controller) may achieve the best level of performance in closed loop, but may only provide limited insight to a structure engineer if the state vector has lost its physical meaning. The majority of order reduction methods developed so far for linear time-invariant continuous-time systems are carried out in open loop and do not take into account closed-loop stability and performance. Although closed-loop order reduction methods were developed [Wor94], [Cet93], no strong link exists between the model order reduction and how the preservation of closed-loop performance could be improved. The main performance criterion used throughout this thesis is the robust performance level of the closed-loop system. Although recent progress in [Beck96] on the open-loop order reduction of uncertain system is to be noticed, no order reduction technique proposed in the literature takes into account a closed–loop robust performance criterion. In the following, we propose methods for order reduction

(model and/or controller) that are more adapted to flexible modes truncation, in a closed-loop framework, and taking into account a robust performance criterion.

3.4.1 Uncertain flexible modes truncation

The robust control setup, which takes explicitly into account the uncertainty in the dynamics of the plant [Bal91a] is extended to represent the neglected flexible dynamics, i.e., the flexible modes we want to truncate [Gaw96]. In the following, we present two methods of order reduction based on two different uncertainty representations.

3.4.1.1 Additive uncertainty reduction

As presented in Chapter 2 the variations in the dynamics of the system can be taken into account in an additive uncertainty model. Assume a nominal system $G(s)=\left[\begin{array}{c|c} A & B \\ \hline C & 0 \end{array}\right]$ containing n flexible modes and represented in its diagonal modal form:

$$A=diag\{A_i\}, A_i=\begin{bmatrix} -\zeta_i\omega_i & \sqrt{1-\zeta_i^2}\,\omega_i \\ -\sqrt{1-\zeta_i^2}\,\omega_i & -\zeta_i\omega_i \end{bmatrix} B=\begin{bmatrix} B_1 & \cdots & B_m \end{bmatrix}, C=\begin{bmatrix} C_1 \\ \vdots \\ C_p \end{bmatrix}, B_i\in\Re^{2n\times 1}, C_i\in\Re^{1\times 2n}.$$

The modes of the full order model are ordered following singular values of A, $\Sigma=diag\{\sigma_1,\ldots,\sigma_{2n}\}$. The reduced model of r flexible modes to be obtained is $G_r(s)$. The additive uncertainty approach proposed, as in [Josh98], is to account for the truncated flexible modes as additive uncertainty $\Delta_a(s)$ acting on a reduced model $G_r(s)$.

$$G(s)=G_r(s)+W_a(s)\Delta_a(s) \tag{3.37}$$

$\Delta_a(s)$ is normalized as $\|\Delta_a(s)\|_\infty<1$ by the use of the weighting function $W_a(s)=G(s)-G_r(s)$ as shown in the following figure:

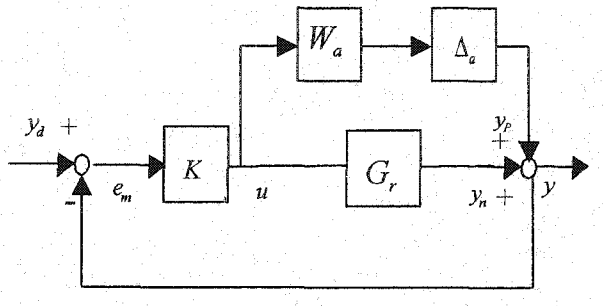

Figure 3.1: Additive uncertainty reduction

The additive uncertainty bound increases according to the number of truncated flexible modes we want, as

$$\|W_a\|_\infty = \|G - G_r\|_\infty = \|G_t\|_\infty \tag{3.38}$$

where $G_t(s) = \sum_{i=n-r}^{n} C_{1:p,i}(sI - A_i)^{-1} B_{i,1:m}$ represents the truncated flexible modes part.

From an open-loop reduction view, the objective is to reduce the model such that: $\min_{G_r} \|W_a\|_\infty$.

Assuming that

$$\|W_a\|_\infty = \|G_t\|_\infty = \sigma_{r+1} \tag{3.39}$$

where $\sigma_{r+1}(\sigma_{r+1} > \ldots > \sigma_n)$ is the Hankel singular value corresponding the $(r+1)$th flexible mode, the open-loop reduction can be carried out by truncating the flexible modes whose corresponding singular values are the smallest. Since we are interested in the closed-loop behaviour, a reasonable objective would be to have a guarantee bound on the norm of the error $\|F_u(F_l(G,K),\Delta) - F_u(F_l(G_r,K),\Delta)\|_\infty$ where $\Delta = \begin{bmatrix} \Delta_p & 0 \\ 0 & \Delta_a \end{bmatrix}$ includes a fictitious uncertainty Δ_p for the performance. From a mathematical point of view, no explicit expression connecting the minimization of the error between the full-order and reduced-order closed-loop systems, and the error in open loop could be obtained. However a heuristic says that, since the reduced model $G_r(s)$ is close to the nominal model $G(s)$, then by increasing the uncertainty bound $W_a(s)$ we should obtain worse closed-loop performance levels with the reduced-order model. Thus the performance criterion used in these uncertain closed-loop reduction methods is: $\|F_u(F_l(G_r,K),\Delta)\|_\infty$. We compare this norm for all possible combinations of *n-r* flexible modes to truncate to decide what the best combination is for truncation, while preserving closed-loop performance.

3.4.1.2 Inverse uncertainty reduction

The additive uncertainty proposed previously has certain deficiencies when the damping ratios of the flexible modes to truncate are small. This implies that the additive uncertainty bound $W_a(j\omega)$ includes peaks in its magnitude due to the truncated flexible modes. Thus, the high uncertainty bound complicates the design of a robust controller with additive uncertainty. From this starting point, we propose a new type of uncertainty used for order reduction. We call it "*inverse uncertainty*".

This type of uncertainty links the reduced-order model to the full-order model as follows:

$$G(s) = [G_r(s)^{-1} + W_{inv}(s)\Delta_{inv}(s)]^{-1} \tag{3.40}$$

where $\Delta_{inv}(s)$, the inverse uncertainty, is normalized as $\|\Delta_{inv}(s)\|_\infty < 1$ using the weighting function $W_{inv}(s) = G^{-1}(s) - G_r^{-1}(s)$ as shown in the following figure:

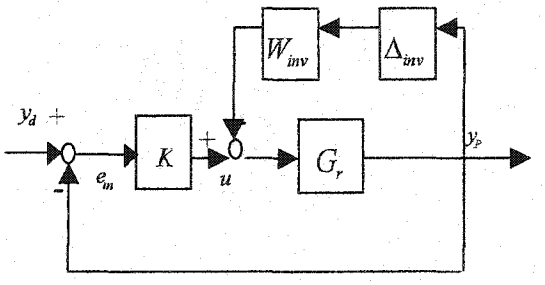

Figure 3.2: Inverse uncertainty reduction

This uncertainty representation often results in a lower bound compared to the additive uncertainty bound. Moreover, when small damping ratios are considered in the truncated part, the inverse uncertainty bound will take into account the inverse of the peak magnitudes which do not increase the bound. This facilitates the design of a robust controller for the reduced-order uncertain plant model considered. As can be noted, the inverse uncertainty approach needs the full-order model $G(s)$ to be invertible. The inverse uncertainty bound $W_{inv}(s) = G^{-1}(s) - G_r^{-1}(s)$ can be rendered proper using a strictly proper filter that neglects the high-frequency dynamics, which are not very important for the performance of the flexible system. The criticism of this uncertainty model is that for open-loop reduction, no specific rule guiding the truncation of the flexible modes such as the one in (3.39) for additive uncertainty could be obtained. However, since we are concerned with closed-loop reduction, such a rule is not required. Rather, a test of closed-loop performance for all possible combinations of flexible modes to truncate is used.

To illustrate the uncertainty based reduction approach and to show the efficiency of the proposed inverse uncertainty approach compared to the additive uncertainty approach, we present the following example.

Example 3.1

The model we use here is similar to the family of three mass system [Gaw96]. In this model, we have three flexible modes with damping ratios $\zeta_1 = 0.07$, $\zeta_2 = 0.2$, $\zeta_3 = 0.3$ and natural frequencies

$\omega_1 = 5,\ \omega_2 = 15,\ \omega_3 = 20$. More precisely, the full-order model can be written as: $G(s) = \sum_{i=1}^{3} G_i(s)$

where $G_i(s) = \dfrac{A_i s + B_i}{s^2 + 2\zeta_i \omega_i s + \omega_i^2}$, $A_1 = 0.1,\ A_2 = 0.1,\ A_3 = 0.5$ and $B_1 = 100,\ B_2 = 100,\ B_3 = 100$. The open loop frequency response of the full order system is given in Figure 3.3:

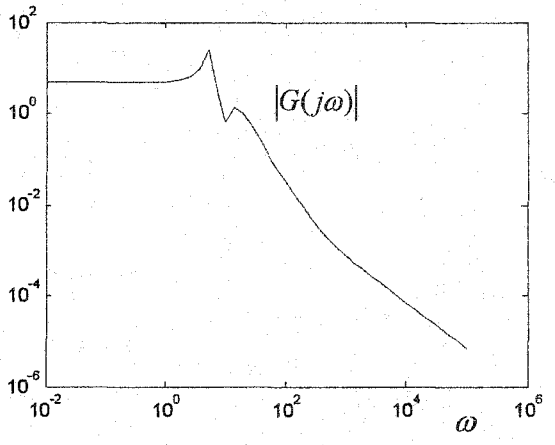

Figure 3.3: open loop frequency response

In this example, we consider the truncation of just one flexible mode from the full-order model. The possible truncations are obviously: flexible mode 1, flexible mode 2 and flexible mode 3. The additive uncertainty approach proposes mode 3 for truncation, which corresponds to the smallest singular value, as the best candidate for open-loop reduction. However, since in this study, consideration is given to closed-loop performance, a check of all possible combinations is required. In Figure 3.4 we show the uncertainty bound $W_a(s)$ for the three possible truncations:

$$W_a(s) = \begin{cases} W_{a_1}(s) = G(s) - G_1(s) \text{ for the first flexible mode to be truncated} \\ W_{a_2}(s) = G(s) - G_2(s) \text{ for the second flexible mode to be truncated} \\ W_{a_3}(s) = G(s) - G_3(s) \text{ for the third flexible mode to be truncated} \end{cases} \quad (3.41)$$

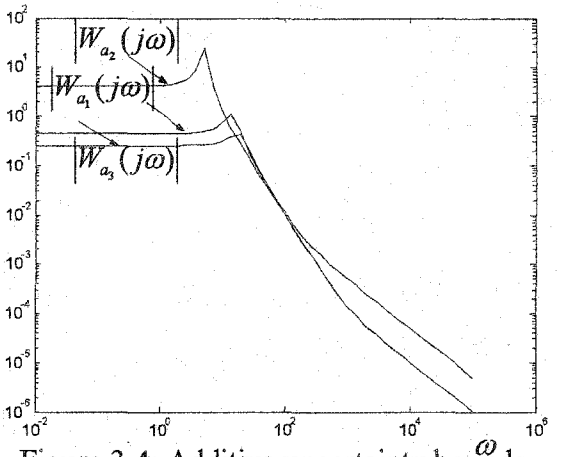

Figure 3.4: Additive uncertainty bounds

The robust controllers designed for the three different possibilities of truncation were obtained using [Gah94b]. The closed-loop performance levels obtained for the three possible truncation of one flexible mode truncation are as follows: $\gamma_{r1} = 25.88$, $\gamma_{r2} = 3.07$, $\gamma_{r3} = 0.765$ This shows that the best possible reduction of one flexible mode is the third flexible mode.

Using the inverse uncertainty approach, and for the three possible truncation modes, the inverse uncertainty bound is given as:

$$W_{inv}(s) = \begin{cases} W_{inv1}(s) = G^{-1}(s) - G_1^{-1}(s) \text{ for the first flexible mode to be truncated} \\ W_{inv2}(s) = G^{-1}(s) - G_2^{-1}(s) \text{ for the second flexible mode to be truncated} \\ W_{inv3}(s) = G^{-1}(s) - G_3^{-1}(s) \text{ for the third flexible mode to be truncated} \end{cases} \quad (3.42)$$

and is shown in Figure3.5.

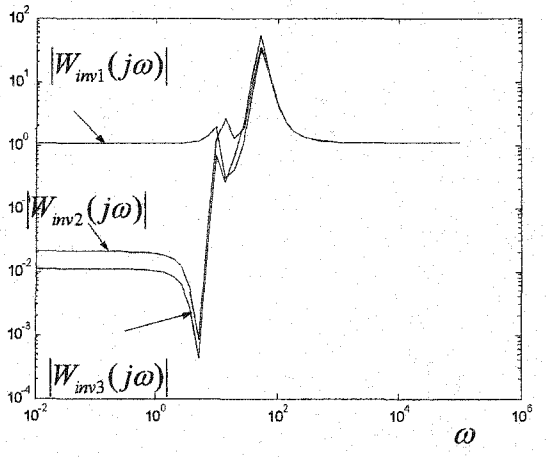

Figure3.5: Inverse uncertainty bounds

Notice, from Figure 3.4 and Figure 3.5, how the inverse uncertainty bound is smaller than the additive uncertainty modes especially in the low frequency interval. This frequency range is the most important in our design since the natural frequencies of the flexible modes belong to that specific range. The closed-loop performance levels obtained for the three flexible modes truncation are as following: $\gamma_{r1} = 0.501$, $\gamma_{r2} = 0.504$, $\gamma_{r3} = 0.73$ the best flexible mode to be truncated following this inverse approach is mode 1, corresponding to the best reduced closed-loop performance γ_{r1}.

Figure 3.6 describes a μ – analysis of the truncation of flexible mode 3 using the two approaches proposed. It is shown that the design obtained using the inverse uncertainty approach achieves better closed-loop robust performance level. Same remark can be made for the other flexible mode truncations, simply by comparing their respective level of performance γ_{r1}, γ_{r2}; Figure 3.7 confirm that for flexible model truncation.

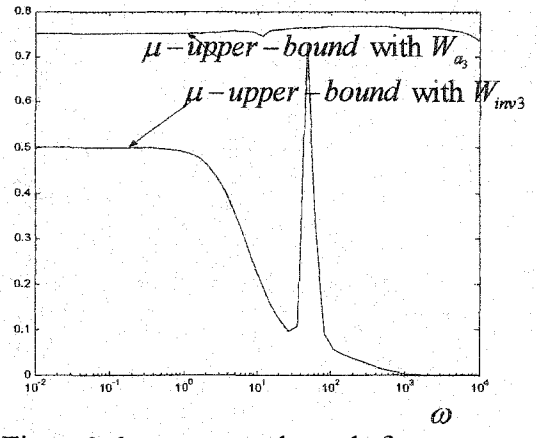

Figure3.6: μ – upper bounds for flexible mode 3 truncation

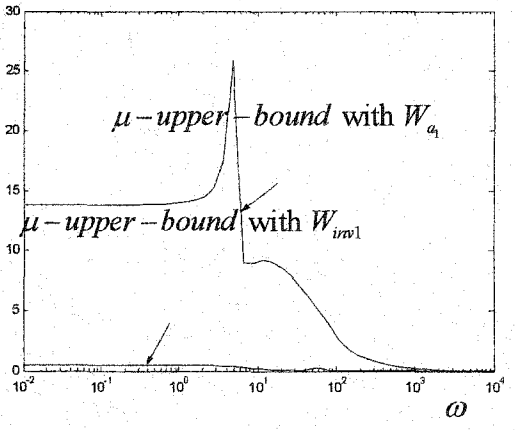

Figure3.7: μ – upper bounds for flexible model truncation

3.4.2 Model and controller reduction for flexible aircraft preserving robust performance

3.4.2.1 Introduction

In this section, we present a systematic approach to reduce the order of a model-controller pair for a flexible aircraft. Numerical examples are given for a flexible model of a B-52 bomber and for a three-mass flexible system.

The method, based on mixed μ-synthesis, determines which flexible modes can be truncated from the full-order model of the aircraft and finds a corresponding reduced-order controller preserving robust closed-loop performance. This method is of interest for practical model and controller reduction for flexible aircraft because in this context it is important to keep the physical interpretation of the truncated and remaining modes.

Our proposed reduction method, inspired from the work of Kavranoglu [Kav96], involves modal truncation, i.e., the truncation of states corresponding to flexible modes of the model. The method then generates an associated reduced-order controller satisfying a closed-loop robust performance specification since in our approach, the main reduction criterion is the achievable closed-loop robust performance level. We use the novel idea of introducing a repeated real parametric uncertainty δ in the flexible modes selected for truncation. This real perturbation, when equal to -1, represents the effect of the truncation of these modes in the aircraft model. Thus, a controller that can maintain some closed-loop performance level for the perturbed full-order aircraft model $\forall|\delta| \leq 1$, can also achieve this robust performance level on the truncated model.

We now describe our reduction procedure. Suppose that it is desired to truncate k flexible modes from the aircraft's full-order model. As a first step, our procedure lists all combinations of k flexible modes from the N flexible modes of the nominal model. This list of mode combinations is shortened by checking specific criteria of robust stability and performance that have to be met. For each candidate combination α of flexible modes to be truncated in the list, a full-order controller $K_{f\alpha}(s)$ is designed and kept in the set $\mathrm{K_F}$ if it achieves the desired robust performance level. Robust performance is measured using the structured singular value with respect to the parametric uncertainty covering the uncertainty in the flexible mode parameters and the truncation of these flexible modes. The result of this first step is the set $\mathrm{K_F}$ of full-order controllers, each one corresponding to a specific combination of flexible modes to be truncated, that meet the desired performance specification both for the full-order aircraft model and its corresponding reduced-order model obtained through a truncation of the k modes.

Since the first step in our approach calls for the design of $\binom{N}{k} = \frac{N!}{k!(N-k)!}$ full-order controllers, it is limited to aircraft models with up to around 15 flexible modes, depending on computing power and

time available for design. Nowadays, it is not unreasonable to assume that a few hours of computations would represent a relatively small cost in the overall design of a new commercial aircraft with flexibilities. What is paramount is to guarantee robust performance with a reduced-order controller.

The second step of our procedure consists of generating a reduced-order controller for the best full-order controller $\hat{K}_f := K_{f\hat{\alpha}} \in \mathsf{K}_F$ corresponding to mode combination $\hat{\alpha}$. The controller reduction problem is set up as a minimization of the weighted error norm between the nominal closed-loop sensitivity matrix and the reduced one, and its solution yields robust performance preservation with the reduced controller. Preservation of robust performance of the reduced model/controller pair is obtained from a structured singular value setup, and controller reduction is thus viewed as a robustness problem against uncertainty in the controller. Any controller reduction technique may be used at this stage, as long as the resulting frequency responses of K_r and $\hat{K}_f$ are close enough to ensure that robust performance is preserved with the reduced-order controller. We treat both model and controller reduction through the same two-step procedure to obtain a good pair of reduced-order model and controller.

3.4.2.2 Problem setup

The nominal finite-dimensional, linear, time-invariant transfer matrix model of a flexible aircraft mapping the control surface inputs u to the measured outputs y, which may be composed of the aircraft's position, angles, linear and angular velocities, and accelerations (available to the controller), can be expressed as:

$$G(s) = G_{rbm}(s) + G_f(s) \tag{3.43}$$

Where the modal state-space realization of the flexible dynamics $G_f(s)$ is given by:

$$G_f(s) = \left[\begin{array}{c|c} A_0 & B_0 \\ \hline C_0 & 0 \end{array}\right] := C_0(sI - A_0)^{-1}B_0 \tag{3.44}$$

In this equation, $A_0 \in \mathbb{R}^{2N\times 2N}$ is in modal form, i.e., $A_0 = diag\{A_i\}$, $A_i = \begin{bmatrix} -\zeta_i\omega_i & \sqrt{1-\zeta_i^2}\,\omega_i \\ -\sqrt{1-\zeta_i^2}\,\omega_i & -\zeta_i\omega_i \end{bmatrix}$ $i = 1,\ldots,N$, and N is the number of flexible modes of the model; ζ_i, ω_i are the damping ratio and the undamped natural frequency of the i^{th} mode, respectively; $B_0 \in \mathbb{R}^{2N\times m}, C_0 \in \mathbb{R}^{p\times 2N}$. The transfer matrix $G_{rbm}(s)$ models rigid-body dynamics and includes any direct feedthrough terms (D_0 matrix) that might appear in the flexible dynamics. Truncation of the i^{th} flexible mode from the nominal model can be seen as eliminating the effect of this mode. Because there is no interaction between the modal states in the modal realization of $G_f(s)$, this truncation corresponds to setting to zero the 2×2 matrix A_i and the corresponding rows and columns of matrices B_0 and C_0, respectively.

3.4.2.3 Uncertainty model

Parametric uncertainty may be less conservative than other types of uncertainty and may lead to a more realistic representation of the differences between the dynamics of a flexible aircraft and its model. In our approach, we treat both this kind of uncertainty and the truncation of the corresponding modes through the same setup, and with the use of a single repeated real scalar perturbation. Robust performance is optimized against this uncertainty in the design of full-order controllers K_f.

For a desired fixed number of flexible modes to be truncated k, we define the set of all possible combinations of k flexible modes to be truncated as follows:

$$\mathsf{A}_k := \left\{\alpha := \{\alpha_1, \ldots\ldots, \alpha_N\} : \alpha_i \in \{0,1\}, \sum_{i=1}^{N} \alpha_i = k\right\},$$

where $\alpha_i = 1$ to truncate and $\alpha_i = 0$ to keep the i^{th} mode. For each mode combination $\alpha \in \mathsf{A}_k$, we define corresponding perturbations of the modal state-space matrices representing modal parameter uncertainty and the truncation effect of these specific modes. First, let $T_\alpha := diag\{\alpha_1 I_2, \ldots, \alpha_N I_2\}$. The perturbed plant model is then defined as follows:

$$G_p(s) := G_{rbm}(s) + G_{fp}(s) \tag{3.45}$$

$$G_{fp}(s) := \left[\begin{array}{c|c} A_0 + \Delta_\alpha^A & B_0 + \Delta_\alpha^B \\ \hline C_0 + \Delta_\alpha^C & 0 \end{array}\right] \tag{3.46}$$

where the perturbations of the state-space matrices are defined by:

$$\begin{bmatrix} \Delta_\alpha^A & \Delta_\alpha^B \\ \Delta_\alpha^C & 0 \end{bmatrix} := \delta \begin{bmatrix} A_\alpha & B_\alpha \\ C_\alpha & 0 \end{bmatrix}, \quad \delta \in \mathbb{R}, \ |\delta| \le 1 \tag{3.47}$$

and the *truncation matrices* $A_\alpha, B_\alpha, C_\alpha$ are given by:

$$A_\alpha = T_\alpha A_0, \ B_\alpha = T_\alpha B_0, \ C_\alpha = C_0 T_\alpha \tag{3.48}$$

The real perturbation δ lies between -1 and 1, covering more than a single objective. The correspondence between values of the parameter δ and the objectives in our design is given as follows:

$\delta = -1$:	Truncate mode combination
$\delta = 0$:	Nominal full-order model
$\delta \in]-1,0[\cup]0,1]$:	Parametric uncertainty of the truncated modes

The latter interval covers variations in the frequencies and damping ratios of the flexible modes to be truncated, as well as their corresponding gains. This uncertainty is useful as the modes truncated from the model are still present (but uncertain) in the aircraft.

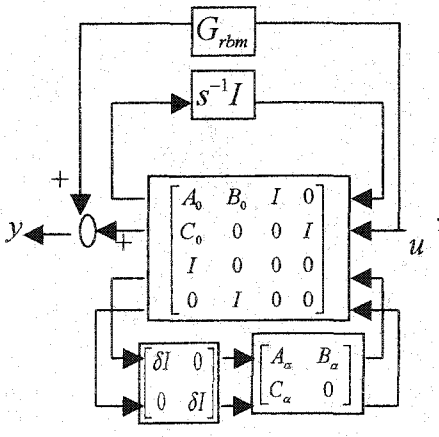

Figure 3.8 :Parametric uncertainty injection

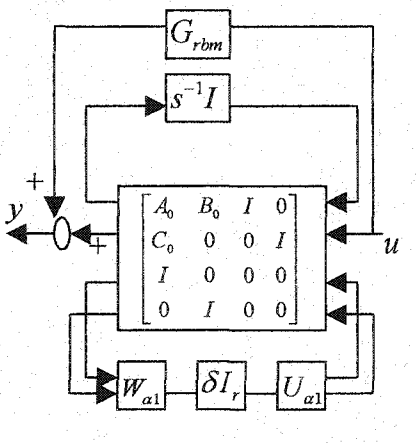

Figure 3.9 :SVD decomposition of the uncertainty

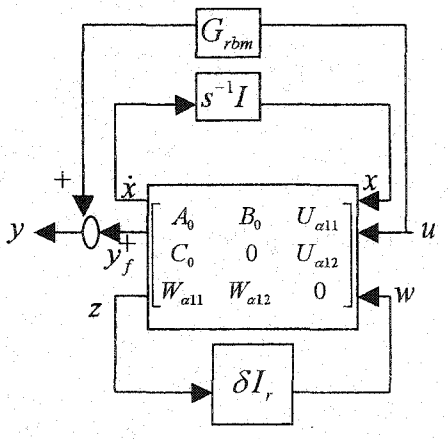

Figure 3.10 :Augmented plant representation

The truncation matrices $A_\alpha, B_\alpha, C_\alpha$ are shown on the block diagram of $G_p(s)$ in Figure 3.8. In fact, these matrices can be lumped in the augmented plant model. However, the multiplicity of the

associated real perturbation δ is high. Using a singular value decomposition of $\begin{bmatrix} A_\alpha & B_\alpha \\ C_\alpha & 0 \end{bmatrix}$, we can reduce the number of repeated perturbations δ, which leads to a less conservative uncertainty model [Zho96]:

$$\begin{bmatrix} A_\alpha & B_\alpha \\ C_\alpha & 0 \end{bmatrix} = U_\alpha \Sigma_\alpha V_\alpha^T = \begin{bmatrix} U_{\alpha 1} & U_{\alpha 2} \end{bmatrix} \begin{bmatrix} \Sigma_{\alpha r} & 0 \\ 0 & 0 \end{bmatrix} \begin{bmatrix} V_{\alpha 1} \\ V_{\alpha 2} \end{bmatrix} = U_{\alpha 1} \Sigma_{\alpha r} V_{\alpha 1} = U_{\alpha 1} W_{\alpha 1} \tag{3.49}$$

where $r = rank \begin{bmatrix} A_\alpha & B_\alpha \\ C_\alpha & 0 \end{bmatrix} \le \max\{2N+m, 2N+p\}$ and $W_{\alpha 1} = \Sigma_{\alpha r} V_{\alpha 1}$. Figures 3.9 and 3.10 show, respectively, how the multiplicity of δ is reduced to r and the matrices $W_{\alpha 1} = \begin{bmatrix} W_{\alpha 11} & W_{\alpha 12} \end{bmatrix}$, $U_{\alpha 1} = \begin{bmatrix} U_{\alpha 11} \\ U_{\alpha 12} \end{bmatrix}$ are incorporated in the augmented plant.

The reduction in the multiplicity of δ yields a less conservative uncertainty set. From Figure 3.10, the transfer function between u and y is given by:

$$G_p(s) = G_{rbm}(s) + \mathcal{F}_L \left[\mathcal{F}_U (M_\alpha, s^{-1} I), \delta I_r \right] \tag{3.50}$$

Where $M_\alpha := \begin{bmatrix} A_0 & B_0 & U_{\alpha 11} \\ C_0 & 0 & U_{\alpha 12} \\ W_{\alpha 11} & W_{\alpha 12} & 0 \end{bmatrix}$ is the real matrix representing the "generalized plant" in Figure 3.10. Define the transfer matrix $H_\alpha(s) := \mathcal{F}_U (M_\alpha, s^{-1} I)$ such that

$$\begin{bmatrix} y_f \\ z \end{bmatrix} = H_\alpha(s) \begin{bmatrix} u \\ w \end{bmatrix} \tag{3.51}$$

Where u is the vector of actuator inputs, w is the output of the repeated real perturbation δI_r, y_f is the output of the flexible part of the aircraft's dynamics, and z is the input of the repeated real perturbation. Reversing the order of the inputs and outputs of $H_\alpha(s)$, we obtain the augmented plant model $Q_\alpha(s)$, as given by Figure 3.11, mapping $\begin{bmatrix} w \\ u \end{bmatrix}$ to $\begin{bmatrix} z \\ y_f \end{bmatrix}$. Figure 3.11 represents a typical setup for robustness analysis against a single repeated real perturbation.

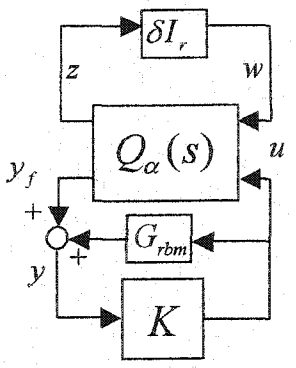

Figure 3.11 : Robust analysis setup

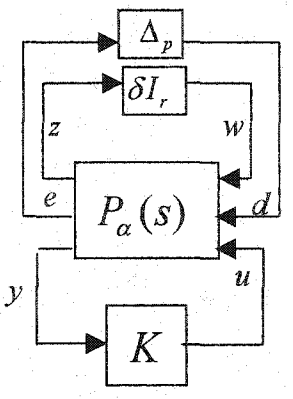

Figure 3.12 : Robust performance setup

Exogenous inputs of interest, e.g., reference signals and disturbances, are grouped together in d, and outputs to be controlled, e.g., tracking error and control signals, are grouped in $\tilde{e}$. These signals are added to $Q_\alpha(s)$ together with the performance weighting function $W_p(s)$ such that $e(s) = W_p(s)\tilde{e}(s)$ to obtain the augmented plant model $P_\alpha(s)$ mapping $\begin{bmatrix} w \\ d \\ u \end{bmatrix}$ to $\begin{bmatrix} z \\ e \\ y \end{bmatrix}$. Note that the rigid-body part of the dynamics $G_{rbm}(s)$ is also embedded in $P_\alpha(s)$ using standard block diagram manipulations.

Figure3.12 shows the $\mu-$synthesis setup for robust performance. The perturbation $\Delta_p \in \mathbb{C}^{n_d \times n_e}$ is a fictitious uncertainty included for performance, linking the exogenous inputs d to the outputs to be controlled e. The uncertainty structure is defined as follows:

$$\Gamma := \left\{ \Delta := \begin{bmatrix} \delta I_r & 0 \\ 0 & \Delta_p \end{bmatrix} : \Delta_p \in \mathbb{C}^{n_d \times n_e}, \delta \in \mathbb{R} \right\} \tag{3.52}$$

and the corresponding set of stable structured perturbations is defined as

$$\mathbf{D}_\Gamma := \left\{ \Delta(s) \in \mathcal{H}_\infty : \|\Delta(s)\|_\infty < 1, \Delta(s_0) \in \Gamma, \forall \mathrm{Re}\{s_0\} > 0 \right\} \tag{3.53}$$

The perturbed plant model is thus given by $\mathcal{F}_U\left[P_\alpha(s), \Delta(s)\right]$, where $\Delta(s) \in \mathbf{D}_\Gamma$.

3.4.2.4 Model and controller reduction

Mixed-μ theory can be used to design a full-order controller achieving the best robust performance index with, e.g., a DGK-iteration or a minimization of $\sup_{\omega \in \mathbb{R}} \mu_\Gamma \left\{ \mathcal{F}_L\left[P_\alpha(j\omega), K_{f\alpha}(j\omega) \right] \right\}$ based on

successive H_2 designs [Yan97]. At the end of the first step, we have the set $\mathrm{K_F}$ of full-order controllers, which achieve robust performance whether or not the corresponding candidate modes have been truncated.

The second step, after the design of the full-order robust controllers, consists of finding a reduced controller $K_r(s)$ of desired order q from the best full-order controller $\hat{K}_f(s) \in K_F$ corresponding to the "best" combination $\hat{\alpha}$ of candidate flexible modes to be truncated. Our proposed controller order reduction method preserves robust closed-loop performance, which is not the case for most earlier works. Consider the optimization problem over the set of stabilizing reduced controllers $K_r(s)$ of desired order q:

$$\inf_{\substack{K_r(s) \\ \text{stabilizing}}} \sup_{\substack{\delta \in \mathbb{R} \\ |\delta| \le 1}} \left\| \mathcal{F}_U \left\{ \mathcal{F}_L \left[P_{\hat{\alpha}}(s), \hat{K}_f(s) \right], \delta I_r \right\} - \mathcal{F}_U \left\{ \mathcal{F}_L \left[P_{\hat{\alpha}}(s), K_r(s) \right], \delta I_r \right\} \right\|_\infty \qquad (3.54)$$

That is, we want the perturbed closed-loop frequency responses with the full-order and reduced-order controllers to be as close as possible, as measured by the ∞-norm. A specification can be expressed with $\rho > 0$ as:

$$\left\| \mathcal{F}_U \left\{ \mathcal{F}_L \left[P_{\hat{\alpha}}(s), \hat{K}_f(s) \right], \delta I_r \right\} - \mathcal{F}_U \left\{ \mathcal{F}_L \left[P_{\hat{\alpha}}(s), K_r(s) \right], \delta I_r \right\} \right\|_\infty \le \rho, \forall |\delta| \le 1 \qquad (3.55)$$

Note that ρ should be chosen such that implies robust performance with the reduced-order controller. For example, if $\sup_{\omega \in \mathbb{R}} \mu_\Gamma[\mathcal{F}_L(P_{\hat{\alpha}}, \hat{K}_f)(j\omega)] = \gamma \le 1$, then one should pick $\rho < 1 - \gamma$. The complex variable s is henceforth dropped to simplify notation. The optimization problem in (3.54) can be represented as in Figure3.13, where:

$$\begin{bmatrix} z_1 \\ e_1 \end{bmatrix} = V \begin{bmatrix} w_1 \\ d \end{bmatrix}, \qquad V := \mathcal{F}_L(P_{\hat{\alpha}}, \hat{K}_f) = \begin{bmatrix} V_{11} & V_{12} \\ V_{21} & V_{22} \end{bmatrix}$$

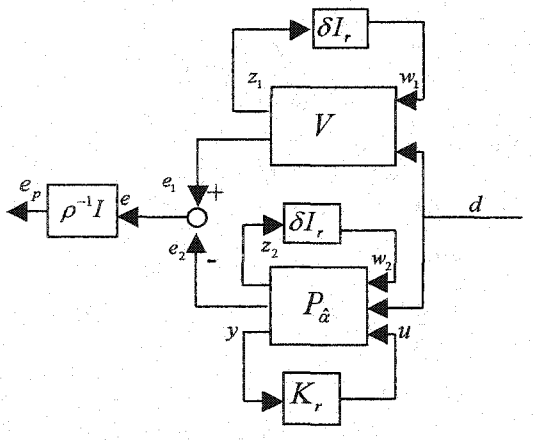

Figure 3.13 : Controller reduction

This setup can be recast in the robust performance design setup shown in Figure3.14:

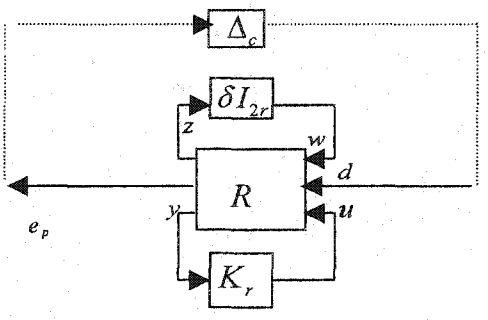

Figure 3.14 Augmented plant with the reduced order controller

where: $\begin{bmatrix} z \\ e_p \\ y \end{bmatrix} = R \begin{bmatrix} w \\ d \\ u \end{bmatrix}, z = \begin{bmatrix} z_1 \\ z_2 \end{bmatrix}, w = \begin{bmatrix} w_1 \\ w_2 \end{bmatrix}, e_p = \rho^{-1}(e_1 - e_2), R = \begin{bmatrix} R_{11} & R_{12} & R_{13} \\ R_{21} & R_{22} & R_{23} \\ R_{31} & R_{32} & R_{33} \end{bmatrix},$

$R_{11} = \begin{bmatrix} V_{11} & 0 \\ 0 & P_{\hat{a}11} \end{bmatrix}, \quad R_{12} = \begin{bmatrix} V_{12} \\ P_{\hat{a}12} \end{bmatrix}, \quad R_{13} = \begin{bmatrix} 0 \\ P_{\hat{a}13} \end{bmatrix}, \quad R_{21} = \begin{bmatrix} V_{21} & P_{\hat{a}21} \end{bmatrix}, \quad R_{22} = V_{22} - P_{\hat{a}22}, \quad R_{23} = P_{\hat{a}23},$

$R_{31} = \begin{bmatrix} 0 & P_{\hat{a}31} \end{bmatrix}, R_{32} = P_{\hat{a}32}, R_{33} = P_{\hat{a}33}.$

With the inclusion of a fictitious perturbation Δ_c for the "closeness" performance objective, the final augmented plant is shown in Figure3.15, where $\Delta_t := \begin{bmatrix} \Delta_c & 0 \\ 0 & \delta I_{2r} \end{bmatrix}$. This robust performance controller design can be transformed into a controller reduction procedure by means of robust performance analysis.

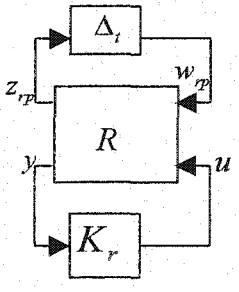

Figure 3.15 : Uncertainty block augmentation

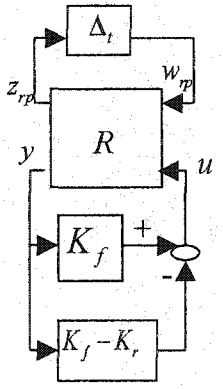

Figure3.16: Introduction of the closeness of the full and reduced controllers

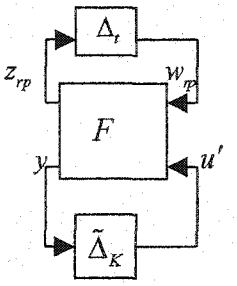

Figure3.17 : Augmentation of the plant by adding $\tilde{\Delta}_K$ uncertainty

From the two equivalent block diagrams shown in Figure 3.15 and 3.16, we obtain in Figure 3.17 a robust performance setup in which $\tilde{\Delta}_K := W_k(\hat{K}_f - K_r)$ is viewed as a normalized controller uncertainty, where W_k is a stable scalar weighting function. The idea is to ensure that K_r is close enough to $\hat{K}_f$ such that the size of $\Delta_K(j\omega) = (\hat{K}_f - K_r)(j\omega)$ is within the admissible uncertainty bound for which the system in Figure 3.17 will be robustly stable.

We use the Main Loop Theorem [Zho96] to prove the following result providing a basis for the proposed controller-order reduction technique. The theorem says that if the reduced-order controller is close enough to the full-order controller, then we can obtain both robust performance, and closed-loop frequency responses that are close to each other. Define the uncertainty structures:

$$\Gamma_1 := \left\{ \Delta := \begin{bmatrix} \delta I_{2r} & 0 & 0 \\ 0 & \Delta_c & 0 \\ 0 & 0 & \Delta_K \end{bmatrix} : \Delta_c \in \mathbb{C}^{n_d \times n_e},\ \delta \in \mathbb{R},\ \Delta_K \in \mathbb{C}^{m \times p} \right\} \tag{3.56}$$

$$\Gamma_2 := \left\{ \Delta_t := \begin{bmatrix} \Delta_c & 0 \\ 0 & \delta I_{2r} \end{bmatrix} : \Delta_c \in \mathbb{C}^{n_d \times n_e},\ \delta \in \mathbb{R} \right\} \tag{3.57}$$

Theorem 3.1

Assume that K_f is a full-order stabilizing controller achieving robust performance, i.e., $\sup_{\omega \in \mathbb{R}} \mu_\Gamma[\mathcal{F}_L(P, K_f)(j\omega)] < 1$ and assume that the reduced-order controller K_r has the same number of unstable poles as K_f. If, for every ω, $\mu_{\Gamma_1}[F(j\omega)] < 1$ and $\left\|(K_f - K_r)(j\omega)\right\| \le \left|W_k^{-1}(j\omega)\right|$, then:

1. K_r stabilizes $\mathcal{F}_U\left[\mathcal{F}_L(P,K_r),\delta I_r\right], \forall \delta \in \mathbb{R}, |\delta| \le 1$,

2. $\sup_{\omega\in\mathbb{R}} \mu_\Gamma[\mathcal{F}_L(P,K_r)(j\omega)] < 1$, and

3. $\left\|\mathcal{F}_U\left[\mathcal{F}_L(P,K_f),\delta I_r\right]-\mathcal{F}_U\left[\mathcal{F}_L(P,K_r),\delta I_r\right]\right\|_\infty < \rho, \forall \delta \in \mathbb{R}, |\delta| \le 1$

Proof:

Assume that $\mu_{\Gamma_1}[F(j\omega)] < 1$ and $\left\|(K_f - K_r)(j\omega)\right\| \le \left|W_k^{-1}(j\omega)\right|$. Then, for any Δ_K such that $K_r = K_f - \Delta_K$ has the same number of unstable poles as K_f and such that $\left\|\Delta_K(j\omega)\right\| \le \left|W_k^{-1}(j\omega)\right|$, we have $\mu_{\Gamma_2}[\mathcal{F}_L(F,\tilde{\Delta}_K)(j\omega)] < 1, \forall \omega$ by virtue of the Main Loop Theorem. In particular, taking $\Delta_K = K_f - K_r$ and working our way back to the equivalent system of Figure 7, we have $\mu_{\Gamma_2}[\mathcal{F}_L(R,K_r)(j\omega)] < 1$ which, by the Main Loop Theorem, implies

$\left\|\mathcal{F}_U\left[\mathcal{F}_L(P,K_f),\delta I_r\right]-\mathcal{F}_U\left[\mathcal{F}_L(P,K_r),\delta I_r\right]\right\|_\infty < \rho, \forall \delta \in \mathbb{R}, |\delta| \le 1.$

Furthermore, $\forall \delta \in \mathbb{R}, |\delta| \le 1$, we have

$$\left\|\mathcal{F}_U\left[\mathcal{F}_L(P,K_r),\delta I_r\right]\right\|_\infty - \left\|\mathcal{F}_U\left[\mathcal{F}_L(P,K_f),\delta I_r\right]\right\|_\infty \le$$
$$\left\|\mathcal{F}_U\left[\mathcal{F}_L(P,K_r),\delta I_r\right]-\mathcal{F}_U\left[\mathcal{F}_L(P,K_f),\delta I_r\right]\right\|_\infty < \rho$$

Hence,

$$\left\|\mathcal{F}_U\left[\mathcal{F}_L(P,K_r),\delta I_r\right]\right\|_\infty \le \left\|\left\{\mathcal{F}_U\left[\mathcal{F}_L(P,K_r),\delta I_r\right]-\mathcal{F}_U\left[\mathcal{F}_L(P,K_f),\delta I_r\right]\right\}\right\|_\infty$$
$$+\left\|\mathcal{F}_U\left[\mathcal{F}_L(P,K_f),\delta I_r\right]\right\|_\infty < \rho+\gamma < 1$$

Finally, the robust stability of $\mathcal{F}_U\left[\mathcal{F}_L(P,K_r),\delta I_r\right]$ follows from the Main Loop Theorem and the small-gain condition coming from the argument that the Nyquist plot of $\det\left[I - K_r\mathcal{F}_U\left(R,\Delta_t\right)\right]$ (Figure 3.16) must not be equal to 0, where $K_r = K_f - \Delta_K$ has the same number of unstable poles as K_f (Zho96).

To get a reduced controller achieving the specifications, we first proceed as follows. With the use of a fine grid of frequency points, an upper bound $\psi(\omega)$ on $\left\|\Delta_K(j\omega)\right\|$ is found such that the feedback interconnection in Figure 3.17 is robustly stable.

This is carried out by using, for each frequency ω_i, a bisection technique to find the upper bound $\psi(\omega_i)$ that leads to $\mu_{\Gamma_1}[F(j\omega_i)]=1$. Then a fitting procedure can be used to obtain the stable weighting function $W_K(s)$ such that $\left|W_K^{-1}(j\omega)\right| \cong \psi(\omega)$. The upper bound $\psi(\omega)$ is also used as a criterion to reject the mode combinations for which the controller cannot be truncated without losing robust performance. For mode combination α, if $\exists\ \omega_j$ for which there is no $\psi(\omega_j) \geq 0$ such that $\left\|\Delta_K(j\omega_j)\right\|_\infty \leq \psi(\omega_j)$ and $\mu_{\Gamma_1}\left[F_\alpha(j\omega_j)\right] \leq 1$, then combination α is rejected because the existence of a corresponding reduced-order controller satisfying the robust performance specifications cannot be guaranteed. The application of this criterion avoids the need to resort to a heuristic in choosing what subset of mode combinations can be safely truncated.

The last step for controller reduction is the following: Given an order $q < \deg\{\hat{K}_f\}$, find a reduced q^{th}-order controller K_r with the same number of unstable poles as $\hat{K}_f$, and such that $\left\|\hat{K}_f(j\omega)-K_r(j\omega)\right\| \leq \left|W_K^{-1}(j\omega)\right|$. If such a K_r cannot be found for $\hat{K}_f$, then the second-best (in terms of the "mu-norm" $\sup_{\omega\in\mathbb{R}}\mu_\Gamma[\mathcal{F}_L(P,K_f)(j\omega)]$) full-order controller can be used, and so forth. Alternatively, the order q may be increased. For this weighted controller approximation problem, any suitable reduction technique can be used, e.g.,[Glo84] [Enn84b]. In the example below, we used the weighted Hankel-norm approximation because of its close upper bound on the norm of the error between the nominal and the reduced controller. Note that since a $\mu-$synthesis may produce an unstable controller, it is suggested that only the stable part be used in the reduction. This ensures that K_r has the same number of unstable poles as K_f, and hence Theorem 1 can be used.

3.4.2.5 Modal reduction over the full flight envelope of a flexible aircraft

For practical flight control applications, one has to keep in mind the changes in aircraft dynamics according to the flight conditions. If these changes can be modeled as slow variations in the modal parameters, one could introduce a suitable complementary uncertainty model capturing these variations for the remaining modes, using for example the technique presented in [Aouf2001]. Our

modal truncation method could then be adapted to yield a reduced-order model which, in closed loop, might achieve the robust performance criterion over the entire flight envelope, provided all possible modal parameter variations over the flight envelope could be covered by the complementary uncertainty model. In this case, it might be possible to truncate the flexible modes in such a single-plant model setup. The truncated modes would then represent the less influent modes in terms of performance degradation over the entire flight envelope.

In the case where all possible modal parameter variations over the flight envelope could not be efficiently represented with a structured perturbation connected to a single generalized plant, our reduction method could be applied for different operating points. Each of these frozen operating points would be chosen such that the uncertainties that cover the modal parameters would produce overlapping sets of perturbed plants with the neighboring operating points. After applying our model order reduction technique at each trim point, one could truncate from all aircraft models their shared flexible modes that can be truncated, if this set were nonempty. This truncation of a common set of modes across all models covering the flight envelope would preserve a consistent model structure. The reduced-order models could then be interpolated to produce a linear parameter-varying (LPV) reduced-order aircraft model covering the full flight envelope, and for which a reduced-order scheduling or LPV controller could be designed.

3.4.2.6 Flexible system example

This example is a flexible system taken from [Gaw96], consisting of three masses $m_1 = 11, m_2 = 5, m_3 = 10$, linked together and to rigid walls through springs of stiffnesses $k_1 = k_4 = 10, k_2 = 50, k_3 = 55$, and dashpots of viscous dampings $d_i = 0.01k_i$, $i = 1,2,3,4$. The input u is applied such that $f_1 = u, f_2 = 2u, f_3 = -5u$ where $f_i, i = 1,2,3$ are the forces applied on each mass respectively. The output is $y_1 = 2q_1 - 2q_2 + 3q_3$, where $q_i, i = 1,2,3$ are the mass displacements. A disturbance d, is added to the plant output y_1 to get the system output $y = y_1 + d$. We represented this system in the state-space modal form such that the nominal damping ratios and frequencies respectively are: $\zeta_1 = 0.0044, \omega_1 = 0.87, \zeta_2 = 0.012, \omega_2 = 2.43, \quad \zeta_3 = 0.025, \omega_3 = 5.12$.

The performance level and the constraint on the controller specified for the nominal model are given by the weighting function $W_p(s) = \begin{bmatrix} \frac{s+3}{60.5s+0.03} & 0 \\ 0 & 1/0.7 \end{bmatrix}$, which specifies that the closed-loop sensitivity should be smaller than 0.01 at low frequencies. The sensitivity consists, in this case, of the transfer function $T_{dy}(s)$ from the disturbance d to the output of the system y. We start by removing one flexible mode to see if it can be truncated without losing robust closed-loop performance. All three "combinations" of one mode are considered. Table3.1 below gives the results obtained for each flexible mode considered for truncation. For the initial design, we selected $\rho = 0.1$, then three full-order controllers of order 28 were designed, with corresponding reduced-order controllers of order 11. Note that the relatively high order of the full controllers comes from the use of various weighting functions and scalings in the minimization of the structured singular value to obtain robust performance.

Table 3.1: Results for truncation of a single flexible mode

	$\max_{\omega_i} \mu_T[\mathcal{F}_L(P_\alpha, K_{f\alpha})(j\omega_i)]$	$\max_{\omega_i} \mu_T[\mathcal{F}_L(P_\alpha, K_{r\alpha})(j\omega_i)]$	$\|W_k(K_{f\alpha} - K_{r\alpha})\|_\infty$
Mode 3	0.7609	0.7609	<1e-015
Mode 2	1.0928	1.0928	0.0005211
Mode 1	1.0544	1.0544	9.1063e-013

Note that if the condition $\|(\hat{K}_f - K_r)(j\omega)\| \le |W_k^{-1}(j\omega)|$ were satisfied with a reduced-order controller with the same number of unstable poles as for $\hat{K}_f$, the performance specification would still be met. Figures 3.18 and 3.19 below represent, respectively the Bode plots of $\Delta_K(s)$ and $W_K^{-1}(s)$, and the upper and lower bounds of $\mu_T[\mathcal{F}_L(P_3, \hat{K}_f)(j\omega)]$ and $\mu_T[\mathcal{F}_L(P_3, K_r)(j\omega)]$ for flexible mode 3 truncated.

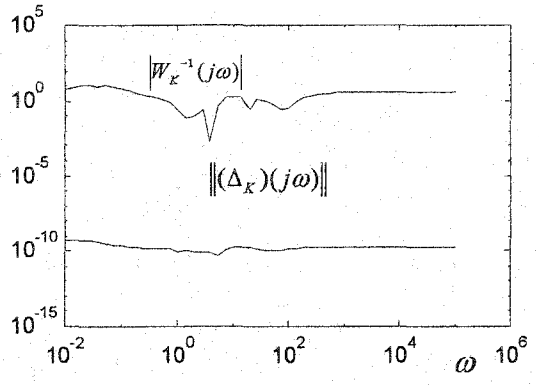

Figure 3.18 : Magnitude of Δ_K and W_k^{-1}

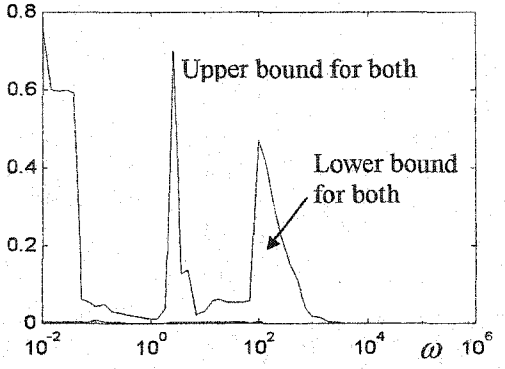

Figure 3.19 : μ bounds for both full and reduced controllers

From the results obtained, we conclude that the best truncation of a single mode that we can do is the truncation of mode 3. It satisfies the required specifications of robust performance, both for the full-order and reduced-order controllers, and the closeness of the corresponding closed-loop sensitivities.

To show the role of the sufficient condition $\|\Delta_K(j\omega)\| \le |W_k^{-1}(j\omega)|$, we tried to obtain a reduced controller of order 8 with the truncation of mode 3. Figure 3.20 shows that this condition was not satisfied. As a consequence, a degradation in performance occurred and we obtained, as shown in Figure 3.21, $\max_{\omega_i} \mu_\Gamma[\mathcal{F}_L(P_3, K_{r3})(j\omega_i)] = 0.9851$, whereas $\max_{\omega_i} \mu_\Gamma[\mathcal{F}_L(P_3, \hat{K}_f)(j\omega_i)] = 0.7609$ as given in Table 3.1.

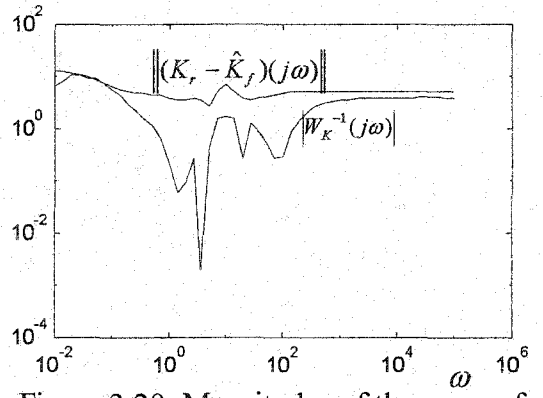

Figure 3.20: Magnitudes of the norm of $(K_r - \hat{K}_f)$ and of W_k^{-1}

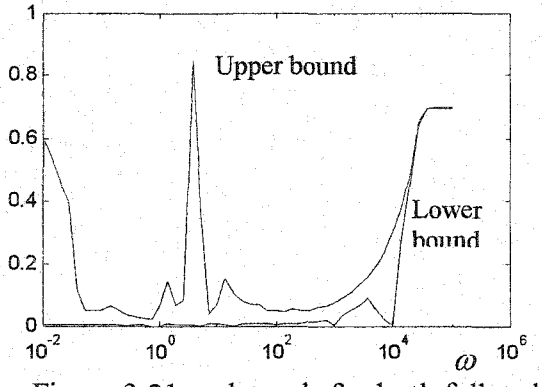

Figure 3.21: μ bounds for both full and reduced controllers

When we tried to truncate two of the three flexible modes, all three possible combinations considered were discarded because these truncations did not meet the evaluation criteria. The results were as follows:

For combination 1 (mode 2 and mode 3): $\max_{\omega_i} \mu_\Gamma[\mathcal{F}_L(P_1, K_{f1})(j\omega_i)] = 1.87$

For combination 2 (mode 1 and mode 3): $\max_{\omega_i} \mu_\Gamma[\mathcal{F}_L(P_2, K_{f2})(j\omega_i)] = 1.74$

For combination 3 (mode 1 and mode 2): $\max_{\omega_i} \mu_\Gamma[\mathcal{F}_L(P_3, K_{f3})(j\omega_i)] = 1.41$

These truncations did not initially achieve the performance specification with the full-order controllers, and obviously with any corresponding reduced-order controller. In the case where we relaxed the performance criteria and were willing to accept the degradation of performance resulting in the truncation of two flexible modes, the best combination retained by our method was combination 3 (mode 1 and mode 2).

3.4.2.7 Flexible aircraft example

We illustrate our reduction approach using a flexible model of a B52 bomber used in chapter2 [Mcl90]. It consists of one short-period rigid-body mode, represented by the angle of attack and the pitch rate, and five bending modes taking into account the flexibility of the airframe. The state-space representation of the aircraft is given as:

$$\begin{aligned} \dot{x} &= Ax + Bu + B_g w_g \\ y &= Cx + Du \end{aligned} \tag{3.58}$$

Where $x \in \mathbb{R}^{12}$ is the state vector given by,

$x^T = [\alpha \;\; q \;\; \eta_1 \;\; \dot{\eta}_1 \;\; \eta_2 \;\; \dot{\eta}_2 \;\; \eta_3 \;\; \dot{\eta}_3 \;\; \eta_4 \;\; \dot{\eta}_4 \;\; \eta_5 \;\; \dot{\eta}_5]$, $u = \begin{bmatrix} \delta_{el} & \delta_{hc} \end{bmatrix}^T \in \mathbb{R}^2$ is the vector of control surface angles [radians], $y \in \mathbb{R}$ is the vertical acceleration [g], $w_g = \begin{bmatrix} w_{g1} & w_{g2} & w_{g3} \end{bmatrix}^T \in \mathbb{R}^3$ is the vertical gust velocity at three stations along the airplane [m/s], $\alpha \in \mathbb{R}$ is the angle of attack [radians], $q \in \mathbb{R}$ is the pitch rate [radians/s], and η_i is the modal coordinate of the i^{th}-mode. The five flexible modes taken into account in the model are characterized by their frequency and damping ratio as given in Table 3.2.

Table 3.2: Flexible modes

	1	2	3	4	5
ω_i [rd/s]	7.40	15.21	19.73	20.24	38.29
ζ_i	0.337	0.056	0.010	0.067	0.023

The control objective is to reduce the effect of the wind gusts acting on the aircraft. This can be achieved by regulating the vertical acceleration of the aircraft subjected to these gusts. Using our order reduction procedure, we want to check what flexible mode(s) can be truncated and how much reduction can be performed on the controller while maintaining the robust performance obtained with the original full-order model/controller pair. Thus, we obtain a reduced model/controller pair that maintains the nominal robust performance level. The weighting functions on the acceleration and the control inputs are given respectively by: $W_{per}(s) = \dfrac{40}{0.05s+1}$, and $W_u = \begin{bmatrix} 1.25 & 0 \\ 0 & 0.25 \end{bmatrix}$, respectively. The weighting function $W_p(s)$ required in our procedure is composed of both $W_{per}(s)$ and $W_u(s)$.

Considering the effect of truncating a single flexible mode, we obtained from our reduction technique that the best choice is to truncate mode 1, the lowest-frequency mode. The resulting full-order controller $\hat{K}_f = K_{f1}$ was of the 40$^{\text{th}}$-order and it achieved the robust performance level of $\max_{\omega_i} \mu_{\Gamma}[\mathcal{F}_L(P_1, K_{f1})(j\omega_i)] = 0.9999$. Choosing $\rho = 10^{-4}$, we found that we could reduce the order of the controller down to 18 with $\left\| W_K (K_r - K_{f1}) \right\|_\infty = 3.0888 \times 10^{-7} < \rho$, and therefore without losing robust performance. Figure 3.22 below shows the magnitude Bode plots of the two entries of $K_r - K_{f1}$ and of W_K^{-1}, while Figure 3.23 shows the mixed-mu bounds for both K_{f1} and K_r (the curves actually sit on top of each other). These figures show that robust closed-loop performance is

preserved for the reduced 18th-order controller, which also achieved $\max_{\omega_i} \mu_T[\mathcal{F}_L(P_1, K_r)(j\omega_i)] = 0.9999$.

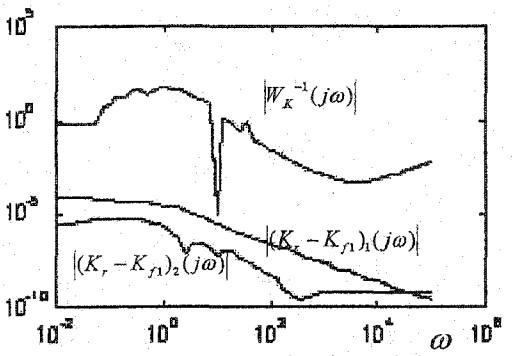

Figure 3.22 : Magnitudes of the two entries of $(K_r - K_{f1})$ and of W_k^{-1}

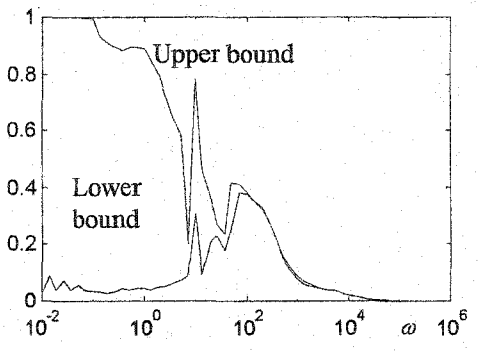

Figure 3.23 : μ bounds for both full and reduced controllers

The other four candidate modes for truncation yielded full-order controllers that could not meet the robust performance specification. Their resulting computed "μ-norms" are given below.

$$\max_{\omega_i} \mu_T[\mathcal{F}_L(P_2, K_{f2})(j\omega_i)] = \max_{\omega_i} \mu_{T_1}[\mathcal{F}_L(P_4, K_{f4})(j\omega_i)] = 1.018$$

$$\max_{\omega_i} \mu_T[\mathcal{F}_L(P_3, K_{f3})(j\omega_i)] = 1.046$$

$$\max_{\omega_i} \mu_T[\mathcal{F}_L(P_5, K_{f5})(j\omega_i)] = 4.20$$

Since robust performance was met with an extremely small margin for the truncation of a single flexible mode, no other flexible mode could be further removed.

3.4.3 Discussion of μ-sensitivity order reduction for flexible structures

To save computation time for the method above, we propose the use of μ-sensitivity tools. Their adaptation to our problem may help determine which mode combination is to be reduced without affecting much the closed-loop robust performance. We shall introduce in the following the notion of μ-sensitivity:

3.4.3.1 μ-sensitivity

Consider a matrix function: $M = \begin{bmatrix} M_{11} & M_{12} \\ M_{21} & M_{22} \end{bmatrix}$ and a corresponding uncertainty block $\Delta = \begin{bmatrix} \Delta_1 & \\ & \Delta_2 \end{bmatrix}$ that fit into the $M-\Delta$ structure shown in Figure2.8. By introducing a scalar weight in the uncertainty structure as: $\Delta = \begin{bmatrix} \alpha I & 0 \\ 0 & I \end{bmatrix}\begin{bmatrix} \Delta_1 & 0 \\ 0 & \Delta_2 \end{bmatrix} = \begin{bmatrix} \alpha\Delta_1 & 0 \\ 0 & \Delta_2 \end{bmatrix}$ that can be included into the augmented plant as: $M(\alpha) = \begin{bmatrix} \alpha I & 0 \\ 0 & I \end{bmatrix}\begin{bmatrix} M_{11} & M_{12} \\ M_{21} & M_{22} \end{bmatrix} = \begin{bmatrix} \alpha M_{11} & \alpha M_{12} \\ M_{21} & M_{22} \end{bmatrix}$. Then the μ-sensitivity with respect to Δ_1 is defined, [Braat91] as: $\delta\mu = \lim_{\Delta\alpha\to 0^+} \left.\dfrac{\mu(M(\alpha)) - \mu(M(\alpha-\Delta\alpha))}{\Delta\alpha}\right|_{\alpha=1}$. $\delta\mu$ can be interpreted as the derivative of μ with respect to α. The higher the value of $\delta\mu$, the more critical the model perturbation Δ_1 is in the value of μ. In practice, $\mu-$bounds are used in the calculation of $\mu-$sensitivity instead of the exact value of μ [Braat91], [Fan91].

3.4.3.2 $\mu-$sensitivity for order reduction

In this proposed approach, we keep the uncertainty model representation introduced in Section 3.4.2.3, which leads to the robust performance setup given by Figure 3.12. For this study, we propose an uncertainty model that corresponds to a combination of reducing all flexible modes of the flexible structure using the methodology of uncertain model used in section 3.4.2.3. With the uncertainty model set up, we proceed to test the $\mu-$sensitivities corresponding to all possible flexible mode combinations of a given number of flexible modes to truncate. Define $\delta\mu_i$, $i=1,...,N$ as the $\mu-$sensitivity of the ith flexible modes combination, then by calculating all the $\mu-$sensitivities the best combination to truncate with respect to robust performance criteria corresponds to the smallest value among the N $\mu-$sensitivities. After finding the best combination to truncate, the corresponding reduced-order controller is deduced using the same methodology of section 3.4.2.4. This approach can be time saving since with one robust control design, we determine the best flexible modes combination for a given number of flexible modes to truncate. However, the conservatism of using all flexible modes of the aircraft in the perturbation can influence the $\mu-$sensitivity results. Research is

underway on the possibility of proving some local additive property of the $\mu-$sensitivity adapted to flexible models, so we can predict the next mode to truncate in the case where we proceed iteratively. By "proceeding iteratively", we mean that if we increase the number of flexible modes to truncate to t_2 from t_1, what is the best flexible mode combination of size t_2-t_1 to be truncated.

Chapter 4:

Uncertainty models and robust complex-rational controller design

4.1 Introduction

Flexible structures are generally characterized by their damping ratios and the frequencies of their flexible modes. These parameters are subject to errors when they are estimated. These uncertainties are important and should be taken into account in a robust controller design.

The proper capture of modal parameter uncertainties in dynamical models of flexible structures for robust control has been the subject of ongoing efforts. Previous research [Bal91a], [Smi94] used additive or multiplicative uncertainty models to take into account the variation in the dynamics of the plant. Another way is to use certain heuristics to facilitate the representation of the parametric uncertainties in the flexible modes by a parametric model [Mad98]. These heuristics represent approximations in the parameter variation that are not generally realistic and lead to conservative controller designs, i.e., designs that cannot provide the desired performance in the face of realistic levels of parametric uncertainty.

Recently, a model to represent parametric uncertainties in the modes of a flexible structure has been discussed in Reference [Bald99]. Note that such models have been developed [Boul97] a few years ago. In the latter reference a model of dynamic uncertainty covering parametric variations in the flexible modes of a flexible structure has been developed. This dynamic uncertainty has the virtue of being non-conservative, but only when the frequencies of the flexible modes are close to each other.

In this section, we propose to represent the variation in the (damping, frequency) pair of each flexible mode by a tight low-order dynamic uncertainty. Thus, we reduce the order of the augmented plant by half, and transform the mixed real/complex robust performance μ – design into an easier complex μ – design representation. We use two techniques: the first is based on the coprime factorization framework [Mcf90] and the second uses a complex diagonal modal representation to model the dynamics of the flexible structure and to take into account the

parametric uncertainties. The advantage of our methods consists in transforming the real modal parametric uncertainties into a smaller number of complex uncertainty blocks. These cover all (damping, frequency) variations in the flexible structures and reduce the complexity of the augmented plant.

The robust controller design we propose takes into account two aspects: the robustness to the uncertainties in the modal parameters, and the closed-loop performance specified for our model. The second uncertainty model proposed results in a complex-rational nominal plant. This led us to develop a new procedure to design a robust controller. A robust complex-rational controller is first obtained via a μ – synthesis, and then a real controller keeping the robust performance level is designed to approximate the frequency response of the complex-rational controller.

4.2 Problem setup

Due to lack of exact knowledge of natural frequencies and damping ratios, the control designer needs to estimate uncertainty bounds for the modal parameters ζ_i and ω_i, $i=1,\ldots,n$. These bounds are used in the design to achieve the required robustness. Suppose that:

$\zeta_i = \zeta_{in} + \delta_{\zeta_i}$ and $\omega_i = \omega_{in} + \delta_{\omega_i}$,

where ζ_{in}, ω_{in} are the *ith* nominal damping ratio and frequency, respectively. The real numbers $\delta_{\zeta_i}, \delta_{\omega_i}$ represent the uncertainty in each parameter and are bounded in magnitude by: $|\delta_{\omega_i}| < t_{\omega_i}$ and $|\delta_{\zeta_i}| < t_{\zeta_i}$.

These uncertainties have to be taken into account in the design of a robust controller. The most used and efficient design to achieve robustness and performance for mixed type of uncertainty is the mixed μ-design based on the *D-G-K* iteration algorithm [You93], [Bal95].

In our design, we considered, respectively for each flexible mode, two parameter variations δ_{ζ_i}, δ_{ω_i}. For these variations, no tight, efficient and realistic parametric model is available in the literature. Consequently, it is difficult to deal with real uncertainties representations to achieve robust performance criteria. Moreover, when the number of scalar perturbations increases, it causes a problem of dimension complexity in the controller design procedure "*D-G-K* algorithm". The order of the system augmented by the *D-G* scales will be very high and the controller synthesis will be difficult. This is even more difficult when the order of the nominal flexible structure is high. Even though the μ-synthesis procedure used in this chapter, which is "μ controller based on H_2 design" from [Yan97], reduces the dimension of the scales by half, a

solution to the parametric uncertainty tightness and conservativeness still has to be found. A novel way to deal with this problem, under a new concept of complex controller design, is proposed.

4.3 Coprime factorization approach

This is the uncertainty modeling technique inspired and adapted from the version presented in [Boul97]. Consider the nominal dynamic equation of the flexible structure, of m inputs and p outputs, in modal coordinates:

$$\begin{aligned} \ddot{\eta} + D\dot{\eta} + \Lambda\eta &= Bu \\ y &= C\eta \end{aligned} \tag{4.1}$$

where: $D = diag\{2\zeta_i\omega_i, ..., 2\zeta_n\omega_n\}$

$\Lambda = diag\{\omega_1^2, ..., \omega_n^2\}$

$B \in \mathbb{R}^{n\times m}, C \in \mathbb{R}^{p\times n}$, $\{\omega_1, ..., \omega_n\}, \{\zeta_1, ..., \zeta_n\}$ are the frequencies and the damping ratios of the flexible modes.

Taking the Laplace transform of (4.1), we obtain

$$\begin{aligned} \eta(s) &= \left(s^2 I + sD + \Lambda\right)^{-1} Bu(s) \\ y(s) &= C\eta(s) \end{aligned} \tag{4.2}$$

Let us define: $G(s) = \left(s^2 I + sD + \Lambda\right)^{-1}$ and let $s^2 + as + b$ be Hurwitz with real zeros.

$G(s)$ can be written as : $G = \tilde{M}^{-1}\tilde{N}$ such that:

$$\begin{aligned} \tilde{M}(s) := \frac{1}{s^2 + as + b} diag\{&s^2 + 2\zeta_1\omega_1 s + \omega_1^2, \\ &..., s^2 + 2\zeta_n\omega_n s + \omega_n^2\} \end{aligned} \tag{4.3}$$

$$\tilde{N}(s) := \text{diag}\left\{\frac{1}{s^2 + as + b}, ..., \frac{1}{s^2 + as + b}\right\} \tag{4.4}$$

$\tilde{M}$ and $\tilde{N}$ form a left coprime factorization of G in RH_∞. The perturbed plant can be written as:

$$G_p = \left(\tilde{M} + \Delta\tilde{M}\right)^{-1}\left(\tilde{N} + \Delta\tilde{N}\right) \tag{4.5}$$

$\Delta\tilde{M}, \Delta\tilde{N} \in RH_\infty$ include all the parameters variations in the flexible modes.

$$\Delta\tilde{M} := \begin{matrix} \text{diag}\left\{ \dfrac{\left[2\zeta_{1n}\delta_{\omega_1} + 2\delta_{\zeta_1}\left(\omega_{1n}+\delta_{\omega_1}\right)\right]s + 2\omega_{1n}\delta_{\omega_1} + \delta_{\omega_1}^2}{s^2+as+b}, \right. \\ \left. \ldots, \dfrac{\left[2\zeta_{nn}\delta_{\omega_n} + 2\delta_{\zeta_n}\left(\omega_{nn}+\delta_{\omega_n}\right)\right]s + 2\omega_{nn}\delta_{\omega_n} + \delta_{\omega_n}^2}{s^2+as+b} \right\} \end{matrix} \tag{4.6}$$

$\Delta\tilde{N} := \text{diag}\{0,\ldots,0\}$

Each element of $\Delta\tilde{M}$, representing a family of strictly proper transfer functions, can be tightly bounded with a second-order weighting function using the bound of each parameter variation t_{ζ_i}, t_{ω_i} $i=1,\ldots,n$. Thus, $\Delta\tilde{M}$ can be bounded by the magnitude of the following weighting function (see Example1):

$$W_{\tilde{M}} := \begin{matrix} \text{diag}\left\{ \dfrac{\left[2\zeta_{1n}t_{\omega_1} + 2t_{\zeta_1}\left(\omega_{1n}+t_{\omega_1}\right)\right]s + 2\omega_{1n}t_{\omega_1} + t_{\omega_1}^2}{s^2+as+b}, \right. \\ \left. \ldots, \dfrac{\left[2\zeta_{nn}t_{\omega_n} + 2t_{\zeta_n}\left(\omega_{nn}+t_{\omega_n}\right)\right]s + 2\omega_{nn}t_{\omega_n} + t_{\omega_n}^2}{s^2+as+b} \right\} \end{matrix} \tag{4.7}$$

The resulting bound is structured, representing complex structured blocks of uncertainty. This bound is more general than the bound obtained in [Boul97], which had the assumption that the modal frequencies of the flexible structure were close to each other.

4.4 Modal coordinates approach

Suppose that the state-space model in modal coordinates of a flexible structure, and particulary a flexible aircraft model, is given as:

$$\begin{aligned} \dot{x} &= Ax + Bu \\ y &= Cx + Du \end{aligned} \tag{4.8}$$

where $A = \text{diag}\{A_i\}$, $i=1,\ldots,n$

$$A_i = \begin{bmatrix} -\zeta_i\omega_i + j\omega_i\sqrt{1-\zeta_i^2} & 0 \\ 0 & -\zeta_i\omega_i - j\omega_i\sqrt{1-\zeta_i^2} \end{bmatrix} \tag{4.9}$$

$(sI - A) = \text{diag}\{sI - A_i\}$.

we use the approximation $\zeta_i << 1$, which is verified in many examples of flexible structures models. Let us define the complex-rational factorization in $\mathbb{C}H_\infty$:

$G(s) = (sI - A)^{-1} = \tilde{M}(s)^{-1}\tilde{N}(s)$ and $\tilde{M} = \text{diag}\{\tilde{M}_i\}$:

$$\tilde{M}_i = \frac{1}{s+\alpha}(sI - A_i) = \frac{1}{s+\alpha}\begin{bmatrix} s+\omega_i(\zeta_i + j) & 0 \\ 0 & s+\omega_i(\zeta_i - j) \end{bmatrix}, \quad \tilde{N} = \text{diag}\left\{\frac{1}{s+\alpha},\ldots,\frac{1}{s+\alpha}\right\} \tag{4.10}$$

where $s+\alpha$ is Hurwitz.

The perturbed model can be written as:

$$G_p = \left(\tilde{M} + \Delta\tilde{M}\right)^{-1}\left(\tilde{N} + \Delta\tilde{N}\right) = \text{blkdiag}\left\{\begin{bmatrix} \begin{pmatrix} s+\omega_{in}(\zeta_{in}+j)+\omega_{in}\delta_{\zeta_i} \\ +\delta_{\omega_i}(\zeta_{in}+j)+\delta_{\omega_i}\delta_{\zeta_i} \end{pmatrix} & 0 \\ 0 & \begin{pmatrix} s+\omega_{in}(\zeta_{in}-j)+\omega_{in}\delta_{\zeta_i} \\ +\delta_{\omega_i}(\zeta_{in}-j)+\delta_{\omega_i}\delta_{\zeta_i} \end{pmatrix} \end{bmatrix}^{-1}\right\} \tag{4.11}$$

$i = 1,\ldots,n$

$$W_{\tilde{M}} := \frac{1}{s+\alpha} \times \text{blkdiag}\left\{\begin{bmatrix} \begin{pmatrix} \omega_{in}\delta_{\zeta_i} + \delta_{\omega_i}(\zeta_{in}+j) \\ +\delta_{\omega_i}\delta_{\zeta_i} \end{pmatrix} & 0 \\ 0 & \begin{pmatrix} \omega_{in}\delta_{\zeta_i} + \delta_{\omega_i}(\zeta_{in}-j) \\ +\delta_{\omega_i}\delta_{\zeta_i} \end{pmatrix} \end{bmatrix}\right\} \tag{4.12}$$

$i = 1,\ldots,n$

$\Delta\tilde{N} := diag\{0,\ldots,0\}$.

The magnitude of each sub-block $\Delta\tilde{M}_i$, such that $\Delta\tilde{M} = \text{diag}\{\Delta\tilde{M}_i\}$, can be tightly bounded by using the maximum on each parameter interval t_{ζ_i}, t_{ω_i}. Because we are interested by the magnitude of the uncertainty that the system is subjected to, it is possible to use the complex-rational weighting function $W_{\tilde{M}}$ given below to bound $\Delta\tilde{M}$ in the design (see Example 2).

$$\Delta\tilde{M}_b(s) := \frac{1}{s+\alpha} \times \mathrm{diag}\left\{\begin{bmatrix} \begin{pmatrix} \omega_{in} t_{\zeta_i} + t_{\omega_i}\zeta_{in} \\ +t_{\omega_i} t_{\zeta_i} + j t_{\omega_i} \end{pmatrix} & 0 \\ 0 & \begin{pmatrix} \omega_{in} t_{\zeta_i} + t_{\omega_i}\zeta_{in} \\ +t_{\omega_i} t_{\zeta_i} - j t_{\omega_i} \end{pmatrix} \end{bmatrix}\right\} \tag{4.13}$$

The uncertainty block in the design will be tightly covered by a modal bound $\Delta\tilde{M}_b(s)$ repeated as many times as there are uncertain parameter pairs of flexible modes.

4.5 Control design

Our control design methodology is based on the coprime factorization obtained from both uncertainty representation approaches. We use the μ-design technique to take into account the robust performance specification. The design concept is explained by Figure 4.1, where $\Delta\tilde{N} := diag\{0,...,0\}$.

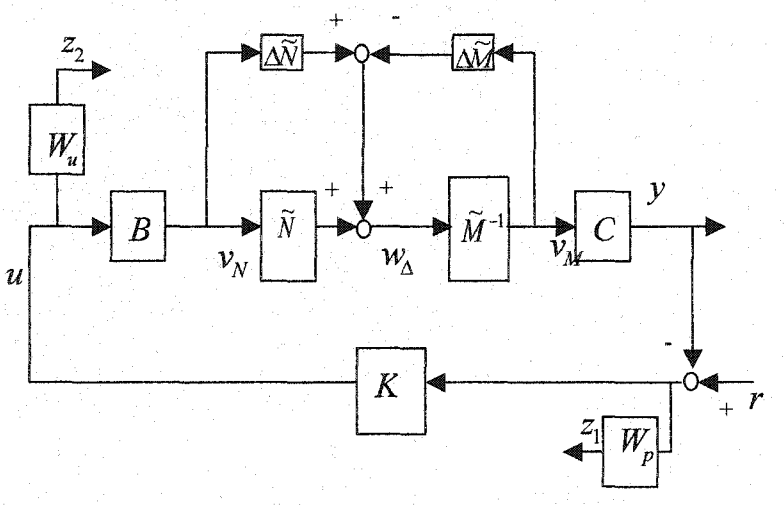

Figure 4.1: Coprime factorization Control

The robust performance is taken into account in the $\mu-$design by including a fictitious uncertainty Δ_p linking the input w to the outputs (z_1, z_2). We transform the scheme given in the previous figure to the classical $\mu-$setup. We obtain the robust design given by Figure 2.8:

Where: $z := \begin{bmatrix} v_M^T & v_N^T & z_1^T & z_2^T \end{bmatrix}^T$, $w := \begin{bmatrix} w_\Delta^T & r^T \end{bmatrix}^T$ $\Delta = \begin{bmatrix} \Delta_c & 0 \\ 0 & \Delta_p \end{bmatrix}$, $\Delta_c = \begin{bmatrix} \Delta\tilde{M} & -\Delta\tilde{N} \end{bmatrix}$,

$$P=\begin{bmatrix} \tilde{M}^{-1} & 0 & \tilde{N} \\ 0 & 0 & B \\ -W_p C\tilde{M}^{-1} & -W_p & -W_p\tilde{N}B \\ 0 & 0 & W_u \\ C\tilde{M}^{-1} & 0 & \tilde{N}B \end{bmatrix} . \qquad (4.14)$$

Since in our case $\Delta\tilde{N}$ is null, then $\Delta_c = \Delta\tilde{M}$ which is in diagonal form and contains the complex uncertainties that cover the parameters variations in each flexible mode.

An advantage that our uncertainty models offer is that we can recast the structured dynamic uncertainties, obtained using our uncertainty models, into one complex block of uncertainty. In fact, for the frequency interval considered, the highest magnitude uncertainty bound:

$\Delta M_{bi} := \dfrac{\left[2\zeta_{in}t_{\omega i} + 2t_{\zeta_i}\left(\omega_{in} + t_{\omega_i}\right)\right]s + 2\omega_{in}t_{\omega_i} + t_{\omega_i}^2}{s^2 + as + b}$ for the coprime factorization approach (and

$\Delta\tilde{M}_{bi} := \dfrac{\omega_{in}t_{\zeta_i} + t_{\omega_i}\zeta_{in} + t_{\omega_i}t_{\zeta_i} + jt_{\omega_i}}{s+\alpha}$ for the modal coordinate approach, respectively) tightly covers the uncertainty set of all the dynamic structured uncertainties obtained. Thus, we reduced the number of perturbations to one complex block of magnitude ΔM_{bi} ($\Delta\tilde{M}_{bi}$). This, in general, will simplify the design of a μ-controller achieving the performance and robustness required.

4.6 Simulation and new control design strategy :

To validate our methods, we chose two flexible systems representing the well-known three-mass system [Gaw96].

Example 1

In the first example, the damping ratios and the frequencies of the flexible modes are $\zeta_1 = 0.072, \zeta_2 = 0.023, \zeta_3 = 0.016$, $\omega_1 = 0.91, \omega_2 = 1.81, \omega_3 = 1.5$. The input matrix B is given by $B = [0 \quad 2.4 \quad 4.4]^T$. We assume that the uncertainties in ζ_i, ω_i, $i = 1,2,3$ are 10% and 0.1% respectively. Thus, the controller to be designed has to be more robust against variations in the damping ratios. The level of performance specified is given by $W_p = \dfrac{s+3}{10.5s + 0.03}$ and the constraint on the controller is specified by: $W_u = 1/0.7$. In this example, we use the first approach described above. Figure 4.2 gives the Bode plots of the first diagonal entry in $\Delta\tilde{M}$ which

concerns all the parameter variations in the coefficients of the first flexible mode and the magnitude of the first diagonal entry of $W_{\tilde{M}}$.

It is easy to see that this magnitude tightly bounds all the variations in the first diagonal entry of $\Delta\tilde{M}$. This observation is valid for the other flexible modes as well. Thus, the weighting function $W_{\tilde{M}}$ represents a tight bound of $\Delta\tilde{M}$.

A μ controller was designed for this example taking into account the complex uncertainty $W_{\tilde{M}}$ covering all the parameters variations in all the flexible modes. Figure4.3 gives the μ – upper bound that we could get with this μ controller. The μ – upper bound obtained is less than 0.72, showing that our controller design effectively guarantees the robust performance specified, in spite of parameter uncertainties in the flexible modes.

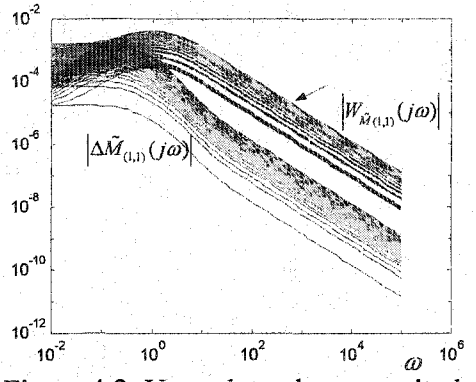

Figure 4.2: Upper bound on magnitudes of perturbations for Example 1

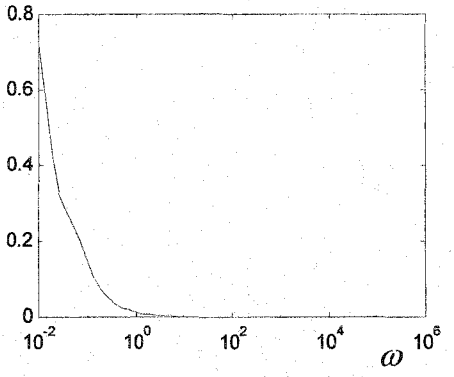

Figure 4.3: Upper bound on μ for Example 1

Example 2

The second example representing the three-mass SISO system is given in a complex modal representation as described above. The damping ratios and the frequencies of the flexible modes are $\zeta_1 = 0.025$, $\zeta_2 = 0.012$, $\zeta_3 = 0.0043$, $\omega_1 = 5.12$, $\omega_2 = 2.43$, $\omega_3 = 0.87$. The uncertainties that the damping ratios and the frequencies of the flexible modes are subjected to represent 10% and 3%, respectively. These uncertainty levels, especially in the frequencies, are quite demanding for a robust control design. The weighting functions W_p and W_u are the same as the ones used in the first example.

Figure 4.4 shows that the magnitude of the first element in $W_{\tilde{M}}$ tightly bounds all the variations in the first entry of $\Delta\tilde{M}$.

The magnitude of the second entry on the diagonal of $\Delta\tilde{M}_1$ is the same as that of the first entry (this also holds for the other flexible modes). Thus, $W_{\tilde{M}}$ is a good candidate for bounding the complex parametric uncertainty in $\Delta\tilde{M}$.

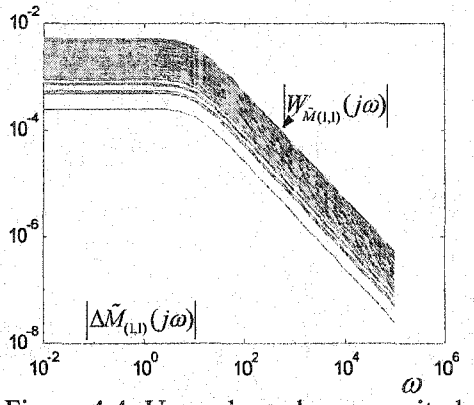

Figure 4.4: Upper bound on magnitudes of perturbations for Example 2

The μ-synthesis setup used for the complex-rational controller design is based on scaled H_2 optimization problems [Yan97]. These optimizations were treated and solved by means of solving two Riccati equations:

$$\begin{aligned}&\left(A-B_2R_1^{-1}D_{12}^*C_1\right)^* X+X\left(A-B_2R_1^{-1}D_{12}^*C_1\right)\\&\quad -XB_2R_1^{-1}B_2^*X+C_1^*\left(I-D_{12}R_1^{-1}D_{12}^*\right)C_1=0\end{aligned} \tag{4.15}$$

$$\begin{aligned}&\left(A-B_1D_{21}^*R_2^{-1}C_2\right)^* Y+Y\left(A-B_1D_{21}^*R_2^{-1}C_2\right)\\&\quad -YC_2R_2^{-1}C_2^*Y+B_1^*\left(I-D_{21}^*R_2^{-1}D_{21}\right)B_1^*=0\end{aligned} \tag{4.16}$$

where: $R_1=D_{12}^*D_{12}$, $R_2=D_{21}D_{21}^*$.

The complex-rational scaled augmented plant P in its simplified state-space representation is given by:

$$P(s):=\left[\begin{array}{c|cc}A & B_1 & B_2\\ \hline C_1 & 0 & D_{12}\\ C_2 & D_{21} & 0\end{array}\right] \tag{4.17}$$

where: $A\in\mathbb{C}^{n_p\times n_p}, B_1\in\mathbb{C}^{n_p\times n_w}, B_2\in\mathbb{C}^{n_p\times n_u}, C_1\in\mathbb{C}^{n_z\times n_p}$, $C_2\in\mathbb{C}^{n_y\times n_p}, D_{12}\in\mathbb{C}^{n_z\times n_u}, D_{21}\in\mathbb{C}^{n_y\times n_w}$. and n_p is the number of modes.

The fact that the state matrices involved in the Riccati equations belong to a complex set gives us the possibility of designing a complex-rational μ-controller achieving the performance and robustness specifications required.

The complex-rational μ controller designed in this case achieved the specified robust performance criterion. Figure 4.5 shows the μ-upper bound obtained for this design. Its maximum equals 0.99.

Note that the μ controller designed is not optimal, and this is because of the uncertainty block structure. This problem of suboptimality of a μ-design has been mentioned in the literature [Bal95]. However, the μ-design still appears to be the best strategy to deal with structured uncertainties in practice. The complex-rational controller design allowed us to deal efficiently with the parametric uncertainties under a complex representation. An uncertainty of up to 3% in the modal frequencies could be tolerated, a level rarely reported in the literature.

After designing a complex-rational controller achieving the robust performance specification, we have to recover a realizable real-rational controller. This controller has to maintain the performance specifications obtained by the complex-rational controller. The problem can be posed as:

$$\min_{K_{rea}} \left\| K - K_{rea} \right\|_{\infty} \tag{4.18}$$

where:

K is the complex-rational controller designed and K_{rea} is the real-rational controller to be found. By enforcing closeness of the frequency responses of the two controllers using the infinity norm, we can ensure that both controllers will act in the same manner on the generalized plant when closing the feedback loop. Thus, the level of performance obtained by the complex-rational controller can be approached by using a real-rational controller. One way to solve the minimization problem above is to fit the magnitude and the phase generated by the complex-rational controller, by a real-rational system K_{rea}. Tools that have the ability to provide a solution in this fitting procedure can be found in Matlab's Identification toolbox [Kol97]. One of the benefits of this real procedure design is the reduction of the real-rational controller. In fact, the typical constraint of maintaining the structure of the original controller in most classical reduction procedures is not present in the fitting procedure proposed here: The structures of the original complex-rational controller and the reduced real-rational controller may differ. Thus, a low order, real-rational controller, achieving robust performance criteria, can be obtained.

A real-rational controller of order 2, achieving a robust performance level of 0.85, was generated for our example. The robust performance level for the real controller is shown in Figure 4.6. The robust complex-rational controller is of order 28. This high order resulted from the number and order of the scales in the μ-design. Due to the non-optimality of the μ-design, the robust performance of the real-rational controller was better than the one obtained by the original complex-rational controller.

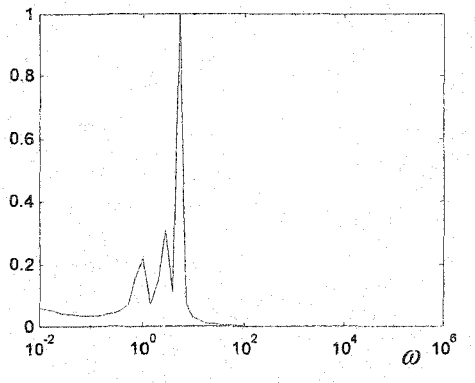

Figure 4.5: Upper bound on μ with complex-rational controller for Example 2

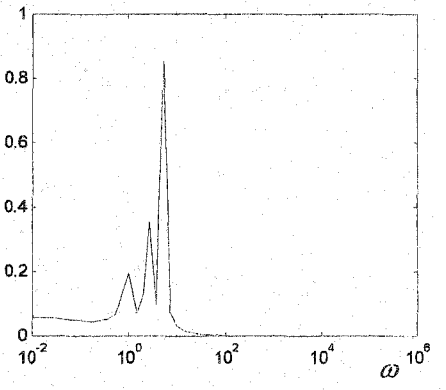

Figure 4.6: Upper bound on μ with real-rational controller for Example 2

Chapter 5

Gain scheduling techniques for STOVL Harrier aircraft

5.1 Introduction

Multivariable gain scheduling has been an open problem until now. Many techniques have been developed from standard interpolation and switching techniques [Hyd91], [Han87] from linear parameter-varying model approaches [Rugh90], [Sham91], to modern interpolation techniques [Stil99]. Applications of these gain-scheduling techniques for flight control have been extensive in the last decade [Hyd91], [Rei92], [Fial97], [Pap98]. The recent developments in linear parameter varying control [Apk95], [Wu95a], [Wu95b] have spurred research on the stability aspects of gain-scheduled controllers that is considered a deficiency of *ad hoc* gain scheduling techniques (interpolation and switching techniques). In this thesis, and due to the complexity of the models we deal with, we preferred to approach the gain-scheduling problem of Chapter 5 and Chapter 6 by proposing new methods, based on *ad hoc* techniques, but improved in terms of stability and performance guarantees.

The research developed in this part of the thesis concerns the gain-scheduling aspect of a control design for a large flight envelope of a Short Takeoff and/or Vertical Landing (STOVL) aircraft. In [Bate99] a robust integrated flight propulsion controller was designed for an experimental STOVL aircraft configuration, using the method of H_∞ loopshaping. Results of piloted simulation trials with a centralized Integrated Flight Propulsion Control (IFPC) system are reported in [Bate2000]. The IFPC system examined in these trials was designed at the 80 knots point of the STOVL flight envelope, where control of the aircraft is starting to pass from purely propulsion system effectors (thrust vectoring nozzles, etc..) to conventional aerodynamic control surfaces. These trials examined the handling qualities of the IFPC system over a range of speeds from 50 to 110kn. While the single controller was found to deliver level 1 handling qualities, [Bate99], at speeds close to its design point, performance was seen to degrade to level 2 quality, [Bate99] as the aircraft moved further away from the 80 kn point of the flight envelope. This degradation in performance is caused by the large changes in both aerodynamics and engine dynamics as the aircraft accelerates from hover to fully wingbourne flight.

In this research study, in order to cope with the performance degradation, we develop the design of alternative scheduling schemes for the IFPC system which provide Level 1 type handling qualities as the Harrier STOVL aircraft, under study here, accelerates from hover to 120 knots, while also keeping the specified engine variables within their safety limits.

Our methodology of control design, based on the H_∞ loopshaping, led us to investigate first how to adapt the observer-form interpolating technique [Hyd91], to our IFPC control design. Furthermore, we propose two other methods trying to improve performance objectives.

The second approach of controller scheduling proposed is a new version of the blending technique implemented successfully for a missile application in [Tich96]. In this technique, we are interested by the output signals of controllers rather than the structure of the controllers themselves.

Adding to the previous scheduling methods proposed, we investigate how we can use a straightforward switching technique between the controllers designed. We develop a new multi-switching methodology based on the Linear-quadratic bumpless transfer technique introduced recently in [Turn2000]. We propose, finally, an innovative scheduling technique based on a partitioned controller obtained from a partitioning procedure applied to the centralized controller designed in the beginning of the IFPC methodology.

5.2 Integrated methodology for propulsion and airframe control

The desire to improve the overall performance of multi-components dynamically coupled systems has stimulated researchers to develop integrated system control design methodologies. One example of interest is the control design of a Short TakeOff and Vertical Landing (STOVL) aircraft. The use of forces and moments produced by the propulsion system to extend the flight envelope of the aircraft results in significant coupling between the airframe and propulsion systems. Traditional control design methodologies, as separate control design for flight and propulsion systems, cannot deal with such coupling. The recent STOVL aircraft include supersonic flight capabilities, which add more complexity in their configurations than subsonic aircraft. This complexity spurred the research in Integrated Flight and Propulsion Control (IFPC) [Garg93a]. The objective of the IFPC research is to consider methodologies to improve the overall system performance. It exploits potentially significant gains in terms of improved flying qualities which may be obtained through the use of propulsive system generated forces and moments for aircraft manoeuvring in the low region of the flight

envelope. These methodologies have to take into account dynamical coupling between the airframe and propulsion systems of STOVL aircraft.

A study program on Design Methods for Integrated Control Systems (DMICS) was undertaken in the 1980's to develop IFPC control laws for an advanced tactical aircraft. The aircraft configuration for the DMICS study included thrust-vectoring and thrust-reversing capabilities that add dynamic coupling between the propulsion and airframe system. The DMICS study proposed two design methodologies: the first one consists in a complex centralized approach that led to a centralized controller design, with the potential to give the best performance, and taking into account all specified criteria. However, this approach is suffering from the complexity of implementing this kind of controller in existing airframe-propulsion control system hardware structures. The second methodology is based on a decentralized hierarchical approach. This approach is highly iterative, leads to lower performance and assumes that the subsystems are weakly coupled, which is not generally the case.

The integrated methodologies for propulsion and airframe control (IMPAC), based on the experience of DMICS study, have the objective to search a new IFPC methodology that takes into account the airframe and the propulsion systems as one integrated system. For this integrated system, initially, a centralized controller design, for each design point, is suggested taking into account all the specifications required, from the performance to the dynamical coupling existing between subsystems. In fact, the starting point of IFPC methodologies was the IMPAC program, which led to good applied results for STOVL aircraft [Garg93b].

5.3 STOVL Harrier Aircraft:

Our research work concerns the well-known STOVL Harrier jump-jet aircraft (Figure 5.1).

Figure 5.1 : A version of STOVL Harrier aircraft

Many versions of this aircraft were developed since the original P1127 Harrier created in 1960. The recent versions include much-advanced avionics and improved handling qualities. The STOVL aircraft are of a particular importance for the military aerospace industry regarding the advantages they offer for military operations. The performance objectives required from recent version of the STOVL Harrier aircraft impose a high workload on the pilot. This is mainly due to the instability of the aircraft for a longitudinal motion at low speed: the inceptor configuration has a difficulty to deal with complex operation moments and the poor decoupling level. A multivariable control technique is then required to reach the specified Harrier aircraft handling qualities while reducing the pilot workload. A modern control strategy was successfully developed for a previous version of the Harrier aircraft in [Hyd91].

In this study, we are concerned with more complex version of the Harrier aircraft. In fact, due to the development of actuator technologies, we could fully integrate the flight and propulsion control systems rather than being restricted to control the longitudinal motion of the aircraft [Hyd91]. The use of the propulsion system to generate forces and moments for aircraft manoeuvring results in significantly increased coupling between the airframe and engine sub-systems. In its simplest form this coupling may be unidirectional (propulsive forces and moments affecting airframe states) but in general the use of novel effectors such as reaction control systems will also affect the engine operating point, [Garg93a], [Garg93b]. This coupling necessitates an integrated approach to the overall flight control system design problem, in order to ensure that (a) optimal use is made of the various propulsion system effectors for aircraft manoeuvring control, and (b) limitations due to engine safety considerations are taken into account in the overall design. This integrated approach is realized in our research study by an Integrated Flight Propulsion Control (IFPC) methodology, which was first successfully developed in [Garg93a].

The aircraft simulation model used in this study has been developed at defense evaluation and research agency (DERA) Bedford (UK) in order to investigate the problems and opportunities associated with the integration of flight and propulsion control systems for STOVL aircraft. The airframe model is based on the nonlinear DERA Bedford Harrier T.Mk4 Wide Envelope Model (WEM). This model has been established through flight trials as being representative of the real aircraft. In order to fully explore the possibilities of advanced engine control under an IFPCS framework, the original Pegasus engine previously included in the WEM has been replaced with a high-fidelity thermodynamic model of the Rolls Royce Spey engine shown in Figure5.2, produced by DERA Pyestock. The Spey is a two–spool reheated turbofan engine with the same basic architecture, for the purposes of control, as the

EJ200, which is used to power the Eurofighter. The thermodynamic model of the Spey allows the control law designer full access to engine parameters such as inlet guide vane angle, fuel flow rate and exit nozzle area. The engine thrust is vectored through four nozzles similar to the standard Harrier. Total thrust and high-pressure bleed flow to the Reaction Control System (RCS) is scaled to match the performance of the Pegasus engine. The effect of high-pressure bleed flow (to the RCS) on the engine operating point is modeled, and the effect of front/rear thrust split on engine performance is assumed to be negligible.

To increase the design difficulty, the front pair of nozzles has been moved forward and downward to displace the center of thrust from the center of gravity and introduce thrust/pitching moment interactions. Also unlike with the standard Harrier, the thrusts from front and rear nozzle pairs can be modulated and vectored independently. Representative nonlinear actuation systems including both rate and magnitude limits (as well as deadzones and hysteresis for the thrust vectoring nozzles) have been placed on all control motivators. The model offers a six-degree of freedom nonlinear simulation over a flight envelope from hover to 250 knots, and linearized models for controller design purposes can be generated over the full flight envelope.

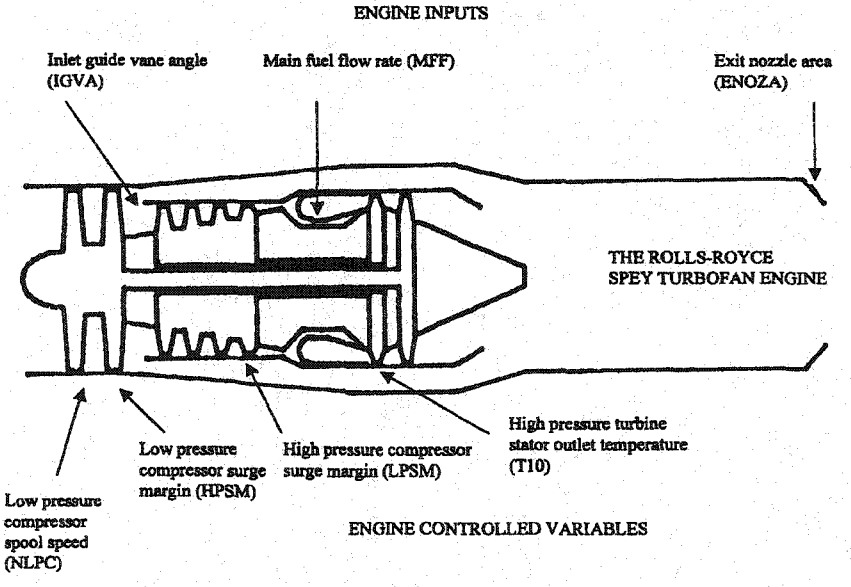

Figure5.2: Spey engine scheme

Nomenclature

γ : Flight path angle (deg).

α : Aircraft angle of incidence(deg).

$\dot{\gamma}$: Flight path angle rate(deg/s).

VT : Velocity along the flight path(knots).

NLPC : Low-pressure compressor spool speed(%).

*T*10 : High-pressure turbine stator outlet temperature(K).

HPSM : High-pressure compressor surge margin(%).

LPSM : Low-pressure compressor surge margin(%).

THM : Thrust magnitude(kN).

ETAD : Elevator position (-15deg to 15deg).

ETASTK : Pitch reaction control system position (-15deg to 15deg).

FNOZ : Front Nozzle position (-5deg to 120deg).

RNOZ : Rear Nozzle position (-5deg to 120deg).

SPLIT : Engine thrust split (0 to 1 : 0= all to front, 1=all to rear).

MFF : Main fuel flow (0 to 1.2 kg/s).

ENOZA : Exit Nozzle area (0.8307 to 0.1602 sine petal angle).

IGV : Inlet guide vane angle (-8deg to 35deg).

The results presented in this chapter relate to the control of the longitudinal axis only, and the control law is required to follow a two-inceptor strategy. In this scheme, fore/aft displacement of the center stick produces a change in flight path angle rate $\dot{\gamma}$, and displacement of the left-hand inceptor demands aircraft velocity *VT* parallel to the flight path. Functional specifications for the IFPC system are given as follows:

a) Flight Path Manoeuvre Demand: The rigid hand pitch control law will command flight path angle rate and should actively hold flight path with the stick centered. Stick displacement will produce a flight path rate demand up to a maximum of $3^{\circ}/\sec$. Flight path demands should aim to be decoupled
from axial manoeuvres, with a maximum demand of ±2knots transient speed change during any flight path manoeuvre.

b)Velocity Demand: Left-hand inceptor displacement will demand velocity parallel to flight path (VT). A maximum transient deviation of $\pm 0.3^{\circ}$ in flight path angle is desirable during velocity changes of up to ± 30knots.

c) Incidence Limit: To avoid extreme incidence angles, which can lead to lateral/directional instability, an incidence boundary is necessary. The aircraft angle of incidence, α, should therefore be kept within $+12^{\circ}$ and -6° during all manoeuvres.

d) Engine Safety Limits: To protect engine components from dangerous over stress and over temperature, and to ensure avoidance of surge conditions, the following set of engine limits are to be respected during all manoeuvres:

1- Low Pressure Spool speed (NLPC) <102%

2- High Pressure Turbine Stator Outlet Temperature (T10) <1430K

3- High Pressure Compressor Surge Margin (HPSM)>10%

4- Low Pressure Compressor Surge Margin (LPSM)>10%

Recommended maximum limits were also provided for five other engine variables – see [Bate2000] for details.

5.4 Centralized IFPC system design

The technique chosen for our IFPC system is the H_{∞} loopshaping procedure described in [Mcf90]. This procedure provides certain advantages over the traditional mixed sensitivity H_{∞} optimization. A report produced by the British Aerospace on full-authority fly-by-wire, [Hyd91], indicates that separating the design into two steps of 1) command feed-forward design and 2) robust closed-loop stabilization leads to an effective design approach. This is typically the case of the H_{∞} loopshaping technique, which offers good handling qualities while maintaining a good stability margin.

Since a comprehensive tutorial on the H_{∞} loopshaping design method is given in Chapter 3, we give only a brief outline of the H_{∞} loopshaping technique used to design the individual controllers. The aircraft nonlinear model was trimmed and linearized at 0,20,50,80 and 120 kn points of the flight envelope. The H_{∞} loopshaping controllers were designed for linearized models of the aircraft/engine dynamics, generated at the operating points specified. The resulting state-space models of the integrated airframe and engine systems, plus actuators, have 35 states and are of the form:

$$\dot{x} = Ax + Bu \tag{5.1}$$

$$y = Cx + Du \tag{5.2}$$

The control inputs are given by

$u = [ETAD, ETASTK, FNOZ, RNOZ, SPLIT, MFF, ENOZA, IGV]$

while the vector of outputs y includes 8 airframe and 19 engine variables. Based on the performance requirements previously detailed, the vector of controlled variables z was chosen as

$z = [\alpha, VT, \dot{\gamma}, NLPC, T10, HPSM, LPSM]$

The angle of incidence α was included in z in order to explicitly minimize deviations from its trim point during maneuvers. The H_∞ loopshaping design method used to design the controllers, [Mcf90], is essentially a two-stage process. First, the open loop plant is augmented by (generally diagonal) weighting matrices to give a desired shape to the singular values of the open-loop frequency response. Then, the resulting shaped plant is robustly stabilized with respect to coprime factor uncertainty using H_∞ optimization. The implementation structure for the H_∞ loopshaping controller used in the piloted simulation trial is shown in Figure 5.3.

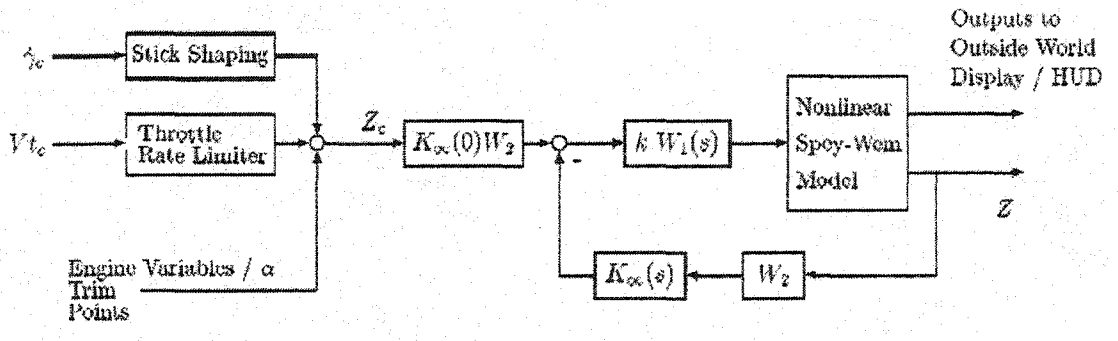

Figure 5.3: H_∞ loopshaping controller implementation for piloted trials

With reference to this figure, the weighting matrix $W_1(s)$ is chosen generally to add integral action and ensure reasonable roll-off rates for the open-loop singular values around the desired crossover frequencies. The scalar weighting matrix k is then used to adjust control actuation requirements to satisfy the various actuator rate and magnitude limits. For each of the linear designs between 0 and 120 knots the weighting function $W_1(s)$, containing pure integrators, was thus chosen to be of the form

$W_1(s) = \frac{s+a}{s}$, with the parameter a varying smoothly between different designs points. Note that in this configuration the nonlinear Spey-Wem aircraft model is assumed to be scaled so as to be approximately normalized with respect to maximum allowable input signals. The scalar matrix W_2 is used to prioritize airframe-controlled variables (which must achieve specific handling qualities characteristics) over engine variables (which have simply to be limited within certain values). For the 50 kn controller for example, the three weighting matrices were chosen as:

$$k = diag(.13,.1,.25,.25,.25,.2,.2,.2),\ W_1 = \frac{s+2}{s} \times I_8$$

$$W_2 = diag(1,1,1,1/200,1/800,1/200,1/500)$$

The second stage of the H_∞ loopshaping design method involves the use of H_∞ optimization to compute a controller block K_∞ which robustly stabilizes the shaped plant against a particular type of uncertainty description, based on stable perturbations to each factors in a normalized coprime factorization of the plant. The K_∞ block controller for each operating design point was respectively designed as described in Chapter 3 by means of the solutions of the Riccati equations given in (2.72),(2.73). The final step of the design procedure is to add the constant prefilter $K(0)W_2$ in order to ensure zero steady-state tracking error, assuming integral action in W_1. The K_∞ controller block for each operating point is of order equal to that of the shaped plant, i.e, for each of our designs K_∞ has 43 states.

5.5 Observer-form implementation and scheduling

In [Sef90], It was shown that the controller resulting from the H_∞ loopshaping procedure can be written as an exact plant observer plus state feedback. Assuming, purely for notational convenience, a strictly proper shaped plant, with stabilizable and detectable state space realization

$$G_s = \left[\begin{array}{c|c} A_s & B_s \\ \hline C_s & 0 \end{array}\right] \tag{5.3}$$

the equations of the plant observer plus state feedback of the H_∞ loopshaping controller are:

$$\dot{\hat{x}}_s = A_s\hat{x}_s + H_s\left(C_s\hat{x}_s - y_s\right) + B_s u_s \tag{5.4}$$

$$u_s = K_s\hat{x}_s \tag{5.5}$$

where $\hat{x}_s$ is the observer state, u_s and y_s, are respectively the input and the output of the shaped plant, and

$$H_s = -Z_s C_s^* \tag{5.6}$$

$$K_s = -B_s^* [I - \gamma^{-2} I - \gamma^{-2} X_s Z_s]^{-1} X_s \tag{5.7}$$

where Z_s and X_s are the appropriate solutions to the generalized algebraic Riccati equations, (2.72), (2.73) for a given $G_s = \left[\begin{array}{c|c} A_s & B_s \\ \hline C_s & D_s \end{array}\right]$. In general an H_∞ controller cannot be written as an exact plant observer combined with a state feedback gain matrix, as there will be a worst-case disturbance term entering the observer state, [Doy89]. However, for a controller produced by the H_∞ loopshaping method, this clear structure exists, as mentioned, and lends itself to gain-scheduling in that the controller matrices K_s and H_s can be simply scheduled as a function of one or more aircraft parameters. Figure 5.4 shows the observer implementation structure of the IFPC system scheduled as a function of aircraft speed. At a given speed *v*, each matrix in the observer structure is linearly interpolated, using the ith and jth (can be (i+1)th or (i-1)th) adjacent designs, as:

$$H_s[\lambda(v)] = [1 - \lambda(v)] H_{si} + \lambda(v) H_{sj} \tag{5.8}$$

where $\lambda(v) \in [0,1]$.

Note that the observer is for the shaped plant G_s, and thus this places some limitations on the choice of weighting functions for each of the linear controller designs – in particular they must have a fixed structure and vary smoothly over the envelope to smooth the dynamics change of the shaped plant. Otherwise, from an implementation point of view, the interpolation of the weighting functions will be difficult and there will be little differences between H_∞ loopshaping controllers written in this form and the classical LQG/LTR structure of modern control theory, [Ste92].

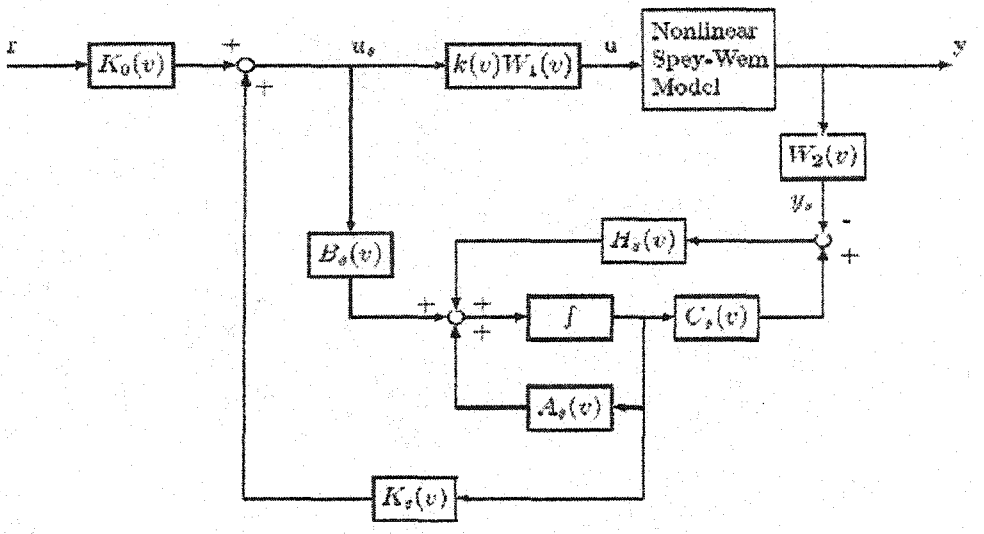

Figure 5.4 : Scheduled Observer implementation of the

For successful operation of the scheduled system it is essential that the controller gains K_s and H_s vary smoothly with operating point. A theorem in [Hyd91] can be used to show that this condition will be satisfied provided the Riccati solutions X and Z and the stability margin γ vary smoothly.

Theorem 5.1

Let $A_s(\theta), D_s(\theta), C_s(\theta)$ be analytic $n \times n$ matrix functions of θ defined on a real interval $[\alpha, \beta]$, with $D_s(\theta)$ positive semi-definite Hermitian, $C_s(\theta)$ Hermitian, and $(A_s(\theta), D_s(\theta))$ stabilizable for every $\theta \in [\alpha, \beta]$ the Riccati equation:

$X(\theta)D_s(\theta)X(\theta) - X(\theta)A_s(\theta) - A_s(\theta)^* X(\theta) - C_s(\theta) = 0$ has a Hermitian solution. Further assume that the number of purely imaginary eigenvalues of $M(\theta) = \begin{bmatrix} A_s(\theta) & -D_s(\theta) \\ -C_s(\theta) & -A_s(\theta)^* \end{bmatrix}$ is constant.

Then the maximum solution $X_m(\theta)$ (given $\theta\ X_m(\theta) > X_i(\theta)\ \forall i$) is an analytic function of $\theta \in [\alpha, \beta]$.

Using the above theorem for the solutions of the Riccati equations used in the H_∞ loopshaping design of a state space realization $\left[\begin{array}{c|c} A_s & B_s \\ \hline C_s & 0 \end{array}\right]$ of a shaped plant G_s, we need the following conditions to hold:

For

$$A_s^* X + X A_s - X B_s B_s^* X + C_s^* C_s = 0 \tag{5.9}$$

1- $B_s B_s^*$ is positive semi-definite Hermitian.

2- $C_s^* C_s$ is Hermitian.

3- $(A_s, B_s B_s^*)$ is stabilizable.

4- $M_c(t) = \begin{bmatrix} A_s & -B_s B_s^* \\ -C_s^* C_s & -A_s^* \end{bmatrix}$ has a constant number of purely imaginary eigenvalues.

For

$$AZ + ZA^* - ZC^*CZ + BB^* = 0 \tag{5.10}$$

5- C^*C is positive semi-definite Hermitian.

6- BB^* is Hermitian.

7- (A, C^*C) is stabilizable.

8- $M_F(t) = \begin{bmatrix} A & -C^*C \\ -BB^* & -A^* \end{bmatrix}$ has a constant number of purely imaginary eigenvalues.

The first three conditions are satisfied trivially, and by assumptions for solution of the normalized coprime factor robust stabilization problem [Mcf90]. Adding to that, if (A, B) and (C, A) are stablizable and detectable respectively, then M_c and M_F have no imaginary eigenvalues. Thus the conditions (4,8) for the Riccati equations (5.9),(5.10) are satisfied.

This result confirms that a smooth interpolation of the parameters of the shaped plant matrices will lead to smooth solutions to the Riccati equations and hence smooth observer and state feedback gains. The shaped plant matrices A_s, B_s, C_s have to vary smoothly with operating point, while also capturing the important changes in the dynamics of the plant over the specified portion of the envelope – knowledge of the aircraft and engine dynamics needs to be used here to decide on the position and number of design points required for interpolation. Some extra freedom can also be introduced by using weighting functions in the interpolation of the different matrices,

$$A_s(v) = (1 - \lambda(v)^p) A_{si} + \lambda(v)^p A_{sj} \tag{5.11}$$

where: $\lambda(v) \in [0 \quad 1]$.

$\lambda(v) = 0$ corresponds to the design i, $\lambda(v) = 1$ corresponds to the design j.

so that the exponent p can be used to get a better match between the interpolated linear system and the actual non-linear system. In fact with our knowledge of the nonlinear model of the aircraft, and

because we interpolate parameters of two linear models, we can give more weight to the state matrices of the most faithful linear model. With that technique, we can also use more weight on the gains of the controllers that we have a confidence in their efficiency around a specific interval of operating points by playing with the tunable exponent p. Note that the constant prefilter must be recalculated at each operating design point to take account of the different structure of the observer-form implementation. Using the linearization of the nonlinear Spey-Wem model around a fixed speed and the structure of the observer-based controller of Figure 5.4, the output of the linearized system is given as:

$$y = -(I + TH_sW_2)^{-1}(TB_s + GW_1k)r \tag{5.12}$$

with

$$T = GW_1kK_s\left(sI - A_s - H_sC_s - B_sK_s\right)^{-1} \tag{5.13}$$

in order to have steady-state error we choose a constant prefilter K_0 given by

$$K_0 = -\left(T(0)B_s + G(0)W_1(0)k\right)^{-1}\left(I + T(0)H_sW_2(0)\right) \tag{5.14}$$

Assuming integral action in W_1 this simplifies to

$$K_0 = \left(I + RB_s\right)^{-1}\left(-RH_sW_2(0)\right) \tag{5.15}$$

where

$$R = -K_s\left(A_s + H_sC_s + B_sK_s\right)^{-1} \tag{5.16}$$

This constant prefilter must then also be scheduled as a function of speed in order to take account of variations in the low-frequency gain of the controller over the envelope.

Simulation results show that the observer-form implementation of the H_∞ loopshaping is suitable in terms of performance. Figure 5.5 (in terms of $\dot{\gamma}$ demands, velocity coupling and engine limits) and Figure 5.8 (in terms of velocity tracking) present improved performance of the observer-form structure comparing to the classical one-degree-of-freedom H_∞ loopshaping structure. This improvement is due mainly to the feedforward block, which was recalculated at each operating design point.

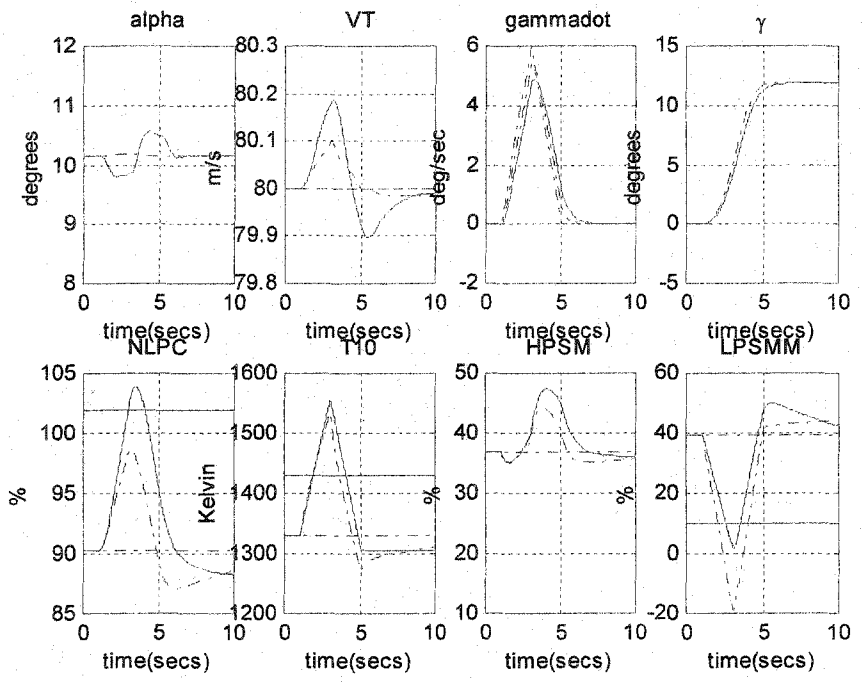

Figure 5.5 : Observer form(dashed)/1DOF H_∞ loopshaping structure for $\dot{\gamma}$ demand. Airframe and engine variables

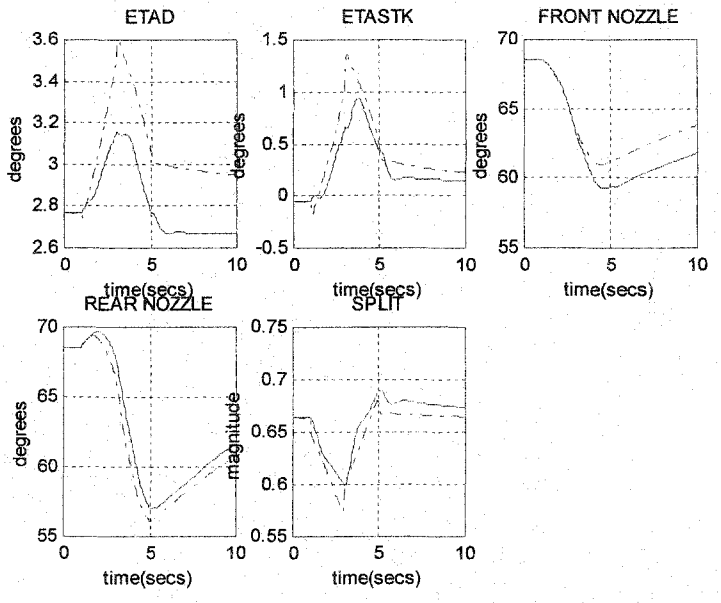

Figure 5.6 : Observer form(dashed)/1DOF H_∞ loopshaping structure for $\dot{\gamma}$ demand. Actuator efforts

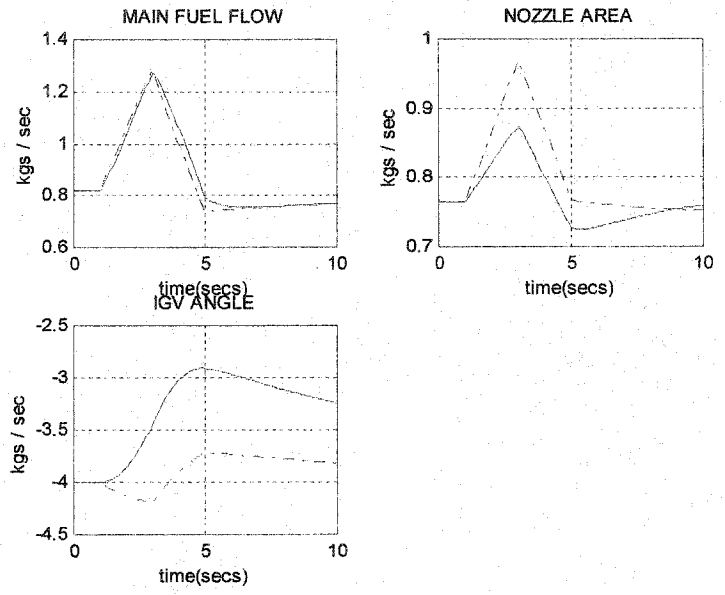

Figure 5.7 : observer form(dashed)/1DOF H_∞ loopshaping structure for $\dot{\gamma}$ demand. Actuator efforts

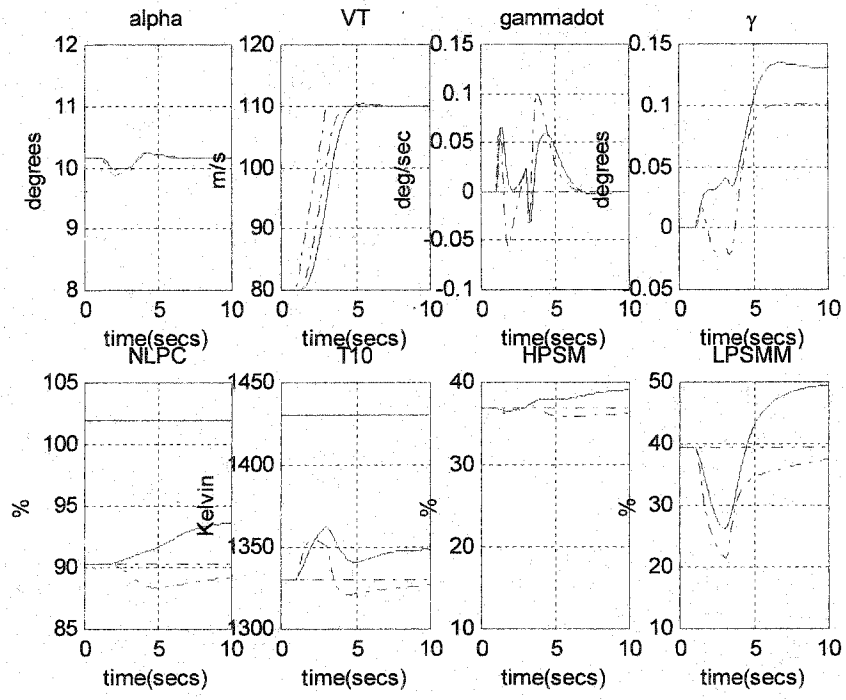

Figure 5.8 : Observer form(dashed)/1DOF H_∞ loopshaping structure for velocity demands: airframe and engine variables

Nonlinear simulation results for the scheduled IFPC system in the acceleration from hover phase are shown in Figures 5.9 to 5.12. The figures show close tracking of velocity demands as the aircraft accelerates from 0 to 120 kns, with only small deviations in flight path angle during the maneuver (comparison with results obtained in [Hyd91]). In addition, the four directly controlled engine variables are kept within their specified limits (Figure 5.12) and α is regulated close to its normal value throughout (Figure 5.9). The necessity for a gain scheduling scheme to preserve performance throughout this portion of the flight envelope is demonstrated in Figure 5.13 to 5.14, which compare the performance of the scheduled IFPC system with a single controller designed at the hover operating condition. As seen from the figures the hover controller, which gives good performance at low speed, is unable to cope with the large changes in the aircraft dynamics as it accelerates to wingbourne flight.

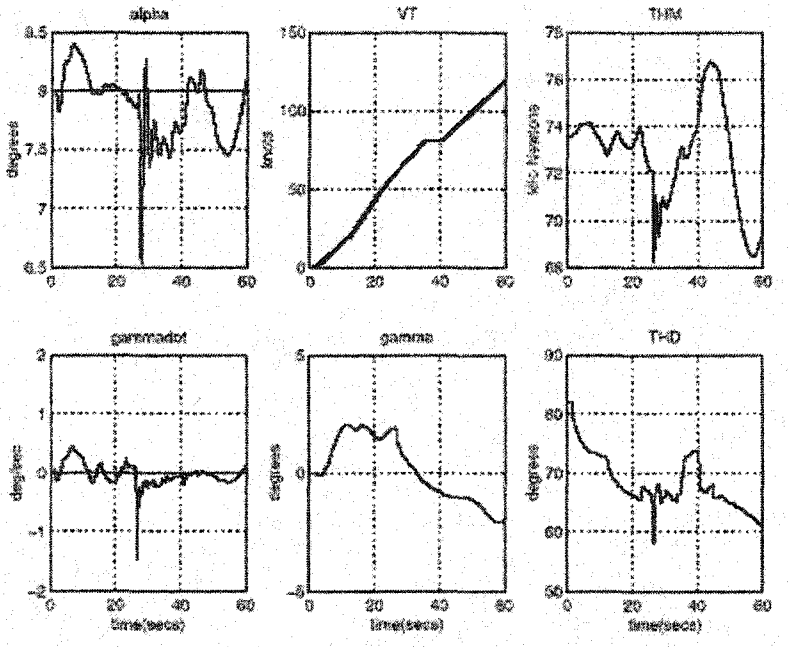

Figure 5.9 : Response of scheduled IFPC system for pilot demands VT in the acceleration from hover

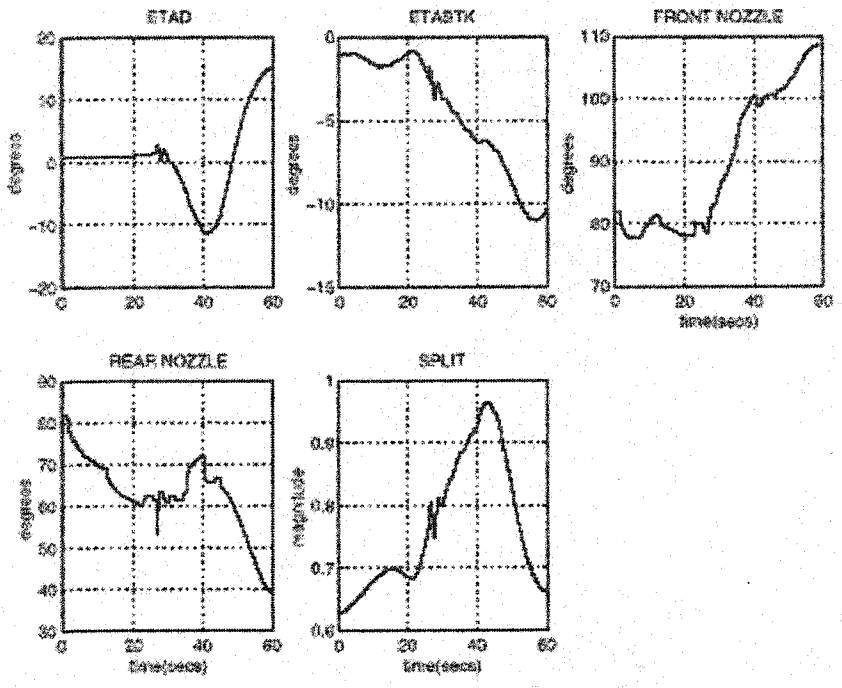

Figure 5.10 : Airframe actuator responses of pilot demands on VT in the acceleration from hover

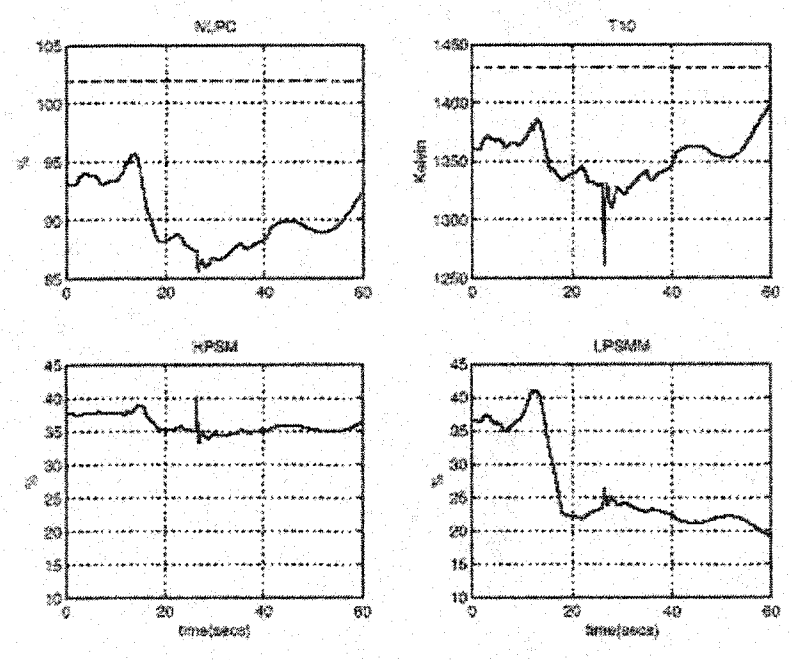

Figure 5.11 : Engine variables of pilot demands on VT in the acceleration from hover

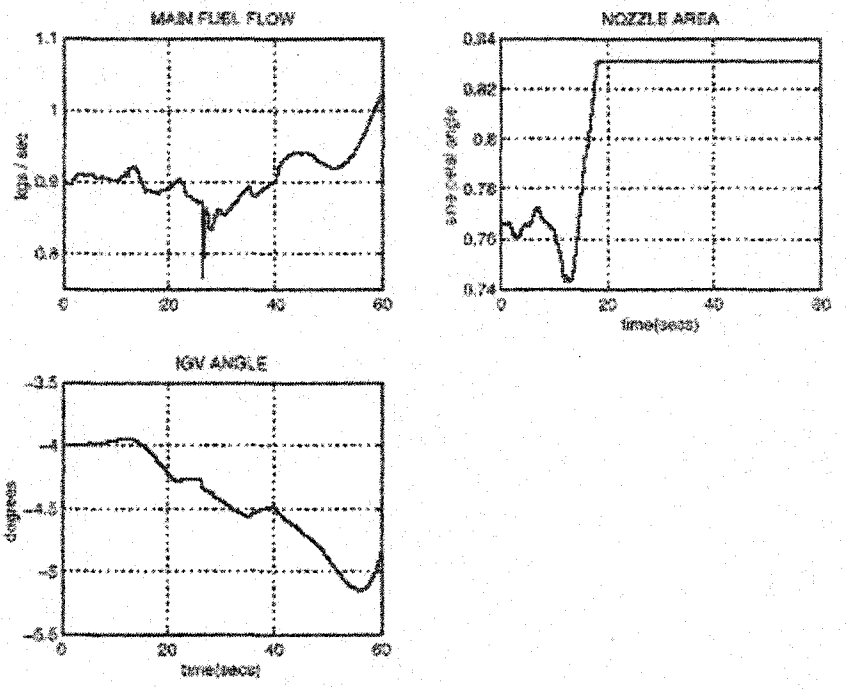

Figure 5.12 Engine actuators of pilot demands on VT in the acceleration from hover

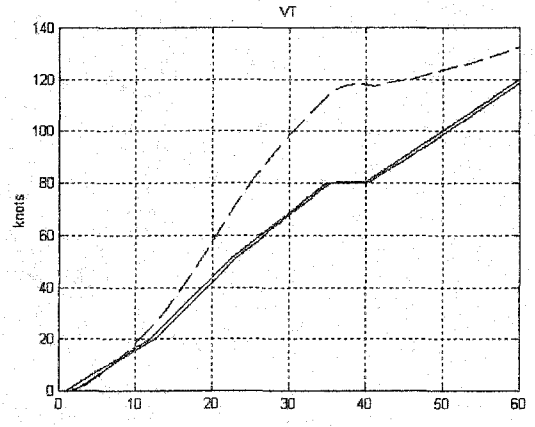

Figure 5.13 : comparison of VT responses to pilot, scheduled IFPC system (-), single controller designed at hover (--)

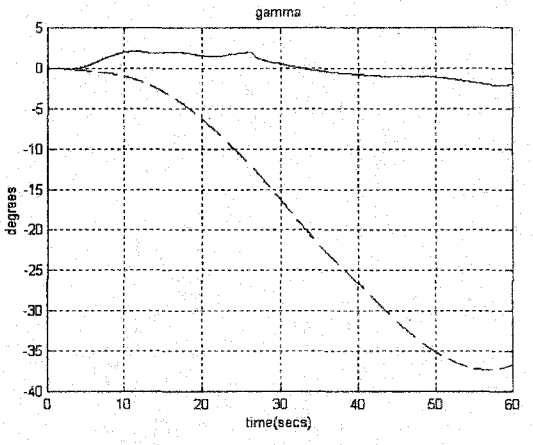

Figure 5.14 :comparison of $\dot{\gamma}$ coupling for pilot demands on VT, scheduled IFPC system (-), single controller designed at hover (--)

5.6 Antiwindup methodology

5.6.1 Problem statement

In this part of the gain scheduling for Harrier aircraft we want to extend the flight envelope over 150kn of velocity. For that, we design a controller at the 150kn operating point. However, a nonlinear simulation of this 150kn controller, depicted in Figure 5.15, shows an increase of the front nozzle effort opposite to the rear nozzle effort. This was not really permitted with previous Harrier aircraft, however the model that is currently in use in this thesis gives more flexibility on the actions of the pair (front nozzle, rear nozzle) actuators.

On the other hand, with this flexibility, we need to prevent saturation of the split causing the actuators to saturate. The results of observer gain scheduling technique from Hover to 150kn, in Figures 5.16, 5.17, 5.18, 5.19 show reduced performance on velocity tracking and coupling with unreasonable actuator effort leading in some cases to saturation. Thus, an antiwindup strategy is needed for better performance results.

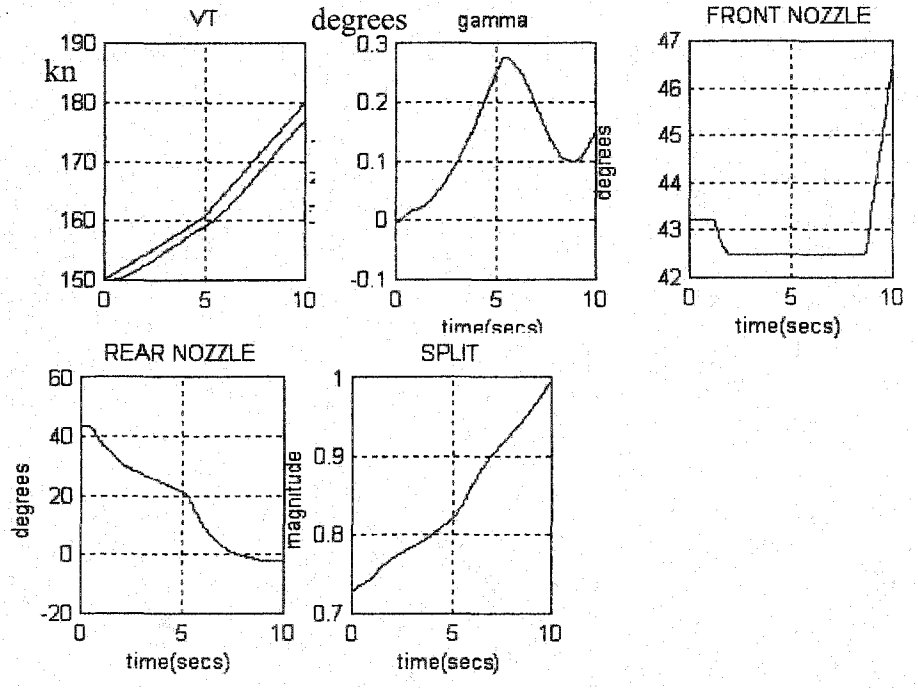

Figure5.15: Results of 150kn controller:
Velocity tracking

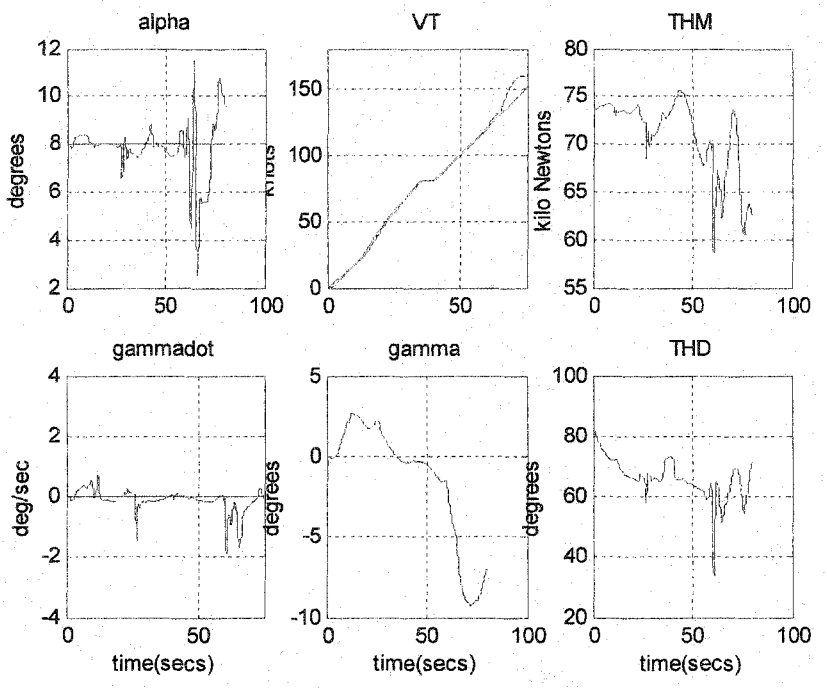

Figure5.16: Results of scheduled controller from hover to150kn without antiwindup technique. (a)

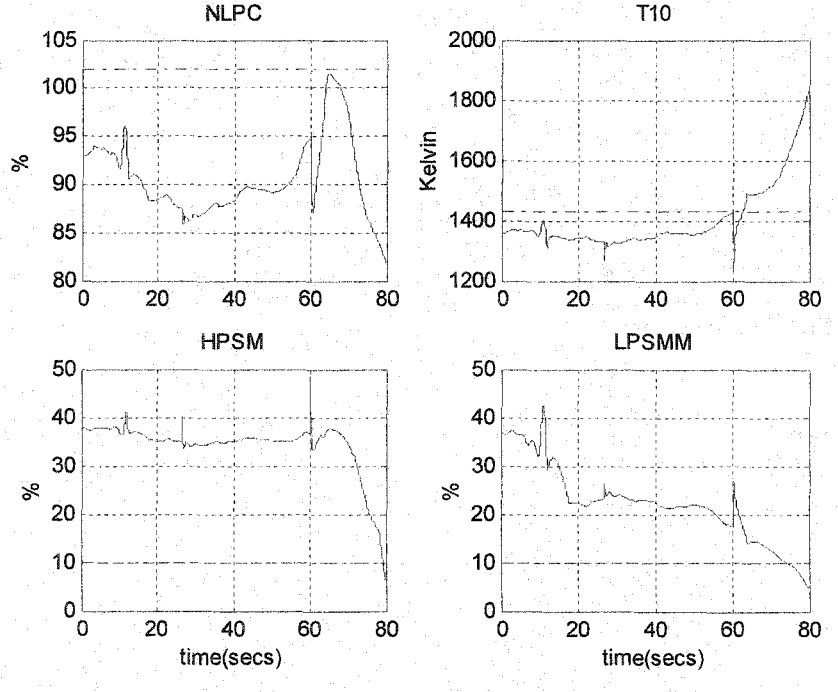

Figure5.17: Results of scheduled controller from hover to150kn without antiwindup technique. (b)

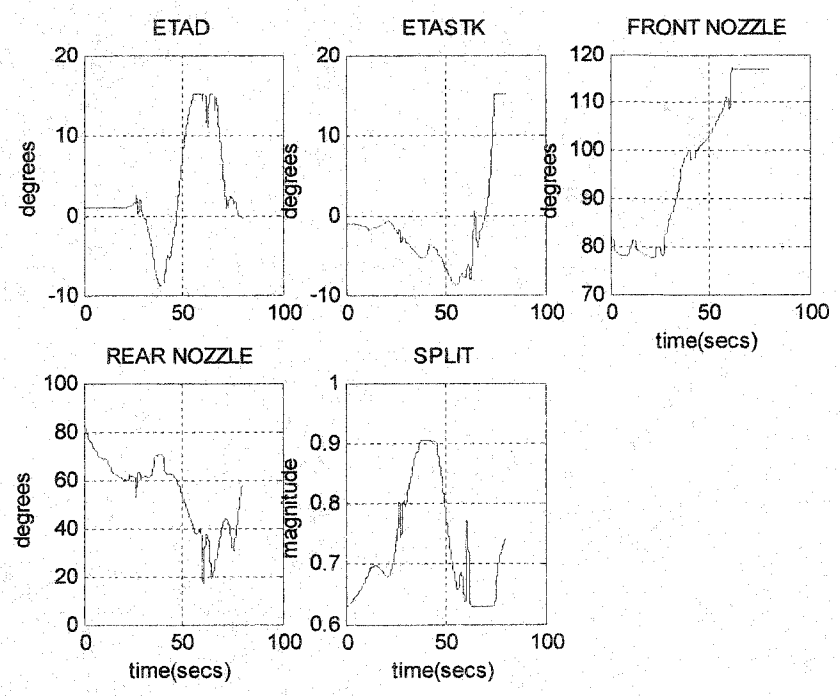

Figure5.18: Results of scheduled controller from hover to150kn without antiwindup technique. (c)

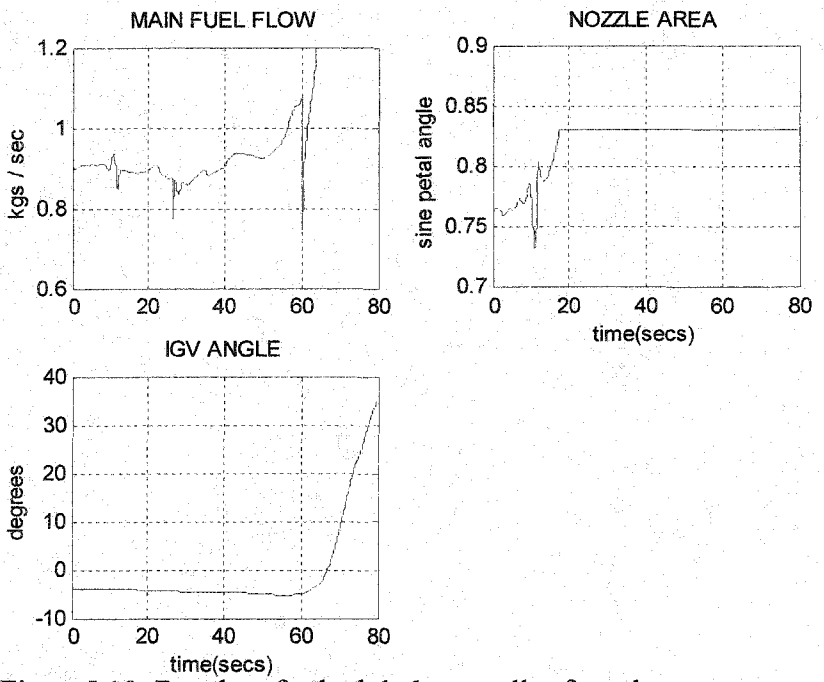

Figure5.19: Results of scheduled controller from hover to150kn without antiwindup technique. (d)

5.6.2 Antiwindup technique

Antiwindup techniques attempt to improve the performance of control systems with saturation constraints. Many such techniques have been reported in the literature and have been implemented for real plant. The most used one is the Hanus conditioning scheme [Han87]. This technique requires the controller to be invertible and minimum phase. The H_∞ loopshaping controllers designed for 0kn, 20kn, 50kn, 80kn, 120kn,and 150kn operating points satisfy those conditions. However, the implementation of this technique showed its limits for the observer-form H_∞ loopshaping controller [Hyd91]. Thus, an observer antiwindup technique is necessary for our 150kn controller. The general setup for this technique is given in Figure 5.20 [Hyd91]:

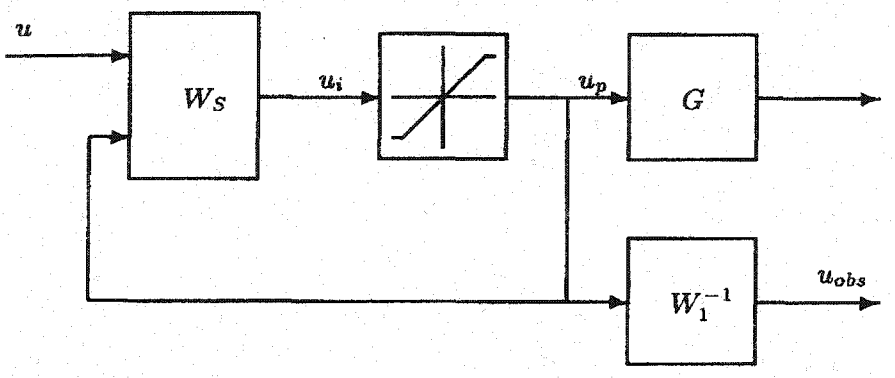

Figure5.20: Observer form antiwindup technique

$$W_1 = \left[\begin{array}{c|c} A_w & B_w \\ \hline C_w & D_w \end{array}\right],\ W_s = \left[\begin{array}{c|cc} A_w - B_w D_w^{-1} C_w & 0 & B_w D_w^{-1} \\ \hline C_w & D_w & 0 \end{array}\right].$$

Without saturation on *up* , the controller W_s is acting as W_1. The actual plant inputs u_p are used to drive the observer form controller, which results in the controller states remains consistent with the plant states. In the opposite to Hanus technique, the observer-form controller uses the signal u_{obs} obtained from the feedback signal u_p through W_1^{-1} (see Figure 5.4).

5.6.3 Application of the observer from antiwindup technique:

Because of the direct effect of the split actuator on the front and rear nozzles, and indirectly on all the actuators, we decided to include antiwindup block just for the split. We designed a 150kn "safe" controller, for which results are shown in Figure 5.21. The performance of the safe controller is lower than results obtained with the original controller without antiwindup. However, with this controller the front and rear nozzles efforts have reasonably decreased compared to the controller without antiwindup.

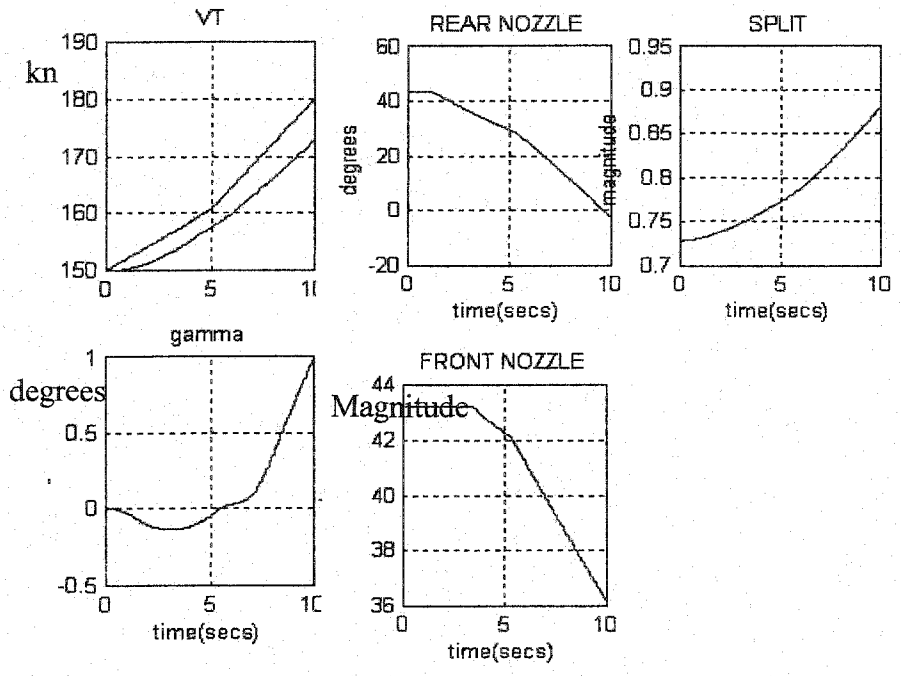

Figure5.21: Results of 150kn safe controller: Velocity tracking

To extend the flight envelope to 150kn velocity, we propose to compare an observer-form scheduling controller using the 150 kn controller without antiwindup, and using the 150 kn controller with antiwindup strategy. Results obtained with the antiwindup strategy show, in Figure 5.22, 5.23, 5.24, 5.25, that by constraining the split effort has a positive effect on all actuator efforts. This can be explained by the fact that the split is responsible on directing the thrust magnitude for front and rear nozzles. In addition, an indirect effect is noticed from split on other actuators. The tracking of the

velocity demands is quite good with small coupling in the flight path angle and reasonable actuator efforts.

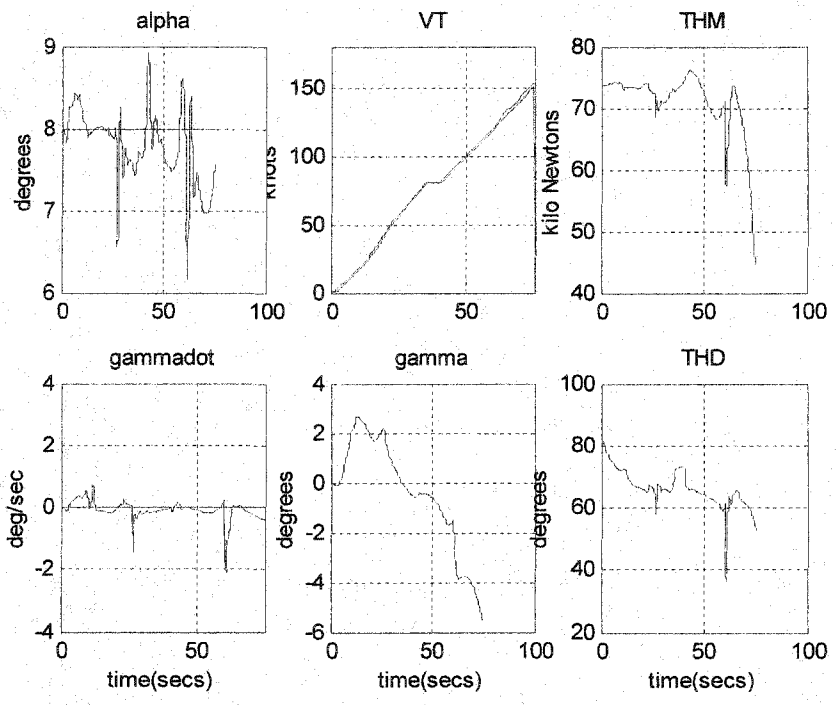

Figure5.22: Results of scheduled controller from hover to150kn with antiwindup technique. (a)

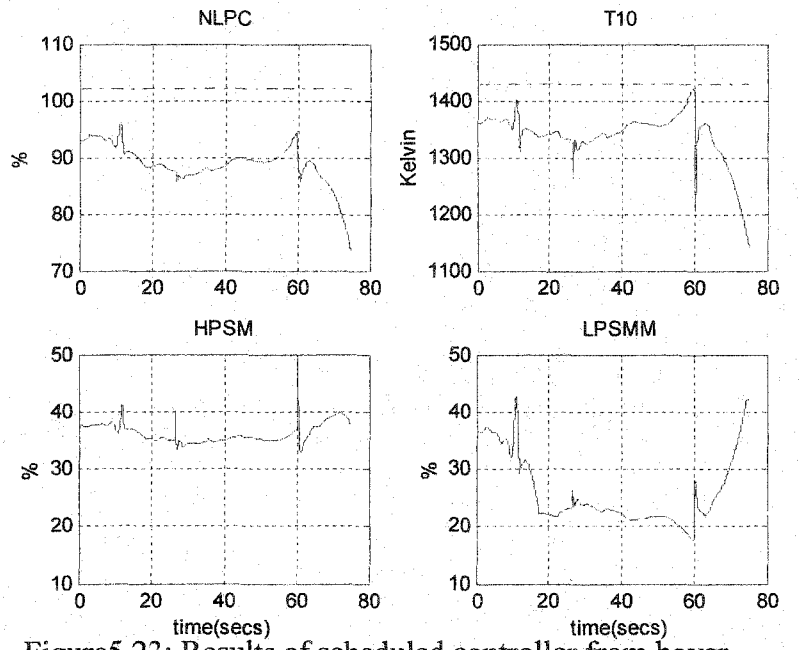

Figure5.23: Results of scheduled controller from hover to150kn with antiwindup technique. (b)

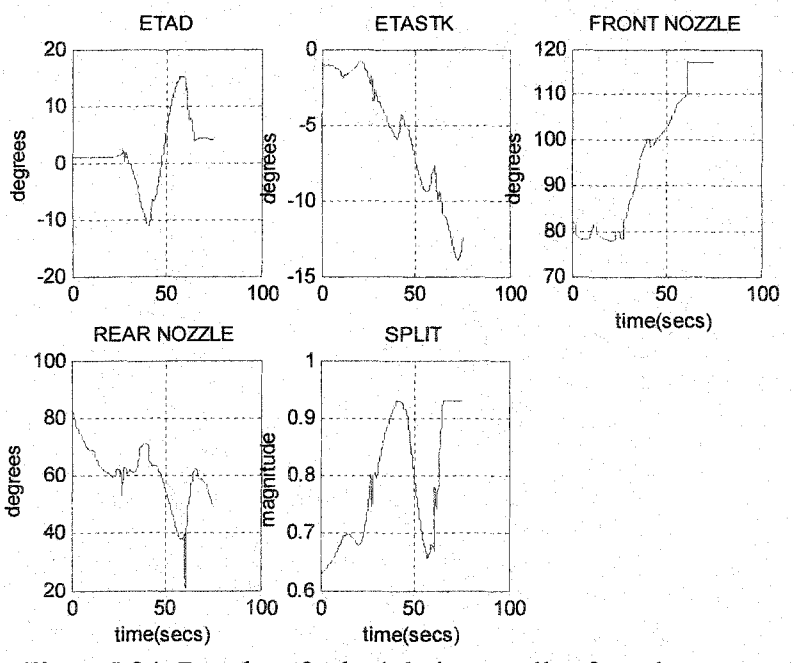

Figure5.24: Results of scheduled controller from hover to150kn with antiwindup technique. (c)

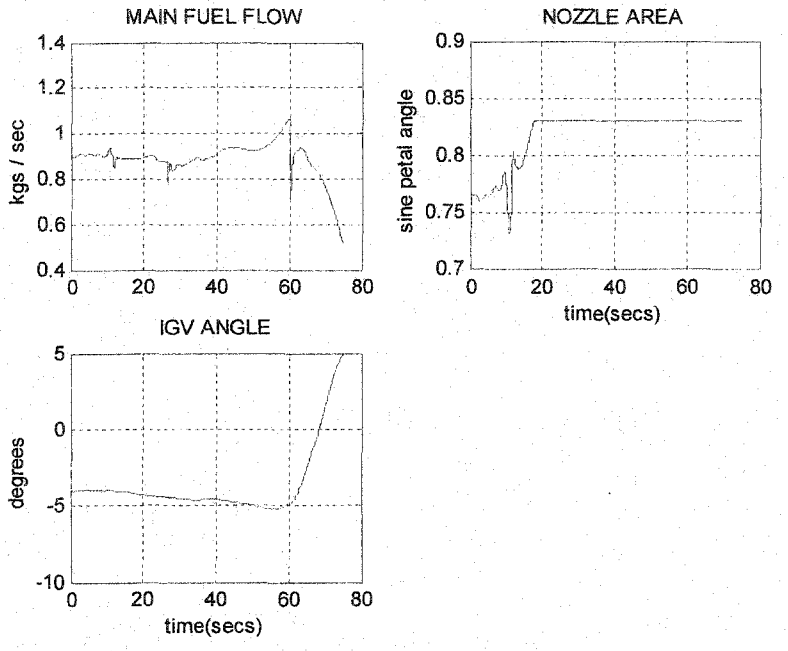

Figure5.25: Results of scheduled controller from hover to150kn with antiwindup technique. (d)

5.7 A control signal blending/interpolating approach:

The approach to scheduling of H_∞ loopshaping controllers described above requires controllers at different operating points in the flight envelope to have the same state-space structure. A drawback of this requirement is that standard usual controller order reduction techniques, [Glo84], cannot be used to reduce the order of each controller prior to scheduling, as this will destroy the consistency of the state-space structure across different designs. This issue is of particular concern for the IFPC problem considered here, which, due to the complexity of the airframe/engine model, results (initially) in high-order controllers at each operating point. Initial attempts at order reduction suggested, however, that these fixed-point controllers could be significantly reduced in order without any change in their closed-loop behavior.

One solution to the above problem would be to try to reduce the order of each controller using technique which preserve the physical interpretation of the state variables, see for example the approach described for an aero-engine control design in [Harf99]. In general such techniques are not well developed and not systematic, however, and so in this study we opted to investigate a second approach for scheduling the fixed-point controllers which imposes no constraint on their structure or order. The approach proposed, called the blending/interpolating method, presents a new version of the approach introduced in [Busch99]. Our method adopted here is different from the one presented in

[Busch99], mainly, in that the controller signals are continuously interpolated as a function of speed with the result that no "bumpless transfer" type conditioning is required. In fact, interpolating the outputs of two controllers, between their adjacent operating points of design, gives us the smooth change of the controller outputs and thus prevent better the bumps that can occur in the classical method presented in [Busch99].

The H_∞ loopshaping controllers are kept in their observer form as this structure was seen previously to provide slightly improved time-domain responses when compared with the implementation structure used in the piloted simulation trials. Now, writing the ith fixed-point controller as

$$\dot{\hat{x}}_s^i = A_s^i \hat{x}_s^i + H_s^i \left(C_s^i \hat{x}_s^i - y_s^i \right) + B_s^i u_s^i \tag{5.17}$$

$$u_s^i = K_s^i \hat{x}_s^i \tag{5.18}$$

then the scheduled controller output is calculated in real-time along the region between two design points i and i+1 as :

$$u_s^i = (1-\lambda) u_s^i + \lambda u_s^{i+1} \tag{5.19}$$

where u_s^i is the output of the ith controller and u_s^{i+1} is the output of the i+1th controller. The interpolation factor $\lambda(v)$ is given by $\frac{v - v^i}{v^{i+1} - v^i}, \lambda \in [0, \quad 1]$.

Where v, v^i and v^{i+1} are the current velocity, velocity at the ith design point and the velocity at i+1th design point, respectively. The structure of the blended/interpolated IFPC system is shown in Figure 5.26. Note that the blending/interpolating of the control signals is done at the input of the shaped plant – the weighting functions for the plant were then interpolated in the same way as for the previous scheduling scheme. This was seen to give better performance than direct blending/interpolating of the control signals at the plant input. A possible reason for this is that, assuming different weighting functions W_1 and including pure integrators, signals after W_1 will have large differences and widely varying blended/interpolated signals will result.

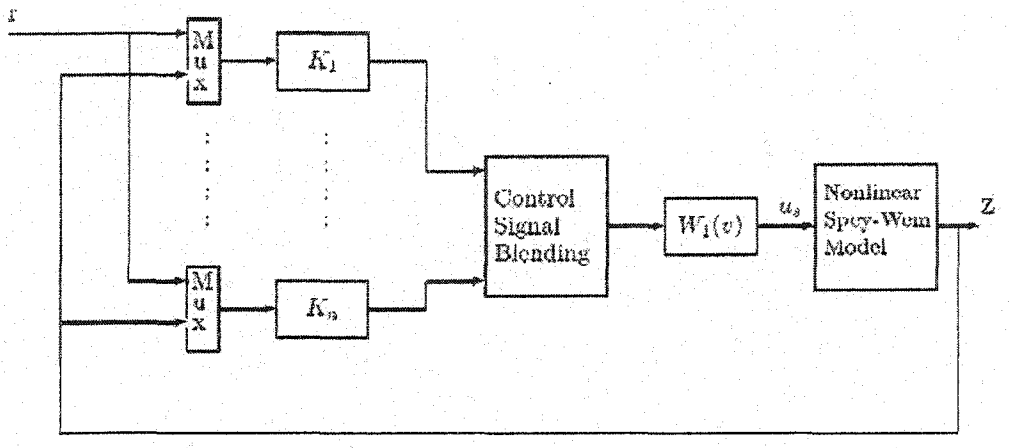

Figure 5.26 : Blended/Interpolated implementation

Each controller we used in this blending/interpolating technique assures stability and achieves reasonable performance in a region around the corresponding operating point (hover, 20, 50, 80 or 120kn). A significant advantage of this approach is that no requirements are placed on the structure or order of the different fixed-point controllers – in fact they could even be designed using different synthesis methods to optimize the performance achieved. This structural freedom was exploited to reduce the order of each individual controller as much as possible without sacrificing performance or robustness properties. With respect to the observer form structure chosen to implement the H_∞ loopshaping controllers, we opt to reduce the order of the shaped plant for each design given by

$$G_s^i = \left[\begin{array}{c|c} A_s^i & B_s^i \\ \hline C_s^i & 0 \end{array}\right] \tag{5.20}$$

where $G_s^i = G_{ss}^i + G_{su}^i$; G_{ss}^i is the stable part of the shaped plant, G_{su}^i is the unstable part of the shaped plant.

to the lowest order shaped plant

$$G_{sr}^i = \left[\begin{array}{c|c} A_{sr}^i & B_{sr}^i \\ \hline C_{sr}^i & 0 \end{array}\right] \tag{5.21}$$

where $G_{sr}^i = G_{srs}^i + G_{su}^i$

such that $\left\| G_{ss}^i - G_{srs}^i \right\|_\infty \le tol$, and then re-calculate the controller gains for the reduced-order shaped plant G_{sr}^i. Note that the unstable part and the stable part were added again at the end of the procedure.

Using this approach we were able to significantly reduce the orders of each fixed-point controllers without losing their respective performance locally. Depending on the point in the envelope, final fixed-point controllers of order 14-19 were obtained.

Nonlinear simulation results for the blended IFPC system are shown in Figures 5.27 to 5.30, for acceleration from 20 to 120 kn. The figures show excellent tracking of velocity demands with minimal coupling into γ and α. In addition, all internal engine variables are held within their specified safety limits.

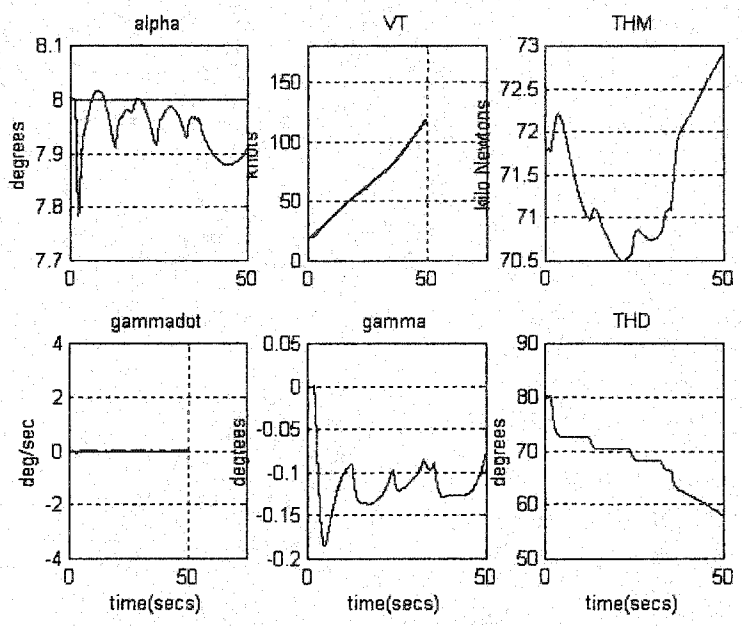

Figure 5.27 : Blending/interpolating scheduling for velocity demands (20kn to 120kn)

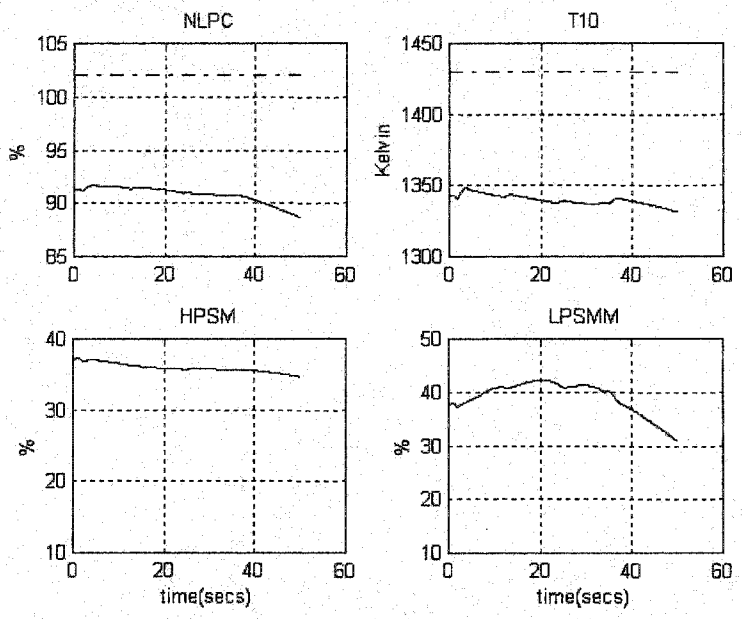

Figure 5.28 Blending/Interpolating scheduling for velocity demands (20kn to 120kn). Engine variables

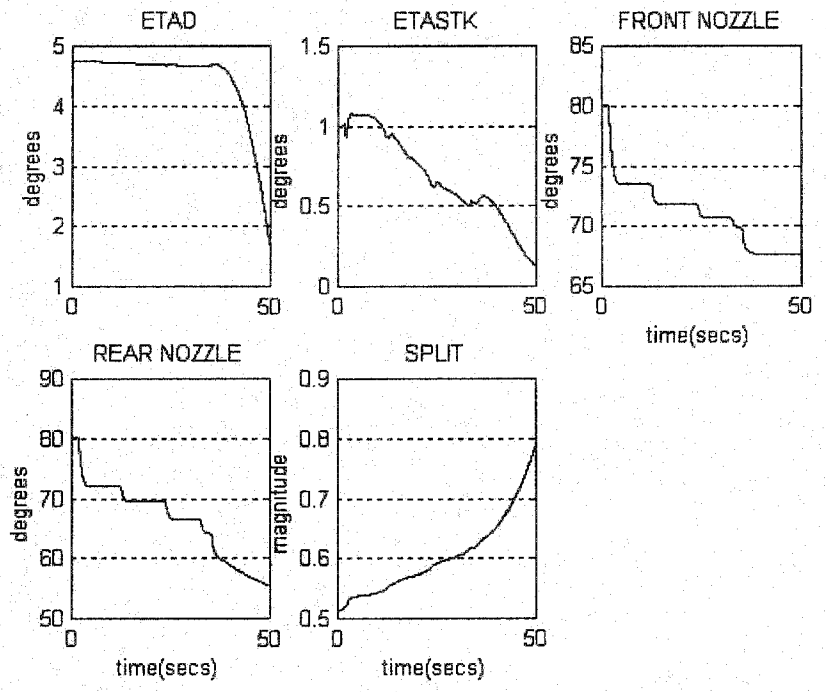

Figure 5.29 : Blending/Interpolating scheduling for velocity demands(20kn to 120kn). Airframe actuators

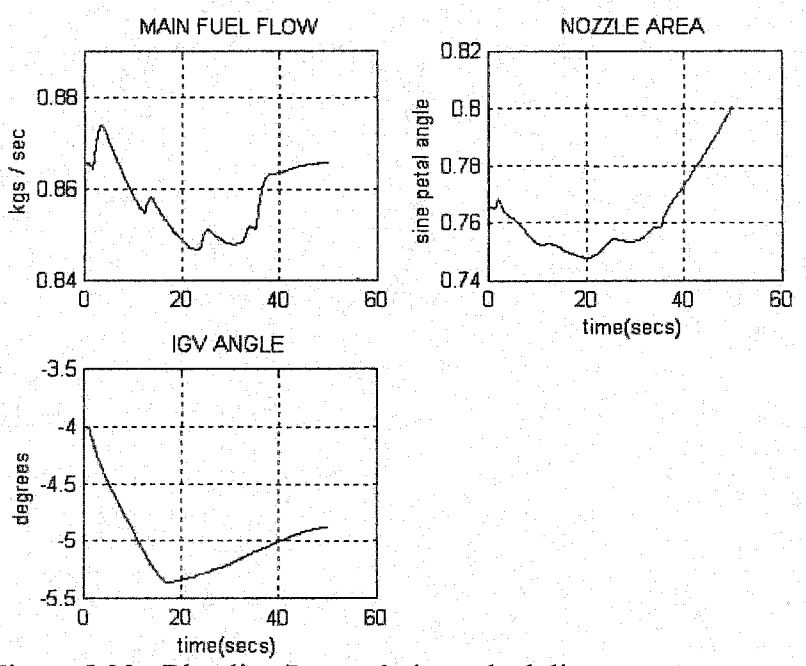

Figure 5.30 : Blending/Interpolating scheduling for velocity demands(20kn to 120kn). engine actuators

Extending the schedule to include the hover flight condition produced the results shown in Figures 5.31 to 5.34. The results show slightly increased coupling into γ due to the large variations in the aircraft dynamics between 0 and 20 kn. Overall the results compare favorably with those achieved with the observer-form scheduling scheme, especially considering that the order of individual controllers has been significantly reduced.

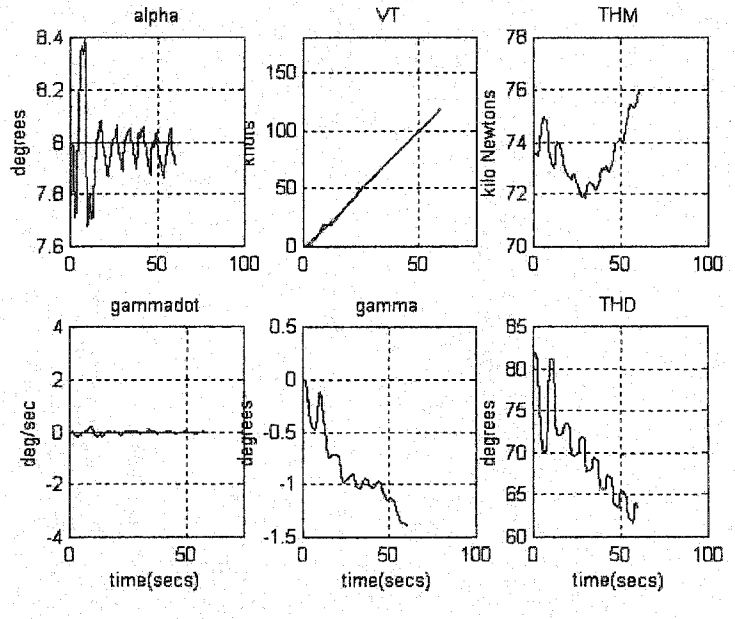

Figure 5.31 : Blending/Interpolating scheduling for velocity demands(0kn to 120kn)

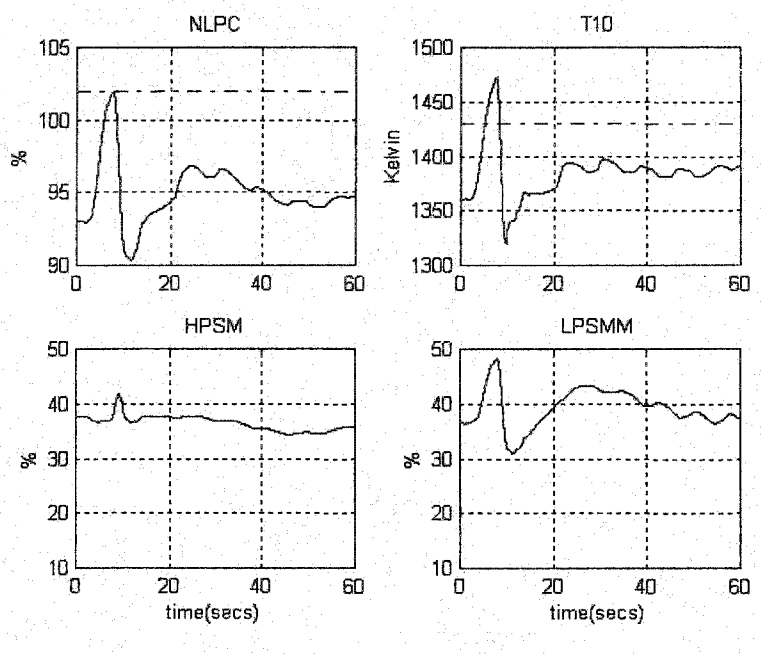

Figure 5.32 : Blending/Interpolating scheduling for velocity demands(0kn to 120kn). Engine

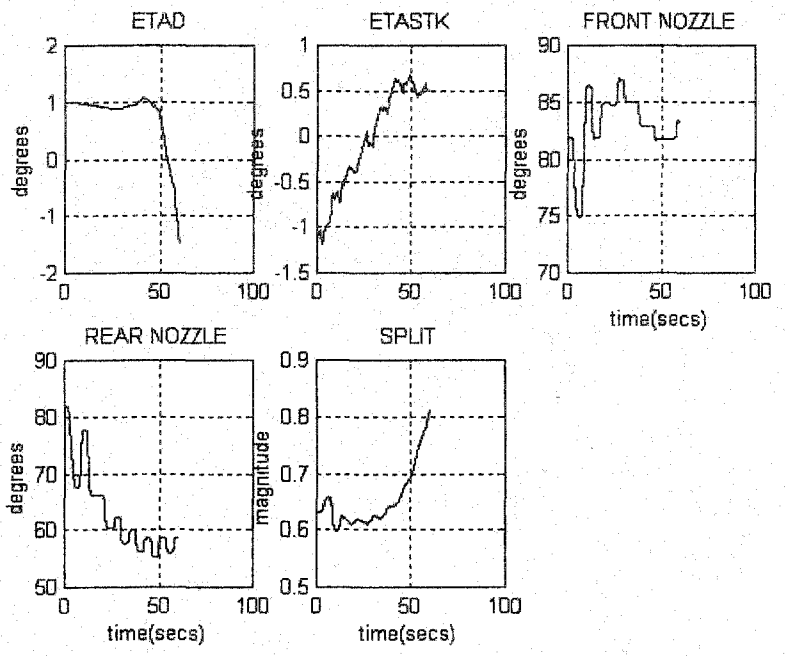

Figure 5.33 : Blending/Interpolating scheduling for velocity demands(0kn to 120kn). Airframe actuators

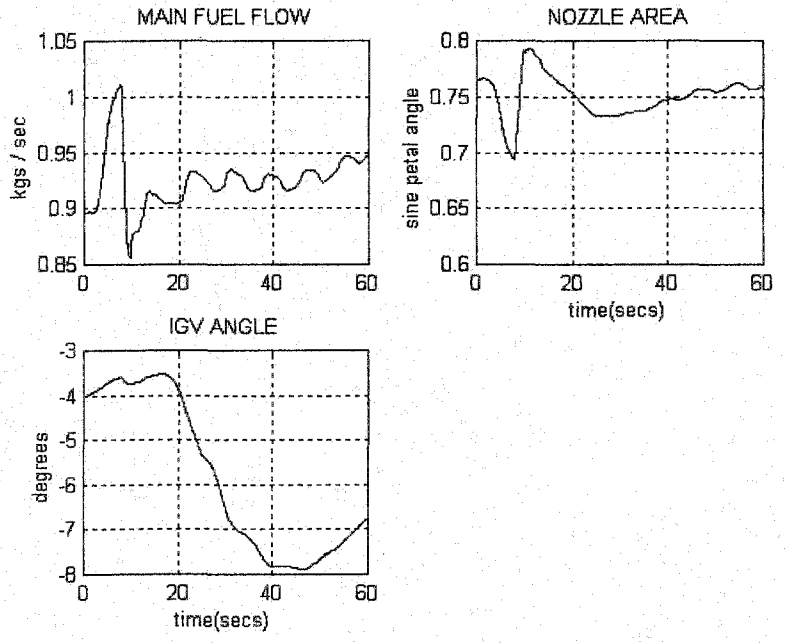

Figure 5.34 : Blending/Interpolating scheduling for velocity demands(0kn to 120kn). engine actuators

5.8 Optimal multi-switching technique

5.8.1 Introduction

The approach in this section is slightly different: we consider several isolated design points as in the interpolated scheduling case, but instead of a blend between two controllers we consider a straightforward switch. This not only has the conceptual advantage of simplicity, but it is often easier to implement switched control architecture than a scheduled one. When compared to previous scheduling approaches it also has advantages in terms of design time and is considerably less computationally demanding. The system under study seems ideally suited to switching (see[Hyd91] for an application of the Hanus technique [Han87] to a simple STOVL Harrier flight control problem) however, which has obvious advantages in the fact that no additional modeling needs to be carried out and, as already stated, in the relatively low computational demands it makes.

It is well known that an abrupt switch between linear controllers can cause transients, or bumps, which can lead to unacceptable closed-loop behavior, both in terms of actuator irregularities and also in system response. These bumps arise out of an inconsistency between the states and graphs of the controllers and, in their most malicious form, may give rise to instability when switching occurs.

Hence, we base our proposed switching strategy on a recently introduced bumpless transfer technique [Turn99],[Turn2000], to reduce the transients at the time of switching. The technique, based on optimal control methods, leads to a feedback matrix, F, which produces a signal, $\alpha(t)$, fed into the off-line controller to ensure that its output tracks the current on-line control signal, while also heeding the difference between $\alpha(t)$ and the current input to the on-line controller. In other words the method seeks to minimize, in a weighted LQ sense, the difference between the responses of the on and off-line controllers, in an attempt to preserve performance.

The LQ bumpless transfer methodology has already been demonstrated on a helicopter example in [Turn2000] and [Turn99]. Here we consider a more complex example, which requires switches between multiple controllers due to the highly nonlinear nature of the plant's dynamics. This leads to an implementation technique to reduce on-line computational burden. Both the LQ bumpless transfer technique and the multi-switch concept are described in more detail later.

5.8.2 Linear quadratic bumpless transfer :

The idea of linear quadratic (LQ) bumpless transfer was introduced in [Turn2000] to facilitate, in an optimal manner, dynamic transfer between two linear controllers.

Essentially the method of attempting to ensure bumpless transfer is a feedback matrix, F, (which we assume has access to the on-line controller's states), which drives the off-line controller in order that its output tracks that of the on-line controller, while also ensuring the off-line controller input does not deviate too sharply from the on-line controller input. In [Turn99], the method was extended to include a low-pass filter in each channel of the vector, $\alpha(t)$ produced by F. The aim behind this was to ensure a less pronounced switch between the on and off-line controllers, albeit at the consequence of introducing dynamics into the bumpless transfer compensation scheme. In our experience this second method works better and thus it was preferred as the basis of the methodology proposed here. In what follows we shall introduce some new modified formulae for the bumpless transfer compensator. This should familiarize the reader with the LQ methodology. Note that the formulae of [Turn99] could not be used directly as that paper only considers strictly proper controllers; the controllers here are not strictly proper.

The subsequent subsections are intended more as an overview of the LQ bumpless transfer method and for more technical details on the derivation of the formulae, the reader is referred to [Turn2000].

5.8.2.1 Finite Horizon compensator formulae

Consider Figure 5.35 where $\tilde{u}(t) \in \mathbb{R}^m$ is the on-line control signal, $u(t) \in \mathbb{R}^m$ is the off-line control signal, $r(t) \in \mathbb{R}^{n_r}$ is the reference demand and $y(t) \in \mathbb{R}^{n_y}$ is the plant output.

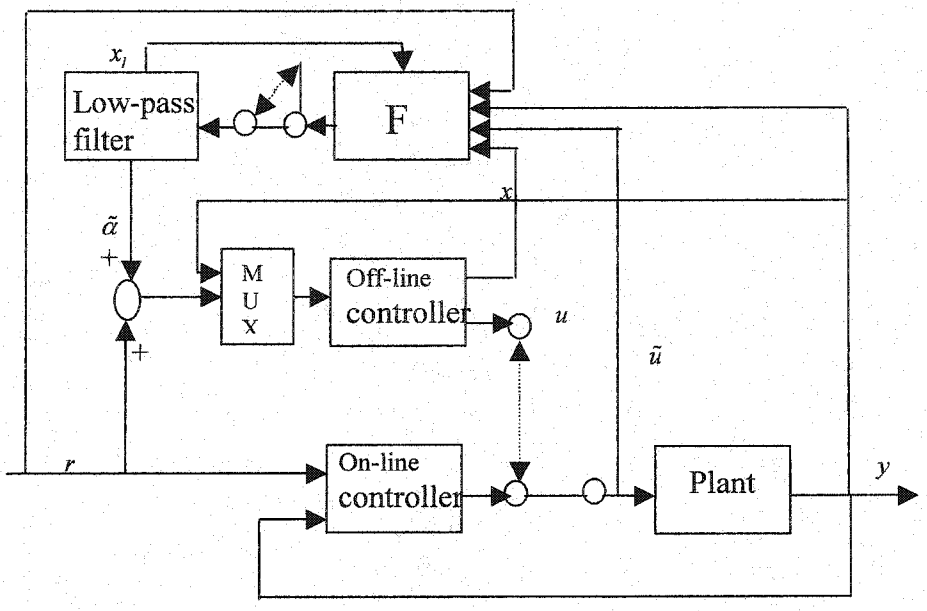

Figure 5.35 : Bumpless transfer scheme

The vector produced by the feedback matrix F is $\alpha(t) \in \mathbb{R}^{n_r}$ and the low-pass filtered version of this is $\tilde{\alpha}(t) \in \mathbb{R}^{n_r}$ .We assume that the off-line controller, $K_{off}(s)$, is governed by the following equations

$$\dot{x} = Ax + B_1(r + \tilde{\alpha}) + B_2 y \tag{5.22}$$

$$u = Cx + D_1(r + \tilde{\alpha}) + D_2 y \tag{5.23}$$

and that the low-pass filter, $L(s)$, is governed by the following equations

$$\dot{x}_l = A_l x_l + B_l \alpha \tag{5.24}$$

$$\tilde{\alpha} = C_l x_l \tag{5.25}$$

Note that we are assuming that the controller has two degrees of freedom. This allows more generality in our results and by making obvious assumptions, the results hold for one-degree-of-freedom controllers. We assume that matrix F has access to both the controller and filter states as well as the vectors $\tilde{u}$, y and r.

Following are the assumptions we made for the method presented:

Assumption 1 : The controllers' state-space realizations are all stabilizable and detectable.

Assumption 2 : Given $K_{off}(s)$ is the off-line controller and $K_{on}(s)$ is the on-line controller, let the following equivalent conditions be satisfied

1.The on and off-line controllers locally stabilize the plant and the intersection of these locally

stabilizing domains is not empty. Furthermore the point of switching is in the intersection of these domains.

2.For the nonlinear plant

$$\mathrm{P}=\begin{cases}\dot{x}_p = f(x_p,u)\\ y = h(x_p,u)\end{cases} \tag{5.26}$$

Let $K_{off}(s)$ be designed at the operating point x_p^v and assume $K_{off}(s)$ stabilizes $P \ \ \forall x_p \in X_p$ where $x_p^v \in \operatorname{int} X_p$.

Let $K_{on}(s)$ be designed at the operating point x_p^μ then $K_{on}(s)$ stabilizes $P \ \ \forall x_p \in X_\mu$ where $x_p^\mu \in \operatorname{int} X_\mu$.

Furthemore, we assume that $X := X_p \cap X_\mu \neq \phi$ and switching takes place in X.

The motivation for Assumption 2 is practical in that we would like to switch between two stabilizing controllers and, furthermore, at the point of switching we would like both controllers to yield stable closed loops. It is unreasonable to expect good behavior from the switched system if the switch takes place at a point in the system's operating regime where one of the controllers does not stabilize it! This is quantified by the assumption that we switch in X , where both controllers are stabilizing.

One could, in principle, make a stronger assumption, given sets $Z_v \subset X_v$ and $Z_\mu \subset X_\mu$ where the respective controllers are not only stable but also yield, in some sense, good performance. The stronger condition would be that the switch takes place in $Z = Z_\mu \cap Z_v \neq \phi$, which would thus guarantee a certain performance level is maintained. This is more difficult to quantify, but some intuition can be used in implicitly determining this set. In practice Z will be used instead of X, as it is normally desirable for some performance, and not purely stability, to be maintained.

The aim of the LQ technique of bumpless transfer is to derive a matrix F such that at the time of switching the transient produced by the controller are minimal. To do this, we would like u and $\tilde{u}$ to be as close as possible at the time of switching, but also we would like $\tilde{\alpha}$ to be as small as possible to ensure that when switching has occurred, any abrupt change at the controller input does not manifest itself at the controller output (plant input). To pose this problem in the LQ framework we consider the minimization of the following functional

$$J(\tilde{u},\alpha,T)=\frac{1}{2}\int_0^T[z_u(t)^T W_u z_u(t)+z_e(t)^T W_e z_e(t)]dt+\frac{1}{2}z_u(T)^T S z_u(T) \tag{5.27}$$

where :

$$z_u(t) = u(t) - \tilde{u}(t) \tag{5.28}$$

$$z_e(t) = \alpha(t) \tag{5.29}$$

Note that we do not minimize $\tilde{\alpha}(t)$ directly, but rather minimize $\alpha(t)$ instead. As the input to the off-line controller is $r(t) + \tilde{\alpha}(t)$ and $\tilde{\alpha}(t)$ is the output of the low-pass filter, this enables the input to the controller to gradually deform into purely $r(t)$ when the off-line controller is switched on-line, which helps avoid a bump at the controller input. In this setup, we assume that the switch between on and off-line controllers occurs at time T, and hence we seek the cost at this time to be minimized also. The matrices W_u and W_e are positive definite matrices which are used to weight the relative importance of ensuring $u \approx \tilde{u}$ and minimizing α.

Combining the dynamics of the off-line controller and the low-pass filter we obtain

$$\dot{\tilde{x}} = \tilde{A}\tilde{x} + \tilde{B}_1 w + \tilde{B}_2 \alpha \tag{5.30}$$

$$u = \tilde{C}\tilde{x} + \tilde{D}_1 w \tag{5.31}$$

where

$$\tilde{A} := \begin{bmatrix} A & B_1 C_l \\ 0 & A_l \end{bmatrix} \quad \tilde{B}_1 := \begin{bmatrix} B_1 & B_2 \\ 0 & 0 \end{bmatrix} \quad \tilde{B}_2 := \begin{bmatrix} 0 \\ B_l \end{bmatrix} \quad \tilde{C} := \begin{bmatrix} C & 0 \end{bmatrix} \quad \tilde{D}_1 := \begin{bmatrix} D_1 & D_2 \end{bmatrix} \quad \tilde{x} := \begin{bmatrix} x \\ x_l \end{bmatrix} \quad w := \begin{bmatrix} r \\ y \end{bmatrix}$$

Substituting this into the performance index (5.27) we obtain

$$J(\tilde{u}, \alpha, T) = \frac{1}{2}\int_0^T [(\tilde{C}\tilde{x} + \tilde{D}_1 w - \tilde{u})' W_u (\tilde{C}\tilde{x} + \tilde{D}_1 w - \tilde{u}) + \alpha' W_e \alpha] dt + \frac{1}{2} z_u(T)' S z_u(T) \tag{5.32}$$

Forming the Hamiltonian [Lew86] yields:

$$H = \frac{1}{2}\left\{(\tilde{C}\tilde{x} + \tilde{D}_1 w - \tilde{u})^T W_u (\tilde{C}\tilde{x} + \tilde{D}_1 w - \tilde{u}) + \alpha^T W_e \alpha\right\} + \lambda^T (\tilde{A}\tilde{x} + \tilde{B}_1 w + \tilde{B}_2 \alpha) \tag{5.33}$$

Invoking standard procedure from LQ optimal control [Lew86], we obtain the first-order necessary conditions for a minimum as

$$\frac{\partial H}{\partial \lambda} = \tilde{A}\tilde{x} + \tilde{B}_1 w + \tilde{B}_2 \alpha = \dot{x} \tag{5.34}$$

$$\frac{\partial H}{\partial \tilde{x}} = \tilde{C}^T W_u \tilde{C}\tilde{x} + \tilde{A}^T \lambda + \tilde{C}^T W_u \tilde{D}_1 w - \tilde{C}^T W_u \tilde{u} = -\dot{\lambda} \tag{5.35}$$

$$\frac{\partial H}{\partial \alpha} = W_e \alpha + \tilde{B}_2^T \lambda = 0 \tag{5.36}$$

These can be combined to obtain

$$\begin{bmatrix} \dot{\tilde{x}} \\ \dot{\lambda} \end{bmatrix} = \begin{bmatrix} \tilde{A} & -\tilde{R} \\ -\tilde{Q} & -\tilde{A}^{'} \end{bmatrix} \begin{bmatrix} \tilde{x} \\ \lambda \end{bmatrix} + \begin{bmatrix} \tilde{B}_1 & 0 \\ -\tilde{C}^{'} W_u \tilde{D}_1 & \tilde{C}^{'} W_u \end{bmatrix} \begin{bmatrix} w \\ \tilde{u} \end{bmatrix} \tag{5.37}$$

where the following definitions have been made

$$\tilde{R} := \tilde{B}_2 W_e \tilde{B}_2^{T} \tag{5.38}$$

$$\tilde{Q} := \tilde{C}^T W_u \tilde{C} \tag{5.39}$$

Using the method of Sweep (i.e, assume the linear relationship $\lambda(t) = \Pi(t)\tilde{x}(t) - g(t)$ and combining this with equation (5.37), α is obtained as

$$\alpha = -W_e^{-1} \tilde{B}_1 \lambda \tag{5.40}$$

where $\lambda := \Pi\tilde{x} - g$ is found from the differential equations

$$\dot{\Pi}(t) + \Pi(t)\tilde{A} + \tilde{A}^T \Pi(t) + \Pi(t)\tilde{R}\Pi(t) + \tilde{Q} = 0 \tag{5.41}$$

$$(\tilde{A} - \tilde{R}\Pi(t))^T g - (\tilde{C}^T W_u \tilde{D} + \Pi\tilde{B}_1) w + \tilde{C}^T W_u \tilde{u} = -\dot{g} \tag{5.42}$$

which are respectively solved from the terminal points

$$\Pi(T) = \tilde{C}^T S \tilde{C} \tag{5.43}$$

$$-g(T) = \tilde{C}^T S \tilde{D}_1 w(T) - \tilde{C}^T S \tilde{u}(T) \tag{5.44}$$

5.8.2.2 Infinite horizon compensator formulae

The finite-horizon formulae are often not appealing from a practical point of view. Firstly, in order for $\alpha(t)$ to be computed, the signals $w(t)$ and $\tilde{u}(t)$ must be known beforehand, which in a flight control situation is not realistic. Secondly, the feedback is time-varying and optimality is associated very much with the horizon length. Therefore these finite horizon results are extended to an infinite time support in order to ease implementation difficulties.

The infinite horizon results assume that the switch between controllers occurs infinitely far in the future $(T \to \infty)$ and one could certainly raise objections to this assumption. However, if the dynamics are such that a steady state is reached relatively fast, and of course the control signal is relatively constant over a period of time, and then one can apply these infinite horizon formulae with some confidence.

It is well known in the optimal control literature [Lew86] and for specific detail [Turn2000] that in order for the solution of the differential Riccati equation, (5.41), to converge to the positive semi-definite stabilizing solution of

$$\tilde{A}'\Pi + \Pi\tilde{A} + \Pi\tilde{R}\Pi + \tilde{Q} \tag{5.45}$$

as $T \to \infty$ we require $(\tilde{A}, \tilde{R}, \sqrt{\tilde{Q}})$ to be stabilizable and detectable. Note from the definitions of $\tilde{R}$ and $\tilde{Q}$ and strict positive definiteness of W_u and W_e, as it was assumed (Assumption 1) that our controller is stabilizable and detectable, then it follows that $(\tilde{A}, \tilde{R}, \sqrt{\tilde{Q}})$ is indeed stabilizable and detectable. Hence a positive semi-definite stabilizing solution to (5.45) always exists and furthermore it satisfies

$$\lim_{T\to\infty} \Pi(t) = \Pi(\infty) = \Pi \geq 0 \tag{5.46}$$

Now consider Equation (5.42) and note that as this develops backwards in time and as $\tilde{A} - \tilde{R}\Pi$ is Hurwitz implies $-(\tilde{A} - \tilde{R}\Pi)$ is anti-Hurwitz, the LQ tracking technique of [Athans66] can be applied. With the assumption that $w(t)$ and $\tilde{u}(t)$ are constant then it follows that

$$\lim_{T\to\infty} g(t) = g = -(\tilde{A} - \tilde{R}\Pi)^{-T}[-(\Pi\tilde{B}_1 + \tilde{C}^T W_u \tilde{B}_1)w + \tilde{C}^T W_u \tilde{u}] \tag{5.47}$$

Inserting this into the expression for α gives

$$\alpha = F\begin{bmatrix} \tilde{x} \\ w \\ \tilde{u} \end{bmatrix} \tag{5.48}$$

where F is given by

$$F = -W_e^{-1}\tilde{B}_2^T\begin{bmatrix} \Pi \\ -((\tilde{A} - \tilde{R}\Pi)^{-T}(\Pi\tilde{B}_1 + \tilde{C}^T W_u \tilde{D}_1))^T \\ ((\tilde{A} - \tilde{R}\Pi)^{-T}\tilde{C}^T W_u)^T \end{bmatrix}^T \tag{5.49}$$

Note that the off-line control loop will be stable as $\Pi \geq 0$ is the stabilizing solution to the ARE, (24); therefore it follows that the off-line 'A' matrix, $(\tilde{A} - \tilde{R}\Pi)$, is Hurwitz (which also ensures the existence of $(\tilde{A} - \tilde{R}\Pi)^{-1}$).

5.8.2.3 Stability

So far we have only given guarantees of the stability of the off-line control loop. Our basic assumption also guarantees the stability of the system at the control design points. However nothing has been said about the stability of the system as a whole; that is the stability of the switched system. In fact plant states would trigger switching and we could have limit cycles in which case the assumption that switching occurs at $t \to \infty$ do not hold.

One of the main problems with a control switching strategy is that it introduces certain technical problems and thus it can be quite difficult to give any rigorous guarantee of stability. The process of switching makes the system's differential equations discontinuous in their right-hand side, and it is therefore nontrivial to guarantee existence and uniqueness of solutions.

It is also worth mentioning that most results on stability of switched systems tend to concentrate on the switching of linear systems. Here we are dealing with an uncertain nonlinear system, so it is not valid to apply results on the stability of switched linear systems.

We thus can make no concrete guarantees of stability, but can offer experience and guidelines, which lend credibility to our approach. Practical results in the literature [hyd91], [Turn2000] have shown that for sensible switching boundaries, stability is never a problem. One could envisage potential stability problems if the switching boundaries were too close and thus limit cycling could occur. However for switching boundaries sufficiently far apart, and maybe with appropriate hysteresis introduced, we believe stability is not likely to be a problem.

5.8.3 A multi-switching technique for controller implementation

5.8.3.1 Supervisory control

In a control system which consists of several switched controllers it is necessary to have some suitable switching protocol to determine the current on-line controller and the points at which control is switched to the other controllers. The mechanism which implements this protocol is often referred to as a "supervisor", the behavior of which has stability and performance implications. There are, broadly, three classes of protocols, which govern control switching

- *Time-based* - the supervisor will switch to a certain controller at a specified time.
  There are generally no stability problems with this method.
- *State-based* - the supervisor will switch to a certain controller when the plant's state crosses a given boundary in the state-space. There are many potential stability problems with this method.
- *Event driven* - the supervisor switches control when an external event takes place. This type of switching protocol is difficult to analyze, particularly if the external event is an indirect function of the plant's state.

Here we consider the second type of protocol, which is the most suitable in the aircraft application. For this type of switching protocol the current on-line controller is determined by the plant state's location in its state-space. The instances at which the control laws are switched can be described by boundaries

in the state-space. In general these boundaries will be manifolds. For example in Figure 5.36, the boundary at which the controller switches from controller K_1 is described by the 1-dimensional manifold $x_1^2 + x_2^2 = r^2$, which happens to be a circle of radius r. When there are several controllers and there are several states on which switching depends, these switching boundaries can appear complex and the study of the switched system's stability is more difficult.

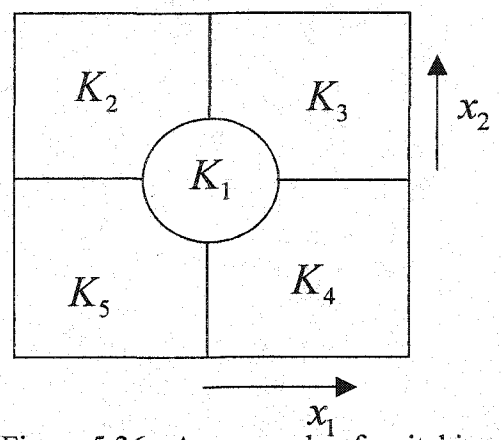

Figure 5.36 : An example of switching boundaries which are manifolds

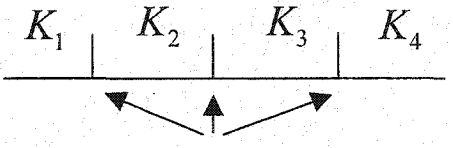

Switching points

Figure 5.37 : Switching points on an interval

In this case we consider a particularly simple form of switching protocol of the state-based class: when the switch only depends on the value of one of the states. We think of this as partitioning the state space, X_p into the Cartesian product $X_p = \Im \times \tilde{X}_p$

where $\Im \subset \mathbb{R}^1$ is the subspace associated with the parameter on which switching is dependent and $\tilde{X}_p \subset \mathbb{R}^{n-1}$ is the remainder of the state-space. Note that switching is independent of the state x_p's position in $\tilde{X}_p$ and is only dependent on the state's position within $\Im$. As $\Im$ is the open line the boundaries at which switching occurs thus become points and, more importantly, induce a certain order in which the controllers can switch.

For example, Figure 5.37, for three controllers, K_1, K_2, K_3, there will necessarily be two switching points. At the first switching point let the switch take place between controllers and K_2; at the second switching point let the switch be between controller K_2 and K_3. Then, providing the resulting switched closed-loop system has a continuous solution, it is evident that a switch is unable to take place directly between the controllers K_1 and K_3 - the only way of getting from K_1 to K_3 is by first switching to K_2.

Extending this idea to N controllers we have the conclusion that K_i can only be switched to K_{i-1} or K_{i+1} $(1 < i < N)$. Of course, if the controller is K_1 it can only be switched to K_2 and if the controller is K_N it can only be switched to K_{N-1} as these controllers are operative at the beginning and end of the line $\Im$.

5.8.3.2 A multi-switch methodology for the VSTOL aircraft

The flight envelope considered in our VSTOL application is simplified as a function of speed alone. To be more specific, we consider the interval between hover (0 kn) and approximately 140kn. This is the region over which there is a significant change of the aircraft's dynamic behavior, and the linearization obtained at, for example, 20 kn differs substantially of the linearization at 120kn. In other words, the subspace we take as $\Im$ is the line, which represents airspeed. In actual fact, we have limited our envelope to be a closed interval within $\Im$ for obvious practical reasons. From the previous subsection, we know that allowing the current on-line controller to depend on the position of one state within an interval allows a sensible, well-defined switching strategy to be used.

To cover the full flight envelope considered for our application, we chose four control design-operating points. Even though we could obtain satisfactory and stable performance with only two extreme controllers, by increasing the number of controllers, we were be able to preserve better the performance objectives over the full flight envelope. The operating design points considered are 20,50,80, and 120kn. Each loopshaping controller designed presents a good performance locally around its design operating point. This region can be seen as a ball with the operating point velocity being one of the coordinates of its center. We noticed that the radius of this ball could be considerably enlarged without losing significant performance criteria. Denoting the controllers, K_{20}, K_{50}, K_{80} and K_{120}, in terms of Assumption 2 we are assuming that:

K_{20} stabilizes P for all $x_p \in X_{20}$.

K_{50} stabilizes P for all $x_p \in X_{50}$.

K_{80} stabilizes P for all $x_p \in X_{80}$.

K_{120} stabilizes P for all $x_p \in X_{120}$.

and that the intersections of these regions are all non-empty.

itching technique presented above we thought about a multi-switching methodology
ve performance objectives, while also ensuring that only three controllers are running
educing computational burden).

of controllers covering the flight envelope considered.
ller, $1 < i \leq N$.
e jth switching point corresponding to a switch between the ith and i+1th controller.
low presents this new methodology:

controllers covering the flight envelope.
witching boundaries (normally a speed).
n/flight with the ith controller.
ing the matrix F, the i-1th and the i+1th controllers. If there is no i+1th controller (the
flight envelope is reached), or there is no i-1th controller (the lower end of the flight
hed), only condition the remaining (adjacent) off-line controller.
j-1th) switching boundary is reached switch to the i+1th (i-1th) controller.
t controller become the i'th controller and go to step 4.

algorithm requires a maximum of three controllers to be run in parallel and only two at
wer end of the flight envelope. This point is useful to note for implementation
ularly when there are a large number of controllers used throughout the envelope.
ewer controllers, which are, conditioned off-line, the less demanding the
equirements are. Heuristically, there would be some hysteresis used in the switching
t possible limit cycles / oscillations arising from change in pilot demand. The level of
quired is likely to depend on the pilot-vehicle system. In our work thus far we have not
sis as so far no piloted simulations have been conducted, although this is anticipated
[Hyd91], hysteresis is used in the switching algorithm proposed for piloted simulation.

in the state-space. In general these boundaries will be manifolds. For example in Figure 5.36, the boundary at which the controller switches from controller K_1 is described by the 1-dimensional manifold $x_1^2 + x_2^2 = r^2$, which happens to be a circle of radius r. When there are several controllers and there are several states on which switching depends, these switching boundaries can appear complex and the study of the switched system's stability is more difficult.

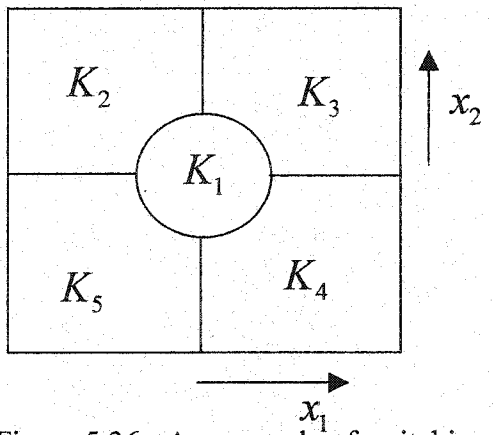

Figure 5.36 : An example of switching boundaries which are manifolds

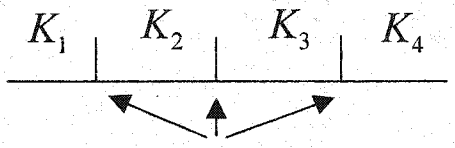

Switching points

Figure 5.37 : Switching points on an interval

In this case we consider a particularly simple form of switching protocol of the state-based class: when the switch only depends on the value of one of the states. We think of this as partitioning the state space, X_p into the Cartesian product $X_p = \Im \times \tilde{X}_p$

where $\Im \subset \mathbb{R}^1$ is the subspace associated with the parameter on which switching is dependent and $\tilde{X}_p \subset \mathbb{R}^{n-1}$ is the remainder of the state-space. Note that switching is independent of the state x_p's position in $\tilde{X}_p$ and is only dependent on the state's position within $\Im$. As $\Im$ is the open line the boundaries at which switching occurs thus become points and, more importantly, induce a certain order in which the controllers can switch.

For example, Figure 5.37, for three controllers, K_1, K_2, K_3, there will necessarily be two switching points. At the first switching point let the switch take place between controllers and K_2; at the second switching point let the switch be between controller K_2 and K_3. Then, providing the resulting switched closed-loop system has a continuous solution, it is evident that a switch is unable to take place directly between the controllers K_1 and K_3 - the only way of getting from K_1 to K_3 is by first switching to K_2.

Extending this idea to N controllers we have the conclusion that K_i can only be switched to K_{i-1} or K_{i+1} $(1 < i < N)$. Of course, if the controller is K_1 it can only be switched to K_2 and if the controller is K_N it can only be switched to K_{N-1} as these controllers are operative at the beginning and end of the line $\Im$.

5.8.3.2 A multi-switch methodology for the VSTOL aircraft

The flight envelope considered in our VSTOL application is simplified as a function of speed alone. To be more specific, we consider the interval between hover (0 kn) and approximately 140kn. This is the region over which there is a significant change of the aircraft's dynamic behavior, and the linearization obtained at, for example, 20 kn differs substantially of the linearization at 120kn. In other words, the subspace we take as $\Im$ is the line, which represents airspeed. In actual fact, we have limited our envelope to be a closed interval within $\Im$ for obvious practical reasons. From the previous subsection, we know that allowing the current on-line controller to depend on the position of one state within an interval allows a sensible, well-defined switching strategy to be used.

To cover the full flight envelope considered for our application, we chose four control design-operating points. Even though we could obtain satisfactory and stable performance with only two extreme controllers, by increasing the number of controllers, we were be able to preserve better the performance objectives over the full flight envelope. The operating design points considered are 20,50,80, and 120kn. Each loopshaping controller designed presents a good performance locally around its design operating point. This region can be seen as a ball with the operating point velocity being one of the coordinates of its center. We noticed that the radius of this ball could be considerably enlarged without losing significant performance criteria. Denoting the controllers, K_{20}, K_{50}, K_{80} and K_{120}, in terms of Assumption 2 we are assuming that:

K_{20} stabilizes P for all $x_p \in X_{20}$.

K_{50} stabilizes P for all $x_p \in X_{50}$.

K_{80} stabilizes P for all $x_p \in X_{80}$.

K_{120} stabilizes P for all $x_p \in X_{120}$.

and that the intersections of these regions are all non-empty.

Based on the switching technique presented above we thought about a multi-switching methodology that would preserve performance objectives, while also ensuring that only three controllers are running simultaneously (reducing computational burden).

Let us define:

N : The number of controllers covering the flight envelope considered.

K_i the ith controller, $1 < i \leq N$.

j, $1 < j \leq N-1$ the jth switching point corresponding to a switch between the ith and i+1th controller.

The algorithm below presents this new methodology:

Algorithm1 :

1- Design the N controllers covering the flight envelope.

2- Choose the switching boundaries (normally a speed).

3- Start simulation/flight with the ith controller.

4- Condition, using the matrix F, the i-1th and the i+1th controllers. If there is no i+1th controller (the upper end of the flight envelope is reached), or there is no i-1th controller (the lower end of the flight envelope is reached), only condition the remaining (adjacent) off-line controller.

5-When the jth (j-1th) switching boundary is reached switch to the i+1th (i-1th) controller.

6- Let the current controller become the i'th controller and go to step 4.

We can see this algorithm requires a maximum of three controllers to be run in parallel and only two at the upper and lower end of the flight envelope. This point is useful to note for implementation purposes, particularly when there are a large number of controllers used throughout the envelope. Obviously, the fewer controllers, which are, conditioned off-line, the less demanding the computational requirements are. Heuristically, there would be some hysteresis used in the switching points to prevent possible limit cycles / oscillations arising from change in pilot demand. The level of the hysteresis required is likely to depend on the pilot-vehicle system. In our work thus far we have not used any hysteresis as so far no piloted simulations have been conducted, although this is anticipated in the future. In [Hyd91], hysteresis is used in the switching algorithm proposed for piloted simulation.

5.8.4 Nonlinear simulation results

5.8.4.1 Without the bumpless transfer scheme

Figures 5.38-5.41 show the system's response to a ramp demand in airspeed V_t, without the bumpless transfer scheme. Note that although reasonably accurate tracking of the V_t demand is achieved, the response is punctuated with small transients. The switch from K_{20} to K_{50} occurs at 12 seconds and the switch from K_{50} to K_{80} occurs at 27 seconds. Although there are certain variables, which show a "bumpy" response, the majority of the variables behave reasonably well.

However when at ≈ 50 seconds the switch to the 120knots controller is made. At this point the aircraft exhibits unacceptable transient behavior. Note that the angle of attack, α, "jumps" suddenly from 8 to almost 5 degrees, before it is regulated back to 8 degrees. This is unacceptable both from a safety point of view (α must stay above 6 degrees at this point in the envelope) and also from a ride quality point of view. Similarly, γ shows an unacceptable excursion to almost -2°, meaning coupling of almost 2.5° which again is unacceptable from a safety perspective.

The engine variables also suffer, as the magnitude of the transient caused by the bump rises $T10$ to a point, which again violates safety limits. Similar large bumps occur in $LPSM$ and $NLPC$. Also of concern is the saturation which occurs in the $SPLIT$ variable and the large jumps in the front nozzle and $ETAD$. The engine actuators shown in

Figure 5.41 also show signs of saturation and large jumps without the bumpless transfer scheme.

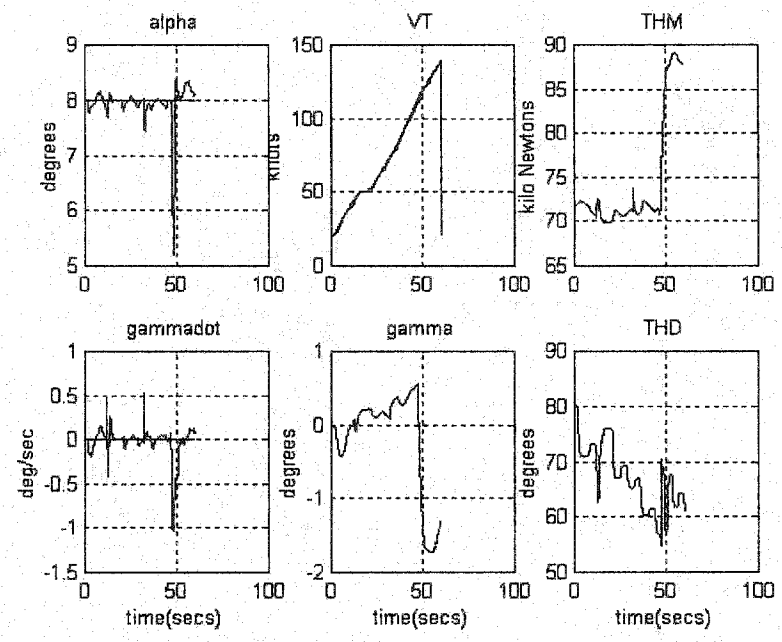

Figure 5.38 : Airframe responses without bumpless transfer scheme

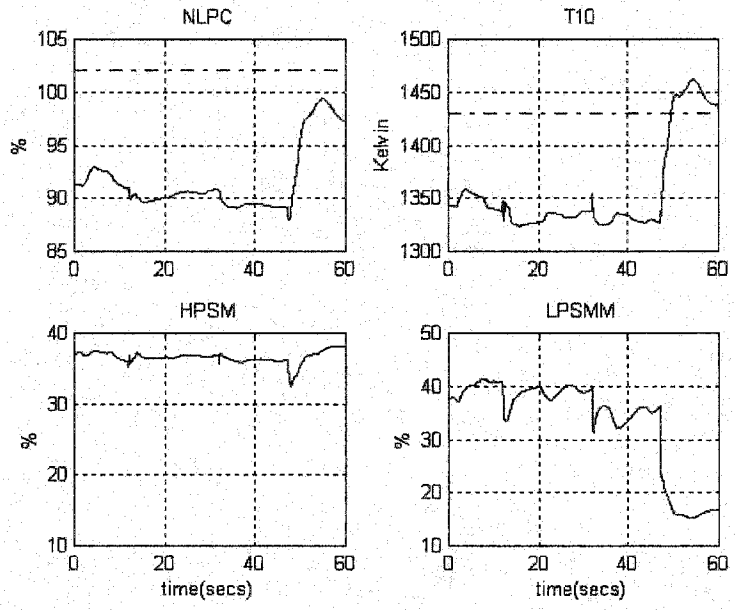

Figure 5.39 : Engine variables without bumpless transfer scheme

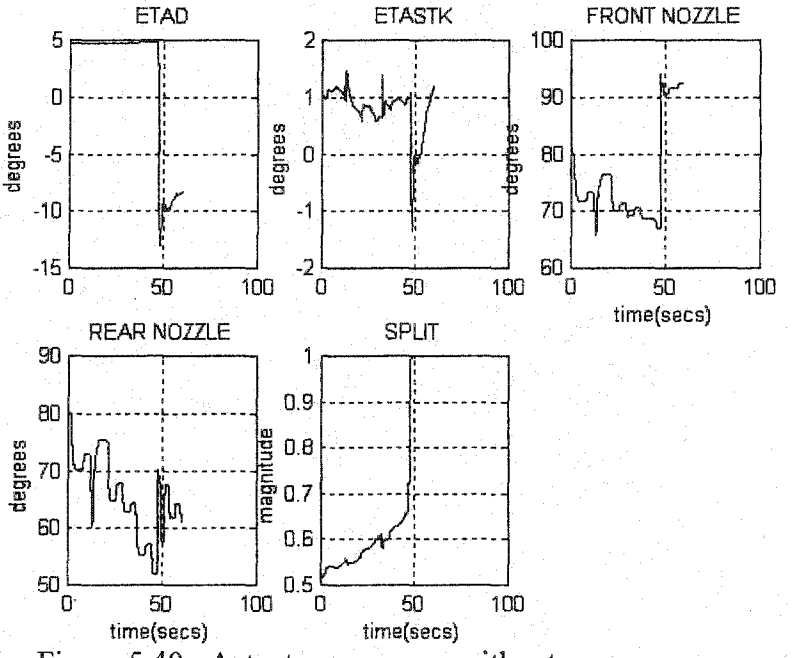

Figure 5.40 : Actuator responses without bumpless transfer scheme

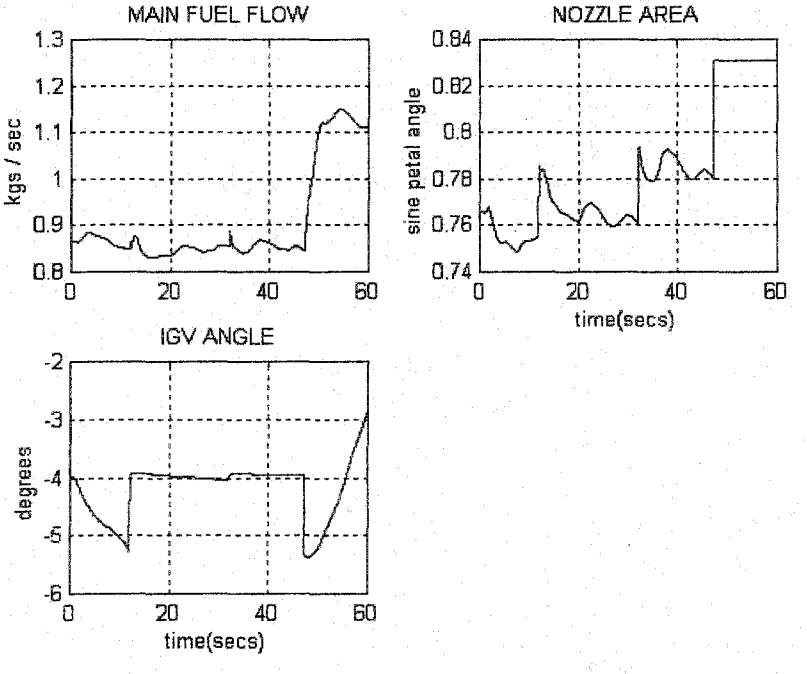

Figure 5.41 : Actuator responses without bumpless transfer sheme.

5.8.4.2 With the bumpless transfer scheme

Figures 5.42-5.45 show the system's response to a ramp demand in airspeed V_t, with the bumpless transfer scheme used to condition the off-line controller. The first thing to notice is that the tracking of the V_t demand is much smoother than before and there appears to be no detectable bumps at the times of transfer (which were the same as before). Notice also how the coupling into α and γ is considerably less than for the case without the bumpless transfer scheme. The bumpless transfer scheme has similar effects on the engine variables (Figure 5.43), where the responses are free from bumps and saturation. The actuator responses tell a similar story. Although the actuator activity changes significantly when K_{120} is on-line, the transition from one type of behavior to another is smooth and *SPLIT* and nozzle area do not saturate as before.

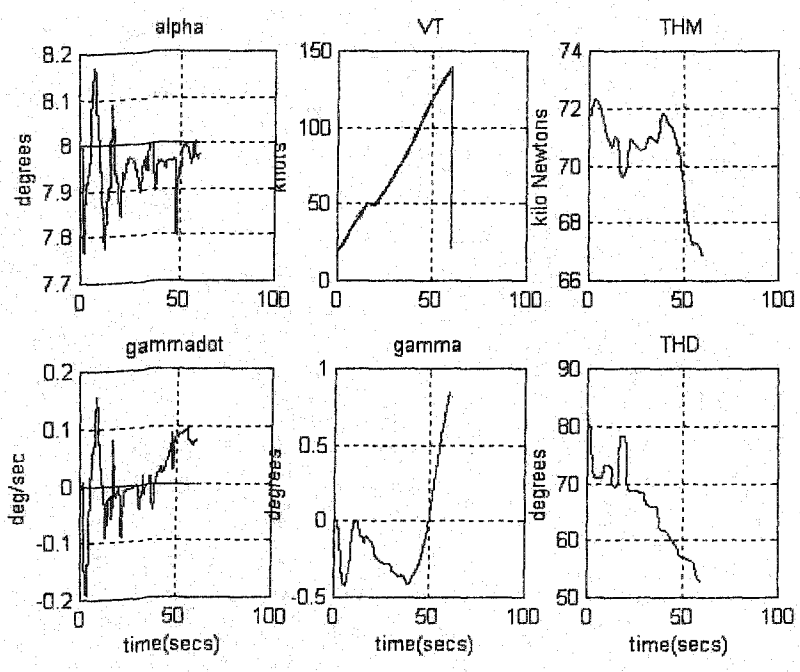

Figure 5.42 : Airframe variables with the bumpless transfer scheme

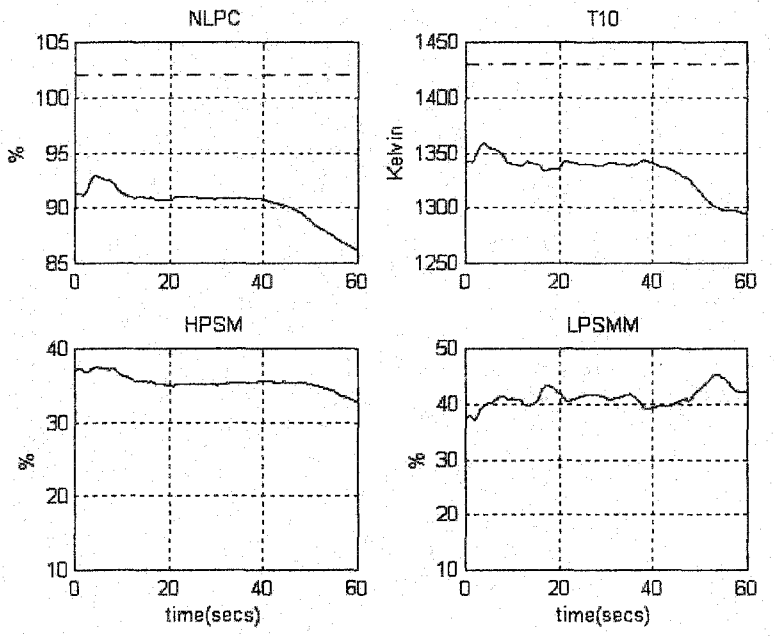

Figure 5.43 : Engine variables with the bumpless transfer scheme

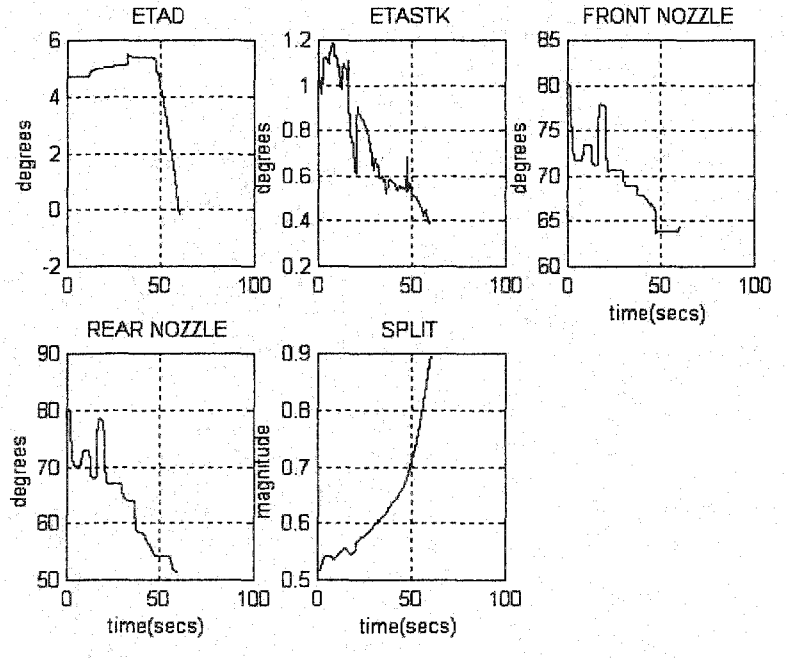

Figure 5.44 : Actuaor responses with bumpless transfer scheme

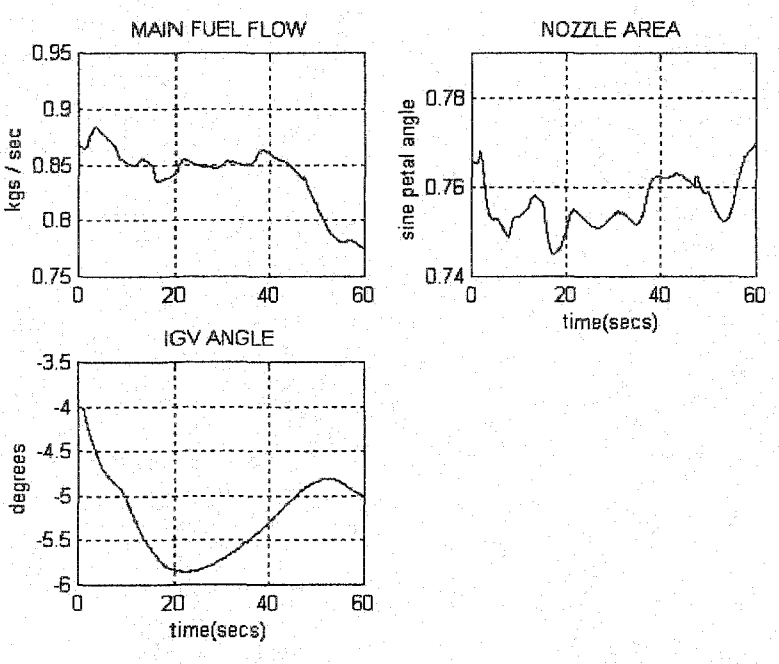

Figure 5.45 : Actuator responses with bumpless transfer scheme

5.9 Partitioning-scheduling of IFPC design

5.9.1 Introduction

The objective of the IFPC research is to consider methodologies to improve the overall system performance. These methodologies have to take into account dynamical coupling between the airframe and propulsion systems of STOVL aircraft. Essentially, an integrated approach has to ensure that optimal use of the various propulsion system into effectors for aircraft maneuvering control and limitation due to engine safety considerations are taken account in the overall design. One approach proposed in [Gar93a] to address integrated flight and propulsion control (IFPC) is to design a single centralized controller for the full-integrated airframe and engine system. This centralized controller is optimal in a sense that it has to take into account the overall performance requirements and the coupling existing between the two subsystems. Multiple criticisms can be addressed to this complex centralized controller. The high order of the centralized controller is its major disadvantage. The centralized controller also suffers from a lack of transparency with regards to subsystems functionality. Independent integrity of both airframe and engine control systems is not maintained. Thus an independent testing and redesign in reality is not possible. The second approach, using mixed

sensitivity H_∞ techniques, was first proposed in [Garg93a]. This method was used to an IFPC system for the VAAC Harrier aircraft in [Sar2000]. It partitions the IFPC system into separate airframe and engine sub-controllers, which are connected via a particular structure, subsequent to the design of a fully centralized controller. The particular structure used for the centralized controller is a static two-degree of freedom of a H_∞ loopshaping controller. In this section, we extend the research done in [Sar2000] by considering the control of a large flight envelope of the Harrier aircraft. We introduce a novel way of gain scheduling using the structure of the partitioned scheme. The blending/interpolating technique proposed in [Aouf2000c] was extended for the partitioned controllers designed for chosen operating points over the flight envelope.

5.9.2 Centralized controller and partitioning procedure

The particular implementation structure for the centralized H_∞ loopshaping controller as two separated blocks, one as feedforward and another as feedback, has been found in practice, [Mcf90] to give better time domain performance, and in particular smaller overshoot in response to reference demands. This is because with this structure the references do not directly excite the dynamics of K_∞. This can often result in large overshoot (classical derivative kick), since K_∞ has been designed in the frequency domain for robustness objectives rather than time-domain performance. The clarity of the observer form structure implementation, adding to the time-domain performance of the H_∞ loopshaping gives us a large potential of a transparent and efficient implementation controller structure. The procedure of partitioning used here can be viewed as a partitioning approach for a static H_∞ loopshaping two-degree-of-freedom controller, as opposed to the original procedure proposed in [Garg93a], [Garg93b], which was applied to a standard mixed-sensitivity H_∞ controller [Doy89]. The particular structure required for the partitioned IFPC system depends on the nature of the interactions between the airframe and engine subsystems, as well as on the various requirements arising from industrial and commercial constraints. In practice, a hierarchical structure has been found to be most appropriate, with the airframe sub-controller generating commands both for the airframe control surfaces, and for those propulsion system variables, which directly affect the airframe. The general framework for controller partitioning is given in Figure 5.46. The centralized IFPC system is partitioned into three separate sub-controllers. The first is related to the airframe part of the aircraft, the second is related to the engines and the third manages the coupling existing between the airframe and the propulsion

systems. A five step procedure, developed in [Sar2000], is described below that leads to blocks of partitioned IFPC systems starting from the centralized H_∞ loopshaping IFPC controller designed.

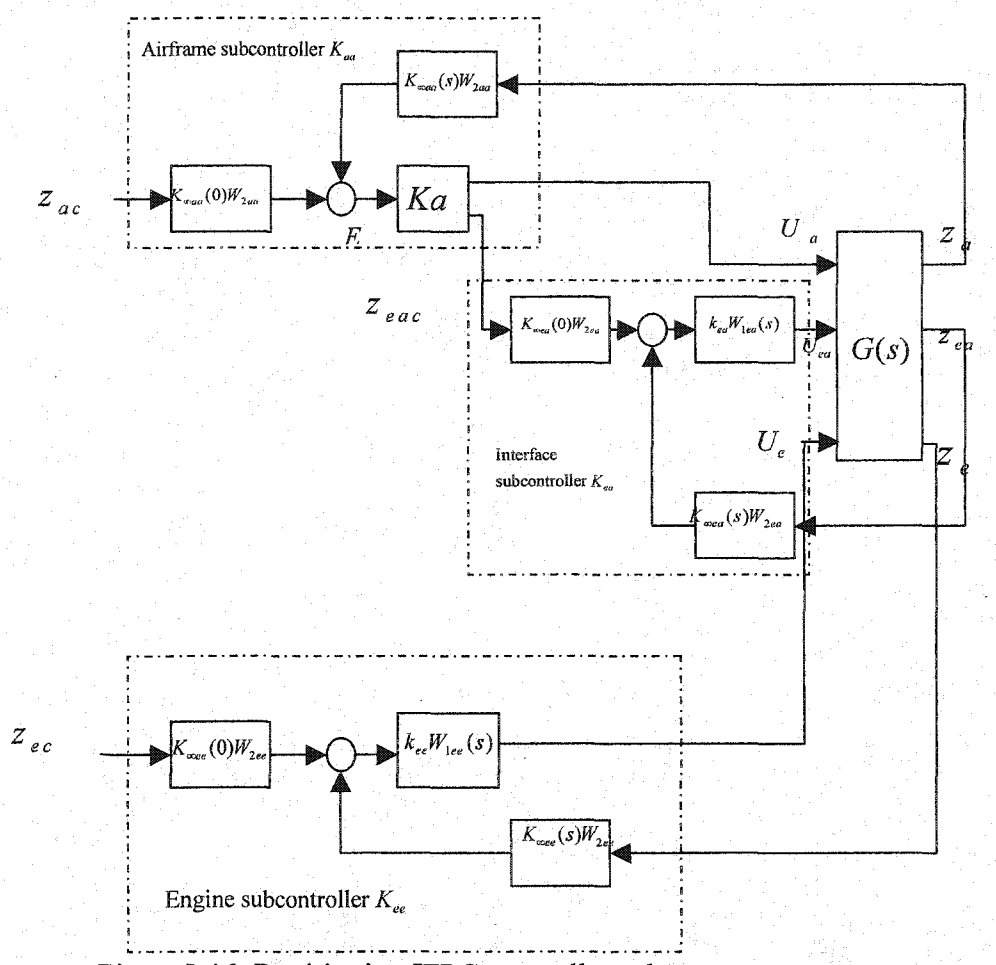

Figure5.46: Partitioning IFPC controller scheme

Step1: Assign the plant's inputs and outputs to be either engine, airframe or interface variables. For the control inputs, this decision is based on control effectiveness rather than the physical location of the actuator. For example, although the front and rear nozzle pairs are physically a part of the propulsion system, the angle of these nozzle pairs directly affects airframe quantities such as α and VT, and so it is natural to consider them as airframe actuators. Variables through which engine control inputs affect indirectly on the airframe variables are not denoted as interface variables. For example a change in main fuel flow may be seen to produce a change in velocity. However, this velocity change is more directly due to the resulting change in thrust magnitude, which we thus denote as an interface variable,

leaving main fuel flow to be considered as part of the engine subsystem. The plant's input, output and interface variables are grouped as presented below:

$U_a = [ETAD, ETASTK, FNOZ, RNOZ, SPLIT]\ U_e = [MFF, ENOZA, IGV]$

$Z_a = [\alpha, VT, \dot{\gamma}]$

$Z_{ea} = [THM, NLPC, T10]$

$Z_e = [HPSM, LPSM]$

where: U_a, U_e are the airframe and engine inputs respectively. Z_a, Z_{ea}, Z_e are the airframe, interface variables and engine outputs, respectively.

We assume that only interactions from engine to airframe are required to be considered. Interactions from airframe to the engine are unwanted disturbances to which the designed IFPC system has to be robust.

Step 2. An internal engine sub-controller K_{ee} is extracted from the centralized IFPC system. This is done by writing the centralized controller $K(s) = W_1(s)kK_\infty(s)W_2$, and partitioning it as:

$$K(s) = \begin{bmatrix} Kaa(s) & Kae(s) \\ Kea(s) & Kee(s) \end{bmatrix}.$$

The internal engine subcontroller K_{ee} is thus written as a reduced order approximation of the Kee block of the centralized system.

Step 3: The control requirements for the interface subcontroller are identified by analyzing the closed-loop frequency responses from the airframe commands Z_{ac} to Z_{ea} with the centralized controller.

Step 4: An H_∞ loopshaping approach was adopted to design the interface sub-controller K_{ea}, which has to meet these control requirements. The full engine sub-controller KE is made up of the internal engine sub-controller K_{ee} and the interface sub-controller K_{ea} connected in parallel.

Step 5: With the engine subsystem closed using the centralized controller, as shown in Figure 5.46, we obtain a state-space representation of the airframe sub-controller block, K_a as a reduced order approximation of the E to $[U_a \quad Z_{ea}]$ transfer function matrix. The airframe sub-controller KA is then made up of the K_a block along with the blocks $K_{\infty a}W_{2a}$ and $K_{\infty a}(0)W_{2a}$, which are simply extracted from the original centralized system.

As can be expected, the overall order of the partitioned IFPC system, shown in Figure 5.46, is greater than the centralized design. However, each individual sub-controller is of low order, leading to easier implementation and greater transparency.

5.9.3 Scheduling the partitioned controllers

Centralized H_∞ loopshaping controllers designed for the particular operating points of 50,80 and 120kn were successfully partitioned following the partitioning procedure described above. In this section, we consider the portion of the STOVL flight envelope from 50 to 120 knots. We present, here, a strategy of gain scheduling that fits with the partitioning IFPC system architecture. The strategy is based on an extension of the blending/interpolating technique, presented in [Aouf2000c], to the controller structure adopted here. Defining $u_{ij}(v)\ i=1,...,p\ ,\ j=1,...,n$ as the *ith* output of the controller system for the *jth* design point, the blending/interpolating technique proposes an interpolation signal to be used for the actuators as:

$u_i(v)=(1-\lambda(v))u_{i,j-1}(v)+\lambda(v)u_{i,j}(v),\ v\in[v_{j-1},v_j[,\ i=1...,p$

where: $0\le\lambda(v)\le 1$ is a function of the aircraft velocity v. v_{j-1} and v_j are the velocities corresponding to the *j-1th* and *jth* design operating point, respectively.

A major advantage of the partitioned IFPC system is that not all of the individual sub-controllers need necessarily be scheduled – in this study; for example, we were able to maintain the sub-controllers for the interface variables and the engine at the 50kn operating point sub-controllers design, and focus our scheduling scheme on the airframe sub-controller. This choice is logical since the most significant changes in the dynamics of the aircraft in this region of the flight envelope relate to the airframe – specifically the control effectiveness of the aerodynamic control surfaces. Thus, the proposed scheduling scheme consists of blending, only, the output control signals of the K_a blocks of the partitioned controllers at 50, 80, and 120kn flight operating points. The blending/interpolating technique in [Aouf2000c] was proposed to interpolate the outputs of adjacent controller designs. For our airframe controller, as shown in Figure5.47, we interpolate the output of K_a at 50kn and 80kn for the flight envelope between 50 and 80kn. We do the same with the airframe controller outputs of K_a at 80 and 120 kn when the aircraft operates between 80 and 120 kn.

Our proposed technique has the advantage of scheduling only the airframe controller rather than scheduling all sub-controllers of the IFPC partitioned controller. This leads to less complexity in the

controller scheme and less time consuming implementation. Notice that by this scheduling method, we deal with an airframe controller of an order smaller than the order of the centralized IFPC controller-scheduling scheme implemented in [Bate99].

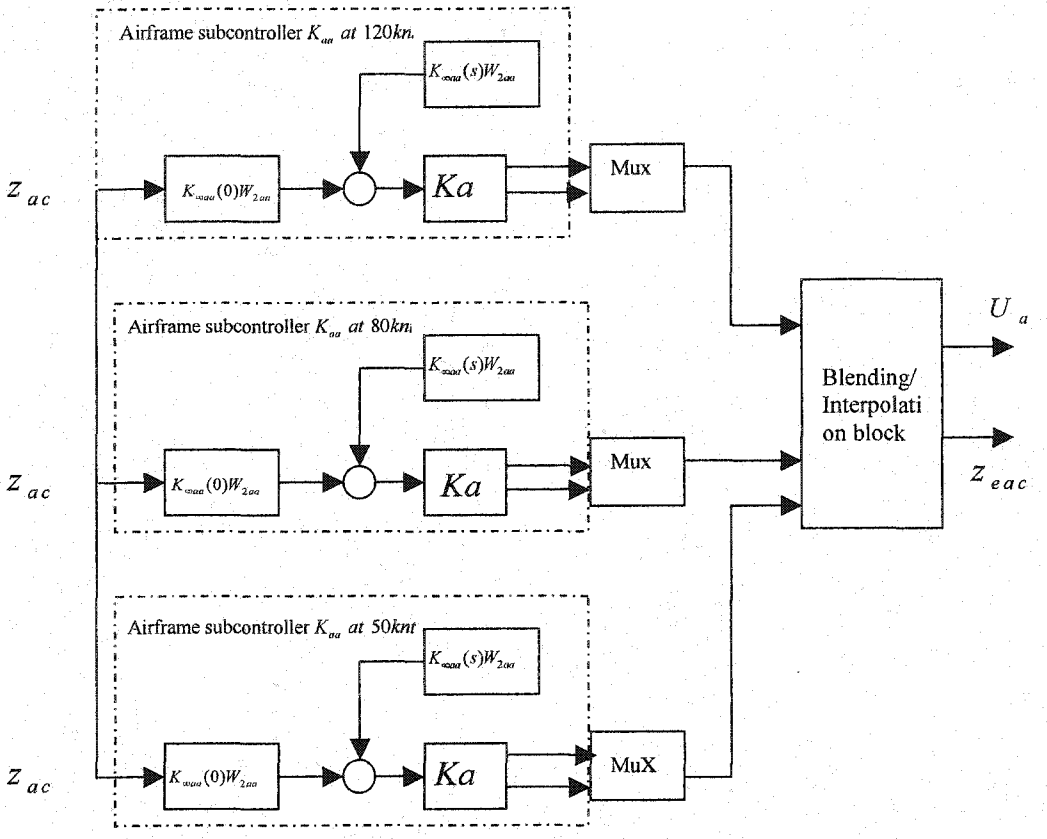

Figure5.47: Blending/interpolating partitioned controller

5.9.4 Nonlinear simulation

The IFPC system designed at the 50 kn operating point could be applied over the full flight envelope considered from 50kn to 120kn velocity - Figures 5.48, 5.49, 5.50, 5.51 present the results of the nonlinear simulation using the partitioned 50 kn controller. However, the performance obtained in terms of decoupling of velocity demands from the flight path angle does not meet the specifications, and in addition, the front nozzle angle is abnormally increasing as the aircraft accelerates from 100 knots to 120 kn. The results of our scheduling technique are given in Figures 5.52, 5.53, 5.54, 5.55. The responses show an improvement in the decoupling of flight path angle, which achieves the limit of ±0.3 degrees required for the portion of the flight envelope considered. Furthermore, all actuator movements now conform to the responses expected.

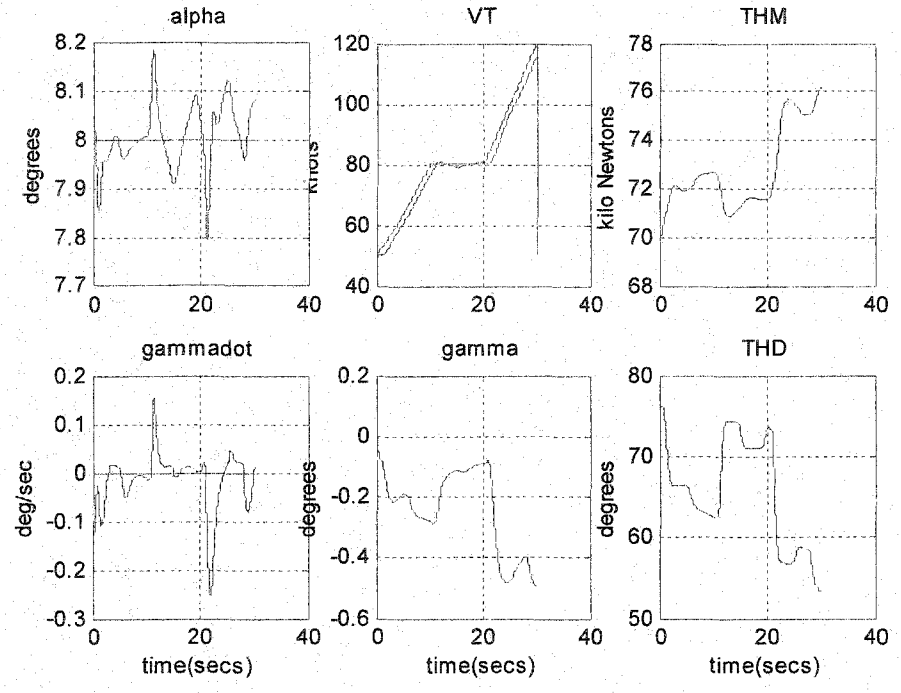

Figure 5.48: Airframe variables with 50kn partitioned controller

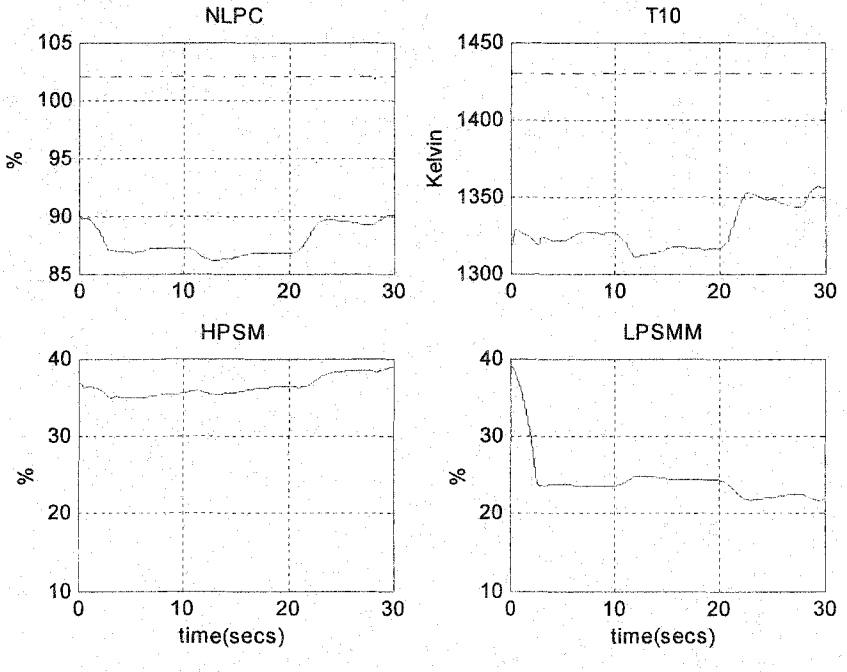

Figure 5.49: Engine variables with 50kn partitioned controller

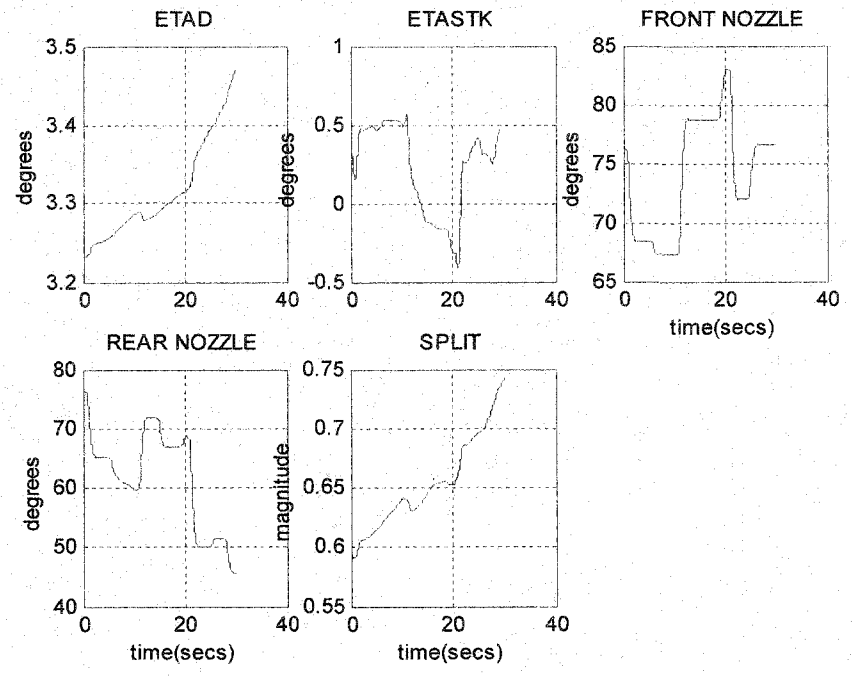

Figure 5.50: Actuator responses with 50kn partitioned controller

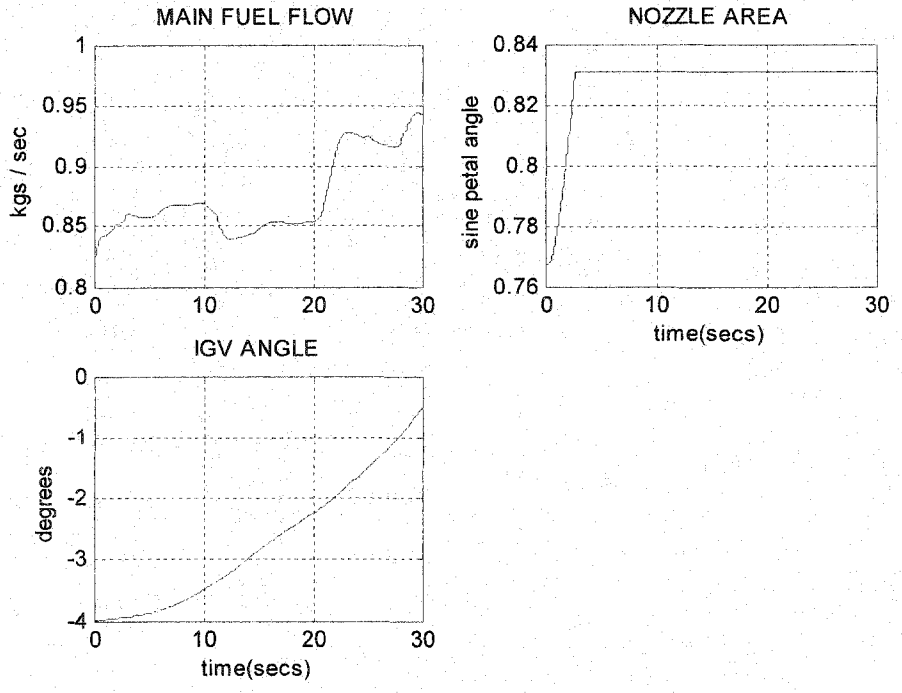

Figure 5.51: Actuator responses for 50kn partitioned controller

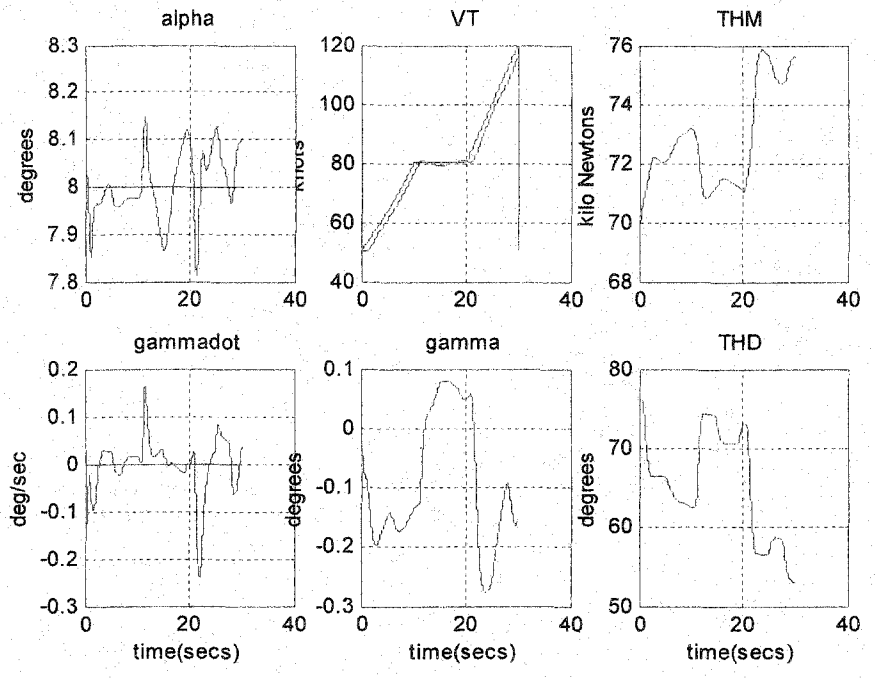

Figure 5.52: Airframe variables with a partitioned scheduled controller

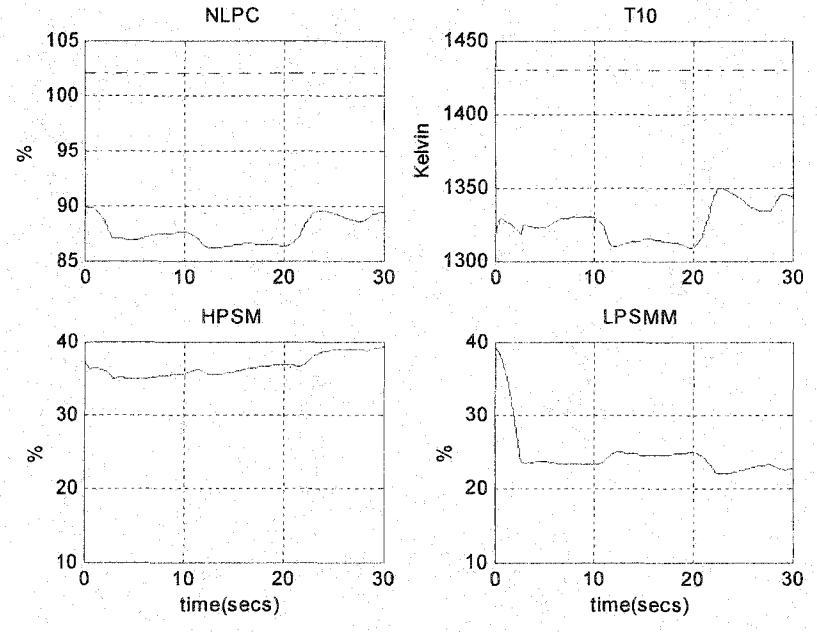

Figure 5.53: Engine variables for scheduled partitioned controller

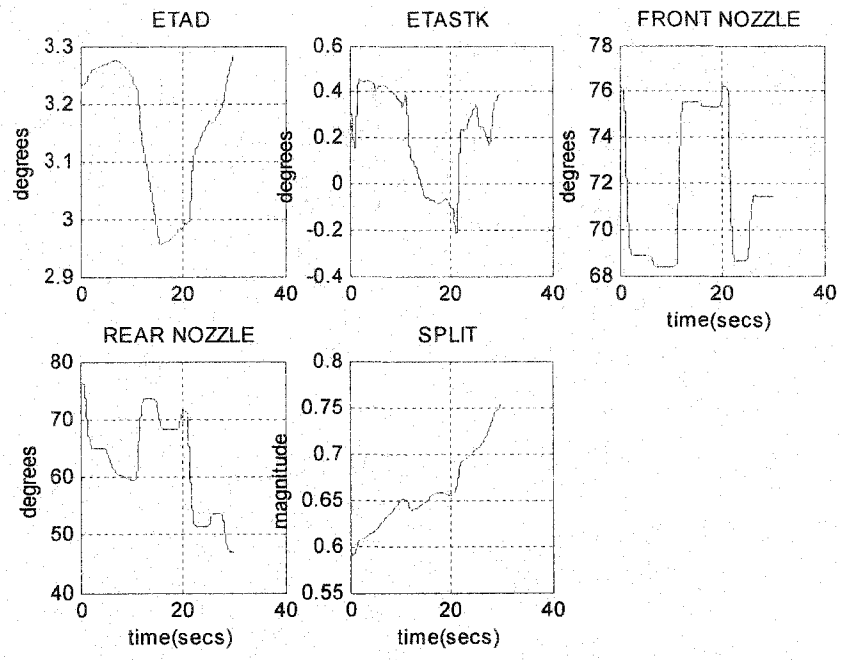

Figure 5.54: Engine variables for scheduled partitioned controller

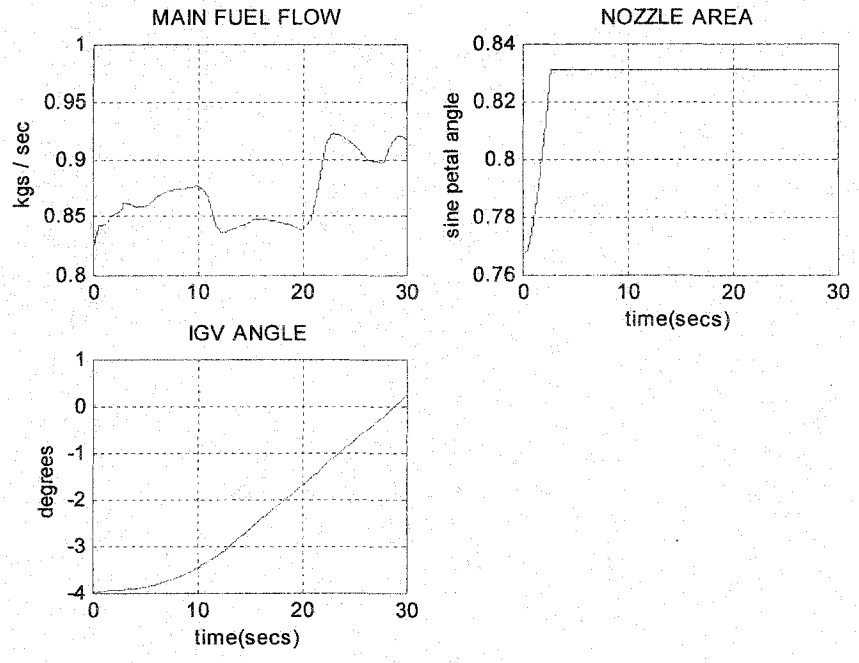

Figure 5.55: Actuator responses for scheduled partitioned controller

Chapter 6

Advanced scheduling techniques for a flexible aircraft

6.1 Introduction

The multivariable scheduling problem is more difficult to deal with than the single-variable case, for which the zeros and poles of the controllers can easily be interpolated. Switching techniques, based on bumpless switching, interpolation techniques [Han87], [AouTurn2000], [Hyd91], and on linear interpolation of the parameters of the observer-form controller [Aouf2000d], have been presented. Methods based on the recent results on linear parameter varying (LPV) designs [Pack96], [Wu95a] are computationally demanding and the solution to get an LPV controller is not guaranteed. Some criticism regarding the lack of stability guarantees have been directed at methods based on the interpolating techniques. On the other hand, a judicious choice of the frozen operating design points with respect to an acceptable range of parameter variation should preserve the stability of the closed-loop system. However, the ease of real-time implementation of those techniques is their major advantage. In this chapter, we present a brief review of the LPV and gain scheduled Linear Fractional transformation (LFT) designs. In addition, we adapt a form of interpolation technique to a B1 flexible aircraft model and we give some new results on a redesign technique and robust performance gain-scheduled interpolated controllers.

6.2 LPV gain-scheduled control theory

Extensive research on LPV gain-scheduled control has been done in the last decades and presented in many papers as in [Wu95a], [Wu95b], [Apk95]. Noting that details and proofs are available in the papers listed above, we present, in the following, the principal ideas of an LPV controller design. A state-space representation of a linear parametrically varying system is given as:

$$\begin{bmatrix} \dot{x}(t) \\ e(t) \end{bmatrix} = \begin{bmatrix} A(\rho(t),\dot{\rho}(t)) & B(\rho(t),\dot{\rho}(t)) \\ C(\rho(t),\dot{\rho}(t)) & D(\rho(t),\dot{\rho}(t)) \end{bmatrix} \begin{bmatrix} x(t) \\ d(t) \end{bmatrix} \tag{6.1}$$

where the vector of parameters ρ(t) is piecewise continuous and lies in a known compact set P [Kar84]. The LPV gain-scheduled controller will depend explicitly on the parameters ρ(t) and guarantee that stability and performance requirements are met for all allowable trajectories of ρ(t) in some known , bounded set. The performance is measured using the L_2-induced norm as:

$$\sup_{\rho \in P} \sup_{\substack{\|d\|_2 \neq 0 \\ d \in L_2}} \frac{\|e\|_2}{\|d\|_2}.$$

The output feedback case for rate-bounded LPV systems requires the closed-loop system to satisfy the following exponential stability Lemma [Wu95b].

Lemma 6.1

Given the state-space parameter-dependent system in (6.1), and nonnegative numbers v_i , if there exists a continuously differentiable function $W : P \to \Re_+$, such that for all $\rho \in P$, $W(\rho) > 0$,

$$\begin{bmatrix} A^T(\rho,\beta)W(\rho) + W(\rho)A(\rho,\beta) + \sum_{i=1}^{s} \beta_i \frac{\partial W}{\partial \rho_i} & W(\rho)B(\rho,\beta) & C^T(\rho,\beta) \\ W(\rho)B^T(\rho,\beta) & -I_{n_d} & D^T(\rho,\beta) \\ C(\rho,\beta) & D(\rho,\beta) & -I_{n_e} \end{bmatrix} < 0 \tag{6.2}$$

where $\beta = [\beta_1 \ldots \beta_s]$.

and $|\beta_i| \leq \upsilon_i$, i=1,2, ⋯ ,s, where s represents the number of varying parameters, then there exists a scalar $\alpha < 1$ such that for any $\rho \in P$, the LPV system of Equation (6.1) is exponentially stable, and if $d \in L_2$ and x(0) = 0, then $\|e\|_2 \leq \alpha \|d\|_2$.

The generalized open-loop interconnection used for robust control design takes on the standard structure, with some regularity assumptions and resulting in matrices depending on only the vector of parameters $\rho(t)$.

$$\begin{bmatrix} \dot{x}(t) \\ e_1(t) \\ e_2(t) \\ y(t) \end{bmatrix} = \begin{bmatrix} A(\rho(t)) & B_{11}(\rho(t)) & B_{12}(\rho(t)) & B_2(\rho(t)) \\ C_{11}(\rho(t)) & 0 & 0 & 0 \\ C_{12}(\rho(t)) & 0 & 0 & I_{n_u} \\ C_2(\rho(t)) & 0 & I_{n_y} & 0 \end{bmatrix} \begin{bmatrix} x(t) \\ d_1(t) \\ d_2(t) \\ u(t) \end{bmatrix} \tag{6.3}$$

where $\rho \in P$, $|\dot{\rho}| \le \upsilon$, the variables to control and the exogenous inputs are $\begin{bmatrix} e_1 & e_2 \end{bmatrix}^T$ and $\begin{bmatrix} d_1 & d_2 \end{bmatrix}^T$ respectively.

A state-space representation of the LPV controller, depending on the parameter ρ, is given as:

$$\begin{bmatrix} \dot{x}_k(t) \\ u(t) \end{bmatrix} = \begin{bmatrix} A_K(\rho(t), \dot{\rho}(t)) & B_K(\rho(t), \dot{\rho}(t)) \\ C_K(\rho(t), \dot{\rho}(t)) & D_K(\rho(t), \dot{\rho}(t)) \end{bmatrix} \begin{bmatrix} x_k(t) \\ y(t) \end{bmatrix} \tag{6.4}$$

and the closed-loop system can be written as:

$$\begin{bmatrix} \dot{x}_{clp}(t) \\ e(t) \end{bmatrix} = \begin{bmatrix} A_{clp}(\rho(t), \dot{\rho}(t)) & B_{clp}(\rho(t), \dot{\rho}(t)) \\ C_{clp}(\rho(t), \dot{\rho}(t)) & D_{clp}(\rho(t), \dot{\rho}(t)) \end{bmatrix} \begin{bmatrix} x(t) \\ d(t) \end{bmatrix} \tag{6.5}$$

where: $x_{clp} = \begin{bmatrix} x \\ x_k \end{bmatrix}$ and

$$A_{clp}(\rho, \dot{\rho}) := \begin{bmatrix} A(\rho) + B_2(\rho) D_K(\rho, \dot{\rho}) C_2(\rho) & B_2(\rho) C_K(\rho, \dot{\rho}) \\ B_K(\rho, \dot{\rho}) C_2(\rho) & A_K(\rho, \dot{\rho}) \end{bmatrix}$$

$$B_{clp}(\rho, \dot{\rho}) := \begin{bmatrix} B_{11}(\rho) & B_{12}(\rho) + B_2(\rho) D_K(\rho, \dot{\rho}) \\ 0 & B_K(\rho, \dot{\rho}) \end{bmatrix}$$

$$C_{clp}(\rho, \dot{\rho}) := \begin{bmatrix} C_{11}(\rho) & 0 \\ C_{12}(\rho) + D_K(\rho, \dot{\rho}) C_2(\rho) & C_K(\rho, \dot{\rho}) \end{bmatrix}$$

$$D_{clp}(\rho, \dot{\rho}) := \begin{bmatrix} 0 & 0 \\ 0 & D_K(\rho, \dot{\rho}) \end{bmatrix}$$

By applying Lemma 6.1 for the closed-loop system representation introduced above, we deduce the solution, in the following theorem, of the LPV control synthesis.

Theorem 6.1 [Wu95a]

The LPV Synthesis "γ-Performance objective/ν-Variation on the varying parameter ρ" is solvable if and only if there exist continuously differentiable real matrix functions X and Y such that for all $\rho \in$ P, $X(\rho) > 0$, $Y(\rho) > 0$, and

$$\begin{bmatrix} Y(\rho)\hat{A}^T(\rho)+\hat{A}(\rho)Y(\rho)+\sum_{i=1}^{s}\pm\left(v_i\frac{\partial Y}{\partial\rho_i}\right)-\gamma B_2(\rho)B_2^T(\rho) & Y(\rho)C_{11}^T(\rho) & B_1(\rho) \\ C_{11}(\rho)Y(\rho) & -\gamma I_{n_{e1}} & 0 \\ B_1(\rho) & 0 & -\gamma I_{n_d} \end{bmatrix} < 0 \tag{6.6}$$

$$\begin{bmatrix} \tilde{A}^T(\rho)X(\rho)+X(\rho)\tilde{A}(\rho)+\sum_{i=1}^{s}\pm\left(v_i\frac{\partial X}{\partial\rho_i}\right)-\gamma C_2^T(\rho)C_2(\rho) & X(\rho)B_{11}(\rho) & C_1^T(\rho) \\ B_{11}^T(\rho)X(\rho) & -\gamma I_{n_{d1}} & 0 \\ C_1(\rho) & 0 & -\gamma I_{n_e} \end{bmatrix} < 0 \tag{6.7}$$

and

$$\begin{bmatrix} X(\rho) & I_n \\ I_n & Y(\rho) \end{bmatrix} \geq 0 \tag{6.8}$$

where: $\hat{A}(\rho) := A(\rho)-B_2(\rho)C_{12}(\rho),\ B_1(\rho)=\begin{bmatrix} B_{11}(\rho) & B_{12}(\rho)\end{bmatrix}$
$\tilde{A}(\rho) := A(\rho)-B_{12}(\rho)C_2(\rho),\ C_1^T(\rho)=\begin{bmatrix} C_{11}^T(\rho) & C_{12}^T(\rho)\end{bmatrix}$ and $\pm v_i$ means that we take into account both rate limits in the inequalities.

If the conditions of Theorem 6.1 are satisfied, then by continuity and compactness, perturb X such that the LMIs of Theorem 6.1 still hold and $(X-Y^{-1})>0$ uniformly on P. Then an n-dimensional strictly proper controller that solves the feedback problem is defined as [Wu95a], [Pack96]:

$$\begin{aligned} A_K(\rho,\dot{\rho}) &:= A+\gamma^{-1}\left[Q^{-1}(\rho)X(\rho)L(\rho)B_{12}^T(\rho)+B_1(\rho)B_1^T(\rho)\right]Y^{-1}(\rho) \\ &\quad +B_2(\rho)F(\rho)+Q^{-1}(\rho)X(\rho)L(\rho)C_2(\rho)-Q^{-1}(\rho)H(\rho,\dot{\rho}) \\ B_K(\rho) &:= -Q^{-1}(\rho)X(\rho)L(\rho) \\ C_K(\rho) &:= F(\rho) \end{aligned} \tag{6.9}$$

where:

$$Q(\rho) := X(\rho)-Y^{-1}(\rho),\ F(\rho) := -\left[\gamma B_2^T(\rho)Y^{-1}(\rho)+C_{12}(\rho)\right],\ L(\rho) := -\left[\gamma X^{-1}(\rho)C_2^T(\rho)+B_{12}(\rho)\right]$$

$$H(\rho,\dot{\rho}) := -\left[A_F^T(\rho)Y^{-1}(\rho)+Y^{-1}(\rho)A_F(\rho)+\sum_i\left(\dot{\rho}_i\frac{\partial Y^{-1}}{\partial\rho_i}\right)+\gamma^{-1}C_F^T(\rho)C_F(\rho)+\gamma^{-1}Y^{-1}(\rho)B_1(\rho)B_1^T(\rho)Y^{-1}(\rho)\right]$$

and $A_F(\rho) := A(\rho)+B_2(\rho)F(\rho),\ C_F(\rho) := \begin{bmatrix} C_{11}(\rho) \\ C_{12}(\rho)+F^T(\rho)\end{bmatrix}$

6.3 Gain-scheduled LFT control theory

The LFT representation is very useful for control design theory, which incites us to present a gain scheduling technique based on LFT. The LFT is also convenient to model plant uncertainty, which is included in our new gain scheduling controller design technique.

Gain-scheduled LFT control assumes that a plant can often be represented as a linear fractional transformation of a nominal plant with physical parameters that vary within a known range. The controller to be scheduled uses these parameters, measured in real time.

Figure 6.1 presents a parameter-dependent plant modeled as an LFT of a time-varying block diagonal matrix $\Delta(t)$, which is assumed measured in real time and takes values in a known set.

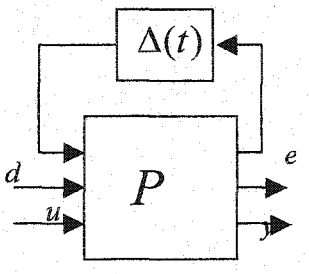

Figure6.1: Parameter-dependent plant

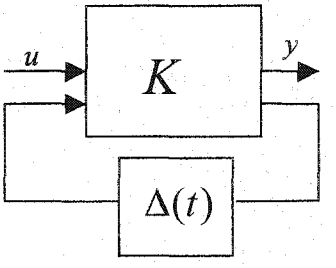

Figure 6.2: Parameter-dependent controller

By interconnecting the parameter dependent plant and controller, the closed-loop system will appear as an uncertain system subject to a time-varying uncertainty $\Delta(t)$.

The parameter-dependent system is written in LFT form as:

$$\begin{bmatrix} e \\ y \end{bmatrix} = F_u\left(P, \Delta(t)\right)\begin{bmatrix} d \\ u \end{bmatrix} \tag{6.10}$$

with P defined as: $P = \begin{bmatrix} P_{\Delta\Delta} & P_{\Delta 1} & P_{\Delta 2} \\ P_{1\Delta} & P_{11} & P_{12} \\ P_{2\Delta} & P_{21} & P_{22} \end{bmatrix}$, $\|\Delta(t)\|_\infty := \sup_{t\in[0,\infty[} \|\Delta(t)\| < 1$ and $P_{LFT} := \begin{bmatrix} P_{11} & P_{12} \\ P_{21} & P_{22} \end{bmatrix}$.

The objective is to obtain an LFT controller $u = F_l\left(K_{LFT}, \Delta(t)\right)y$, $K_{LFT} = \begin{bmatrix} K_{11} & K_{1\delta} \\ K_{\delta 1} & K_{\delta\delta} \end{bmatrix}$

such that the closed-loop system $T := F_l(F_u(P_{LFT}, \Delta(t)), F_l(K_{LFT}, \Delta(t)))$ is internally stable for all parameter trajectories with $\|\Delta\|_\infty < 1$, $\max_{\sigma(\Delta(t))<1} \max_{d\in L_2} \frac{\|Td\|_2}{\|d\|_2} < 1$.

where T is the transfer matrix linking the disturbances d to the errors e.

The closed-loop interconnection structure can be rearranged into the diagram shown in Figure 6.3

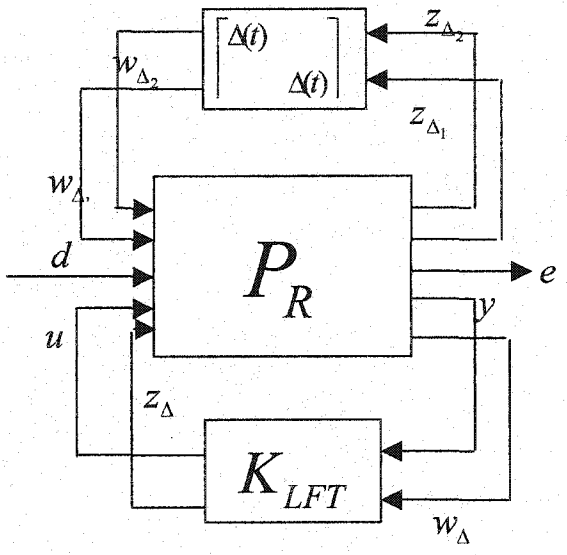

Figure 6.3: Gain scheduled LFT control setup

K_{LFT} is the central part of the gain-scheduled controller. The structure presented in Figure 6.3 is well adapted to use the small-gain theorem introduced in Chapter 2. However, the conservatism due to the time-varying nature of the uncertainties spurred the research in [Pack93] to propose a type-scaling matrix to reduce this conservatism.

With the scaling matrices $J \in \mathcal{J}$ ($\mathcal{J}$ as defined in [Pack93]), the LFT control synthesis problem is formulated as:

Search for $J \in \mathcal{J}$ and a stabilizing controller K_{LFT} such that:

$$\left\| \begin{bmatrix} J & 0 \\ 0 & I_{n_z} \end{bmatrix} F_l(P_R, K_{LFT}) \begin{bmatrix} J^{-1} & 0 \\ 0 & I_{n_d} \end{bmatrix} \right\| < 1 \qquad (6.11)$$

This optimization problem is expressed as the feasibility of a finite-dimensional affine matrix inequality [Boy94] (AMI), which renders the problem numerically tractable because of the convexity of these AMIs.

6.4 Riccati solutions interpolation technique

6.4.1 Introduction

A technique, based on the interpolation of the solutions of the Riccati equations of frozen H_∞ designs, is used for gain scheduling of the full flight envelope of a flexible aircraft. The aircraft model consists of a linear parameter-varying model of a flexible B1 bomber that varies with the Mach number from 0.2 to 0.8Mach. The performance objectives are to track the pitch demand and to alleviate the loads due to wind gusts acting on the aircraft. The flexibility of the aircraft is taken into account through four flexible modes. The method presented is shown to provide good results over the full flight envelope, while allowing for a simple implementation structure.

Modeling the structural flexibility existing in large aircraft is sensible, and makes the control system design challenging for gust load alleviation objectives. In fact, it can be argued that the detrimental effect of turbulence (gusts) acting on the aircraft is increased through the bending modes of the aircraft.

At frozen linear models covering the flight envelope, controllers based on the mixed-sensitivity H_∞ technique were designed. The same weighting functions for performance were used for the different controller designs. This allowed us to automate the design and to unify the performance objectives along the Mach number variation. The scheduling technique used to cover the full flight envelope while preserving performance is based on a linear interpolation of the solutions of the two Riccati equations used in the H_∞ controller design. A version of this method was first introduced and successfully implemented for a small missile model in [Rei92]. Our approach is different from the version presented in that paper in the sense that the controller at the intermediate design points is a function of only the interpolated Riccati solutions variables. In [Rei92], the controller depends on the interpolated solution of the Riccati equation and other parameters viewed as exogenous inputs upon which the nonlinear dynamics are dependent. Another advantage to be noticed, in this approach, is the use of a linear parameter-varying model. In fact, in [Rei92], a nonlinear model is linearized at each point of the flight envelope to be used in the construction of the controller. This will certainly complicate the implementation of the controller over the flight envelope. We believe that the mixture of the LPV models and the interpolating techniques solving the control design problem offers easier implementation and good results. We propose this approach since the classical LPV control design is

time-consuming and suffers, as presented earlier, from the difficulty of solving an LMI problem for high-order systems.

6.4.2 Problem setup

6.4.2.1 Aircraft model

A B-1 bomber is the aircraft under study, and a model of it [Was88], [Van99] taking into account the structural flexibility is used. The aircraft's dynamics are assumed typical for a high-speed transport aircraft, but it includes a ride quality control system (RQCS) that was installed to diminish the unacceptable vibration due to the turbulence that was apparent in the previous version of that aircraft. The longitudinal, linear parameter-varying, B-1 model can be represented as:

$$\begin{cases} \dot{x} = A(\rho)x + B(\rho)u \\ y = C(\rho)x + D(\rho)u \end{cases} \tag{6.12}$$

where: $x = [\alpha \; q \; \eta_1 \; \eta_2 \; \eta_3 \; \eta_4 \; \dot{\eta}_1 \; \dot{\eta}_2 \; \dot{\eta}_3 \; \dot{\eta}_4]^T$ is the state vector which contains the angle of attack, the pitch rate, and the coordinates of the four flexible modes.

$u = [w_g^T \; \dot{w}_g^T \; \delta_{ele}^T \; \delta_{cv}^T]$ are the gust vector, the elevator, and the canard actuators respectively.

$y = [y_q \; y_{acc}]^T$ are the pitch rate and the acceleration of the aircraft measured by the rate gyro and the accelerometer, respectively. $\rho = Mach\ number$: is the parameter varying between 0.2Mach and 0.8Mach.

The following model gives the dynamics of the actuators:

$$\begin{bmatrix} \delta_{ele} \\ \delta_{cv} \end{bmatrix} = \left[\begin{array}{c|c} A_{act} & B_{act} \\ \hline C_{act} & D_{act} \end{array}\right] \begin{bmatrix} \delta_{ele}^{cmd} \\ \delta_{cv}^{cmd} \end{bmatrix} \tag{6.13}$$

where : $[\delta_{ele}^{cmd} \quad \delta_{cv}^{cmd}]^T$ are the actuator commands, and

$$A_{act} = \begin{bmatrix} -10 & 0 \\ 0 & -50 \end{bmatrix}, B_{act} = \begin{bmatrix} 10 \\ 50 \end{bmatrix}, C_{act} = \begin{bmatrix} 1 & 0 \\ 0 & 1 \end{bmatrix}, D_{act} = \begin{bmatrix} 0 \\ 0 \end{bmatrix} \tag{6.14}$$

The transfer function representing the turbulence acting on the aircraft is given as:

$$\begin{bmatrix} w_g \\ \dot{w}_g \end{bmatrix} = \left[\begin{array}{c|c} A_{wg} & B_{wg} \\ \hline C_{wg} & D_{wg} \end{array}\right] d_g \tag{6.15}$$

where: $A_{wg}=\begin{bmatrix}-2V_0/L_{wg} & 1\\ -(V_0/L_{wg})^2 & 0\end{bmatrix}, B_{wg}=\begin{bmatrix}\sigma_{wg}\sqrt{3}(V_0/L_{wg})^{0.5}\\ \sigma_{wg}(V_0/L_{wg})^{1.5}\end{bmatrix}, C_{wg}=\begin{bmatrix}1 & 0\\ -2(V_0/L_{wg}) & 1\end{bmatrix}, D_{wg}=\begin{bmatrix}0\\ \sigma_{wg}\sqrt{3}(V_0/L_{wg})^{0.5}\end{bmatrix}$

σ_{wg}, L_{wg}, d_g : are the intensity, the turbulence scale length and a gaussian white noise, respectively.

The four flexible modes are characterized by their damping ratios $\varsigma_1=\varsigma_2=\varsigma_3=\varsigma_4=0.02$ and their modal frequencies $\omega_1=12.57, \omega_2=14.07, \omega_3=21.17, \omega_4=22.05 rd/s$. The flexible modes have an effect at high frequencies and thus can be separated from the rigid-body modes. To be as realistic as possible, we preferred to use all the flexible modes in the design rather than using conventional techniques such as notch filters to cope with the reduction of flexible modes.

The high level of flexibility in the B-1 bomber model acts negatively on the aircraft and exhibits high-frequency transient motions for the pitch rate open-loop response. Thus, a feedback controller design is needed to improve the pitch rate response and to decrease the acceleration of the aircraft due to turbulence effects.

6.4.2.2 Controller design

Linear parameter-varying model is used to generate frozen linear models corresponding to a set Λ of chosen Mach numbers (operating points). The flight envelope covers the variation of the Mach number from 0.2 to 0.8 for a given altitude. Hence, our choice of the frozen operating points corresponds to the set $\Lambda=\{0.2, 0.25, 0.3, 0.35, 0.4, 0.45, 0.50, 0.55, 0.6, 0.65, 0.7, 0.75, 0.8\}$. The general setup of the frozen controller designs is given by the figure below:

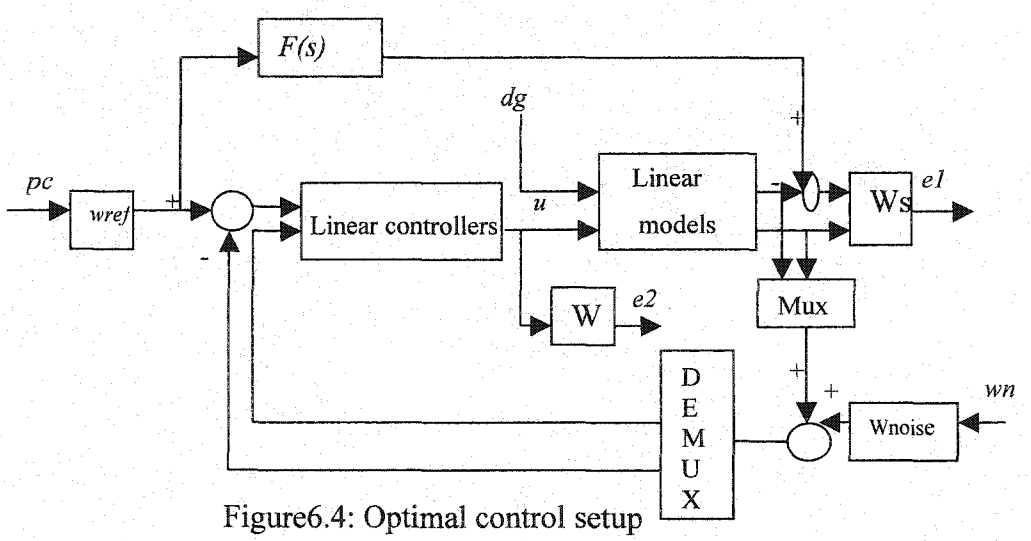

Figure6.4: Optimal control setup

Our control objectives are to track the pilot's pitch demand and to alleviate the gust load by reducing the acceleration of the aircraft due to the effect of the turbulence. For the tracking objective we used a filter $F(s)=\frac{16}{s^2+5.2s+16}$ to shape the response imposed to the closed-loop pitch response. $W_s=\begin{bmatrix}\frac{800}{s+1} & 0\\ 0 & \frac{10}{s+15}\end{bmatrix}$ specifies levels of performance desired from both design objectives. $W_u=\begin{bmatrix}\frac{180}{15\pi} & 0\\ 0 & \frac{180}{15\pi}\frac{(s+15)}{(s+0.01)}\end{bmatrix}$ is used to constrain the effort of the actuators to reasonable and realistic limits which are 15° for the elevator and 15° with zero deflection at the steady-state for the control vane actuator. $W_{noise}=\begin{bmatrix}3\times10^{-4} & 0\\ 0 & 0.01\end{bmatrix}$ represents sensor noise and is used to ensure well-posedness of the H_∞ control design.

Note that the performance objectives were unified for all $\rho_i \in \Lambda$, by having the same weighting functions for the augmented plant along the flight envelope. The controller designs in Figure6.4 can be recast into the general H_∞ controller design framework [Doy89], where the augmented frozen linear models can be represented in the state-space form as:

$$\begin{cases}\dot{x}=A_a(\rho_i)x+B_a(\rho_i)u\\ y=C_a(\rho_i)x+D_a(\rho_i)u\end{cases} \tag{6.16}$$

where: $\rho_i \in \Lambda$

With some simplifying assumptions, [Doy89], we consider the state-space representation of the augmented system as:

$$G_{a_i}(s):=\left[\begin{array}{c|cc}A_a(\rho_i) & B_{a1}(\rho_i) & B_{a2}(\rho_i)\\ \hline C_{a1}(\rho_i) & 0 & D_{a12}(\rho_i)\\ C_{a2}(\rho_i) & D_{a21}(\rho_i) & 0\end{array}\right] \tag{6.17}$$

A suboptimal H_∞ controller [Doy89], for the augmented plant, can be written in its state-space form as:

$$K_{sub}(s) := \left[\begin{array}{c|c} \hat{A}_\infty & -Z_\infty L_\infty \\ \hline F_\infty & 0 \end{array}\right] \tag{6.18}$$

where: $F_\infty := -B_{a2}^* X_\infty$

$$\hat{A}_\infty := A_a + \gamma^{-2} B_{a1} B_{a1}^* X_\infty + B_{a2} F_\infty + Z_\infty L_\infty C_2$$

$$L_\infty := -Y_\infty C_{a2}^*$$

$$Z_\infty := (I - \gamma^{-2} Y_\infty X_\infty)^{-1}$$

The assumption that the terms D_{a11}, D_{a22} are equal to zero is not verified in general, and in our case study in particular. In this case, we use results from $\mathcal{H}_\infty$ control theory [Doy89] that permit to resolve the general problem posed. These results are:

a- The controller in the case of $D_{a22} \neq 0$ is $K_{sub}(I + D_{a22} K_{sub})^{-1}$, if we suppose K_{sub} is the sub-optimal controller of G_a with the asssumption that $D_{a22} = 0$.

b- If $D_{a11} \neq 0$ and without loss of generality, by normalizing D_{a12} and D_{a21} , we shall assume that the augmented plant can be written as:

$$G_{a_i}(s) := \left[\begin{array}{c|cc} A_a(\rho_i) & B_{a1}(\rho_i) & B_{a2}(\rho_i) \\ \hline C_{a1}(\rho_i) & \begin{bmatrix} D_{a1111}(\rho_i) & D_{a1112}(\rho_i) \\ D_{a1121}(\rho_i) & D_{a1122}(\rho_i) \end{bmatrix} & \begin{bmatrix} 0 \\ I \end{bmatrix} \\ C_{a2}(\rho_i) & \begin{bmatrix} 0 & I \end{bmatrix} & 0 \end{array}\right] \tag{6.19}$$

such that: $\tilde{D}_{12} = \begin{bmatrix} 0 \\ I \end{bmatrix}, \tilde{D}_{21} = \begin{bmatrix} 0 & I \end{bmatrix}$.

If we normalize $\gamma = 1$, then there exists a controller K that internally stabilizes G_a and $\left\| \mathcal{F}_L(G_a, K) \right\|_\infty \leq 1$ if and only if there is $\tilde{K}$ that stabilizes M and $\left\| \mathcal{F}_L(M, \tilde{K}) \right\|_\infty \leq 1$. where:

$$M := \left[\begin{array}{c|cc} \tilde{A} + \tilde{B}_1 R_1^{-1} \tilde{D}_{11}^* \tilde{C}_1 & \tilde{B}_1 R_1^{-1/2} & \tilde{B}_2 + \tilde{B}_1 R_1^{-1} \tilde{D}_{11}^* \tilde{D}_{12} \\ \hline \tilde{R}_1^{-1/2} \tilde{C}_1 & 0 & \tilde{R}_1^{-1/2} \tilde{D}_{12} \\ \tilde{C}_2 + \tilde{D}_{12} R_1^{-1} \tilde{D}_{11}^* \tilde{C}_1 & \tilde{D}_{21} R_1^{-1/2} & \tilde{D}_{21} R_1^{-1} \tilde{D}_{11}^* \tilde{D}_{12} \end{array}\right]$$

$$\tilde{D}_{11} := \begin{bmatrix} D_{1111} & D_{1112} \\ D_{1121} & D_{1122} + D_\infty \end{bmatrix}, D_\infty = -D_{1122} - D_{1121}(I - D_{1111}^* D_{1111})^{-1} D_{1111}^* D_{1112}$$

$R_1 := I - \tilde{D}_{11}^* \tilde{D}_{11}, \tilde{R}_1 = I - \tilde{D}_{11} D_{11}^*$.

Thus, an H_∞ controller can be calculated for our particular models where $D_{a11} \neq 0$ and $D_{a22} \neq 0$. Algorithms for this general H_∞ control problem can be found in [Bal95].

6.4.3 Scheduling technique:

The H_∞ controllers designed for the frozen design points $\rho_i \in \Lambda$ depend essentially on the solutions of the two Riccati equations needed in each H_∞ control design.

Define:

$K_i := f(\Im_i, X_i, Y_i)$ as the ith H_∞ controller for the ith design, where:

$$\Im_i := \left[\begin{array}{c|cc} A_a(\rho_i) & B_{a1}(\rho_i) & B_{a2}(\rho_i) \\ \hline C_{a1}(\rho_i) & D_{a11}(\rho_i) & D_{a12}(\rho_i) \\ C_{a2}(\rho_i) & D_{a21}(\rho_i) & D_{a21}(\rho_i) \end{array}\right] \tag{6.20}$$

is the state space representation of the ith augmented plant.

X_i, Y_i: are the ith solutions of the ith Riccati equations pair used in the ith frozen design.

The advantage of our method is the on-line availability of a faithful linear model at any point of the flight envelope, using the LPV model available. This model facilitates considerably the implementation in contrast to the procedure of linearization, which was used at each point of the flight envelope in [Rei92]. The model $\Im_j$ can be evaluated for each jth parameter $\rho_j \in [0.2, 0.8]$. If we suppose that $\rho_j \in [\rho_i, \rho_{i+1}]$ we use the ith and the (i+1)th controllers designed, K_i and K_{i+1} respectively, to calculate the controller K_j. The solutions of the two Riccati equations at any jth design point are linearly interpolated from the solutions (X_i, Y_i) and (X_{i+1}, Y_{i+1}) as follows:

$$X_j = (1-\mu_j)X_i + \mu_j X_{i+1},\ \mu_j = (\rho_j - \rho_i)/(\rho_{i+1} - \rho_i):\ \mu_j \in [0,1] \tag{6.21}$$

and similarly for Y_j. Once the jth solutions of the Riccati equations are evaluated and using the state matrices of $\Im_j$, the H_∞ controller at jth point of the flight envelope is calculated as shown in the previous section as: $K_j = f(\Im_j, X_j, Y_j)$.

The use of this technique of controller scheduling has the advantage that it does not require any special structure for the frozen controllers. It can be an H_2 controller, an H_∞ controller or an H_∞ loopshaping

controller. These modern controllers have the common specification to be calculated based on solutions of Riccati equations.

6.4.4 Results and nonlinear simulation

The frozen designs made are based on a mixed-sensitivity H_∞ setup. The performance objectives were unified for all frozen design points. The performance indices γ obtained are given in the following table.

Table 6.1: Operating points and performance indices

γ	1.1	1.09	1	0.93	0.86	0.80	0.74	0.76	0.80	0.84	0.88	0.93	0.98
ρ	0.2	0.25	0.3	0.35	0.4	0.45	0.5	0.55	0.6	0.65	0.7	0.75	0.8

Thus, the performance specifications, concerning the pitch demand tracking, the gust load alleviation and the controller output constraints, were basically satisfied for all the frozen designs. Figure 6.5 shows closed-loop responses and actuator deflections for 0.55Mach. It confirms the good pitch tracking obtained for pilot pitch demand $pc = 3\pi/180\ rd$ and the reduction of the acceleration with the $\mathcal{H}_\infty$ design [Aou2000b] using reasonable actuator deflections. The full flight envelope controller outputs using the technique presented in this work is shown by Figure 6.6. Notice the good performance level for the pitch-tracking objective. Concerning the gust load alleviation objective, we obtained a degradation of performance compared to the frozen design results.

However, the worst level of acceleration obtained is equal to $-1.5m/s^2 = -0.15g$ which is still reasonable, taking into account that we are operating over the full flight envelope. We have to comment that the gust load alleviation problem is in general not easy to deal with for just one operating point. To our knowledge, our approach to deal with this problem over a full flight envelope is presented in this thesis for the first time, with good performance results. The actuator responses are still in the acceptable range of $\pm 15^\circ$ for both the elevator and the control vane actuator. We notice that certain bumps essentially for control vane actuators. These bumps are due essentially to the high degree of change in the dynamics of the aircraft. This change is noticed even between two adjacent operating points. Although these are undesirable effects on the deflection actuator responses, these bumps can be handled by the actuators, which are bounded in magnitude and variation rate. We went

further in our research, trying to avoid those undesirable bumps for the actuator response. We used a safety technique that consists in constraining the actuator deflections to safe ranges of deflection. Figure 6.7 shows, respectively, the closed-loop pitch response, the acceleration of the aircraft and the constrained actuator deflections. We were able to reduce the actuator bumps in magnitude and variation rate into more homogenous deflections without significantly affecting the performance obtained in the unconstrained actuator case.

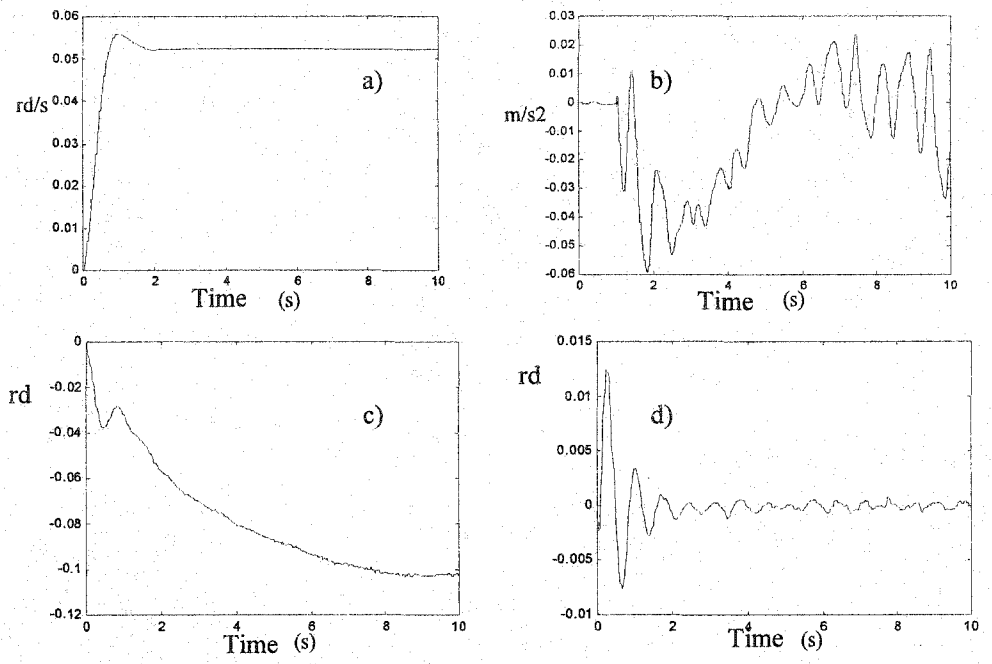

Figure 6.5: Frozen controller results (pitch tracking and actuator responses)

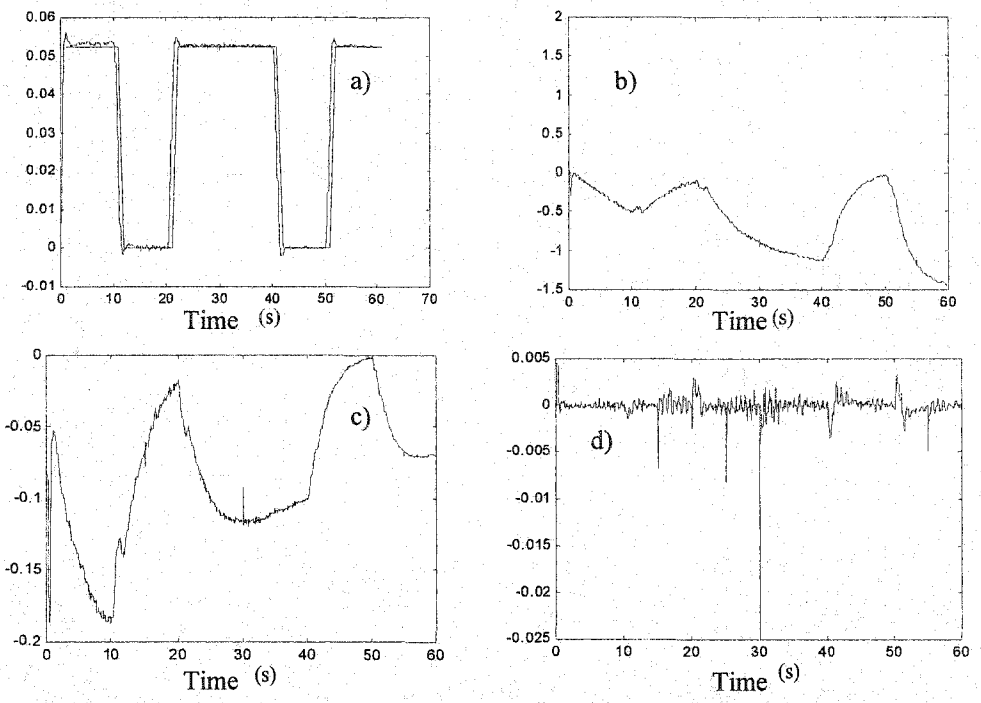

Figure 6.6: gain scheduled controller results (pitch tracking and actuator responses)

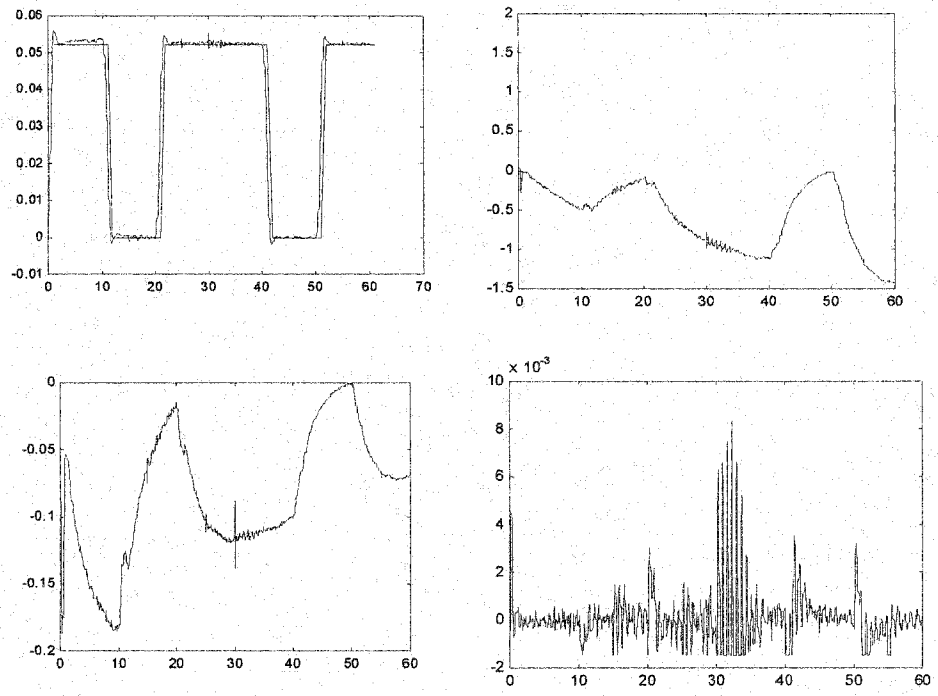

Figure 6.7: Constrained gain scheduled controller results (pitch tracking and actuator responses)

6.5 Concept of online redesign of controller

In the following, we limited our application example to the pitch angle-tracking problem. Our aircraft model is a two-input (actuators), one-output (pitch angle) system. We believe that with the progress of computer capabilities these days, an approach based on an online controller design can make sense. Figure 6.8 proposes the concept of online controller redesign adopted for the simplified B1 flexible model.

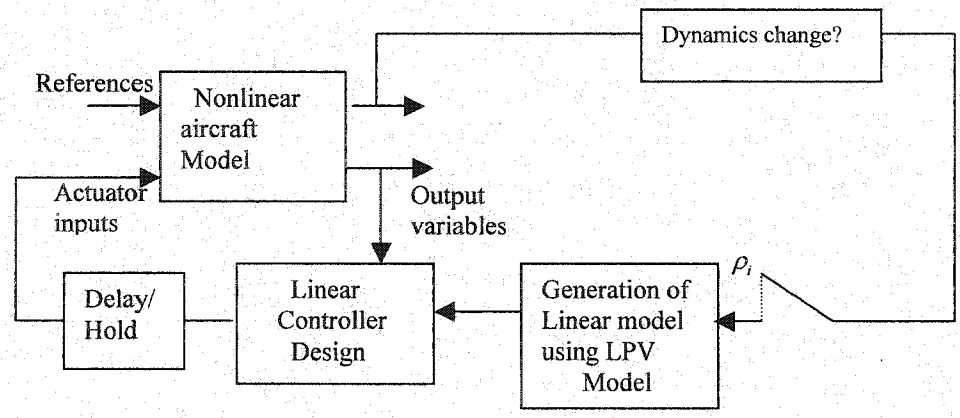

Figure 6.8: Controller redesign setup

The nonlinear model in this case has an accurate approximation consisting in the LPV model. The inputs of the nonlinear model are the references (pilot demands), in this case the Mach number (the velocity of the aircraft), and the actuators efforts. As outputs we obtain the measured Mach number, which is used to generate the corresponding linear model from the LPV model representation if a change in dynamics is noticed. At each corresponding change in dynamics a design of a linear controller achieving the performance objectives could be used to compute the control signals to actuators for the nonlinear model.

A controller redesign can be efficient and easy to implement if the following conditions are satisfied:

1-The controller design algorithm has to be systematic and robust for any linear model corresponding to a trim point of the flight condition.

2-The performance objectives specified by performance weighting functions have to be unified for all l linear designs or varying with the parameter of the flight condition.

3-The block Delay/Hold can overcome differences in timing between a change in dynamics and the controller redesign time.

The second condition is, obviously, needed to make the approach systematic online. However, the first condition is obligatory since it minimizes the time taken for redesign and allows the approach to be implemented. Since we based the controller design approach earlier on a mixed-sensitivity H_∞ design, which is based on an iterative H_∞ optimization, an online redesign controller would appear difficult. Thus, we propose in our approach to use weighted H_2 optimization [Aou2000a] or an H_∞ loopshaping control technique, which are both computable through a single pair of Riccati equations. The objective in our application example consists of tracking the pitch angle with reasonable actuators efforts. The $\mathcal{H}_\infty$ loopshaping technique [Mcf90] is used for the controller design. This technique, as presented in Chapter 2, proposes to shape the plant model by appropriate input and output weighting functions resulting in the shaped plant $G_s = W_1 G W_2$, and a robust stabilization procedure is used for the shaped plant G_s to obtain an H_∞ loopshaping controller K_∞ implemented as $W_2 K_\infty W_1$. A static gain used to adjust the steady-state gain is also computed. The weighting functions W_1 and W_2 used in our design are the same over the entire flight envelope. Note that the portion of the global flight envelope considered here is from 0.2Mach to 0.5Mach. Figure 6.9 presents the design index γ for the controller redesign along the flight envelope considered.

The inverse of the performance index represents the stability margin obtained through the robust stabilization procedure. Figure 6.9 shows that the interval of stability margin along the flight envelope is kept close to the level of 36% stability margin.

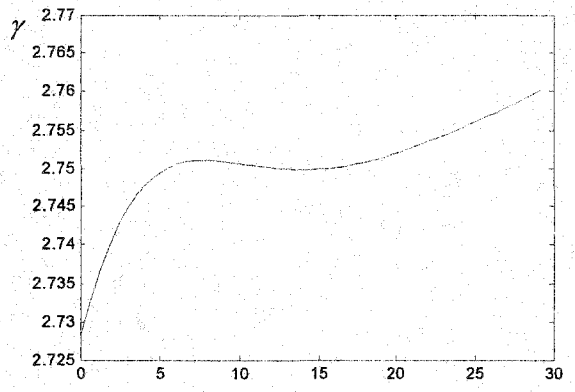

Figure 6.9: Robustness measures

Figure 6.10 gives the pitch angle tracking results for the B1 flexible model through the nonlinear simulation framework proposed in Figure 6.8.

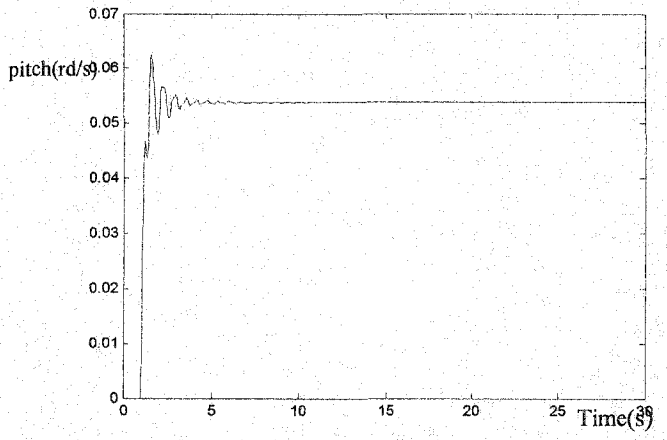

Figure6.10: pitch angle tracking for redesigned controller

A good pitch angle tracking response is obtained, quick in reaching steady-state, and reasonable actuators effort, under the physical limits required as shown in Figure 6.11.

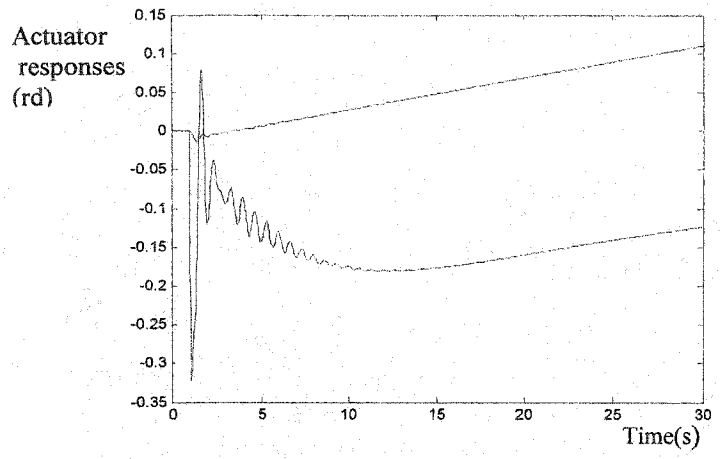

Figure 6.11: actuator responses for redesigned controller

6.6 Robust gain scheduling controller design

6.6.1 Introduction

Intensive research in control over the last two decades led to well developed design techniques [Doy89],[Bal95],[Ske88]. These techniques sometimes, known as modern approaches, introduced and improved important closed-loop properties such as robust stability and robust performance. These techniques, usually sub-optimal, are based on linear design methodologies. This means that the performance obtained, as for all linear techniques, is guaranteed only around specific operating points. Aerospace applications need control laws that maintain acceptable performance levels over the entire flight envelope considered for aerospace vehicles, which implies nonlinear dynamics. For this reason, research efforts turned to develop gain scheduling methods such as interpolation of frozen controllers, and to study their real-time on-board implementation [Hyd91]. Other techniques are based on linear parameter varying (LPV) models and lead to LPV controllers designed via LMI's (Linear matrix inequalities). The main advantage of interpolation techniques, compared to other gain scheduling methods such as LPV methods, is their simple implementation, which is a major issue in the aerospace industry.

A new interpolation based approach; called blending/interpolating technique [Aouf2000c] is proposed in this section. This approach has the virtue to avoid restrictions on the type, structure and order of the interpolated controllers as opposed to the observer-based interpolation technique in [Hyd91]. As mentioned earlier, the main criticism regarding interpolation techniques is the lack of guarantees on

stability of the closed-loop system. These "ad-hoc" techniques, with a judicious choice of operating points covering the flight envelope for the frozen designs, may often give satisfactory stability margins. However, stability guarantees are needed to reassure aerospace engineers whom may be tempted to try this type of technique. In this section, we present a robust controller design, based on a blending/interpolating method, that guarantees stability and performance over the entire flight envelope of aerospace vehicles. This methodology is successfully applied to a B1 flexible aircraft model. The extension of this methodology to any gain scheduling problem is straightforward. The variation along the flight envelope is captured by a time-varying uncertainty representation, which is treated in a μ – synthesis framework.

6.6.2 Uncertain model representation

Aerospace vehicles operating over a large flight envelope are represented by nonlinear models depending on operating conditions. Obviously, to use linear controller design we need linear models around chosen operating points. This can be obtained by classical linearization procedures for chosen operating points. Nonlinear models can also be formulated as linear parameter-varying models for use in an LPV controller design framework. In this section, we represent nonlinear dynamics of the aircraft models by uncertain systems in linear fractional transformation (LFT) representation used for a μ – setup. The general μ – setup is given in Figure 6.12.

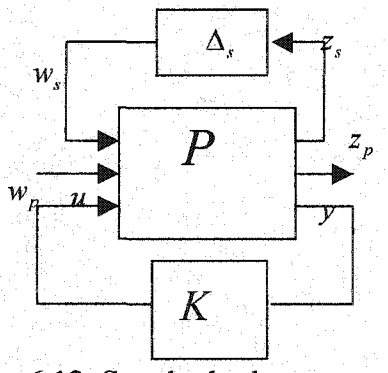

Figure6.12: Standard robust controller setup

The objective is stated as: Assuming a model $P(s) = \begin{bmatrix} P_{11} & P_{12} & P_{13} \\ P_{21} & P_{22} & P_{23} \\ P_{31} & P_{32} & P_{33} \end{bmatrix}$ subject to an uncertainty model

$\Delta_s(s) \in \Re H_\infty : \|\Delta_s\|_\infty \le 1$, design a controller $K(s)$ such that: $\|F_u(F_l(P,K),\Delta_s)\|_\infty \le 1$ and $\|P_{11}\|_\infty \le 1$.

In the literature, methods where proposed [Fial97],[Hyd91] to construct an LFT model that approaches the behavior of the nonlinear model along the flight envelope portion considered.

Let us consider $\Lambda = \{\rho_1, ..., \rho_n\}$ a set of operating design points, where ρ_i represents a vector of flight parameter conditions, e.g., as aircraft velocity, for the *ith* chosen operating point. The nonlinear model is linearized on those chosen operating design points leading to linear state-space representation:

$$\begin{cases} \dot{x} = A_i x + B_i u \\ y = C_i x + D_i u \end{cases} \tag{6.22}$$

for each $\rho_i \in \Lambda$.

Where: $A_i \in \Re^{n \times n}, B_i \in \Re^{n \times p}, C_i \in \Re^{m \times n}, D_i \in \Re^{m \times p}$.

For simplification, we assume $C_i = C, D_i = 0 \ \forall i = 1, .., n$, which means that changes over the entire flight envelope are restricted to matrices A and B. We further assume that a single parameter ρ of the aircraft is varying; call z its scaled version.

Assume that matrices $\{A_i\}_{i=1}^n$ and $\{B_i\}_{i=1}^n$ are interpolated by polynomials of order t with matrix coefficients:

$$\begin{aligned} P_A(z) &:= \sum_{i=1}^{t} \mathcal{A}_i z^i, \ z \in [-1,1] \\ P_B(z) &:= \sum_{i=1}^{t} \mathcal{B}_i z^i, \ z \in [-1,1] \end{aligned} \tag{6.23}$$

That is, at the points $\{z_j\}_{j=1}^n$, we have:

$$\begin{aligned} &P_A(z_j) = A_j \\ &P_B(z_j) = B_j \\ &j = 1, ..., n \end{aligned} \tag{6.24}$$

Note that the interpolation is assumed to be performed entry by entry of the matrices to fit. In other words, each scalar polynomial entry of $P_A(z)$ and $P_B(z)$ interpolates the same entry in matrices $\{A_i\}$ and $\{B_i\}$ respectively.

Define the matrix M including the system dynamics and the matrices $\mathcal{A}_i, \mathcal{B}_i$ as

$$M = \begin{bmatrix} 0 & 0 & I & 0 & 0 & 0 & 0 & 0 \\ 0 & 0 & 0 & I & 0 & 0 & 0 & 0 \\ 0 & 0 & 0 & 0 & I & 0 & 0 & 0 \\ 0 & 0 & 0 & 0 & 0 & I & 0 & 0 \\ 0 & 0 & 0 & 0 & 0 & 0 & I & 0 \\ 0 & 0 & 0 & 0 & 0 & 0 & 0 & I \\ 0 & 0 & 0 & 0 & 0 & 0 & D & C \\ \mathcal{B}_l & \mathcal{A}_l & . & . & \mathcal{B}_1 & \mathcal{A}_1 & \mathcal{B}_0 & \mathcal{A}_0 \end{bmatrix} \tag{6.25}$$

then an uncertain system, in an LFT form as in Figure 6.12, [Hyd91], covering the flight envelope considered, could be retrieved as: $F_u(P,\Delta_s)$ where $P = F_l(M, s^{-1}I)$ and $\Delta_s = \delta I_r . \delta$ is an uncertain repeated parameter, $-1 < \delta < 1$, that depends on the vector of the flight condition parameters. Note that δ is variable z in the matrix polynomials $P_A(z)$ and $P_B(z)$. By varying δ from –1 to 1, we are varying the flight condition parameter to cover the flight envelope considered. In the example below, δ depends on the Mach number. Thus varying the parameter δ means a variation in the Mach number that the nonlinear model depends on.

6.6.3 Parameterization of stabilizing controllers

The parameterization of stabilizing controllers is important for the development of the method proposed in this section since it provides a sub-optimal controller with a free-parameter that can be tuned for performance objectives. Let us consider the nominal system of Figure 6.13 relating the inputs $\begin{bmatrix} w^T & u^T \end{bmatrix}^T$ to outputs $\begin{bmatrix} z^T & y^T \end{bmatrix}$:

$$P_n = \begin{bmatrix} P_{22} & P_{23} \\ P_{32} & P_{33} \end{bmatrix} = \left[\begin{array}{c|cc} A & B_1 & B_2 \\ \hline C_1 & D_{11} & D_{12} \\ C_2 & D_{21} & D_{22} \end{array}\right] \tag{6.26}$$

which its realization is assumed detectable and stabilizable. An internally-stabilizing, observer-based controller $K(s)$ can be obtained as: $K(s) = \left[\begin{array}{c|c} A + B_2F + LC_2 + LD_{22}F & -L \\ \hline F & 0 \end{array}\right]$ whose F and L are a state feedback and observer gain such that $A + B_2F$ and $A + LC_2$ are stable.

It has been shown in the literature [Doy89] that all stabilizing controllers for a system P_n can be parameterized as a central controller with a free parameter called "Youla parameter" as in Figure 6.13:

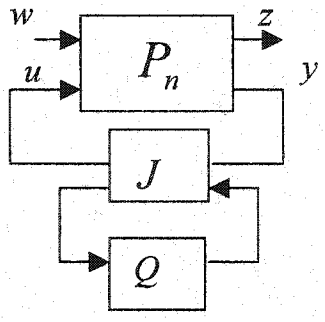

Figure 6.13: Parameterization of stabilizing controller

The family of all stabilizing controllers is given as follows:

$\mathbf{K} = \{F_l(J,Q) : Q \in \Re H_\infty \text{ and } I + D_{22}Q(\infty) \text{ non-singular}\}$

$$J = \left[\begin{array}{cc|c} A + B_2F + LC_2 + LD_{22}F & -L & B_2 + LD_{22} \\ F & 0 & I \\ \hline -(C_2 + D_{22}F) & I & -D_{22} \end{array}\right] \tag{6.27}$$

The closed loop system $\Im$ depends on the free Youla parameter $Q(s)$ as:

$\Im = F_l(T,Q) = \{T_{11} + T_{12}QT_{21} : Q \in \Re H_\infty, I + D_{22}Q(\infty) \text{ invertible}\}$

$$T = \begin{bmatrix} T_{11} & T_{12} \\ T_{21} & T_{22} \end{bmatrix} = \left[\begin{array}{cc|cc} A + B_2F & -B_2F & B_1 & B_2 \\ 0 & A + LC_2 & B_1 + LD_{21} & 0 \\ \hline C_1 + D_{12}F & -D_{12}F & D_{11} & D_{12} \\ 0 & C_2 & D_{21} & 0 \end{array}\right] \tag{6.28}$$

H_∞ controllers can also be parameterized as a central controller with a free Youla parameter:

$\mathbf{K} = \{F_l(J,Q) : Q \in \Re H_\infty \text{ and } \|Q\| < \gamma\}$

$$J = \left[\begin{array}{c|cc} A_\infty & -Z_\infty L_\infty & Z_\infty B_2 \\ \hline F_\infty & 0 & I \\ -C_2 & I & 0 \end{array}\right] \tag{6.29}$$

$$
\begin{aligned}
A_\infty &= A+\gamma^{-2}B_1B_1^{'}X_\infty + B_2F_\infty + Z_\infty L_\infty C_2 \\
F_\infty &= -B_2^{'}X_\infty \\
L_\infty &= -Y_\infty C_2^{'} \\
Z_\infty &= (I-\gamma^{-2}Y_\infty X_\infty)^{-1}
\end{aligned}
\tag{6.30}
$$

X_∞, Y_∞ and γ are solutions of the standard Riccati equations used for the H_∞ design for the augmented systems state-space representation: $\begin{bmatrix} A & [B_1 \quad B_2] \\ \begin{bmatrix} C_1 \\ C_2 \end{bmatrix} & 0 \end{bmatrix}$.

6.6.4 Robust performance gain scheduling approach

The proposed approach in this section is based on the blending/interpolating technique, [Aouf2000c], that assumes controllers achieving local performance for chosen operating points have been designed. Suppose, as earlier, that Λ is the set of chosen operating points for linear design and define $u_j(\rho)\ j=1,..,n$ as the controller output for the *jth* design point then the blending/interpolating technique proposes a linearly blended signal to be used for the actuators as:

$$
u(\rho) = (1-\lambda(\rho))u_{j-1}(\rho) + \lambda(\rho)u_j(\rho),\ \rho \in [\rho_{j-1}, \rho_j[,\ j=1,...,n \tag{6.31}
$$

where: $0 \le \lambda(\rho) \le 1$ is a function of the aircraft parameter ρ. ρ_{j-1} and ρ_j are the velocity corresponding to the (j-1)st and jth design operating point, respectively.

In the following, the blending/interpolating strategy outlined above is shown to yield a robust stability and performance over the entire flight envelope of the aircraft. Suppose we have two adjacent operating points *j-1* and *j* where controllers are designed using (6.27) or (6.29) and shown as in Figure 6.13 and suppose the nonlinear model is represented by an uncertain linear parameter-varying system in LFT form as presented in (6.25). Then an implementation of blending/interpolating control at operating point $\rho_i \in \left[\rho_{j-1}, \rho_j\right]$ is given as in Figure 6.14:

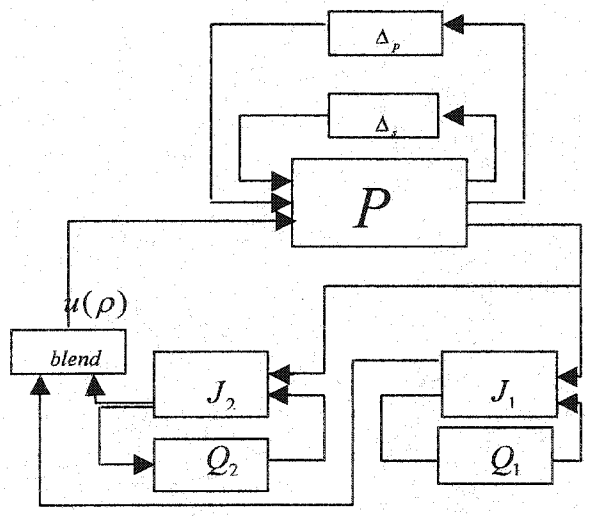

Figure 6.14: Blending/interpolating parameterized controllers

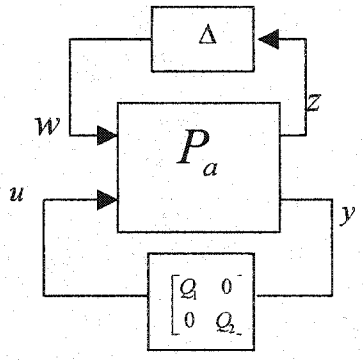

Figure 6.15: Augmented system into robust controller setup

The controller signal vector $u(\rho)$ depends on $\lambda(\rho)$ which is a function of the operating parameter ρ. This parameter ρ is in turn proportional to the uncertain parameter δ used in the uncertainty block Δ_s as previously mentioned. Figure 6.14 can be recast into a μ – framework as in Figure 6.15:

Where the plant P is augmented into: $P_a = f(P, J_1, J_2, \mathrm{h})$, the uncertainty block is augmented into

$$\Delta = \begin{bmatrix} \Delta_p & & \\ & \delta I_{2p} & \\ & & \Delta_s \end{bmatrix} \tag{6.32}$$

and h is a scaling function $\lambda = \mathrm{h}(\delta)$, $z = \begin{bmatrix} z_p^T & z_{\Delta_2}^T & z_{\Delta_1}^T \end{bmatrix}^T$, $w = \begin{bmatrix} w_p^T & w_{\Delta_2}^T & w_{\Delta_1}^T \end{bmatrix}^T$, Δ_p a fictitious performance uncertainty.

The following theorem gives the necessary and sufficient condition under a μ – framework that guarantees that a blended/interpolated controller, based on a stabilizing controller parameterization, will achieve robust performance over the entire flight envelope considered.

Theorem6.2:

For a slowly-varying operating point which leads to a slowly-varying system, and for constant D-scaling matrices $D \in \mathbb{D} = \left\{ D \in \Re^{n_\Delta \times n_\Delta} : D^T D = I_{n_\Delta} \text{ and } D\Delta = \Delta D \right\}$ then:

The closed-loop parameter-varying system of Figure 6.15 is stable and achieves the desired performance objectives if and only if $\exists D \in \mathbb{D}$ such that $\left\| DTD^{-1} \right\|_\infty \leq 1$ where $T = F_l(P_a, diag\{Q_1, Q_2\})$.

Proof:

The use of real constant D-scalings to take into account the time-varying uncertainties is proven in [Sham94]. Referring to Figure 6.15 and using the results of robust performance μ-controller design, the rest of the proof is straightforward.

6.6.5 Optimization based control

The objective is to obtain a controller-parameter $Q_{opt}(s) = \begin{bmatrix} Q_1(s) & 0 \\ 0 & Q_2(s) \end{bmatrix}, Q_1(s), Q_2(s) \in \Re H_\infty$ such that:

$$\min_{Q_1, Q_2} \max_{\omega} \inf_{D} \bar{\sigma}(DT(j\omega)D^{-1}) \tag{6.33}$$

where $\bar{\sigma}$ is the maximum singular value.

This problem cannot be treated efficiently as a $\mu - controller$ design [Bal95], because of the stability constraint on the controller-parameter Q_{opt}, which is not guaranteed under $\mu - framework$ and also because of the dimensionality of the resulting LFT representation in (6.21). Therefore, an optimization technique for parameters of a fixed structure controller-parameter Q_{opt} is proposed. Since stability and performance are guaranteed for two design points, our objective is to obtain a "controller-parameter" Q_{opt} that guarantees performance with stability between the two extremities of the operating point trajectory. We propose a simple structure of controller-parameter Q_{opt} to facilitate the design. The proposed structure of Q_{opt} is given as: $Q_{opt}(s) = \begin{bmatrix} Q(s) & 0 \\ 0 & Q(s) \end{bmatrix}$ where $Q(s) = \frac{1}{s+a} I_{2pm}, a \in \Re^+$.

Although the choice of the structure of the controller Q_{opt} may be different from the structure proposed here, we highly recommend a simple structure of controller.

Different optimization techniques can be formulated for the optimization problem (6.33) posed above, from nonlinear programming techniques, to least-square minimization. Two of the simplest methods using gradient descent of the function $\bar{\sigma}(DT(j\omega)D^{-1})$, which is well adapted to our fixed controller structure design, are presented. In [Mora89], an optimization procedure for the free parameter $Q(s)$ of an Internal Model Control (IMC) structure has been proposed. An analytic expression of the gradient of the upper bound on μ given in [Mora89], can be derived as:

$\min_{Q_1,Q_2\in\Re H_\infty} \max_{\omega\in\Omega} \inf_{D\in\mathcal{D}} \bar{\sigma}(DT(j\omega)D^{-1}) \Leftrightarrow \min_{a\in\Re^+} \max_{\omega\in\Omega} \inf_{D\in\mathcal{D}} \bar{\sigma}(DT(j\omega)D^{-1})$ where: Ω is the frequency interval considered and $\mathcal{D}=\{d\times I_{n_w n_z} : d\in\Re\}$. If we define $\Phi(a)=\max_{\omega\in\Omega} \inf_{D\in\mathcal{D}} \bar{\sigma}(DTD^{-1})$, then $\frac{\partial\Phi}{\partial a}=\frac{\partial\sigma_1(D_{op}T(j\omega_{op})D_{op}^{-1})}{\partial a}$ where the $\max_{\omega}(.)$ is attained at $\omega=\omega_{op}$, the $\inf_{D}\bar{\sigma}(DT(j\omega_{op})D^{-1})$ is obtained at $D=D_{op}$ and $D_{op}T(j\omega_{op})D_{op}^{-1}$.

Consider the closed-loop system $T=F_l(P_a,Q_{opt})$ to be normalized at its performance inputs/outputs w_p/z_p as $T=W_pHW_i$ where $H=\begin{bmatrix} H_{11} & H_{12} & H_{13} \\ H_{21} & H_{22} & H_{23} \\ H_{31} & H_{32} & H_{33} \end{bmatrix}$. An SVD decomposition of:

$$D_0H(j\omega_0)D_0^{-1}=\begin{bmatrix}\mathrm{u}_1 & U\end{bmatrix}\begin{bmatrix}\sigma_1 & \\ & \Sigma\end{bmatrix}\begin{bmatrix}\mathrm{v}_1^{\mathrm{T}} \\ V^T\end{bmatrix} \tag{6.34}$$

is needed.

Considering $W_i=I$, an analytic expression of the gradient of $\Phi(a)$ is given as [Mora89]:

$$\frac{\partial\Phi}{\partial a}=\mathrm{Re}\left[\mathrm{u}_1^{\mathrm{T}}D_{op}\begin{pmatrix}H_{13}\\ W_pH_{23}\end{pmatrix}\left(I-K_{op}H_{33}\right)^{-1}\frac{\partial Q_{opt}(j\omega_{op})}{\partial a}\left(I-H_{33}Q_{opt}\right)^{-1}\begin{pmatrix}H_{31} & H_{32}\end{pmatrix}D_{op}^{-1}\mathrm{v}_1\right] \tag{6.35}$$

A procedure to obtain a satisfactory solution of the minimization in (6.33) can be proposed as follows:

1-Choose an initial value of the parameter a.

2-Obtain ω_{op} from the frequency interval considered and obtain the D-scaling matrix D_{op}.

3-Do the SVD decomposition in (6.30).

4-Calculate the gradient $\frac{\partial\Phi}{\partial a}$

5-Readjust the value of the parameter a as $a=a-\varepsilon\frac{\partial\Phi}{\partial a}$, $0<\varepsilon<1$.

The optimization proposed based on an analytic expression of the gradient can sometimes be inefficient since the gradient depends on the results ω_{op} and D_{op} that are difficult to estimate. Therefore we propose another helpful way to optimize (6.33) numerically. It is actually a simple gradient-based method where the gradient function $\frac{\partial \Phi}{\partial a(i)}$ for the *ith* iteration search is evaluated as:

$$\frac{\partial \Phi}{\partial a(i)} = \frac{\Phi(a(i)) - \Phi(a(i-1))}{a(i) - a(i-1)} \tag{6.36}$$

where $\Phi(a(i-1))$ is the result of the previous iteration. $\Phi(a(i))$ is evaluated, using the "mu" command in Matlab [Bal95] , as the minimum value obtained for a constant *D-scaling.* The parameter a is then readjusted in step 5.

6.6.6 Robust performance analysis technique

A lack of tools for stability assessment of gain scheduling controllers based on interpolation technique led us to extend the design proposed earlier for stability and performance analysis over the entire flight envelope. The accurate uncertainty description of the nonlinear system, introduced above in (6.25), is adopted in the current section.

We assume that two stabilizing controllers K_1, K_2 are designed for the extremities of the portion of the flight envelope considered. These controllers can be designed using any type of linear control technique. The blending/interpolating controller implementation in Figure 6.14, where $F_l(J_1, Q_1)$ and $F_l(J_2, Q_2)$ are substituted for K_1 and K_2 respectively, is used.

Thus an $S-\Delta$ block structure as given in Figure 6.16 is obtained using the uncertainty block augmentation as in (6.32) and where:

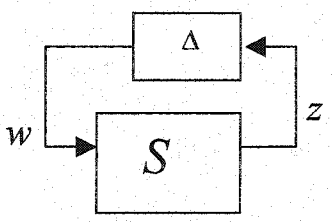

Figure6.16: $S-\Delta$ structure

$S = f(P, K_1, K_2, \mathrm{h})$ and $\Delta = \begin{bmatrix} \Delta_p & 0 & 0 \\ 0 & \delta I_{2p} & 0 \\ 0 & 0 & \Delta_s \end{bmatrix}$, $z = \begin{bmatrix} z_p^T & z_{\Delta_2}^T & z_{\Delta_1}^T \end{bmatrix}^T$, $w = \begin{bmatrix} w_p^T & w_{\Delta_2}^T & w_{\Delta_1}^T \end{bmatrix}^T$. This structure can be used to analyze the performance and robust stability objectives through standard $\mu-$analysis [Bal95].

We propose to analyze the blending/interpolating controller to gain confidence in the safety of a real-time implementation of this controller over the entire flight envelope considered. The following lemma, adapted from [Sham94], gives the main result of stability and performance analysis of the blending/interpolating controller.

Lemma 6.2

Stability over the entire flight envelope considered is guaranteed if and only if for $D \in \mathbb{D} = \left\{ D \in \Re^{n_{\Delta stab} \times n_{\Delta stab}} : D^T D = I_{n_{\Delta stab}} \text{ and } D\Delta_{stab} = \Delta_{stab} D \right\}$, $\left\| DS_{22} D^{-1} \right\|_\infty \leq 1$ where $S = \begin{bmatrix} S_{11} & S_{12} \\ S_{21} & S_{22} \end{bmatrix}$ and $\Delta_{stab} = \begin{bmatrix} \delta I_{2p} & 0 \\ 0 & \Delta_s \end{bmatrix}$. Furthermore a specified level of performance γ is preserved if and only if: for $D \in \mathbb{D} = \left\{ D \in \Re^{n_\Delta \times n_\Delta} : D^T D = I_{n_\Delta} \text{ and } D\Delta = \Delta D \right\}$, $\left\| DSD^{-1} \right\|_\infty \leq 1$.

6.6.7 Application example:

The example showing the applicability of the results and design methodologies of the previous section consists of a simplified version of the B1 flexible model [Aouf2002]. In this application, we are interested in a pitch angle-tracking problem. Mixed-sensitivity H_∞ approach is used to design H_∞ controllers for the two extremities (0.2Mach and 0.3Mach) of the flight envelope portion considered. The tracking results and actuator efforts for 0.2Mach and 0.3Mach are comparable to the results shown in Figure 6.10, 611 for the redesign approach proposed earlier. The robust analysis method, given in Lemma6.1 is applied for the blending/interpolating H_∞ controller based on the frozen 0.2Mach and 0.3Mach H_∞ controller designs. The specified level of performance required in this H_∞ controller design is given by $W_s = \dfrac{800}{s+1}$ as in the online control design concept. Figure 6.16 presents the robust performance $\mu-$bound of the worst-case blending/interpolating controller over the flight envelope [0.2Mach,0.3Mach].

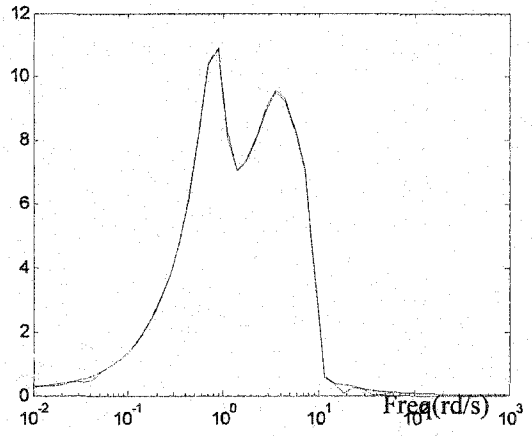

Figure 6.17: $\mu - bounds$ for robust performance

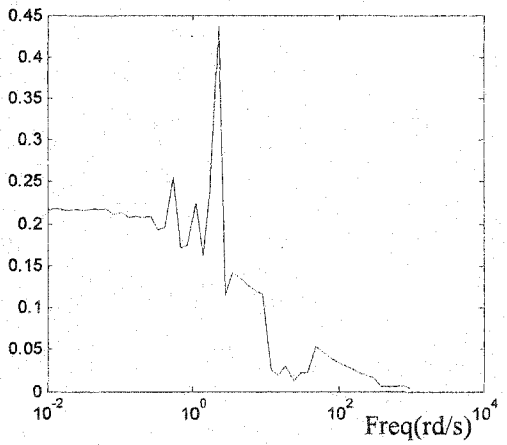

Figure 6.18: $\mu - bounds$ for robust stability

Since a robust stability analysis of this worst case blending/interpolating controller shows, in Figure 6.17, that robust stability is maintained over the flight envelope, we decided to decrease the specified level of performance to be able to meet the robust performance criterion. Choosing the performance weighting function as: $\frac{40}{s+1}$, we obtained a reasonable upper bound of μ for the worst-case blending /interpolating controller over the flight envelope as shown in Figure 6.18.

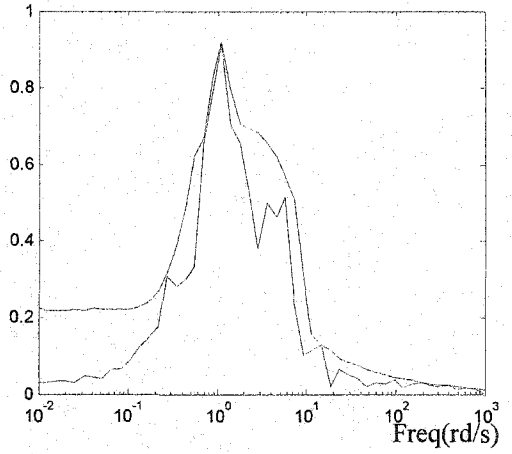

Figure 6.19: $\mu - bounds$ with relaxed performance specification

In the following, we propose to design a robust performance controller design for the flight envelope of the B1 flexible model based on the methodology proposed in this part of the current chapter. We kept the weighting function of performance to $\frac{40}{s+1}$. The varying-parameter in this case study is the Mach number, i.e., the velocity of the aircraft. A good perturbed model, as in (6.25), is obtained for the nonlinear dynamics of the aircraft model over the flight envelope considered. The designs of frozen controllers at the extremities of the flight envelope were done using weighted H_2 control. We preferred this design technique over classical H_∞ for its simplicity, and to show that for the method proposed optimality is not required in the frozen designs step. In fact, the optimization over the best sub-controller $Q_{opt}(s)$ compensates in a way to find a good sub-optimal blending/interpolating controller. Figures 6.19, 6.20 present the pitch angle tracking and the actuator responses for the weighted H_2 controller designed at 0.3 Mach.

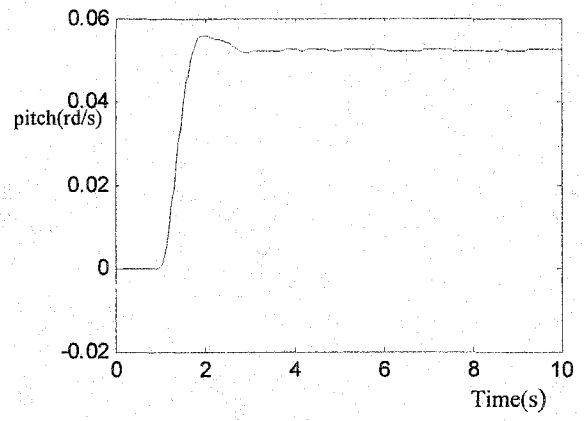

Figure 6.20: pitch tracking for weighted H_2 control

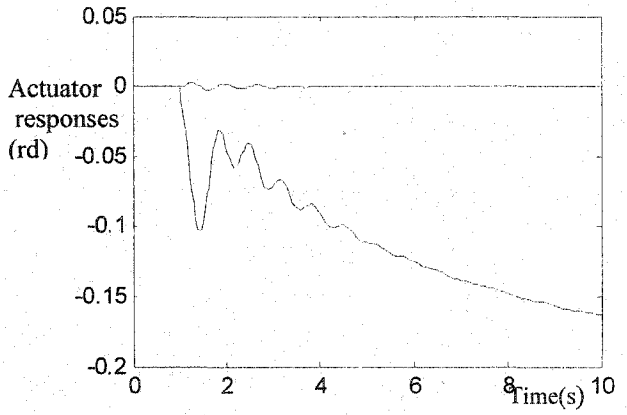

Figure 6.21: actuator responses for weighted H_2 control

The objective, as presented in (6.33), is to obtain the best sub-controller $Q_{opt}(s)$, thus the best parameter 'a', that assures the robust performance criterion of the closed-loop parameter-varying system presented in Figure 6.15.

A gradient-based optimization method, as presented earlier, is used to search for positive parameter a. The best values for the parameter a and the D-scaling are obtained equal to 0.14, 0.809, respectively.

The $\mu-$value of the closed loop system with the corresponded sub-controller controller $Q_{opt}(s)=\begin{pmatrix} \frac{1}{s+a}I_{2\times1} & 0 \\ 0 & \frac{1}{s+a}I_{2\times1} \end{pmatrix}$ is shown to be reasonable on Figure 6.22.

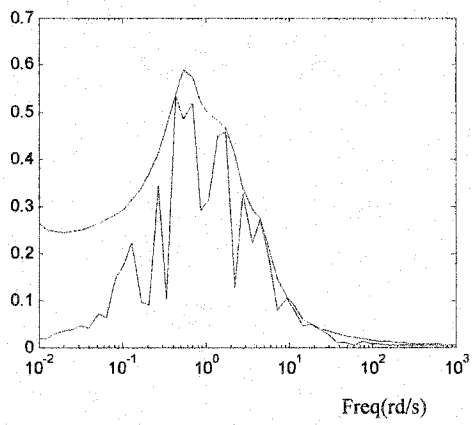

Figure 6.22: $\mu-$*bounds* for robust performance

To test the blending/interpolating controller, we proposed to do nonlinear simulation over the entire flight envelope considered. Figure6.22 shows the pitch angle tracking result and figure6.23 presents the actuator outputs over [0.2Mach,0.3Mach]. The results obtained from this non-linear implementation shows a good pitch angle tracking with acceptable range of controller outputs.

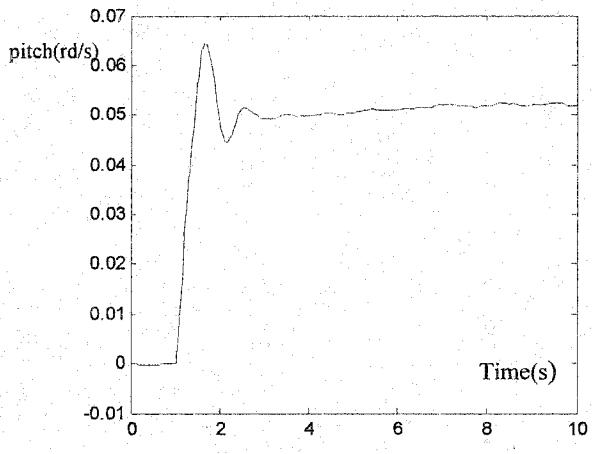

Figure 6.23: pitch tracking for robust gain scheduling control

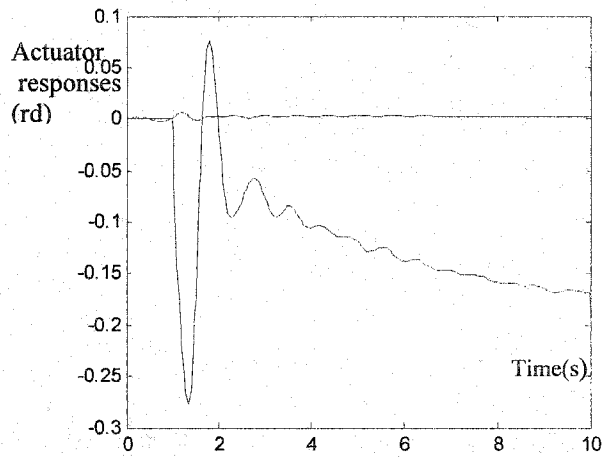

Figure 6.24: pitch tracking for robust gain scheduling control

Chapter 7

Summary and Conclusion

In Chapter 1, we presented different robust flight control objectives treated in this thesis. In addition to this, we introduced the modeling aspect for an aircraft. Furthermore, we gave details on flexible aircraft modeling. These flexible aircraft models are one of the main applications interest in this thesis since they are realistic and their sensitivity to turbulence effects has been of great interest in recent flight control research. Formal models of gust generation are also presented in Chapter 1.

In Chapter 2, details of optimal H_2 and H_∞ control theory are given along with a description of recent advances in their respective controller design under the LMI framework. We described the usual uncertainty modeling that is used for robust control design such as $\mu-$synthesis. The classical $\mu-$design via the D-K iteration algorithm [Bal95] presents conservatism when dealing with high-order uncertain system, as is the case for flexible aircraft. Thus, we presented $\mu-$synthesis based on iterative H_2 designs, which showed better results in many cases. In addition to these techniques, details on the H_∞ loopshaping procedure are given since we use this design technique in Chapter 5.

The adaptation of robust control techniques such as weighted H_2, H_∞ and $\mu-$synthesis to gust load alleviation problem is also given in Chapter 2. Interest in this research problem grew in the eighties, where progress in modern control techniques, such as LQR and LQG, is noticed. In this chapter, motivation for using optimal H_∞ control techniques is provided. H_∞ control laws developed for formal gust generation models show their efficiency in reducing undesirable accelerations of the flexible aircraft due to severe gust effects. A huge difference in terms of gust load alleviation is noticed between modern control techniques and robust control techniques, the latter proving superior in a comparison made in Chapter 2. In addition, we extended favorably the H_∞ control design to a $\mu-$design when uncertainties in the aircraft dynamics are taken into account.

Working with flexible aircraft models means that we deal with high-order systems that complicate the robust control design and render it conservative when uncertainty is taken into account. Thus, in Chapter 3 we investigated model order reduction techniques, to be able to use reduce-order flexible models that facilitate the robust control design.

We presented an overview of different open-loop model order reduction methods and recent techniques using closed-loop specifications. In this chapter, we introduced a new order reduction

technique, adapted for flexible aircraft and respecting the physical interpretation of the flexibility in the aircraft that provides a reduced, compatible model/controller pair while preserving robust performance specifications. Under a robust performance μ – setup, we propose a two-step procedure:

1. By a robust performance full-order controller design and μ – analysis, we deduce the best flexible mode combination to truncate for a given number of flexible modes to truncate.
2. Then, we present in Theorem 3.1 a sufficient condition under which, starting from the full-order controller of the best flexible mode combination, and under certain conditions a reduced-order controller preserving the robust performance specifications obtained by the full-order controller can be obtained.

The method is extended with μ – sensitivity theory, used in the first step of our technique, in order to save time and render the whole procedure more systematic.

In addition to this important result, we develop a new uncertainty model that we call "inverse uncertainty". This model proposes a lower uncertainty bound than bounds usually generated by common additive and multiplicative uncertainty models. The inverse uncertainty is adapted to robust control design techniques and shows good results when used for order reduction purposes in a closed-loop framework.

The order reduction techniques presented in Chapter 3 fill the void of methods adapted for flexible models. They offer order reduction tools that are indeed needed by aerospace engineers.

In Chapter 4, we propose uncertainty models able to represent tightly the uncertainty in the flexible aircraft model dynamics through the flexible mode parameter variations. The two models presented in this chapter are based on the coprime factorization representation and the modal coordinates representation. The efficiency of these models is tested on flexible systems and they present favorably good results in tightly bounding the flexible mode parameter variations and also in the robust performance levels obtained. Note that with the modal coordinates model, we are led to a new complex-rational controller design methodology that shows its efficiency under a robust control framework. For the implementation issue, we can recover a real-rational controller that preserves the robust performance obtained by the complex-rational controller.

In Chapter 5 and Chapter 6 we treat research problems related to gain scheduling. We introduce the IFPC design for the STOVL Harrier aircraft. This methodology is needed to take into account the propulsion system (engines) and its interaction with the airframe system. For this complex aircraft model, we have to provide gain-scheduling techniques to cover the entire flight envelope. First, we adopt an observer-form controller interpolation strategy, which results in good performance from hover to 120kn. We extend, by means of an observer form antiwindup technique, the flight envelope to 150kn of velocity. Because of the controller order reduction limits of this approach, we propose a new

approach consisting of a blending/interpolating approach that shows good results in nonlinear simulations. In addition, we propose an optimal multi-switching methodology, which is successfully implemented on a nonlinear model of the Harrier aircraft. The complexity of this model induces complexity in the H_∞ loopshaping frozen controllers designed and used to cover the entire flight envelope. Thus, a partitioning technique is used to obtain decentralized controllers which is easy to implement, and for which we develop and successfully implement a new scheduling-partitioning scheme.

In Chapter 6, after a brief presentation of LPV and LFT gain scheduled control theory, a Riccati based interpolation method, and a redesign control technique have been developed for a B1 flexible aircraft. Simulation results for both methods and for pitch tracking and gust load alleviation objectives are shown to be satisfactory. In addition, with the robust performance gain scheduling controller approach proposed, based on the blending/interpolating technique of Chapter 5, we enhanced the so-called *ad hoc* methods with guarantees on robust stability and performance of the closed-loop system. The gain-scheduled controller is obtained through an optimization based control approach, for μ specifications. Under a robust performance $\mu-$setup, and by using Theorem 6.1 (Lemma 6.1 is for robust performance analysis) that proves the robust performance of the gain scheduled controller, we are able to use the blending/interpolating technique safely. The positive results with this proposed method obtained for the B1 flexible model will certainly be useful to the aerospace researchers usually adept at methods based on interpolation techniques.

7.1 Future research

7.1.1 Order reduction

Using $\mu-$sensitivity for closed-loop order reduction for flexible aircraft preserving robust performance is a promising research direction that can be extended for iterative model order reduction. In fact, proving an additive property of the $\mu-$sensitivity, as is the case with H_∞ norm, we can predict the (i+1)th flexible mode to truncate such that $i=1,...,n$ and n represents the global number of the flexible modes to truncate.

Flexible modes reduction technique over a flight envelope will give the possibility of using frozen model order reduction over the flight envelope. Then the resulting reduced model could be used, under linear parameter varying representation, to derive a reduced-order scheduled controller. Research ideas related to that topic could be of a practical interest to the aerospace industry.

7.1.2 Uncertainty and gain scheduling:

Accurate uncertainty models presented in this thesis can be used with flight test data to give tight bounds on the variations in aeroelastic parameters of the aircraft. A joint project related to this research is being explored with NASA Dryden research center.

For the gain scheduling problem, the research reported in this thesis in terms of the gain-scheduled controller based on blending/interpolating technique and guaranteeing robust stability and performance opens new horizons for the *ad hoc* techniques. In fact, we think it is possible to extend this methodology to the parameter rate variation, which will be useful in analyzing the permissible region of acceleration of the aircraft without missing any important specification such as aircraft stability.

BIBLIOGRAPHY

[Abel82] Abel, I., Perry III, B. et Newsom, J.R "Comparison of Analytical and Wind-Tunnel Results for Flutter and Gust Response of a Transport Wing With Active Controls" NASA- TP-2010 1982.

[And86] Anderson, B.D.O "Weighted Hankel-norm approximation: calculation of bounds. Systems and Control letters 1986, (7) pp247-255.

[And89] Anderson, B.D.O and Liu, Y. "Controller reduction: Concept and approaches" IEEE Transactions on Automatic Control, 34(8), Aug 1989.

[Aou2000a] Aouf, N. Boulet, B., Botez, R. "$\mathcal{H}_2$ and $\mathcal{H}_\infty$ optimal gust load alleviation for a flexible aircraft." *Proc. 2000 American Control Conference,* Chicago, June 28-30, 2000, pp. 1872-1876.

[Aou2000b] Aouf, N. Boulet, B., Botez, R. "Robust gust load alleviation for a flexible aircraft." Canadian aeronautics and space journal 2000, Vol 46(3) pp.131-139.

[Aouf2000c] Aouf, N., Bates, D.G., Postlethwaite, I., and Boulet, B "Scheduling of integrated flight and propulsion control laws for a V/STOL aircraft in the acceleration from hover" Submitted to Control engineering practice.

[Aouf2002] Aouf, N., Boulet, B., Botez, R., "Gain scheduling for a flexible aircraft" Submitted American Control Conference 2002.

[Aouf2000d] Aouf, N, Bates, D.G, and Postlethwaite, I., "Observer-form scheduling of $\mathcal{H}_\infty$ loopshaping V/STOL aircraft control law in the acceleration from hover" Proceedings AIAA conference on Navigation, Control and Dynamics 2000.

[Aouf2001] Aouf, N. and Boulet, B., "Uncertainty modeling and complex-rational controller design for flexible structures" Proceedings of the AIAA Conference on Guidance, Navigation and Control, Montreal, August 6-9, 2001.

[Apk95] Apkarian, P., and Gahinet, P., "A convex characterization of gain –scheduled $\mathcal{H}_\infty$ controllers" IEEE Trans. on Automatic Control 1995 Vol 40(5), pp.853-864.

[Athans66] Athans, M., Falb, P.L., "Optimal control, an introduction to the theory and its applications" McGraw-Hill, New York, 1966.

[Att61] Attwood, J.L., Cannon, J.M., Johnson, J.M., Andrew, G.M. "Gust Alleviation System" US Patent 1961, 2, 985, pp. 409.

[Bal91a] Balas, G.J., and Doyle, J.C., "Robustness and tradeoffs in control design for flexible structures" Proceedings American Control Conference. 1991.

[Bal91b] Balas, G.J., Doyle, J.C., Glover, K., and Packard, A.K. "The robust and multivariable course" 1991, Cambridge, UK.

[Bal95] Balas, G.J., Doyle, J.C., Glover, K., Packard, A., Smith, R. "μ-Analysis and synthesis toolbox." 1995 MUSYN Inc, and the MathWorks, Inc.

[Bald99] Baldelli, D.H., and Sanchez Pena, R.S. "Uncertainty Modeling in Aerospace Flexible Structures" *AIAA J. of Guidance, Control and Dynamics*, Vol. 22, No.5, 1999.

[Ban92] Banda, S., Sparks, A. "Application of structured singular value synthesis to a fighter aircraft" Wright Laboratory, Wright Patterson Report 1992, pp 1301-1305.

[Bar89] Barmish, B., Khargonekar, P., Shi, Z., and Tempo, R. "Robustness margin need not to be continuous function of the problem data" Systems and Control letters 1989, vol.15, pp91-98.

[Bate99] Bates, D.G., Gatley, S.L., Postlethwaite, I., and Berry, A.J. "Integrated flight and propulsion control design using Hinfinity loopshaping techniques" Proceedings Conference on Decision and Control 1999, pp1523-1528.

[Bate2000] Bates, D.G., Gatley, S.L., Postlethwaite, I., and Berry, A.J. "Design and piloted simulation of robust integrated flight and propulsion controller" Journal of Guidance Navigation and Control 2000, Vol23 (2), pp269-277.

[Beck96] Beck, C. "Model reduction and minimality for uncertain systems" PhD Thesis 1996, California Institute of Technology, Passadena, CA, USA.

[Bon82] Bonvin, D., and Mellichamp, D.A. "A unified derivation and critical review of modal approaches to model reduction" International Journal of Control 1982, Vol 35, pp.829-848.

[Bot99] Botez, R., Boustani, I. and Vayani, N. "Optimal control laws for gust load alleviation." *Proc. 46th Annual CASI Conference,* Montréal, May 3-5, 1999, pp. 649-655.

[Boul97] Boulet, B., Francis, B.A., Hughes, P.C. and Hong, T. "Uncertainty Modeling and Experiments in H-infinity Control of Large Flexible Space Structures" *IEEE Trans. Control Systems Technology*, Vol. 5, No. 5, Sept. 1997, pp. 504-519.

[Boy94] Boyd, S., El Ghaoui, L., Feron, E., and Balakrishnan V. "Linear matrix inequalities in system and control theoty" 1994, Studies in Applied Mathematics SIAM 1994.

[Braat91] Braatz, R.P., Morari, M. "μ-sensitivity as an aid for robust identification" American Control Conference pp. 231-236, 1991.

[Bur68] Burris, P.M., Bender, M.A. "Aircraft Load Alleviation and Mode Stabilization (LAMS) – B52 system analysis, synthesis and design" AFFDL-TR-68-161, WPAFB, Dayton, Ohio.

[Busch99] Buschek, H. "Full flight envelope missile autopilot design using gain scheduled robust control" Journal of Guidance Control and Dynamics Vol22 (1), pp.115-123.

[Cet93] Ceton, C., Wortelboer, P., and Bosgra, O. "Frequency weighted closed-loop balanced reduction" Proceedings European Control Conference 1993, pp.697-701.

[Dec76] Decoster, M., and Cauwenberghe, A.R. "A comparative study of different reduction methods part I" Journal of Aircraft 1976, Vol 17, pp.68-74.

[Dev87] Devillemagne, C., and Skelton, R.E. "Model reductions using a projection formulation" International Journal of Control 1987, 46(6), pp.2141-2169.

[Doy82] Doyle, J.C. "Analysis of feedback systems with structured uncertainty" IEE Proceedings 1982 vol. 129, pp.242-250.

[Doy84] Doyle, J.C. "Matrix interpolation theory and optimal control" PhD Thesis 1984 University California Berkley.

[Doy85] Doyle, J.C. "Structured uncertainty in control system design" Proceedings Conference on Decision and Control 1985 pp.260-265.

[Doy89] Doyle, J.C., Glover, K., Khargonekar, P., Francis, B. "State space solutions to standard $\mathcal{H}_2$ and $\mathcal{H}_\infty$ control problems." IEEE Trans. Automatic Control 1989 AC34(8), pp.831-847.

[Enn84a] Enns, D. "Model reduction with balanced realizations: an error bound and frequency weighted generalization" Proceedings of the 23rd IEEE Conference on Decision and Control, Las Vegas, Dec. 1984, pp. 127-132.

[Enn84b] Enns, D."Model reduction for control system design" Phd thesis 1984, Stanford University USA.

[Fan91] Fan, M, K. H., Tits, A. L., and Doyle, J. C. "Robustness in the presence of mixed parametric uncertainty and unmodeled dynamics" IEEE Trans on Automatic Control 1991, Vol. 36, pp.25-38.

[Ferr98] Ferreres.G., and Biannic, J.M. "A μ analysis technique without frequency gridding" Proceedings of the American Control conference 1998.

[Fial97] Fialho, I., Balas, G.J., Packard, A.K., Renfrow, J., and Mullaney, C. "Linear Fractional Transformation control of the F-14 aircraft lateral-directional axxxis during powered approach landing" Proceedings American Control conference 1997, pp.128-132.

[Gah93] Gahinet, P., and Apkarian, P. "An LMI-based parametrization of all H_∞ controllers with applications" Proceedings Conference on Decision and Control 1993, Vol 1, pp.656-661.

[Gah94a] Gahinet, P., and Apkarian, P. "A linear matrix inequality approach to H_∞ control" International Journal of Robust and Nonlinear Control 1994, 4: pp.421-448.

[Gah94b] Gahinet, P., Nemirovskii, A., Laub, A.J., and Chilali, M. " The LMI control toolbox" Mathworks 1994.

[Garg93a] Garg, S. "Robust Integrated flight/propulsion control design for a STOVL aircraft using Hinfinity control design techniques" Automatica Vol29 (1), pp.129-145.

[Garg93b] Garg, S. " partitioning of centralized integrated flight propulsion control design for decentralized implementation" IEEE Control Systems Technology 1993, Vol1(2), pp.93-100.

[Gaw96] Gawronski, K. "Balanced control for flexible structures" in Lecture notes in Control and Information Sciences 211, Springer-Verlag, 1996.

[Glo84] Glover, K. "All optimal Hankel-norm approximations of linear multivariable systems and their L_∞ bounds" IEEE Transactions on Automatic Control, 1984 39(6): pp.1115-1193.

[Godd93] Goddard, P.J., Glover, K. "Controller reduction: weights for stability and performance preservation" Proceedings of the 32nd IEEE Conference on Decision and Control, 1993, Vol. 3, pp. 2903 -2908.

[Godd98] Goddard, P.J., Glover, K. "Controller approximation: approaches for preserving H_∞ performance" IEEE Trans on Automatic Control 1998, Vol 43 (7), pp.858-871.

[Gre95] Green, M., Limebeer, D.J. "Linear robust control" Englewood Cliffs, N.J, Prentice Hall 1995.

[Gup80] Gupta, N.K. "Frequency-shaped cost functionals; extension of linear-quadratic-gaussian design methods" Journal of Guidance and Control 1980, pp.529-535.

[Had89] Haddad, W.M., and Bernstein, D.S. " Combined L_2/H_∞ model reduction" International Journal of Control 1989, Vol 49 (5), pp.1523-1535.

[Han87] Hanus, R., Kinnaert, M., and Henrotte, J.L. "Conditioning technique, a general anti-windup and bumpless transfer method" Automatica Vol23 (6) pp.729-739.

[Har94] Harn, Y.L., and Kosut, R.L. "Optimal low order controller via LQG-like parametrization" IFAC Automatica 1993, Vol29, pp.1377-1394

[Harf99] Harefors, M. "A study in jet engine control- Control structure selection and multivariable design" PhD thesis 1999, Chalmers university Sweden.

[Hay90] Hayland, D.C., and Richter, S. "On direct versus indirect methods for reduced-order controller design" IEEE Trans. on Automatic Control 1990, Vol35 (3), pp.377-379.

[Helm95a] Helmersson "A finite frequency method for μ- analysis" Proceedings 3rd European Control Conference 1995, pp171-176.

[Helm95b] Helmersson "Model reduction for an H_∞ / LMI perspective" Proceedings 3rd European Control Conference 1995.

[Hob88] Hoblit, F.M. "Gust loads on aircraft: concepts and applications" Washington D.C: American institute on aeronautics and astronautics 1988.

[Horn85] Horn, R.A., and Johnson C.R., " Matrix analysis" Cambridge Univ. Press 1985.

[Hyd91] Hyde, R. "The application of robust control to VSTOL aircraft" PhD thesis 1991, University of Cambridge, UK.

[Hyl85] Hyland, D.C., and Bernstein, D. "The optimal projection equations for model reduction and the relationships among the methods of Wilson, Skelton and Moore" IEEE Trans. On Automatic Control 1985, AC30 (12), pp.1201-1211.

[Jonc83] Jonckheere, E.A., and Silverman, L.M. "A new set of invariants for linear systems-application to reduced order compensator design" IEEE Trans. Automatic Control 1983, AC28, pp.953-964.

[Josh98] Joshi, S.M., Kelkar, A. "Inner loop control of supersonic aircraft in the presence of aeroelastic modes" IEEE Trans Control systems technology 1998, Vol 6(6), pp.730-739

[Kal60] Kalman, R.E. "Contributions to the theory of optimal control" Pol. Soc. Mat. Mex, 1960 Vol 5 pp.102-119.

[Kar84] Karmen, E., and Khargonekar, P. "On the control of linear systems whose coefficients are functions of parameters" IEEE Trans on Automatic Control 1984, Vol29(1), pp.25-33.

[Kav93] Kavranoglu, D., and Bettayed, M. "Characterization of the solution to the optimal H_∞ model reduction problem" Systems and Control letters 1993, 20, pp.99-107.

[Kav94] Kavranoglu, D. "A computational scheme for H_∞ model reduction" IEEE Trans on Automatic Control 1994, Vol39 (7) pp.1447-1451.

[Kav96] Kavranoglu, D. "Controller reduction for uncertain systems" Proceedings of the 35th Conference on Decision and Control, Kobe, Japan, December 1996, pp. 887-892.

[Kol97] Kollar, I. "Frequency domain identification toolbox" The Mathworks, 1997.

[Krag79] Krag, B. "Active control technology for gust alleviation" Von Karman Institute for Fluid Dynamics, Lecture Series 1979 1, pp.1-78.

[Kuc72] Kucera, V. "A contribution to matrix quadratic equations" IEEE Trazns on Automatic Control" 1972 Vol AC17 (3) pp.344-347.

[Len88a] Lenz, K.E., Khargonekar, P.P., and Doyle, J.C. "Controller order reduction with garanteed stability and performance" Proceedings American Control Conference 1988, pp.1697-1698

[Len88b] Lenz, K.E ."Topics in applied H_∞ control" PhD thesis 1988, University of Minnesota, USA

[Lew86] Lewis, F.L. "Optimal control" Wiley International 1986.

[Mad98] Madelaine, B and Alazard, D. "Flexible structure model construction for control system" Proceedings of the AIAA Conference on Guidance Navigation and Control, Boston, 1998, pp. 1165-1175.

[Mats88] Matsuzaki, Y., Matsushita, H. "Gust load alleviation of transport-type wing : test and analysis" Journal of Aircraft 1988 Vol 26, No 4.

[McF90] McFarlane, D.C., and Glover, K. "Robust control design using normalized coprime factor plant description" Springer-Verlag, 1990.

[Mcl78] Mclean, D. "Gust load alleviation control systems for aircraft." Proc. IEE, Vol.125, No.7, July 1978, pp. 675-685.

[Mcl90] Mclean, D. "Automatic flight control systems." Prentice Hall International, Series in Systems and Control engineering 1990.

[Moo81] Moore, B.C. "Principal component analysis in linear systems: controllability, observability and model reduction" IEEE Transactions on Automatic Control 1981, 26(1).

[Mora89] Morari, M., and Zafriou, E. "Robust procedd control" Englewood Cliffs, N.J, Prentice Hall, 1989.

[Must89] Mustafa, D. " H_∞ -characteristics values" Proceedings Conference on Decision and Control 1989, pp.1483-1487.

[Muk92] Mukhopadhyay, V. "Digital robust control law synthesis using constrained optimization" Journal of Guidance, Control and Dynamics 1992, Vol. 12, No. 2, pp.175-181.

[New95a] Newman, B., and Schmidt, D.K. "Model simplification and robustness with elastic flight vehicles" Trans of the ASME: Journal of dynamics Systems, measurements and Control 1995 117(3) pp.336-342.

[New95b] Newman, B., Buttrill, C. "Conventional Flight Control for an Aeroelastic Relaxed Static Stability High-Speed Transport" Proceedings AIAA GN&C Conf., Aug. 1995, Baltimore, MD, pp.717-726.

[Nie96] Niewoehner, R.J., and Kaminar, I.I. "Design of an autoland controller for an F-14 aircraft using $\mathcal{H}_\infty$ synthesis." Journal of Guidance, Control, and Dynamics, Vol. 19, No 3, May 1996, pp.656-663.

[Osb94] Osborne, C. "Reduced-order $H\infty$ compensator design for an aircraft control problem" Journal of Guidance, Control and Dynamics 1997, Vol. 17, No. 2, pp.342-345.

[Pack88] Packard, A.K., and Doyle, J.C. "Structured singular value with repeated scalar blocks" Proceedings American Control Conference, 1988, pp.1213-1218.

[Pack93a] Packard, A.K., Pandey, P. "Continuity properties of the real/complex structures singular value" IEEE on Automatic Control 1993, vol. 38, pp.415-427

[PacK93b] Packard, A.K and Doyle, J.C "The complex structured singular value". Automatica, 1993 Vol.29, pp.71-109.

[Pack94] Packard, A.K. "Gain scheduling via Linear Fractional Transformations" Systems and Control letters 1994, Vol22(2), pp.79-92.

[Pack96] Packard, A and Kantner, M "Gain scheduling the LPV way" Proceedings Conference on Decision and Control 1996, pp3938-3941.

[Pap98] Papageorgiou, G. "Robust Control System Design : H-infinity Loop Shaping and Aerospace Applications" PhD thesis, University of Cambridge 1998.

[Rei92] Reichert, R. "Dynamic scheduling of modern robust control autopilot designs for missiles" Control Systems Magazine 1992 pp.35-42.

[Rugh90] Rugh, W.J."Analytical framework for gain scheduling" Proceedings American Control Conference 1990, pp.651-656.

[Saf90] Safonov, M.G., Chiang, R.Y., and Limebeer, D.J.N. "Optimal Hankel model reduction for nominimal systems" IEEE Trans. On Automatic Control 1990, 35(4).

[Sara2000] Sarah, G., Bates, D.G., Postlethwait, I "A partitioned integrated flight and propulsion control system with engine safety limiting" Control engineering practice 8 pp. 845-859, 2000

[Saw97] Sawan, M., Rokhsaz, K. "Mixed $H_2/H\infty$ method suitable for gain scheduled aircraft control" Journal of Guidance, Control and Dynamics 1997 Vol. 20, No. 4, pp.699-706.

[Sef90] Sefton, J.A., and Glover, K. "Pole/Zero cancellations in the general Hinfinity problem with reference to a Two block design" Systems and Control letters 1990, 14, pp.295-306

[Sham91] Shamma, J.S., and Athans, M. "Guaranteed properties of gain scheduled control for linear parameter-varying plants" Automatica 1991, Vol27 (3), pp.559-564.

[Sham94] Shamma, J.S. "Robust stability with time-varying structured uncertainty" IEEE Trans. Automatic Control 1994, Vol39(4), pp.714 -724

[Sid89] Sideris, A., and Sanchez-Pena, R,S. "Fast computation of the multivariable stability margin for real interrelated uncertain parameters" IEEE Trans Automatic Control 1989, vol.34, pp.1272-1276.

[Sid90] Sideris, A., and Sanchez-Pena, R,S. "Robustness margin calculation with dynamic and real parametric uncertainty" IEEE Trans Automatic Control 1990, vol.35, pp.970-974.

[Ske80] Skelton, R.E. "Cost decomposition of linear systems with application to model reduction" International Journal of Control 1980, 32 (6), pp.1031-1035.

[Ske88] Skelton, R.E. "Dynamics systems control" John Wiley&Sons, New York 1988.

[Ske90] Skelton, R.E., and Hu, A. "Model reduction with weighted modal cost analysis" Proceedings Conference on Guidance Navigation and Control AIAA1990.

[Smi94] Smith, R.S., Chu, C.C., and Fanson, J.L. "The design of H-infinity controllers for an experimental noncollocated flexible structure" IEEE Trans. Control Systems Technology 1994, Vol. 2, pp.101-109.

[Ste92] Steven, B., and Lewis, F.L. "Aircraft simulation and control" Wiley 1992.

[Stil99] Stilwell, D., Rugh, W.J. " Interpolation of observer state feedback controllers for gain scheduling" IEE Trans. Automatic Control 1999, Vol44 (6), pp.1225 -1229

[Sto73] Stockdale, C.R., Poyneer, R.D. "Control Configured Vehicle – Ride Control System" AFFDL-TR-73-83, WPAFB, Dayton, Ohio.

[Tich96] Tischler, M.B. "Advances in aircraft flight control" Taylor and Francis chap6 1996.

[Turn99] Turner, M.C., and Walker, D.J. "Modified linear quadratic bumpless transfer" Proceedings American Control Conference 1999, pp.2285-2289.

[Turn2000] Turner, M.C. "Robust control of systems subject to input nonlinearities with application to high performance helicopters" PhD thesis 2000, University of Leicester UK.

[Turn2001] Turner, M.C., Aouf, N., Bates, D.G., Postlethwaite, I., and Boulet, B. "A switching scheme for full-envelope control of a V/STOL aircraft using LQ bumpless transfer" Submitted to International Journal of Control, Special Issue on Switched Systems 2002.

[Vane99]Van Etten, C. "Linear parameter-varying structural mode control" Master Thesis Delft University 1999.

[Van86] Van Gelder, P.A. "Design of an integrated control system for flutter margin augmentation and gust load alleviation, tested on a dynamic wind tunnel model" AIAA 1986, pp.802-811.

[Vid95] Vidyasagar, M., Deodhar, G. " $H\infty$ Design of robust flight controllers to meet flying quality specifications" Proceedings of the 31st Conference on Decision and Control 1995, pp.562-563.

[Vin94] Vincent, J.H., Emami-Naeini, A., Khraishi, N.M. "Case Study Comparison of Linear Quadratic Regulator and $\mathcal{H}_\infty$ Control Synthesis" Journal of Guidance, Control, and Dynamics 1994, Vol. 17, No. 5, pp.958-965.

[Von37] Von Karman, T. "Fundamentals of the Statistical Theory of Turbulence" Journal of Aeronautical Science 1937, 4, pp. 131-138.

[Wan98] Wang, H.S, Yung, C.F and Chang, F.R. "Bounded real lemma and H_∞ control for descriptor systems" IEE Proceedings Control Theory and Applications 1998, Vol 145, pp.316-322.

[Wang2001] Wang, G., Sreeram, V., and Liu, W.Q. "Performance preserving controller reduction via additive perturbation of the closed loop transfer-function" IEEE Trans. Automatic Control 2001 Vol 46 (5), pp.771-775.

[Was88] Waszak, M., Shmidt, D. "Flight dynamics of aerolastic vehicles" Journal of Aircraft 1988 Vol25 (6) pp.563-571.

[Wil70] Wilsson "optimum solution of model-reduction problem" Proceedings IEE 1970, Vol117, pp.1161-1165.

[Wil74] Willsson "Model reduction for multivariable systems" International Journal of Control 1974, Vol20, pp.57-64.

[Woe85] Woerkom, P.Van. "Mathematical models for flexible spacecraft dynamics: a survey of order approaches" Proceedings of Automatic Control in Space, 1985.

[Wor93] Wortelboer, P. , Bosgra, O.H., and Ceton, C. "Frequency-weighted balanced reduction in closed loop systems" Selected Topics in Identification, Modelling and Control Vol6, Delft University Press, pp.133-141.

[Wor94] Wortelboer, P. "Frequency-weighted balanced reduction of closed-loop mechanical servo-systems: Theory and Tools" PhD thesis 1994, Delft University Netherlands.

[Wu95a] Wu, F. "Control of linear parameter varying systems" Phd thesis, 1995, University of California, Berkley.

[Wu95b] Wu, F., Packard, A.K., and Balas G.J. "LPV control design for pitch-axis missile autopilots" Proceedings Conference on Decision and Control 1995, pp.188-193.

[Yan97] Yang, C.-D. , Chang, C.-Y., and Y.-P. Sun. "Mixed μ-Synthesis via H_2-Based Loop-Shaping Iteration" Journal of Guidance, Control and Dynamics 1997, Vol 21 No 1.

[You90] Young, P. M., Doyle, J. C. "Computation of μ with real and complex uncertainties" Proceedings 29th Conference on Decision and Control 1990 pp.1230-1235.

[You92] Young, P. M., Newlin, M. P., and Doyle, J. C. "Practical computation of the mixed μ problem" Proceedings American Control Conference, 1992, pp.2190-2194.

[You93] Young, P. M. "Robustness with parametric and dynamic uncertainty" PhD. Dissertation 1993, California Institute of technology.

[Zam66] Zames, G. "On the input-output stability of non-linear time-varying feedback systems, PartI and II" IEEE Trans. On Automatic Control1966, 11, pp.228-238 and pp.465-476.

[Zho96] Zhou, K., Doyle, J.C., and Glover, K. "Robust and Optimal Control" Prentice-Hall: New-Jersey, 1996, 596 pages.